THE ROLE OF LIPID-INDUCED INTEGRATED STRESS RESPONSE IN METAFLAMMATION AND ATHEROSCLEROSIS

A DISSERTATION SUBMITTED TO

THE GRADUATE SCHOOL OF ENGINEERING AND SCIENCE

OF BILKENT UNIVERSITY

IN PARTIAL FULFILLMENT OF THE REQUIREMENTS FOR

THE DEGREE OF

DOCTOR OF PHILOSOPHY

IN

MOLECULAR BIOLOGY AND GENETICS

By

Umut İnci Onat

June, 2019

THE ROLE OF LIPID-INDUCED INTEGRATED STRESS RESPONSE IN METAFLAMMATION AND ATHEROSCLEROSIS

By Umut İnci Onat

June, 2019

We certify that we have read this dissertation and that in our opinion it is fully adequate, in scope and in quality, as a thesis for the degree of Doctor of Philosophy.

Ebru Erbay
(Advisor)

Michelle Marie Adams

Murat Alper Cevher

Çağdaş Devrim Son

Erkan Yılmaz

Approved for the Graduate School of Engineering and Science

Ezhan Karaşan
Director of the Graduate School of Engineering and Science

ABSTRACT

THE ROLE OF LIPID INDUCED INTEGRATED STRESS RESPONSE IN METAFLAMMATION AND ATHEROSCLEROSIS

Umut İnci Onat
Ph.D. in Molecular Biology and Genetics
Advisor: Ebru ERBAY
June 2019

Chronic inflammation resulting from metabolic overloading of organelles (such as the endoplasmic reticulum (ER) and mitochondria that control cellular homeostasis) is a major cause of metabolic disorders including diabetes, obesity and atherosclerosis. ER is an organelle that plays a critical role in cellular metabolism through biosynthesis of lipids, protein maturation and secretion, and calcium storage. Furthermore, a stressed endoplasmic reticulum maintains cellular homeostasis by initiating a conserved stress response pathway that is known as Unfolded protein response (UPR). UPR is activated in response to diverse stimuli that disrupts ER functions and serves asva pro-survival mechanism to regain ER homeostasis. However, in prolonged or severe ER stress, chronic UPR can promote inflammation and apoptosis. Activated UPR, inflammation and necrosis are observed in and causally associated with atherosclerosis. UPR has three branches, one of which is initiated by the protein kinase RNA (PKR) like ER kinase (PERK) and signals to eukaryotic initiation factor 2α (eIF2α). This signaling arm of the UPR is also part of a larger, translational control pathway known as the integrated stress response (ISR). Activation of ISR has been observed in atherosclerosis and could promote atherosclerosis To study the contribution of ISR to atherogenesis, I took advantage of three small molecule inhibitors that can modulate this pathway. I also used a chemical-genetic approach, known as the Adenosine triphosphate (ATP) analog sensitive kinase (ASKA) technology, to interrupt PERK kinase activity. With these multiple tools, I was able to specifically interfere with ISR signaling at multiple molecular nodes in order to study the role of lipid-induced ISR in inflammation, inflammasome activation and atherosclerosis. I discovered that during lipid-induced ER stress, PERK to Activating transcription factor 4 (ATF4)

signaling resulted in transcriptional induction of a mitochondrial protease, Lon protease 1 (LONP1), which degrades PTEN induced putative kinase 1 (PINK1) and blocks Parkin-mediated mitochondria clearance (or mitophagy). This in turn causes an increase in mitochondrial reactive oxygen species (ROS) production, inflammasome activation and pro-inflammatory cytokine secretion such as interleukin-1β (IL-1β) in both mouse and human macrophages. I also discovered that these inhibitors are also effective in reducing hyperlipidemia-induced inflammasome activation in Apolipoprotein E-deficient ($Apoe^{-/-}$) mice and consequently, in preventing atherosclerosis progression. These results point out that intercepting with ISR signaling in hypercholestrolemia can be considered as a novel therapeutic approach that could be developed against atherosclerosis.

Keywords: ER stress, integrated stress response, mitochondrial ROS, inflammasome, atherosclerosis, ATP analog sensitive kinase allele, IL-1β

ÖZET

ENTEGRE STRES TEPKİSİNİN METAFLAMASYON VE ATHEROSKLEROZDAKİ ROLÜ

Umut İnci Onat
Moleküler Biyoloji ve Genetik, Doktora
Tez Danışmanı: Ebru ERBAY
Haziran 2019

Hücresel ve metabolik homeostazı sağlayan endoplazmik retikulum (ER) ve mitokondri gibi organellerde metabolik aşırı yüklenme sonucu oluşan kronik metabolik inflamasyon, tip II diyabet, obezite ve ateroskleroz gibi metabolik hastalıklara neden olur. Endoplazmik retikulum, lipid biyosentezi, protein olgunlaşması ve kalsiyum depolaması gibi hücresel metabolizmadaki kritik rollerine ilaveten katlanmamış protein yanıtı (KPY) olarak adlandırılan bir stres yanıtı yolu ile hücresel homeostazı korumaktadır. Hücresel homeostazı bozan çeşitli çevresel uyarıcılara cevap olarak, KPY hücresel fonksiyonları yeniden kazanmak için hayatta kalma yanlısı bir mekanizma olarak aktive edilir. Ancak, uzun süreli Endoplazmik Retikulum (ER) stresi durumlarında KPY hücreleri inflamasyon ve apoptik ölüme sürükler. Aktif KPY, artmış inflamasyon ve apoptoz, ER'i metabolik hastalığa bağlayan ve aterosklerozda aktif olan belirteçlerdir. KPY'in inhibisyonunun ateroskleroz gelişimini önlediği deneysel olarak gösterilmiştir. KPY'in bir kolu olan protein kinaz R benzeri ER kinaz (PERK) – ökaryotik inisiyasyon faktörü 2α (eIF2α) ve entegre stres tepkisi (EST) adlı bir başka stress yanıti ile örtüsmektedir. EST eif2α'ın fosforilasyonu ile genel proteine çevrim mekanizmasını bloke eder. EST'in belirteçlerinin aterosklerotik plaklarda aktive oldukları bilinmektedir ve aterosklerozun ilerlemesine neden olabileceği düşünülmektedir. Bu metabolik yolaklara ateroskleroz sürecinde ve makrofajlarda müdahale etmek için yakın zamanda keşfedilen üç küçük moleküler inhibitörden yararlandım. Bu yöntemde ADKA (ATP analoguna duyarlı kinaz aleli) teknolojisini PERK kinaza uygulayarak, kimyasal-genetik yöntem ilede bu kinazın aktivitesini ateroskleroz sürecinde ve makrojalarda kapatabildim. Bu değişik yöntemler ile EST stres yolağına birçok moleküler seviyede müdahale etme şansım oldu. Bu teknololojileri EST'nin, özellikle KPY ile örtüşen PERK-eIF2α yolağının makrofajlarda yağ yüklemesiyle artan

mitokondriyel reaktif oksijen türevlerinin (mtROT) üretimi, inflamazom aktivasyonu ve interlökin-1 beta (IL-1β) gibi inflamatuvar sitokinlerin salınımı ve bunların aterosklerozdaki rolünü incelemek için kullandım. Yağ kaynaklı ER stres koşullarında, PERK'den Aktifleştirici Transkripsiyon Faktörü 4 (ATF4)'e sinyalizasyon, Uyarılmış Putatif Kinaz-1(PINK1) sinyal yolunun, PINK1'ı parçalayan ve uyarılmış putatif kinaz 1 (PINK1)'ı parçalayan ve PINK1 / Parkin mitofaji yolağını bloke eden mitokondriyal proteaz Lon Proteaz 1 (LONP1)' in transkripsiyon düzeyinde yapımını indüklediğini ve bunun sonucunda mtROT üretiminde, inflamazom aktivasyonunda ve interlökin 1- beta (IL-1β) salınımında bir artışa neden olduğunu keşfettim. Ayrıca, inhibitörlerin bu etkilerinin *in vitro* çalışmalar ile sınırlı olmadığını, aynı zamanda hiperkolesterolemik apolipoprotein – $E^{-/-}$ ($apoE^{-/-}$) farelere tatbik edilmesiyle hiperlipideminin neden olduğu inflamazom aktivasyonunu sınırlandırdığını ve sonuç olarak aterosklerozun ilerlemesini baskıladığını keşfettim. Bu sonuçlar, hiperkolesterolemi ile artan EST sinyal yolağının baskılanmasının aterosklerozu azaltmak için terapötik bir yaklaşım olarak kullanılabileceğine işaret etmektedir.

Anahtar sözcükler: ER stres, entegre stres tepkisi, mitokondriyal reaktif oksijen türleri, inflamazom, ateroskleroz, ATP analoğuna hassas kinaz aleli, interklökin-1β

To my Family…

Acknowledgements

Firstly, I am very thankful to my supervisor Dr. Ebru Erbay for her scientific and personal guidance and support. I feel honored and very lucky to have had a chance to study in her lab. Dr. Erbay's scientific lead and guidance and support during my scientific discoveries and publishing in one of the leading journals in cardiovascular research helped me surpass these challenging times.

I also want to thank Bilkent University for giving me the opportunity to do carry out my doctoral research under their academic roof. During my PhD, I improved my scientific knowledge, my personal skills, gained problem solving as well as detailed planning capabilities.

I appreciate the helps and scientific contributions of my thesis committee members Dr. Michelle Adams and Dr. Alper Murat Cevher. Furthermore, I would like to thank Dr. Erkan Yılmaz and Dr. Çağdaş Devrim Son for guidance during my dissertation and for their contribution as members of my thesis jury.

I am thankful for the contributions of our collaborators, Dr. Moshe Arditi, Dr. Roberta Gottlieb, Dr. Jon Sin, Dr. Kenichi Shimada and Dr. Shuang Chen, and for their assistance and support in difficult times during the revision of the studies for publication.

I also want to thank to my friends and colleges for their help and support during my Ph.D studies. I received a lot of support during my Ph.D. study in scientific manners as well as in friendship.

First of all, I want to thank Aslı Dilber Yıldırım for her friendship, help and contribution to the published work. She performed every task with great care and enthusiasm, and nothing I can say here can describe my great appreciation of her efforts.

I would like to also express my appreciation to Dr. İsmail Çimen for training me in animal experiments.

I express my appreciations to Dr. Begüm Kocatürk for training me in flow cytometry

and giving me scientific perspective in immunostaining procedures.

I express my appreciations to Dr. Özlem Tufanlı Kireççibaşı for her scientific lead, support and friendship during my Ph.D studies.

I also want to thank Dr. Hamid Sayed Muhammed, Zehra Yıldırım and Aslı Ekin Doğan for their support and friendship.

I would like to express my gratitude to Buket Gültekin for her help with problems regarding laboratory equipment, effort to supply research materials and for her friendship.

I want to thank to our veterinarian, Dr. Gamze Aykut for her technical support with animal experiments.

I cannot find enough words to express my gratitude and appreciation for the Zehra Veli's help Whenever I was in trouble, unhappy or unmotivated, Zehra was always there for me as a great listener, friend and supporter. I did not know how to handle the unpredictability during the revision process prior to publication of my thesis work, but she was not there and supporting me. She is one of the most important persons in my life, who helped me keep going in the last two years.

I also want to thank for the funding that enabled me to complete my thesis; Scientific and Technological Research Council of Turkey (TUBITAK)-COST grant 113Z023, European Molecular biology Organization (EMBO) for Installation Grant and European Research Council (ERC) Starting Grant 336643.

And, most precious is my family. I want to express my deep gratitude and my love for my husband Dr. Onur Emre Onat for his outstanding support as a scientist, great friend and life partner. I would not be able to succeed or cope with the difficulties of a PhD study without him.

I also want to express my gratitude for my parents for bringing me this far, and doing every-thing in their power to support my education.

But most of all I want to thank god and my husband for their outstanding gift to me, my daughter, Zeynep. She is my strength, my love, and my dearie that gives me

emotional support and power. I am very lucky to have her. Her existence is the most powerful energy that led me go this far to reach this stage in my academic studies…

Contents

ABSTRACT ..... **II**

ÖZET ..... **IV**

ACKNOWLEDGEMENTS ..... **VII**

CONTENTS ..... **X**

LIST OF FIGURES ..... **XV**

LIST OF TABLES ..... **XIX**

ABBREVIATIONS ..... **XX**

CHAPTER 1. INTRODUCTION **23**

1.1. The Endoplasmic Reticulum **23**

1.1.1. Endoplasmic Reticulum Function 24

1.1.2. The Endoplasmic Reticulum Stress and Unfolded Protein Response 26

1.2. Unfolded Protein Response Signaling **27**

1.2.1. IRE1 27

1.2.2. PERK 28

1.2.3. ATF6 29

1.3. Integrated Stress Response **30**

1.4. Endoplasmic Reticulum Stress and Immune Response **33**

1.4.1. UPR Connection to Inflammatory Pathways 35

1.4.2. UPR Connection with Inflammasome Activation 37

1.5. Endoplasmic Reticulum and Mitochondria **40**

1.5.1. Mitophagy and inflammation 42

1.6. Atherosclerosis **46**

1.6.1. Initiation and Progression of Atherosclerosis 47

1.6.2. Endoplasmic Reticulum Stress in the Progression of Atherosclerosis 51

1.6.3. Therapeutic Approaches in Atherosclerosis 52

1.7. Hypothesis and Study Aims **55**

CHAPTER 2. MATERIALS AND METHODS 57

2.1. Materials 57

2.1.1. Reagents 57

2.1.2. Cell Culture Reagents 59

2.1.3. Antibodies 60

2.1.4. Study Specific Reagents and Kits 61

2.1.5. Solutions 62

2.1.6. Transgenic Mice Used 64

2.1.7. Diets used in mouse atherosclerosis studies 64

2.2. Methods 65

2.2.1. General Study Design 65

2.2.2. Cell Culture and Treatments 65

2.2.3. Mitochondria Isolation & Mitophagy Experiments 67

2.2.4. siRNA Electroporation 67

2.2.5. mtROS Staining and Quantification 67

2.2.6. Western Blot Analysis 68

2.2.7. RNA isolation and Quantitative Real Time Polymerase Chain Reaction 68

2.2.8. Mouse Cytokine Measurements with Enzyme Linked Immunosorbent Assay 69

2.2.9. Mouse Studies and Treatments 69

2.2.10. Plasma Lipids and Lipoprotein Analysis 70

2.2.11. Flow Cytometry 70

2.2.12. Immunohistochemistry 71

2.2.13. *En face* Aorta Lesion Analysis 72

2.2.14. Statistical Analysis 72

CHAPTER 3. IN VITRO RESULTS 73

3.1. Regulation of Inflammasome Activation 73

3.1.1. The Impact of Silencing PERK Under Lipid-induced ER Stress Conditions in Bone-marrow Derived Macrophages 73

3.1.2. Effect of Silencing PERK Kinase Activity Under Lipid-induced ER Stress Conditions in Bone-marrow Derived Macrophages 74

3.1.3. Alternative Approach Confirms of PERK Kinase Activity is Necessary for Lipid-Induced Activation of Inflammasome Activation in Macrophages and *In Vivo* 75

3.2. Contribution of the Integrated Stress Response to Inflammasome Activation 77

3.2.1. The Impact of eIF2α Phosphorylation on Inflammasome Activation ... 77

3.2.2. Delineating eIF2α to Inflammasome Signaling 79

3.3. The Impact of Silencing ISR on Lipid-Induced Activation in Human Macrophages 81

3.4. Regulation of Mitochondrial Oxidative Stress by the Integrated Stress Response 82

3.4.1. Regulation of Mitochondrial Reactive Oxygen Species (mtROS) Production by PERK 82

3.4.2. Regulation of Mitochondrial LON Protease by ISR Signaling 83

3.4.2.1. Regulation of Mitochondrial LON Protease by ISR in Mouse BMDMs 83

3.4.2.2. Regulation of Mitochondrial LON Protease by PERK in Human Macrophages 85

3.4.3. Regulation of Mitochondrial Reactive Oxygen Species (ROS) Production by LONP1..... 86

3.4.4. Regulation of Inflammasome Activation by LONP1 87

3.4.5. Regulation of PINK1 by PERK-eIF2α-LONP1 Signaling Axis 89

3.5. Regulation of Mitophagy by ISR 90

3.5.1. PINK1-Parkin Dependent Mitophagy Response 90

3.5.2. Confirming the Role of Mitophagy in Inflammasome Regulation by ISR 91

CHAPTER 4. PERK'S ROLE IN HIGH FAT-INDUCED INFLAMMATION AND ATHEROGENESIS *IN VIVO* 93

4.1. In vivo Administration of GSK2606414 to Inhibit PERK Kinase Activity in A Mouse Model of Atherosclerosis 93

4.1.1. General Study Design and Correlation of The Efficacy of GSK2606414 *In Vivo* 93

4.1.2. Analysis of Bodyweight, Blood Glucose and Plasma Insulin Levels in Animals 95

4.1.3. Analysis of Atherosclerotic Lesion Formation in PERK Kinase – Inhibited Apoe$^{-/-}$ Mice 96

4.1.4. The Impact of PERK Inhibition on Atherosclerotic Plaque Cellular Composition 98

4.1.4.1. Analysis of Aortic Sinuses for P-eIF2α and LONP1 Axis 98

4.1.4.2. Analysis of PERK Kinase Inhibitor's Impact on Macrophage and T Cell Content in the Aortic Sinus Atherosclerotic Plaque Areas 100

4.1.4.3. Analysis of Inflammatory Cytokine Levels 101

4.1.4.4. PERK Kinase Inhibitor's Impact on Aortic Plaque Collagen Content 106

4.1.5. PERK Kinase Inhibitor's Impact on Inflammatory Cell Numbers in the Circulation 108

4.1.6. The Impact of PERK Kinase Inhibitor on T Lymphocytes in the Apoe$^{-/-}$ Mice in Western Diet 108

4.1.7. The Impact of PERK Kinase Inhibitor on Lipoprotein Profiles of Apoe$^{-/-}$ Mice Fed with Western Diet 110

4.1.8. Analysis of Aortic Lesion Progression or Aortic in PERK Kinase Inhibitor-Treated Mice 112

4.2. Modulating ATP Analog- Sensitive Kinase Allele of PERK *In Vivo* 113

4.2.1. General Study Design and Correlation of The Efficacy of 1-NAPP1 *In Vivo* 113

4.2.2. Analysis of Bodyweight and Blood Glucose 115

4.2.3. The Impact of PERK ASKA Kinase Inhibition by 1-NAPP1 on Atherosclerotic Plaque Development 116

4.2.4. 1-NAPP1 Treatment Reduces Stress, Inflammation and Atherosclerosis Progression in the Aortic Roots of ASKA-Apoe$^{-/-}$ Mice 119

4.2.4.1. Analysis of Aortic Sinuses for P-eIF2α and LONP1 119

4.2.4.2. The Impact of PERK Inhibition on Plaque Immune Cell Content 121

4.2.4.3. PERK Kinase Inhibition Suppressed Hyperlipidemia-Induced Inflammatory Cytokine Levels 122

4.2.5. The Impact of PERK Kinase Inhibition on Lipid Profiles of Mice 125

CHAPTER 5. EFFECT OF INTEGRATED STRESS RESPONSE IN ATHEROSCLEROSIS 126

5.1. The Impact of ISRIB on Hyperlipidemia-Induced Inflammation and Atherosclerosis *In Vivo* 127

5.1.1. General Study Design and The Efficacy of ISRIB *In Vivo* 127

5.1.2. The Impact of ISRIB on Metabolic Parameters 129
5.1.3. The Impact of ISRIB on Atherosclerotic Plaque Development 129
5.1.4. The Impact of ISRIB on Plaque Immune Cell Composition 131
5.1.4.1. The Impact of ISRIB on Hyperlipidemia-Induced LONP1 Expression in Plaques 131
5.1.4.2. The Impact of ISRIB on Plaque Immune Cell Content 132
5.1.4.3. The Impact of ISRIB on Inflammatory Cytokine Levels Induced by Hyperlipidemia 133
5.1.5. The Impact of ISRIB on Circulating Immune Cell Counts 136
5.1.6. The Impact of ISRIB on Systemic Lipoprotein and Lipid Profiles in Apoe$^{-/-}$ Mice Fed with Western Diet 137
5.1.7. The Impact of ISRIB on Atherosclerosis Progression 138
5.2. The Impact of Higher Dose of ISRIB Administration on Atherosclerosis 139
5.2.1. The Impact of Higher Dose of ISRIB Administration on Metabolic Parameters 139
5.2.2. The Impact of Higher Dose of ISRIB Administration on Atherosclerosis 140
CHAPTER 6. DISCUSSION 141
CHAPTER 7. FUTURE PERSPECTIVES 147
BIBLIOGRAPHY 149
COPYRIGHT PERMISSIONS 172
PUBLICATION 179

List of Figures

Figure 1.1. Endoplasmic Reticulum Stress and Unfolded Protein Response.....27

Figure 1.2. Schematic representation of ISR.....33

Figure 1.3. ER Stress, Inflammation and Metabolic Disease.....35

Figure 1.4. UPR Engages Inflammatory Pathways.....36

Figure 1.5. Relationship Between PERK Signaling Pathway and Inflammation.....37

Figure 1.6. Mitophagy Pathways.....44

Figure 1.7. Mitophagy Reduces Inflammation and Inflammasome Activation.....46

Figure 1.8. Four Stages of Atherosclerotic Lesion Formation.....48

Figure 1.9. Role of UPR in the Progression of Atherosclerosis.....52

Figure 3.1. PERK expression silencing with siRNA can suppress lipid-induced NLRP3 inflammasome activation in BMDM cells.....74

Figure 3.2 Inhibition of PERK kinase activity leads to suppression of lipid-induced NLRP3 inflammasome activation in BMDMs.....75

Figure 3.3 Design of PERK_ASKA mice and successful breeding of homozygous mice.....76

Figure 3.4 PERK kinase activity is critical for robust activation of the NLRP3 inflammasome by lipids was confirmed in peritoneal macrophages by an alternative approach involving chemical genetics.....77

Figure 3.5 Sephin1 prolongs eIF2α phosphorylation and bypassess PERK inhibitor's suppression of NLRP3 inflammasome.....78

Figure 3.6. ISRIB inhibits NLRP3 inflammasome activation in lipid stressed BMDMs.....79

Figure 3.7. ATF4 mediates lipid-induced NLRP3 inflammasome activation in BMDMs.....80

Figure 3.8. ISR signaling plays a critical role in lipid-induced inflammasome activation in human macrophages.....81

Figure 3.9. Regulation of lipid-induced mtROS production by ISR.....83

Figure 3.10 Mitochondrial LONP1 is regulated by ISR in lipid-stressed macrophages.....84

Figure 3.11 Lipid-induced mitochondrial LONP1 is dependent on ISR signaling in human macrophages.....85

Figure 3.12 Regulation of mtROS production by LONP1 86

Figure 3.13. LONP1 regulates lipid-induced inflammasome activation kinase.....88

Figure 3.14. PERK regulates inflammasome activation through mitochondrial LONP1 and PINK1.....89

Figure 3.15. PERK-eif2α-LONP1 signaling axis regulates mitophagy.....90

Figure 3.16. Inflammasome regulation via PERK–LONP1 axis is dependent on PINK1-PARKIN-mediated mitophagy.....92

Figure 4.1. Inhibition of PERK kinase Activity In Vivo During Athersclerosis progression.....94

Figure 4.2. Metabolic characterization of 30mg/kg/day GSK2606414-treated mice.....95

Figure 4.3. PERK inhibition leads to reduction in atherosclerotic plaque formation *in vivo*.....97

Figure 4.4. Loss of PERK kinase activity reduces of p-eIF2α and LONP1 levels in Apoe$^{-/-}$ mice in vivo.....99

Figure 4.5. Loss of PERK kinase activity mitigates hyperlipidemia induced immune cell accumulation in Apoe$^{-/-}$ mice.....101

Figure 4.6. Inhibition of PERK kinase activity reduces hyperlipidemia-induced IL-1β production in aortic plaque macrophages.....102

Figure 4.7. Inhibition of PERK kinase activity reduces hyperlipidemia-induced cleaved caspase1 levels in aortic plaque macrophages.....103

Figure 4.8. Inhibition of PERK kinase activity suppresses hyperlipidemia-indued cytokine levels in the Apoe$^{-/-}$ mice on WD.....105

Figure 4.9. Analysis of VCAM-1 and Cell Death in Plaques from PERK kinase-inhibited Apoe$^{-/-}$ Mice.....106

Figure 4.10. Loss of Perk kinase activity does not affect smooth muscle cell migration or collagen secretion.....107

Figure 4.11. Loss of Perk kinase activity does not affect numbers of immune cells in bloodstream.....108

Figure 4.12. Inhibition of PERK kinase activity impacts Th lymphocyte differentiation induced by hyperlipidemia in Apoe$^{-/-}$.....110

Figure 4.13. Plasma Lipid and Lipoprotein Profiles from 30mg/kg/day GSK2606414-treated and control Apoe$^{-/-}$ mice.....111

Figure 4.14. The impact of PERK kinase inhibitior on atherosclerosis progression.....112

Figure 4.15. Experimental Design for Monospecific Inhibition of ASKA mutant in vivo during atherosclerosis development.....114

Figure 4.16. Bodyweight and glucose levels in 60mg/kg/day 1-NAPP1 injected Apoe$^{-/-}$ (control) vs ASKA-Apoe$^{-/-}$ mice *in vivo*.....115

Figure 4.17. 1-NAPP1 does not effect atherosclerosis in control Apoe$^{-/-}$ mice.....117

Figure 4.18. 1-NAPP1 administration to ASKA-Apoe$^{-/-}$ mice reduced atherosclerosis development.....118

Figure 4.19 PERK kinase activity is critical for hyperlipidemia-induced eIF2α-LONP1 signaling in vivo.....120

Figure 4.20. Inhibition of PERK kinase activity reduces hyperlipidemia-induced macrophage infiltration in plaques.....121

Figure 4.21. Inhibition of PERK kinase activity reduces hyperlipidemia-induced inflammasome activation in mice.....123

Figure 4.22. Inhibition of PERK kinase activity reduces hyperlipidemia-induced serum and plaque cytokine levels in mice.....124

Figure 4.23. Selective inhibition of PERK kinase activity with 60 mg/kg/day 1-NAPP1 does not affect blood lipid measurements in ASKA-Apoe$^{-/-}$ mice on western diet.....125

Figure 5.1. Experimental design and the efficacy of ISRIB administration *in vivo*.....128

Figure 5.2. Analysis of metabolic parameters in ISRIB-treated Apoe$^{-/-}$ mice.....129

Figure 5.3. Blocking ISR by ISRIB alleviates atherosclerosis in Apoe$^{-/-}$ mice.....130

Figure 5.4. ISRIB supresses LONP1 expression in *Apoe*$^{-/-}$ aortic root sections.....131

Figure 5.5. ISRIB supresses hyperlipidemia-induced inflammation in *Apoe*$^{-/-}$ mice.....132

Figure 5.6. ISRIB supresses hyperlipidemia-induced IL-1β and cleaved caspase-1 levels in vivo.....134

Figure 5.7. ISRIB administration reduces serum and plaque cytokine levels in Apoe$^{-/-}$ mice.....135

Figure 5.8. Blockade of ISR with ISRIB does not alter circulating immune cells counts.....136

Figure 5.9. ISRIB administration does not affect systemic lipid measurements.....137

Figure 5.10. ISRIB Prevents Atherosclerosis Progression.....138

Figure 5.11. Experimental design and metabolic characteristics of ISRIB administration in vivo.....139

Figure 5.12. Blocking ISR by higher dose of ISRIB alleviates atherosclerosis.....140

Figure 6.1. Lipid-induced ISR tegulates mitochondrial clearance, mitochondrial oxidative stress and subsequent inflammasome activation.....146

List of Tables

Table 2.1. Chemicals and reagents that are used in laboratory generally.....57

Table 2.2. Reagents, chemicals and kits used in cell culture.....59

Table 2.3. Antibodies used in all procedures.....60

Table 2.4. Study specific Reagents, chemicals and kits.....61

Table 2.5. Solutions used in this study.....62

Table 2.6. q-RT PCR Primers used in the study.....69

Abbreviations

Abbreviation	Explanation
1-NAPP1	1-(1,1-Dimethylethyl)-3-(1-Naphthalenyl)-1H-Pyrazolo [3,4-D] Pyrimidin-4-Amine
Ab	Antibody
Ag	Antigen
AIM	Absent in Melanoma-2 Receptors
APC	Allophycocyanin
ASC	Apoptosis Associated Speck-Like Protein Containing a CARD
ATF	Activating Transcription Factor
ATP	Adenosine Triphosphate
BMDM	Bone Marrow-Derived Macrophages
CARD	Caspase Recruitment Domains
CDDO	2-Cyano-3,12-Dioxo-Oleana-1,9(11)-Dien-28-oic Acid Methyl Ester
CHOP	CCAAT-Enhancer-Binding Protein Homologous Protein
DAMPs	Danger-Associated Molecular Patterns
DAPI	4',6-Diamidino-2-Phenylindole
DNA	Deoxyribonucleic Acid
ECL	Enhanced Chemiluminescence
EDTA	Ethylenediaminetetraacetic Acid
eIF2α	Eukaryotic Initiation Factor 2
ELISA	The Enzyme-Linked Immunosorbent Assay
ER	Endoplasmic Reticulum
ERAD	ER Associated Degradation
FACS	Fluorescence-Activated Cell Sorting
FBS	Fetal Bovine Serum
FDA	Food and Drug Administration
GADD34	Growth Arrest and DNA Damage 34
GAPDH	Glyceraldehyde-3-Phosphate Dehydrogenase

Abbreviation	Explanation
GSK 2606414	7-Methyl-5-(1-{[3-(Trifluoromethyl) Phenyl] Acetyl}-2,3-Dihydro-1H-Indol-5-Yl)-7H-Pyrrolo[2,3-D] Pyrimidin-4-Amine
HEPES	4-(2-Hydroxyethyl)-1-Piperazineethanesulfonic Acid
IFN	Interferon
IRE1	Inositol-Requiring Enzyme-1
ISR	Integrated Signal Response
ISRIB	N,N'-Trans-1,4-Cyclohexanediylbis [2-(4-Chlorophenoxy) Acetamide]
IκB	Inhibitor of NF-Kb
i.p.	Intraperitonel
KLF	Kruppel-Like Factor
LDL	Low Density Lipoprotein
LP	Lipoprotein
LPS	Lipopolysaccharide
MAM	Mitochondria Associated Membranes
MAPK	Mitogen-Activated Protein Kinase
MDP	Muramyl Dipeptidemitochondrial Antiviral Signaling Protein
MHC	Major Histocompatibility Complex
MOMA	Monocyte/Macrophage Marker Antibody
MSU	Uric Acid Crystals
NK	Naturel Killer
NLR	Nucleotide Binding And Oligomerization Domain (NOD)-Like Receptors
PAMP	Pathogen-Associated Molecular Patterns
PBS	Phosphate Buffer Saline
PDGF	Platelet-Derived Growth Factor
PERK	Protein Kinase RNA-Like ER Kinase
PMSF	Phenyl-methane Sulfonyl Fluoride
PRRs	Pattern Recognition Receptors
RNA	Ribonucleic Acid
RT-PCR	Reverse Transcriptase PCR

Abbreviation	Explanation
siRNA	Small Interfering RNA
SMC	Smooth Muscle Cell
STAT	Signal Transducer And Activator of Transcription
TBS	Tris-Buffered Saline
Th	Helper T Cell
TLR	Toll-Like Receptor
TNF	Tumor Necrosis Factor
TRAF	TNF Receptor Associated Factor
Treg	Regulatory T Cells
TUDCA	Tauroursodeoxycholic Acid
TUNEL	Terminal Deoxynucleotidyl Transferase dUTP Nick End Labeling
TXNIP	Thioredoxin Interacting Protein
UPR	Unfolded Protein Response
UPRE	Unfolded Protein Response Element
XBP1	X-Box Binding Protein 1

CHAPTER 1.

Introduction

1.1 The Endoplasmic Reticulum

Endoplasmic Reticulum (ER) is an organelle that is surrounded by a single, continuous membrane. ER membranes spread from the nucleus forming a network of membranes that reaches the plasma membrane. ER is also quite a dynamic organelle with branching tubules (1,2). ER can be subdivided into compartments according to specific functions. Those ER parts that associate with ribosomes during protein synthesis are known as 'rough', whereas the other non-ribosome associated parts are known as the 'smooth' ER. The ER plays a critical role in modification and folding of secreted and transmembrane protein, which relocate to the Golgi and to the plasma membrane. ER also makes membrane synapses/contacts with organelles such as the mitochondria. The contact sites between the ER and mitochondria are known as the Mitochondria Associated Membranes (MAMs). MAMs are known to have critical roles in metabolism as well as in initiating inflammatory responses (1,3). The functions of all the ER proteins are not known as the identity of ER proteins in the inter-organelle contact sites. The recent proteomic science advances and their application to discovering ER proteins and inter-organelle contact site proteins will generate a better understanding about this organelle and its functions and collaboration with other organelles in the cell (1).

1.1.1 Endoplasmic Reticulum Function

ER is a very important organelle in regulation of intracellular calcium levels as it is the major storage site for cellular calcium, from which controlled calcium release can occur in certain circumstances. Another major role of ER is in protein folding, modification and eradication of mis-folded proteins. Lastly, ER is important metabolic organelle with a major role in the synthesis of major lipid species.

Proper Protein Synthesis, Folding and Maturation

ER plays a critical role in folding of secreted and transmembrane proteins. Rough ER membranes harbor ribosomes that translate these proteins, but these ribosomes are transiently associated with ER membranes and they can be released into the cytosol post-translation. The growing polypeptide chains are transferred from these ribosomes into the ER lumen through membrane-spanning channels. The nascent proteins are folded properly in the ER lumen and and transferred back to ER membrane to be shipped to its target destinations such as plasma membrane, ER and other organelle membranes or to the Golgi, if the protein is to be secreted outside of the cell. ER is not only the place for proper protein folding but also for modifications such as oligomerization of proteins, disulfide bond formation and N-glycosylation, which are required for reaching the protein's target destination or for function (2,4). If any of these processes go wrong, ER has its own mechanism to destroy these undesired forms of proteins called as ERAD (5).

Endoplasmic Reticulum - Associated Degradation (ERAD)

ERAD is a quality check pathway that prevents the accumulation of unwanted improper folded or immature proteins in ER lumen. Misfolded proteins in ER lumen are transferred back to cytosol, where ERAD acts. Any modifications on these proteins are removed before translocating to the cytosol and they are ubiquitinylated and tagged for proteasomal degradation.

Calcium (Ca^{2+}) Metabolism

ER is a central player in cellular calcium homeostasis (6). As ER is the main calcium storage compartment of the cell, there is a huge difference between calcium

concentration between the ER, cytosol and extracellular compartments (~ 100μM, 100nM, 2nM, respectively) (7).

Calcium is a secondary messenger that regulate a multitude of cellular processes. Calcium is important for re-shaping the ER after neurotransmitter release or after a muscle contraction. Calcium also important for protein function, protein-protein, protein – nucleic acid, protein-organelle interactions (2,8). Another important impact of calcium is on cellular metabolism and homeostasis. For example, increased in calcium transfer into the mitochondria can regulate alter mitochondrial metabolism, membrane permeability, and ATP production. In turn mitochondria calcium concentration can determine cell death or survival (9-11).

As a calcium storing organelle, ER harbors many calcium channels (Sarcoplasmic Reticulum Ca^{2+} ATPase (SERCA) pump), inositol 1,4,5-triphosphate receptors (IP3R), and ryanodine receptors on its membranes that it uses for import and export of calcium based on the cellular need (2,7). Mitochondria also has calcium channels on its outer and inner membranes such as the Voltage Dependent Anion Channel (VDAC) family of calcium transporters and the mitochondrial Ca^{2+} uniporter (MCU), respectively (12).

Membrane Lipid Biogenesis

ER is also an important organelle involved in lipid biogenesis. Two key-players of cell membranes, phospholipids and cholesterol, are both synthesized on ER. Together with Golgi and mitochondria, ER forms an endomembrane compartment that is responsible for lipid synthesis. Lipids synthesized on the ER are transported from ER membrane to these organelles, where further modifications take place (3).

To initiate the synthesis of lipid-bilayer cell membrane, two fatty acids are added to glycerol phosphate backbone (providing the diacylglycerol phosphate (DGP) precursor for phospholipids) on the cytosolic side of the ER membrane. Phosphatidylcholine (PC), the most abundant glycerophospholipid is synthesized in the ER and Golgi (3)..ER-mitochondria contact sites are also important locations where phospholipid biosynthesis enzymes such as phosphatidylserine decarboxylases are abundant. Mainly phosphatidylserine (PS) is transported to ER-mitochondria contact sites and PS is converted to phosphatidylethanolamine (PE) and

Phosphatidylcholine (PC) (13,14).

As ER is responsible for the lipid synthesis, it is also responsible for the regulation of genes that are required for lipid synthesis. ER exerts its effects by the Sterol Regulatory Element Binding Protein (SREBP) family of transcription factors that are normally found on the ER but in an inactive state. On the course of lipid synthesis, SREBP is first translocated to Golgi and then to nucleus to initiate transcription of the genes for lipid synthesis and uptake. These transcription factors a re-located to and modified in the Golgi because of their lipid-sensing capabilities. Then they move to the nucleus to play their role in initiating lipid synthesis and maturation (15-17).

1.1.2. The Endoplasmic Reticulum Stress and Unfolded Protein Response

Due to its role in protein folding and maturation of transmembrane and secretory proteins, ER has a tremendous amount of work-load. Unfolded or immature proteins are first transported to ER lumen through its membrane and folding and modifications by the help of chaperons, foldases and cofactors take place in the ER lumen (4). However, a portion of the proteins are not properly folded in the ER. ER has intrinsic mechanisms that sense the unfolded proteins and initiate the ERAD response that can eliminate these unwanted or potentially harmful proteins (18,19).

There are conditions that can cause ER dysfunction. Cells often endure metabolic changes that occur due to changing physiological or environmental conditions. These include decreased ATP levels, viral infections, oxidative stress, genetic abnormalities or increased amount of protein synthesis. Also in certain metabolic conditions that cause excess influx of cholesterol or fatty acids (such as in obesity and dyslipidemia) can also disrupt ER functions. The disturbance in ER functions is perceived as ER stress and initiates an elaborate stress signaling pathway that aims to cope with this (19,20). This signaling is known as the unfolded protein response (UPR) (21,22). UPR signaling is initiated by three ER resident transmembrane stress sensor proteins leading to transcriptional and translational changes in the cell. These are inositol-requiring-enzyme-1 (IRE1), protein kinase RNA (PKR) like ER kinase (PERK) and the activating transcription factor 6 (ATF6) (Figure 1.1). Misfolded proteins are sensed through protein-protein interactions with the stress sensors. These sensors normally

bind Binding-immunoglobulin protein / Glucose Regulated Protein 78 (Bip/Grp78) chaperone within the ER lumen. Upon ER stress, Bip dissociates from the sensors to associate with the misfolded proteins, initiating the UPR cascade. If ER stress is prolonged and the re-association of chaperone with stress sensors is delayed, then ER can adopt two measures: First ER can activate a survival response that involves transcriptional and translational mechanisms to induce the production of ER chaperon proteins to reduce misfolded proteins and re-gain ER homeostasis. However, if ER cannot re-establish cellular homeostasis by this measure, then the same stressor proteins engage apoptotic cascades to eliminate the stressed cell (21,23,24).

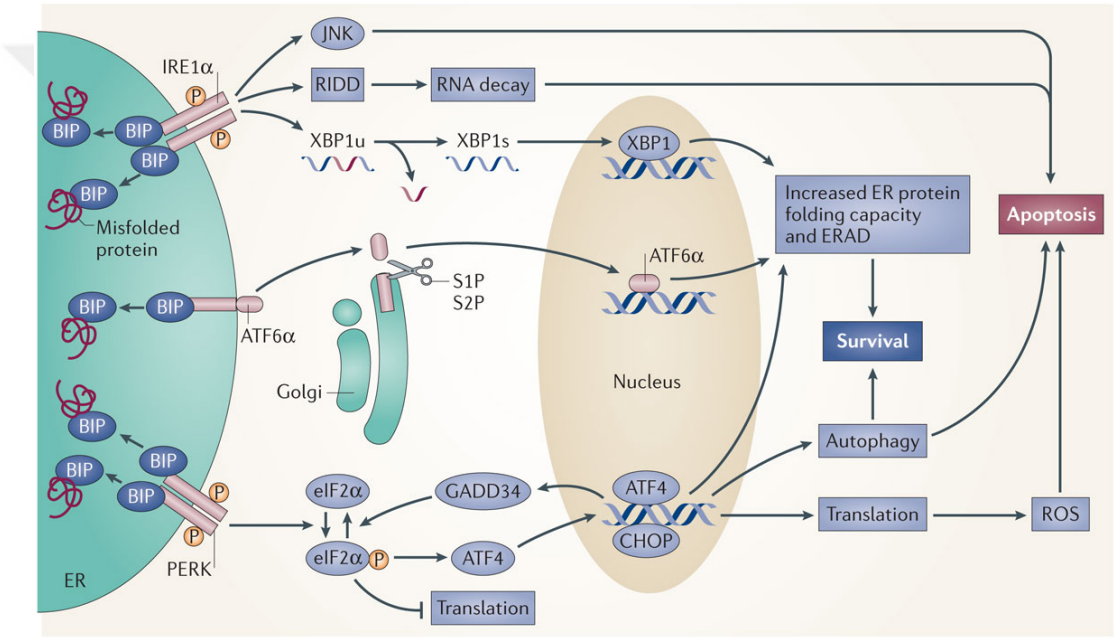

Figure 1.1 Endoplasmic Reticulum Stress and Unfolded Protein Response

1.2. Unfolded Protein Response Signaling

Unfolded protein response is directed by three ER transmembrane proteins, IRE1, PERK and ATF6.

1.2.1. IRE1

IRE1 is the first UPR kinase that was identified in yeast ER membranes and is conserved across the species. In mammals, however, there are two IRE1 homologs, namely IRE1α and IRE1β. The expression of IRE1β is limited only to respiratory and gastrointestinal tract, but IRE1α is ubiquitously expressed.

IRE1 is composed of three domains: luminal, transmembrane and cytosolic domains. The cytosolic domain harbors two enzymatic activities, namely kinase and endoribonuclease (RNase) activities. The domain that senses misfolded or unfolded proteins is the luminal domain of IRE1. Upon sensing, IRE1 oligomerizes and auto-phosphorylates. The RNase domain activation requires autophosphorylation. The RNase domain can initiate either death or survival pathways according to the nature and the duration of ER stress. The classically known IRE1 RNase domain substrate is X-box protein 1 (XBP1) messenger RNA(mRNA)(25). When IRE1 is activated, it splices XBP1 mRNA leading to deletion of a 26-base portion of an intron and frameshift. Spliced XBP1 (sXBP1) mRNA produces a larger protein, which is an active transcription factor. sXBP1 protein can activate transcription of genes such as chaperons or components of ERAD pathway to relieve ER stress (26,27). IRE1 was recently shown to also degrade mRNAs that associates with the ribosomes for translation. This leads to decrease in the protein load in the ER and is known as the IRE0dependent decay (RIDD) pathway (35,36).

1.2.2. PERK

PERK is another major transmembrane ER stress sensor protein. It is normally found on ER membrane as a monomer and bound to Bip/Grp78. PERK has three domains: The luminal domain mediates stress sensing and is the binding place for Bip/Grp78. There is a transmembrane domain that anchors PERK into ER membranes and PERK's cytosolic domain harbors kinase activity (28). Under ER stress conditions, when Bip/Grp78 dissociates in order to bind misfolded proteins, the PERK monomers can oligomerize. And auto-phosphorylate itself at threonine-980. After this phosphorylation, the active PERK kinase can phosphorylate its substrate, eukaryotic initiation factor 2 α (eIF2α) on serine 52. Phosphorylation of eIF2α, leads to global translation attenuation via inhibiting cap dependent translation. An exception to this rule is a select group of genes that can be translated through upstream alternative open reading frame (ORF). The activating transcription factor-4 (ATF4) is one of the proteins made during PERK-induced translational attenuation and is an important transcription factor that activates the transcription of homeostatic genes involved in metabolism, oxidative stress, amino-acid import and synthesis, autophagy and survival. The outcome of PERK-ATF4 signaling can be different depending on the

degree of ER stress the duration of the ER stress (28-30). In early stages of stress, PERK-ATF4 signaling acts as a cytoprotective mechanism through inducing the Heme oxidase-1 (HO-1) antioxidant response. This occurs by the induction of activating transcription factor 5 (ATF5), autophagy related 7 (ATG7) and Unc-51 like serine threonine kinase-1 (ULK1). Another protein that plays important role in antioxidant response through PERK signaling is nuclear factor erythroid 2- related factor-2 (Nrf2) in conjunction with kelch like ECH – associated protein 1 (Keap1). Nrf2 is also shown to cross-talk with nuclear factor κ B (NFκB); in the absence of Nrf2, NFκB is inhibited. PERK directly interacts with Nrf2 to exert antioxidant effects (31). However, if ER stress cannot be resolved, then PERK–ATF4 signaling pathway induces C/EBP-homologous protein (CHOP), which inhibits B-cell leukemia 2 (BCL-2) family proteins and induce BH3-only proteins, leading to apoptosis. eIF2α phosphorylation is temporary and it is dephosphorylated sometime after ER stress initiation by protein phosphatase-1 regulatory subunit015A (PP1R15A) or growth arrest and DNA damage-34 (GADD34), which is transcriptionally induced by CHOP. Therefore, the role of eIF2α dephosphorylation is re-instating ER homeostasis by re-activating the attenuated protein translation (32).

PERK has been shown to be activate the NFκB inflammatory pathway. PERK exert its effects on this pathway through a translational regulation mechanism, in which phosphorylation of eIF2α blocks translation of the inhibitory protein κB (IκB), in turn releasing NFκB transcription factor which goes to nucleus to activate pro-inflammatory genes (33).

In summary, PERK is a multifunctional kinase that can impact a multitude of cellular responses including inflammation, antioxidant effects, protein synthesis, autophagy, apoptosis and thereby, can contribute to cellular homeostasis and determine cell fate.

1.2.3. ATF6

ATF6 is the third transmembrane ER stress sensor that acts as a transcription factor when activated. ATF6 is a multi-domain protein consisting of a luminal domain, which binds to Bip/Grp78 to sense misfolded proteins. It also has a cytosolic domain, which has a bZIP motif (a DNA binding motif), and transmembrane domain, which contains

Golgi translocation signal to target Golgi for proteolytic cleavage (34,35). Activation of ATF6 takes place in the Golgi. After ER stress, ATF6 protein is transported to Golgi by ER –budded vesicles that contain the coat protein complex II (COPII) protein aiding in the translocation to Golgi. When ATF6 is transferred to Golgi, it undergoes two proteolytic cleavages by the membrane-bound transcription factor site-1 and site-2 proteases (S1P and S2P). S1P cleaves the luminal domain and S2P cleaves the transmembrane domain, leaving the active cytosolic domain (ATF6-N) that contains bZIP motif. ATF6-N is transported from golgi to nucleus to act as a transcription factor for UPR target genes (36-38). These target genes are important for proper protein synthesis, increasing ER protein folding capacities (chaperons) and decreasing protein-folding load of ER (via ERAD) to activate pro-survival mechanisms (39-42).

1.3. Integrated Stress Response

Integrated stress response (ISR) is a multiplex stress signal pathway that is activated in response to both physiological/metabolic demand and in pathological conditions(43-47). The main activators of ISR pathway include heme deprivation, amino acid deprivation, ER stress and viral infections (44,46-50). According to the type of the activator the proximal stress sensing protein (or eiF2α kinase) changes (51). For example, ER stress is sensed via PERK while heme deprivation is sensed via Heme-regulated eIF2α kinase (HRI). On the other hand, viral infections are sensed via the Double-stranded RNA-dependent proteins kinase (PKR) and amino acid deprivation is sensed via the General control non-derepressible-2 (GCN2) kinase (as shown in Figure 1.2) (52). The common and central player in the ISR is eIF2α. All 4 kinases mentioned can phosphorylate eIF2α on serine 51 to initiate the ISR pathway (43). As explained in the previous sections, phosphorylation of eIF2α causes global protein translation block and permits the translation of only select proteins such as ATF4, which favors survival and cellular homeostasis to be re-established (53). However, in severe or prolonged stress conditions ATF4 can switch to a pro-apoptotic gene activation program. As a result, phosphorylation of eIF2α and activation of ATF4 can have opposing effects on the cell depending on the duration of stress response (54-56).

GCN2 is a highly conserved kinase (57). Binding of GCN2 to de-acetylated transfer

RNAs (tRNA) initiates the ISR pathway in the absence of amino acids (58). It is also shown that glucose deprivation causes GCN2 activation (49). The reason for this may be the higher consumptions of amino-acids due to the absence of glucose to supply the energy needs of cells) (49).

PKR is activated by binding to double stranded RNA (dsRNA), which typically originates from the infecting virus. PKR auto-phosphorylates upon binding dsRNA on threonine 446, and this phosphorylation results in the activation of PKR and eIF2α phosphorylation by PKR(59-63). Consequently, PKR activation leads to the inhibition of viral protein synthesis along with a global translation attenuation (59,64,65). Also, PKR was shown to be activated by other stress conditions such as ER stress, oxidative stress or bacterial infections, but these mechanisms of activation are not clear (66-69).

HRI is abundant in erythroid cells (70). HRI activation also happens by dimerization and auto-phosphorylation but upon heme deprivation (71,72). Normally heme bound to HRI and keeps the monomers in an inactive form, inhibiting its kinase activity (70,73). Upon heme deprivation, HRI actively dimerizes and initiates the ISR by phosphorylating eIF2α (70).

PERK is resident on the ER and senses the accumulation of unfolded or misfolded proteins (74,75). PERK also senses oxidative stress, energy, calcium levels, but how this happens is not clear (44). PERK can also be activated during glucose deprivation, whereas ATP deprivation leads to dysregulated ER calcium ATPase pump (76,77).

eIF2α is the central player in ISR and also the major component of eIF2 complex, which consists of eIF2β and eIF2γ in addition to eIF2α. eIF2 recognizes the translation start site (AUG codon) and binds to mRNA to initiate translation(78,79). eIF2 is part of the pre-initiation complex (PIC) for RNA translation(80,81). eIF2 is complexed with GTP when bound to mRNA in the PIC, but dissociates during translation initiation upon the hydrolysis of eIF2 bound GTP to GDP. The GDP-GTP exchange is executed by eIF2B. However, the activation of ISR and consequent phosphorylation of eIF2α inhibits the eIF2B regulated GDP-GTP exchange and this mechanism prevents 5' cap dependent translation(78-82). There are a select group of proteins that are preferentially translated via alternative upstream-ORFs (uORF) and include ATF4,

ATF5, CHOP and Growth arrest DNA-inducible protein (GADD34 or PPPR15A) (82-84). ATF4, ATF5, and CHOP are regulatory proteins for cellular homeostasis and GADD34 de-phosphorylates eIF2α. Constitutive repressor of eIF2α phosphorylation (CreP)(PPPR15B) on the other hand is constitutively expressed and bound to GADD34, leading to continuous removal of the phosphate groups on eIF2α(85,86). However, GADD34 is not normally translated but induced as a consequence of ISR and downstream of ATF4. De-phosphorylation of eIF2α is crucial for survival, which requires re-activates the translation (87,88).

ATF4 is a central transcription factor in the ISR and is controlled by transcriptional, translational and post-translational manners during ISR (44). ATF4 is a basic leucine zipper domain (bZIP) type of transcription factor and can dimerize with a variety of partners for differential gene regulation by binding CCAAT-enhancer binding proteins / Activating Transcription factor (C-EBP/ATF) response elements (44,89-92). ATF4 can also form homo or hetero dimers with other DNA binding proteins such as CHOP. This formed hetero-dimer has been shown to activate the transcription of genes including ATF3, ATF5, PPP1R15A (89,93,94). The interaction partner determines how ATF4 will alter the cellular fate (such as survival vs death). There is little ATF4 present in non-stress conditions. It has two ORFs upstream of coding sequence. Normally ribosomes initiate translation of ATF4 through uORF 2, which overlaps with the coding sequence and this prevents the translation of ATF4 mRNA(95) . However, under stress conditions, translation is initiated from uORF1, from which bound ribosomes can detect the start codon in coding sequence (CDS) region of ATF4 (89,95,96). ATF4 is also regulated transcriptionally by factors such as NRF2 that induces ATF4 transcription during oxidative or ER stress(97). Another regulation of ATF4 is post- translational stability. It has a very short half-life - less than 1 hour (98,99). Post-translational modification of ATF4 mainly includes phosphorylation and ubiquitination. ATF4 is phosphorylated on four sites: Serine 219 and serine 224 phosphorylation both cause its proteasomal degradation(98). Serine 245 phosphorylation by ribosomal protein S6 (RPS6K) or serine 254 by protein kinase A (PKA) both induce the activity and stability of ATF4 (100,101).

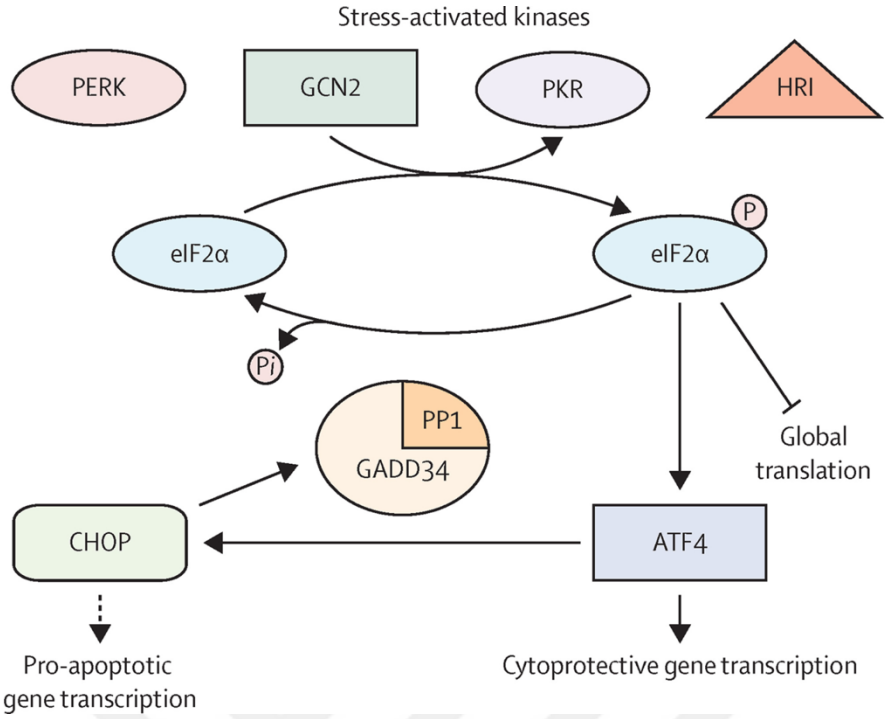

Figure 1.2 Schematic Representation of ISR

In conclusion, ISR is a very important and complex signaling response that controls global translation and cell death pathways in response to diverse stress stimuli. It is mainly cell protective and seeks to regain cellular homeostasis, however, this pathway can switch the balance from survival to cell death depending on the nature and duration of stress.

1.4. Endoplasmic Reticulum Stress and Immune Response

Unfolded protein response is a critical homeostatic pathway in mammals, however, not all of the stress sensors proteins are conserved across the species. The most conserved and ancient protein in the UPR is IRE1, found in all eukaryotic species from yeast to mammals. However, other UPR sensors, PERK and ATF6, are not found in yeast (102,103). In plants, PERK is expressed, however only IRE1 and ATF6 participate in plant UPR activation. As in mammals, UPR in plants try to controls the protein load, however plants experience different stresses such as heat shock (103). Plant IRE1 is active in abiotic conditions and has a role in antibacterial host defense by increasing selective translation of foldases that aid in the maturation of plant host defense proteins (104,105)

Caenorhabditis elegans is an organism where UPR complexity increases. Here, all three branches of UPR are active (106). The mode of action of proteins are much more similar to mammals. All three arms work for preventing protein load, however, only IRE1 arm causes selective activation of host defense proteins in this organism (106,107).

In mammals, UPR is initially aims to re-instate homeostasis, but it can also engage inflammatory pathways in addition to pro-apoptotic pathways depending on the nature of the stress. Mammalian UPR is also activated with increased amounts of lipids and glucose and plays a role in metabolic stress conditions (108,109). UPR is also activated by pro-inflammatory cytokines (109,110).

Reactive oxygen species (ROS) is an agent that induces inflammation and inflammasome activation in macrophages. ER stress can increase ROS production from both the ER and the mitochondria during metabolic stress conditions (111,112). ER stress leads to Ca^{2+} transport from the ER to mitochondria via the MAMs (113,114). This transfer couples ER and mitochondria by potentiating ROS production.

ER stress and UPR is activated via metabolic stress such as in dyslipidemia and obesity. Also, increased inflammation in these metabolic conditions augments UPR activation. UPR activation in return disrupts metabolism and aggravates the inflammatory response, causing a feed-forward, chronic inflammatory process that underlies metabolic disease progression in obesity, atherosclerosis and diabetes (Figure 1.3) (110,115-118).

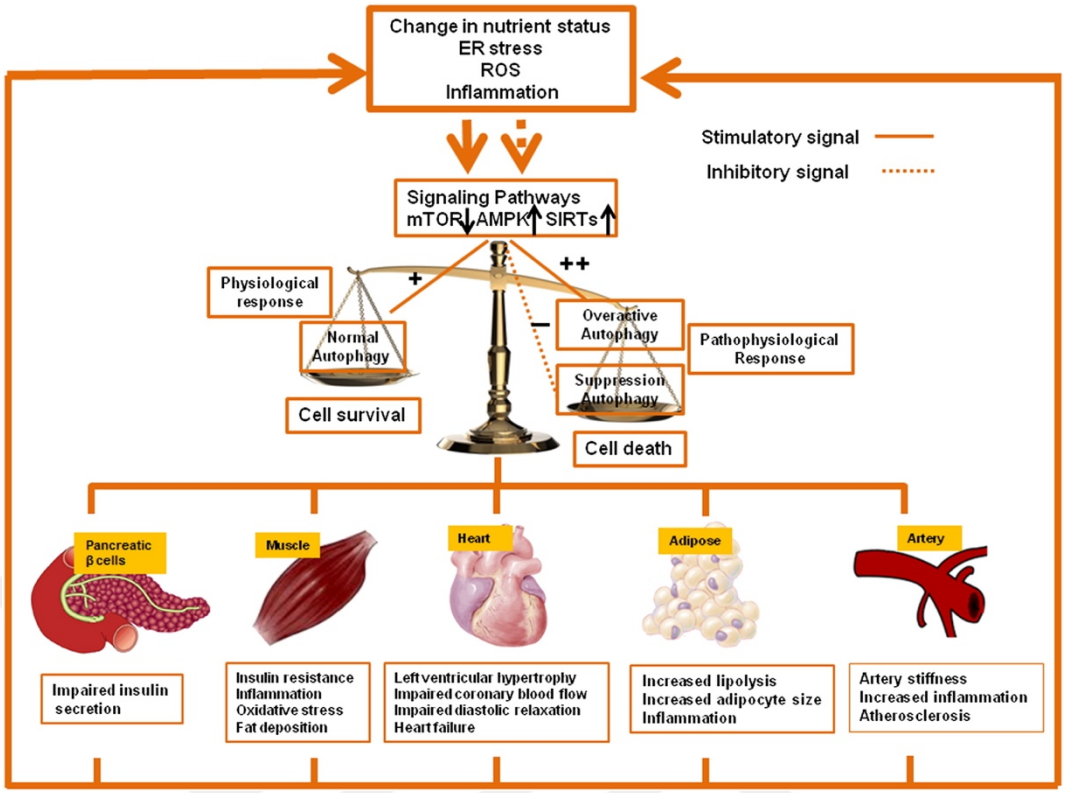

Figure 1.3 ER Stress, Inflammation and Metabolic Disease

1.4.1. UPR Connection to Inflammatory Pathways

The UPR can engage Toll like receptor (TLR) signaling as well as the NFκB pathway shown in Figure 1.4 (119-121). Nuclear Factor Kappa B(NFκB) pathway is one of the major inflammatory pathways and all three branches of UPR activates NFκB pathway in response to ER stress to induce inflammation (122,123). NFκB is a transcription factor that is normally found in cytosol bound to its inhibitor, IκB, in an inactive state. The activation of NFκB requires first the phosphorylation of IκB by the IκB kinase (IKK) and dissociation of IκB from NFκB, allowing the free NFκB to translocate into the nucleus and initiate pro-inflammatory gene transcription (124). All three branches of UPR can activate inflammation through NFκB pathway, however by different mechanisms. Auto-phosphorylated IRE1α activates NFκB indirectly by recruiting TNF receptor-associated factor 2 (TRAF2) to itself. TRAF2 then recruits IκB kinase (IKK) and mediates the phosphorylation of IκB, in turn releasing NFκB to translocate into the nucleus for pro-inflammatory cytokine genes' transcriptional activation (119). IRE1 can also activate NFκB pathway, via TRAF2-oligomerization domain

containing protein (NODs) to activate NFκB and induce cytokine production (125).

PERK, activates NFκB through translational inhibition of IκB. NFκB and IκB are constitutively translated proteins; NFκB enables cells to initiate sudden inflammatory responses while IκB prevents an undesired inflammatory response. The translation inhibition of IκB, during PERK activation, results in the accumulation of larger numbers of NFκB free to translocate into the nucleus for pro-inflammatory cytokine gene transcriptional activation (124,126).

ATF6 activates NFκB pathway in a different way than both IRE1 and PERK. ATF6 induces mTOR pathway and inhibits Akt. Akt in turn phosphorylates IKK to inhibit IκB and release NFκB for further pro-inflammatory cytokine release (127-129)

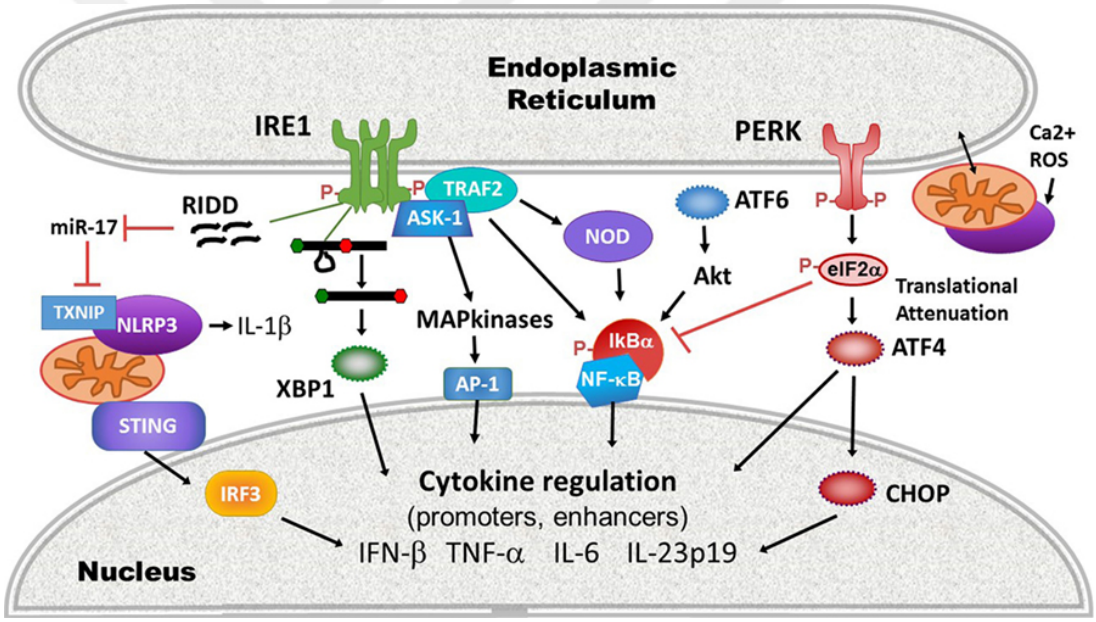

Figure 1.4 UPR Engages Inflammatory Pathways (130)

PERK and IRE1 initiates inflammatory pathways through additional other mechanisms. IRE1 and PERK can both upregulate Thioredoxin interacting protein (TXNIP), which induces inflammasome activation and inflammatory cytokine release. PERK induces TXNIP through a selectively translated transcription factor (during ER stress) known as the activating transcription factor 5 (ATF5). On the other hand, IRE1 induce TXNIP through regulated IRE1 dependent decay (RIDD) pathway(131). IRE endoribonuclease activity degrades pre-miR17 and inhibits the biogenesis of miR17,

which normally suppresses TXNIP expression (132). IRE1 can also activate immune response through the Mitogen Activated Protein kinase (MAP kinase)Jun N Terminal Kinase1(JNK1)- Activator Protein 1 (AP-1) pathway, which is activated by TRAF2 association with autophosphorylated IRE1 (133,134). Also, the RNase substrate of IRE1, sXBP1, can regulate cytokine transcription (such as TNFα, IL-6 and IFNβ) (135,136). PERK also activates inflammation through ATF4 and CHOP, which contribute to IFNβ, IL-6, IL-8 and IL-23 transcription (119,137). ATF4 can also bind to IL-6 promoter to activate gene expression (138). Also PERK interaction with nuclear fator erythroid 2-related factor 2 (Nrf2) causes TNFα production (139) (Figure 1.5).

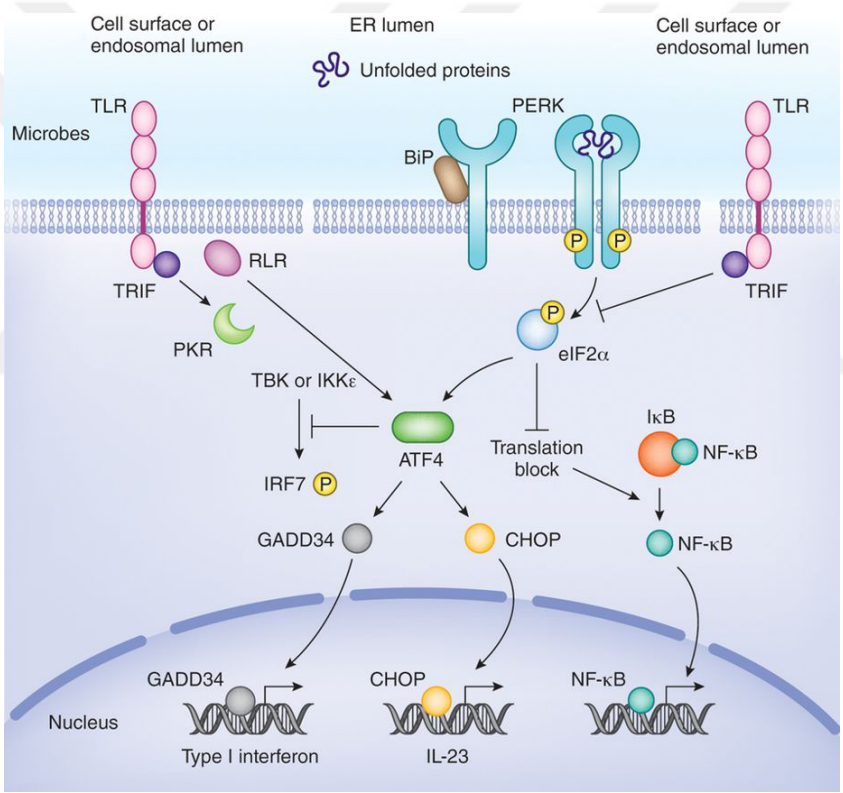

Figure 1.5 Relationship Between PERK Signaling Pathway and Inflammation

1.4.2. UPR Connection with Inflammasome Activation

Inflammasome

The pattern recognition receptors (PRR) are expressed in immune cells (such as macrophages, dendritic cells and neutrophils) as well as in epithelial cells and airway resident smooth muscle cells. These receptors bind to either damage associated

molecular patterns (DAMP) or pathogen associated molecular patterns (PAMP) and activate an innate immune response for clearance of damaged cells or pathogens. Extracellular ATP can serve as a DAMP that activates PRRs as does intracellular accumulation of reactive oxygen species (ROS), cholesterol crystals, uric acid crystals and intracellular release of the mitochondrial DNA. PAMPs include stimuli such as bacterial lipopolysaccharides (LPS), bacterial endotoxins, or pathogen associated RNA and DNA molecules. PRRs that recognize these PAMPs and DAMPs are many and differ in their function and structure. These PRRs are: Nucleotide binding and oligomerization domain (NOD) -like receptors (NLRs), absent in melanoma-2 receptors (AIMs) and pyrin. Upon recognizing the DAMPs and PAMPS, PRR leads to the assembly and activation of cytoplasmic inflammatory response complexes that are called 'inflammasomes' (140,141). NLR family of receptors can be subdivided into two according to the effector proteins. Nucleotide binding and oligomerization domain (NOD) -like receptors family of PRRs contains a pyrin domain (NLRP), whereas nucleotide binding and oligomerization domain (NOD) -like receptors family of PRRs contains a caspase activation and recruitment domain (CARD) (NLRC). NLR family of PRRs can activate the inflammasome complex by binding both PAMPs and DAMPs (140,141).

After assembly of inflammasome complex in the cytosol, pro-IL-1β and pro-IL-18 are subjected to proteolytic cleavage and maturation by the mature caspase-1(142). Mature IL-1β and IL-18 activate other inflammatory pathways and lead to pro-inflammatory cytokine release, recruitment of inflammatory cells, and T cell polarization (143). Best known NLRP and NLRC members of inflammasomes are NLRP1, NLRP3 and NLRC4, which are activated via different stimuli. For example NLRP1 inflammasome is mainly activated by direct biding of the bacterial muramyl dipeptide (MDP) or bacterial anthrax toxin (144). NLRC4 inflammasome on the other hand needs an adaptor, the apoptosis inhibitory protein (NAIP), to sense and bind ligands such as bacterial flagellin (145,146). As opposed to NLRP1 and NLRC4, NLRP3 inflammasome has multiple activators that are DAMPS (such as cholesterol crystals, ATP, ROS, uric acid crystals, PAMPs (such as peptidoglycans, bacteria and virus originated nucleic acids, bacterial, fungal and viral toxins) as well as environmental effectors (such as aluminum crystals, asbestos and silica) (147).

Inflammasome activation is also detected in a variety of metabolic diseases such as the fatty liver disease, obesity, and diabetes, in which metabolites such as free cholesterol and fatty acids have been shown to activate NLRP3 (148).

The last member of inflammasome family, AIM2 inflammasome, also binds to caspase-1 through the apoptosis-associated speck-like (ASC) Pyrin Domain Containing-Caspase activation and recruitment domain (PYD-CARD) domain. Upon caspase-1 maturation and activation as in the other inflammasome complexes, cleavage and maturation of pro-IL-1βand IL-18 occurs. AIM2 however, is activated via different stimuli such as cytoplasmic nucleic acids that can bind its hematopoietic interferon-inducible nuclear antigens with 200 amino acid repeats (HIN200) domain (149).

Among all the inflammasomes NLRP3 is the one that is most studied in literature. NLRP3 inflammasome activation in cell culture for experimental purposes requires two signals. First signal is needed for the activation of NFκB pathway and for transcriptional upregulation of pro-IL-1β and pro-IL-18. This first signal is called priming step. The most frequently used PAMPs for this purpose is lipopolysaccharide (LPS), which is a bacterial cell wall component that binds to TLR4 receptors to activate NFκB signaling pathway. The activation of NFκB pathway is also the trigger for NLRP3 inflammasome assembly on mitochondria-ER associated membranes (MAMs)(141,150,151). Second signal comes from the DAMPs such as extracellular ATP, cholesterol crystals, monosodium urate crystals (MSU) or increased levels of ROS. The second signal leads to translocation of the assembled NLRP3 inflammasome complex to the cytosol, which results in the activation of caspase-1 and cleavage and maturation of pro-IL-1β and pro-IL-18 (151,152).

ER stress, UPR and Inflammasome

Thioredoxin – interacting protein (TXNIP) has been recently shown to be induced by ER stress and UPR activation. TXNIP is a protein regulated by glucose metabolism and its expression is shown to be increased in diabetes. In literature, TXNIP was shown to induce NLRP3 inflammasome activation (131,132,153). Based on these publications, TXNIP induction occurs after prolonged ER stress and is one of the

molecular links that connects UPR signaling to inflammasome activation. IRE1α induces TXNIP through by cleaving and degrading pre-miR17, which is an inhibitor of TXNIP expression. By depleting miR17, IRE1 induces TXNIP expression during prolonged ER stress. As TXNIP causes inflammasome activation under ER stress, it is a link that connects IRE1 to inflammasome activation (132). In addition to this mechanism, IRE1α can directly induce NLRP3 inflammasome components transcription and activation under lipid induced ER stress in macrophages without altering TXNIP levels (154).

PERK also induces TXNIP under ER stress via promoting selective translation of ATF5, which binds to TXNIP promoter region to activate TXNIP's transcription, providing a link between PERK and inflammasome activation (131). Another study revealed that NLRP1 inflammasome can be induced through ATF4, which is also downstream to PERK (155). On the other hand, another study described PERK is dispensable for inflammasome activation(156,157). While these contradictory findings exist, it is also not well understood how metabolic stress and in particular, saturated fatty acid-induced stress, is mediated to the inflammasome through UPR activation.

1.5. Endoplasmic Reticulum and Mitochondria

Mitochondria

Mitochondria are essential organelles in cells with important roles in maintaining cellular homeostasis not only by being a cellular energy power house but also as an organelle that is involved in regulating cellular metabolism and immune responses (158). These vital functions are conducted on mitochondria's membrane and inter-membrane spaces. Mitochondria are comprised of outer membrane, intermembrane space, inner membrane and the mitochondrial matrix. Citric acid cycle takes place in mitochondrial matrix whereas oxidative phosphorylation is carried out on the inner mitochondrial membrane (159). Mitochondria also has its own DNA, which encodes, together with the nuclear DNA, a total of 13 mitochondrial proteins (160).

As mitochondria is the place for respiration and subsequent oxidative phosphorylation, reactive oxygen species (ROS) and other radicals such as hydrogen peroxide (H_2O_2)

and superoxide radicals (O^-) are produced. These radicals are purged with the help of scavengers in healthy mitochondria, however, if mitochondrial dysfunction and resulting membrane potential loss occurs, these free radicals and ROS are released from mitochondria, leading to cellular oxidative stress. This oxidative stress can cause or potentiate stress in the neighboring ER s(111,112). The release of ROS through dysfunctional mitochondria as well as release of the mitochondrial DNA (mtDNA) from the disrupted mitochondrial membranes can also lead to inflammasome activation and further stress for the cell (161-163).

The Relationship of ER and Mitochondria

ER and mitochondria are similar as they are both dynamic organelles, which can modify their structures and their functions in response to changing environmental conditions and signals. ER and mitochondria are connected functionally through calcium and lipid metabolism and physically through ER-mitochondria membrane contact sites (MAMs) (13,164). Some of the MAM proteins identified include ion channels and calcium transporters (such as voltage dependent anion channels (VDAC), inositol 1,4,5-triphosphate receptors (IP3Rs) and Ca^{2+} ATPases), mitochondrial fusion proteins, and ubiquitin ligases. Among these, the mitochondrial fusion proteins help stabilizes the physical contacts between ER and mitochondria(165). Finally, both PERK and IRE1 can be found at the MAMs (166,167).

One of the most important duties of MAMs is Ca^{2+} transport between ER and mitochondria. Some portion of the Ca^{2+} that resides in ER in normal conditions is released to the cytoplasmic space for mitochondrial uptake. Calcium is released by IP3R calcium receptors, whereas mitochondrial uptake is done by VDAC or Ca^{2+} uniporters (168).

Another protein at the MAMS and for the stabilization of MAMs is a molecular chaperon known as mitochondrial Grp75, which stabilizes the IP3R at MAMs. These IP3R are which are very prone to proteasomal degradation, but Grp75 forms a bridge between IP3R and VDACs to stabilize the calcium transfer between ER and mitochondria (169). IP3Rs are stabilized on the mitochondria side with Grp75,

wherease, Sigma-1 Receptor (Sig1R) and Grp78/Bip stabilizes it from the ER side, allowing for a prolonged ER mitochondria calcium signaling (170).

Other poteins and chaperons that are found at the MAMs are calreticulin and calnexin as well as Phosphofurin Acidic Cluster Sorting Protein 2 (PACS2). Calreticulin and calnexin are ER molecular chaperons that regulate the IP3R controlled calcium release. They also interact with Sarcoplasmic Reticulum Ca^{2+} ATPase (SERCA) pump that regulates calcium import into the ER. Calnexin and PACS2 also serve to stabilizes the MAMs (171-173).

Prolonged ER stress leads to increase Ca^{2+} release from ER to mitochondria, disrupts the mitochondrial membrane potential and leading to depolarization of inner membrane and the release of cytochrome c release into the cytosol. This in return, activates B-cell lymphoma 2 associated X (Bax)/ B-cell lymphoma 2 homologous antagonist killer (Bak)-regulated apoptosis. Also apoptosis protease -activating factor 1(Apaf1)/ caspase-9 related pathway of apoptosis is activated through this mechanism (174).

1.5.1. Mitophagy and Inflammation

Autophagy is an organelle clearance process in cell, basically eliminating non-functional or problematic organelles via formation of double-membrane encapsulated autophagosomes that fuse with lysosomes for lysosomal degradation of the cargo (175). Mitophagy is a form of autophagy that specifically clears the dysfunctional mitochondria (158). In mammals, two different pathways are used for mitophagical clearance of damaged mitochondria as shown in Figure 1.6. These are ubiquitin dependent and ubiquitin independent (receptor mediated) signaling cascades (158,176).

Ubiquitin Mediated Mitophagy

Phosphatase and tensin homolog (Pten)-induced putative kinase-1 (PINK1), a serine-threonine kinase, and Parkin, an E3 ubiquitin ligase, are two important effector proteins that regulate the Ubiquitin-dependent mitophagy. Disruption of mitochondrial membrane potential, increase in mitochondrial calcium concentration and enhanced release of mitochondrial ROS blocks constitutive degradation of PINK1 by

mitochondrial protease and which goes on in normal conditions. The uncleaved PINK1 remains on the outer mitochondrial membrane (OMM) and recruits and phosphorylates an E3 ubiquitin ligase known as Parkin on serine 65 (177,178). Further phosphorylation of ubiquitin by PINK1 leads to more Parkin accumulation on the OMM as Parkin has high affinity for its substrate ubiquitin (179). Other proteins are recruited to the OMM. These proteins are adaptor proteins that can recognize and bind the phosphorylated ubiquitin chains. The binding of adaptor proteins such as p62/sequestesome 1(p62/SQSTM1), optineurin (OPTN) and nuclear domain 10 protein 52 (NDP52) then recruits Microtubule-associated proteins 1A/1B light chain 3B (LC3) through their LC3 recognition motifs (LIR)(180). Also, there is another pathway that is Parkin independent. According to literature, PINK1 phosphorylation of ubiquitin also can recruit SQSTM1/P62, OPTN and NDP52 without Parkin presence. These three adaptors are enough for LC3 recruitment and the formation of autopagosome in a Parkin-independent manner (158,181-183).

Receptor Mediated Mitophagy

Another pathway of mitophagy that is independent of ubiquitination is called the receptor-mediated mitophagy. The mitochondrial OMM receptors NIP3-like protein (NIX), FUN14 domain-containing-1 (FUNDC1) and B-cell lymphoma 2 (BCL2)/adenovirus E1B 19 kDa protein interacting protein-3 (BNIP3) are recruited to the micothondria upon cellular metabolic stress, hypoxia or membrane potential loss, and activate mitophagy by binding to LC3 through the LIR domain (176).

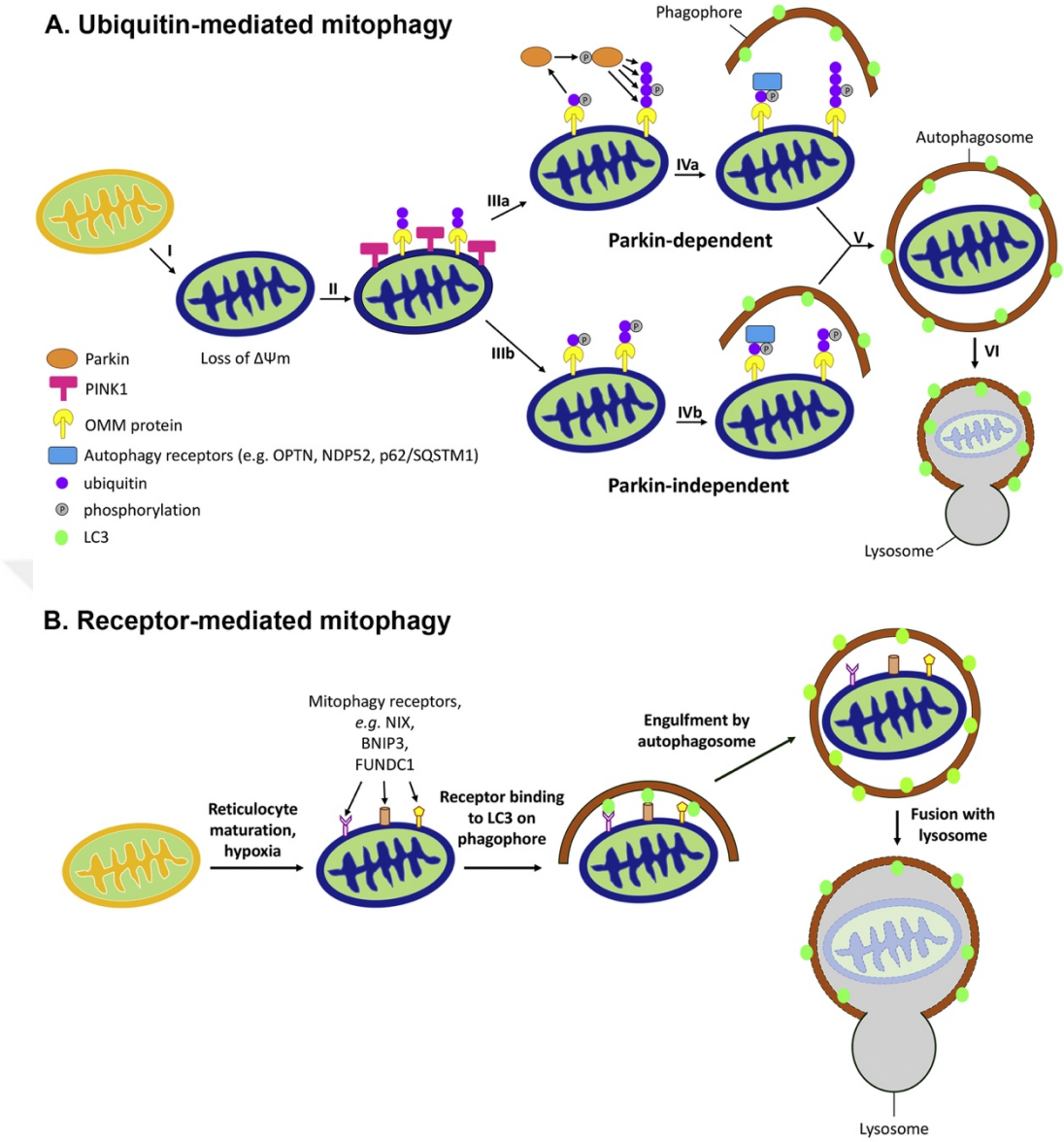

Figure 1.6 Mitophagy pathways

UPR and Mitophagy

In previous sections, I explained the close relationship between mitochondria and ER and the conditins and mechanisms that activate mitochondrial clearance. According to literature there are links between PERK/ATF4 and mitophagy pathways (184). Parkin expression is ATF4 dependent, which may interconnect UPR and Parkin-dependent mitophagy and cell curvival mechanisms(185). PERK is also co-locatized with mitofusin2 (MFN2) at MAMs for stabilization. Mitofusins are proteins that are responsible for mitochondrial integrity and promoting cell survival by inducing mitochondria fusion. Cells lacking either PERK or MFN2 show the same

characteristics in mitochondrial morphology; mitochondria are fragmented and susceptible for mitophagic clearance (166). Whether PERK impacts PINK1-Parkin mediated mitophagy pathway is not known. However, one clue is that Lon Protease1(LONP1), which has been shown to be responsible for cleavage and degradation of PINK1 in healthy mitochondria, can be induced by PERK. Whereas ER stress can induce LONP1 epxression, $PERK^{-/-}$ cells show decreased amounts of LONP1 under ER stress conditions (186). This suggests that LONP1/PINK1 regulation by PERK under ER stress conditions can induce or augment existing mitophagy.

ATF6 has been linked to mitochondrial biogenesis by activation of peroxisome proliferator-activated receptor gamma, coactivator 1 alpha (PGC1α), which induces mitochondrial biogenesis. PGC1α is activated upon ER stress together with ATF6 for stress response and survival mechanisms (187). However, ATF6's role in mitophagy is also not known.

Mitophagy and inflammation

The disruption in mitochondrial functions in response to changed membrane potential, increased calcium and increased ROS levels have been shown to activate inflammatory responses. Impaired mitophagical clearance of damaged mitochondria lead to accumulation of mitochondrial ROS and activates inflammatory cytokine release by activating the inflammasome. Not only ROS production but also the release of mtDNA from damaged mitochondria activates NLRP3 inflammasome. Induction of NLRP3 in cells with impaired mitophagy such as in $Parkin^{-/-}$ cells leads to increased levels of pro-inflammatory cytokines (188). Moreover, macrophages that are deficient for P62 show exacerbated inflammasome activation and release in pro-inflammatory cytokines (189). These findings show, mitophagic clearance of damaged mitochondria can reduces mitochondrial ROS production and prevent inflammasome activation (shown in Figure 1.7).

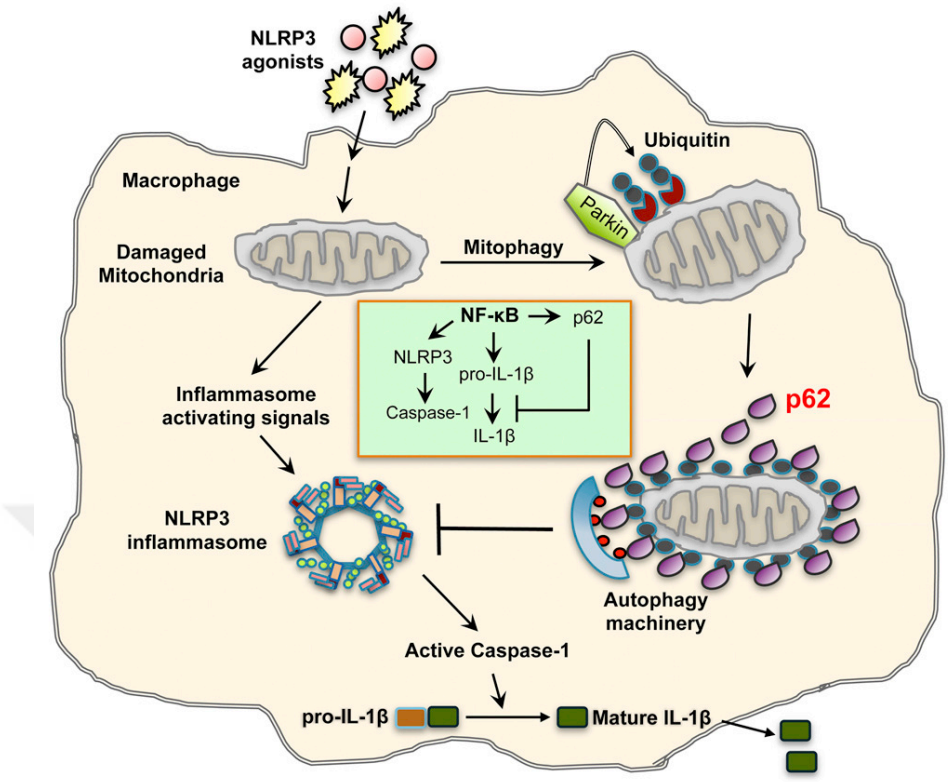

Figure 1.7 Mitophagy Reduces Inflammation and Inflammasome Activation

1.6. Atherosclerosis

Metabolic diseases such as type 2 diabetes, insulin resistance, dyslipidemia, obesity and fatty liver disease are important risk factors for atherosclerosis and its complications (118,190). These diseases combined are account for one in every three deaths in the world (191). Atherosclerosis is a vascular disease that was first described as 'arteriosclerosis' by a pathologist in 1829 (191). The connection between atherosclerosis and inflammation came later (192,193). Rudolf Virchow was the first one to show the role of inflammation in the development of atherosclerosis. After that, scientists described cholesterol is a major risk factor for atherosclerosis and showed that calcification and cholesterol crystals were permanent characteristics of the progressive atherosclerotic human disease. In one of the earlier studies, scientists showed that rabbits fed with cholesterol-rich diets present signs of atherosclerosis (194,195). Nowadays atherosclerotic risk factors include stress, diet, smoking, hypertension, diabetes, obesity, and some infections (196).

1.6.1. Initiation and Progression of Atherosclerosis

Lipoprotein particles are synthesized from liver and carry the water insoluble cholesterol and triglycerides to other cells according to the organism's metabolic needs. Lipoprotein particles are synthesized in liver as very low density lipoprotein (VLDL). VLDLs are composed of cholesteryl esters and triglycerides. Then they are converted to low density lipoprotein (LDL) or high density lipoprotein (HDL). LDL is converted from VLDL by addition of triacylglycerides (TAG) in the liver and it contains apoliporotein B(ApoB) (197). The initiation of atherosclerosis occurs when ApoB containing lipoproteins (LDL) accumulate in the arterial walls of blood vessels at the intima (198). The accumulation and retention of the LDL occurs at vessel branch points where blood flow rate is reduced. After the retention, LDL particles are oxidized (ox-LDL) mainly by free radicals. Ox-LDL particles settle down in the arterial wall and induce a low-grade inflammatory response: First, endothelial cells on the arterial lining are activated by exposure to ox-LDL and then, they begin to express chemokines and other cytokines that attract the monocyte infiltration to the area. Furthermore, other inflammatory cells such as dendritic cells, T cells and B cells and mast cells are recruited to the lesion area (199,200). Also, this inflammatory response activates the resident smooth muscle cells to proliferate and migrate, leading to the formation of a fibrous cap over the lesion. This fibrous cap serves to protect the plaque from the rupture and prevents the release of pro-thrombotic material into the circulation. A lesion with a well-organized fibrous cap is called an established lesion. But there are also vulnerable plaques without a strong fibrous cap. These are prone to rupture and present a risk of thrombosis. An ineffective phagocytosis of lipid material by on-site differentiated macrophages can also trigger rupture. In vulnerable plaques, the lipid debris-filled dead macrophages (or foam cells) form a necrotic core. Fibrous cap thickness loosens in these types of lesions prior to rupture upon enduring shear stress produced by blood flow (Figure 1.8) (201-203).

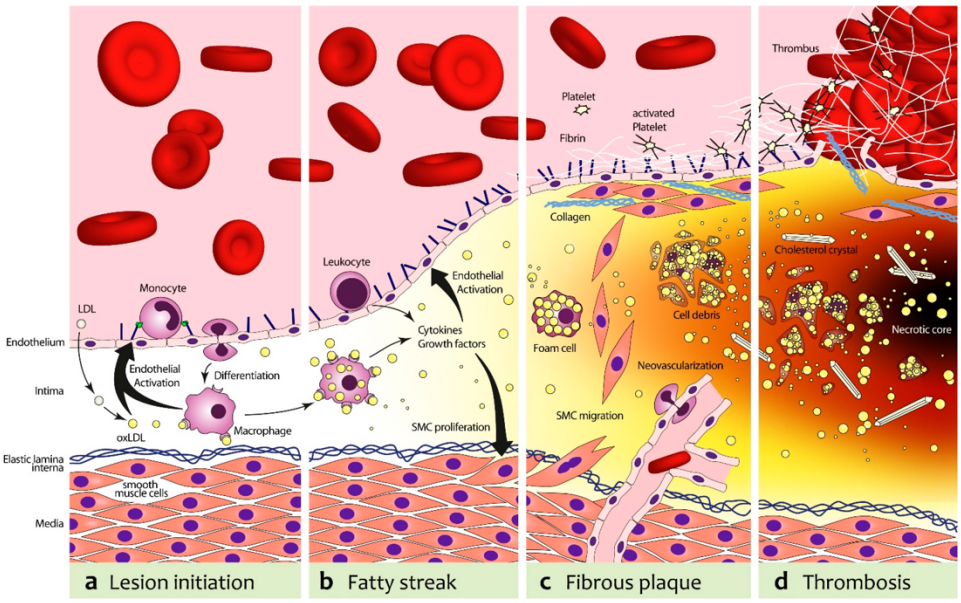

Figure 1.8. Four Stages of Atherosclerotic Lesion Formation (204)

The atherosclerotic lesion area is composed of three main cell types: Endothelial cells (EC) constitute the internal lining of the arterial walls, the intimal smooth muscle cells form the fibrous cap and immune cells that accumulate inside the atherosclerotic plaques. Initiation, progression and rupture of atherosclerotic plaque depends on these three types of cells as well as other immune cells recruited to the plaque (205).

Endothelial Cells

There are two distinct morphologies and functions of ECs at the straight vs branched vessel areas. Straight vessel areas are so called atherosclerosis-resistant areas vs branched vessel areas are called atherosclerosis-susceptible areas. Blood flow at the straight vessel areas is fast but slower at the branched areas. Because of the slow blood-flow, there is more potential for ox-LDL to settle in those areas. Also, in atherosclerosis resistant vessel area, there is uniform laminar flow and high shear stress, however in atherosclerosis-susceptible vessel area there is low shear stress and non-uniform laminar flow (206). At the atherosclerosis-resistant areas, ECs are aligned in the same direction as the laminar flow. However, in atherosclerosis-susceptible areas, the ECs are more cuboidal and interfere with the blood flow to recruit lipids or immune cells to area easily. Also, these cells are more prone to cell death (205-207).

The inflammatory phenotype of these two types of blood vessel regions are also

different. Due to the shape and morphology of endothelial cells as well as due to the high blood shear stress caused by uniform laminar flow in atherosclerosis-resistant areas, kruppel-like factor 2 (KLF2) and KLF4 gene expression is activated. These are transcription factors responsible for proliferation, which serves anti-atherogenic purpose. It was shown in previous studies that KLF2-deficient ($KLF2^{-/-}$) and Apoe-deficient ($Apoe^{-/-}$) mice are protected from atherosclerosis compared to control $Apoe^{-/-}$ mice (205,208). Also KLF4 over expression in mice led to an anti-inflammatory phenotype (209). On the other hand, in the atherosclerosis-prone areas, due to disturbed endothelial cell morphology/function, non-uniform laminar flow and shear stress, NF-κB pathway is activated. When ox-LDL is accumulated in those areas, NF-κB pathway is further augmented and aggravates the inflammatory response on the vessel wall (210,211).

Smooth Muscle Cells (SMCs)

To form a fibrous cap, resident smooth muscle cells change their phenotypes and migrate to intimal region of the plaque. The activation of smooth muscle cells is a result of lipoprotein accumulation and endothelial cell activation and the subsequent inflammatory response, which leads to the secretion of IL-1β, tumor necrosis factor-α (TNFα) and platelet-derived growth factor (PDGF) (205). The activation and migration of smooth muscle cells to lesion area is a dynamic process that continues to evolve during atherosclerosis progression (212). Smooth muscle cells do not only protect the lesion from rupturing by forming the fibrous cap, but also they help the stabilization of lesions by secreting collagen to increase the flexibility of the fibrous cap against the shear stress (213,214). SMCs also produce proteoglycans and components of the extracellular matrix to further stabilize the lesion area (212).

Immune Cells

The recruitment of monocytes to lesion area is stimulated by factors released from the activated endothelial that are known as chemoattractant proteins. Moreover, the activated endothelial cells secrete colony-stimulating factors that activate and promote the differentiation of recruited monocytes to macrophages or dendritic (215,216). Modified ox-LDL particles are internalized by these differentiated macrophages

through their scavenger receptors. The interaction of macrophages with modified lipoprotein particles such as ox-LDL activates their inflammatory receptors such as TLR and NLRs (217). This results in the activation of NFκB pathway and the release of monocyte chemoattractant protein 1 (MCP-1) and pro-IL-1β, TNFα and IL-6. In turn, these factors help recruit and activate more monocytes to the lesion area. Second, the ingestion of ox-LDL by macrophages leads to the formation of a lipid-laden foam cell. This foam cell formation is important for atherosclerosis progression as wells as the necrotic core formation and through their death, it can trigger plaque rupture (218). In addition, NLRP3 inflammasome is activated in the lipid-loaded macrophages mainly as a consequence of cholesterol crystal accumulation and mitochondrial dysfunction (leading to oxidative stress and subsequent mitochondrial DNA release) (219,220). Macrophages can trigger rupture also through the matrix-metalloproteinases that they secrete and which degrades the extracellular matrix, leading to disruption of the fibrous cap. Macrophages can further inhibit the collagen synthesis from SMCs, which can decrease the strength and flexibility of fibrous cap (203).

Monocytes retained in plaques can also differentiate into dendritic cells (DC) (221). As opposed to macrophages, DCs exert their effects by adaptive immunity that is based on T cells. DCs present antigens to T cells and also regulate the activation and differentiation of T cells. The subtypes of T cells that are mostly present in atherosclerotic lesions are T helper cells (Th) and T regulatory cells (Treg). Th1 subtype of Th cells are pro-atherogenic as they secrete Interferon gamma (IFN-γ), and promote pro-inflammatory macrophages (M1) that secrete pro-inflammatory cytokines (222). On the other hand, Th2 cells mainly secrete IL-4, which is known to generate teh anti-inflammator macrophage subtype (M2) and therefore, these are viewed as anti-atherosclerotic. However, in some studies, Th2 cells are induced by hypercholesterolemia (222). In general, Th1 and Th2 cells counteract each other, by secreting IFN-γ vs IL-4. Mostly Th2 has been shown to be athero-protective, but also the absence of IL-4 has been shown to be associated with reduced atherosclerotic plaque formation (223-225). It remains to be clarified the exact role of IL-4 in plaque formation. Treg cells on the other hand are viewed to be athero-protective due to their ability to increasing collagen content of the fibrous cap and stimulating the secretion

of anti-inflammatory transforming growth factor beta (TGFβ) and IL-10 (226).

There are other immune cell types that are observed in in atherosclerotic lesions during different stages. Among these, natural killer (NK) cells and mast cells are both shown to be pro-atherogenic (227,228).

1.6.2. Endoplasmic Reticulum Stress in The Progression of Atherosclerosis

As mentioned in earlier sections, the atherosclerotic lesion is an abundant source of ER stressors such as oxidative stress, saturated fatty acids, cholesterol, hypoxia, and inflammation, all of which can either activate or aggravate the UPR (229,230).

UPR is activated not only in inflammatory cells in atherosclerotic lesion area but also in endothelial cells and smooth muscle cells on the vascular wall. In fact, in cultured endothelial cells that were treated with tunicamycin, pro-inflammatory cytokines such as MCP1 were induced, and these could be blocked by ablating ATF4 or sXBP1 (231). Also, smooth muscle cells and macrophages in plaque area show increased GRP78 and CHOP levels (230). UPR activation, particularly the activation of the PERK branch, was detected in many lesion cell types and all three stages of progressing atherosclerotic lesions, early, mid and advanced atheroma(232).

ER stress contributes to apoptosis and atherosclerotic lesion progress. This leads to formation of necrotic core and plaque rupture in further progression. In advanced atherosclerotic lesions, the abundance of cell death and necrosis correlates with ER stress markers such as increased CHOP levels and with inflammatory signaling such as enhanced expression of STAT2-JNK, and p38 mitogen activated kinase (108,233,234).

Evidence connects chronic ER stress to increased inflammation that is associated with atherosclerosis initiation and progression, however, further mechanistic insights into how UPR engages the inflammatory pathways during atherogenosis is needed (232).

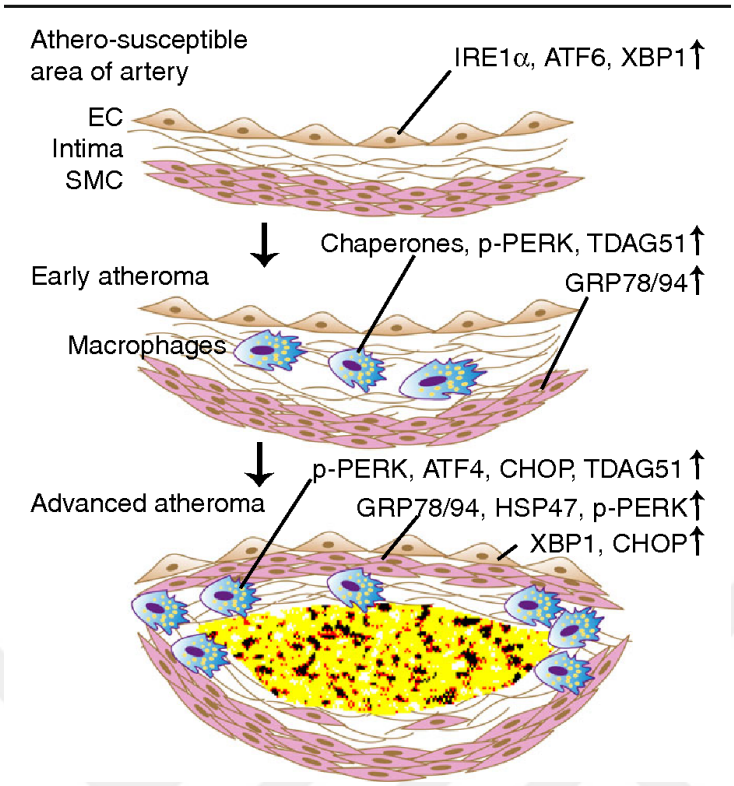

Figure 1.9 Role of UPR in the Progression of Atherosclerosis

1.6.3. Therapeutic Approaches in Atherosclerosis

Throughout the world cardiovascular disease remains the top reason for mortality (191). Despite the advances such as by-pass surgery that can treat a minor percentage of the events (235,236), there is still a critical need to develop novel therapeutic approaches based on well-understood mechanisms. Ongoing studies to prevent atherosclerosis have involved anti-inflammatory drugs and nutraceuticals (dietary supplements), which also have anti-inflammatory and anti-ER stress effects (237-239). Some examples for nutraceuticals are olive oil or hydroxytyrosol, which were shown to prevent the modification of LDL and their use is associated with reduced the atherosclerotic plaque size (240-242). Furthermore, vitamin C and E have been shown to reduce inflammation and atherosclerotic plaque formation (243,244). Poly-unsaturated fatty acids such as Omega-3 and -6 have been shown to reduce pro-inflammatory cytokine expression in atherosclerotic plaque area (238,245). More recently, a mono-unsaturated fatty acid, palmitoleic acid (also known as Omega-7), was shown to reduce inflammation and atherosclerosis (246).

Atherosclerosis is mainly caused and progressed by inflammation, but an

atherosclerosis prevention strategy targeting inflammation has not been developed. However, many studies are being conducted assessing anti-inflammatory drugs or antagonists of known inflammatory cytokines. These strategies include CC motif chemokine ligand - CC motif chemokine receptor 2 (CCL2-CCR2) inhibitors, leukotriene inhibitors (5-lipoxygenase inhibitors), agents that stabilizes TNFα, phospholipase A2 inhibitors and IL-1β antagonists (247-252).

All of these treatments have pros and cons. The very important requirement for these new therapeutic approaches is that must have minimal side effects but maximum effect on disease in a chronic treatment scheme. For example, studies revealed that inhibition of CCL2-CCR2 pathway is beneficial for the prevention of atherosclerosis, however, as it is one of the most important host defense mechanisms in immunity, silencing this pathway would have major consequences by increasing susceptibility to infections or even worsen infection by compromising host defense (253,254).

Leukotrienes are the compounds that mediate inflammation by attracting leukocytes to the lesion area. They are produced by leukocytes themselves through the oxidation of arachidonic acid and eicosapentaenoic acid (EPA), which is an Omega-3 fatty acid. This conversion is done by the enzyme 5-lipoxygenase, and the inhibitors of this enzyme can reduce leukocyte infiltration and the progression of atherosclerosis (255-258).

Phospholipase A2 is an important enzyme for the modification of lipoprotein particles. Considering the important role of modified lipoprotein particles in the initiation and the progression of atherosclerosis, inhibiting this enzyme should be beneficial. However, more studies needed to assess the impact of this treatment on atherosclerosis (250).

Also, there are widely used approaches that target the lipid metabolism to prevent atherosclerosis. The best one known is a drug called statin that is used for cholesterol reduction in patients through statin-induced inhibition of cholesterol synthesis. Statins are also considered to be anti-inflammatory agents. Statins inhibit T cell activation and Th1 lymphocytes proliferation as well as macrophage activation and polarization (248,259,260)

IL-1β is a major cytokine causally associated with atherosclerosis progression. It activates EC cells for cytokine release, stimulates vascular cell adhesion protein (VCAM) adhesion proteins for leukocyte attraction, and induces monocyte chemoattractant protein1 (MCP1) to chemoattract monocytes. Inhibition of this cytokine was achieved with 'anakinra', which is a recombinant IL-1 receptor antagonist (IL-1ra) to compete with the endogenous IL-1β binding to the receptor., initially used for treatment of rheumatoid arthritis(261). Evidence from an engineered mouse of IL-1ra also showed significant reduction in inflammation and atherosclerosis(262-264) .

Interfering with IL-1ra had good effects in diabetes, however, because the blockade of the receptor inhibits both IL-1α and IL-1β, host defense compromise and increased susceptibility to infections remained concerning. In the clinical trial 'CANTOS', a neutralizing antibody against IL-1β, 'Canakinumab', reduced inflammation in cardiovascular disease without effecting cholesterol levels. The neutralization of IL-1β does not appear to cause any severe problems with host defense as IL-1α remained intact (265).

In recent years ER stress and UPR has gained attention as a central pathogenic mechanism in a variety of metabolic diseases including but not limited to diabetes, obesity, fatty liver, and atherosclerosis. UPR drives cells to re-gain cellular homeostasis, however, in prolonged ER stress conditions, UPR activates cell death and inflammatory pathways (232,266,267). So, a strategy to limit ER stress or UPR activity to prevent the metabolic diseases is being evaluated by multiple groups. In literature, chemical mimics of ER chaperoning activity such as phenylbutyrate (PBA) or Tauroursodeoxycholic acid (TUDCA) was shown to reduce diabetes, fatty liver and atherosclerosis (268,269). There are other small molecule inhibitors devised to reduce ER stress effects such as Growth arrest DNA-inducible protein (GADD34/PPPr15a) inhibitors (sephin1, guanabenz, salubrinal), CHOP pathway inhibitor SB203580, and inhibitors for downstream signaling that is induced by ER stress such as C-Jun terminal kinase (JNK) inhibitor SP600125, etc. (268,270-272). While blocking ER stress as a strategy for treatment of metabolic diseases is attractive, it must be taken account that UPR is an essential homeostatic pathway. It can be dangerous to completely ablate a UPR pathway that promotes cellular homeostasis and survival.

The regulation of survival and apoptosis outputs of UPR has not been fully enlightened at the molecular level. Also in terms of metabolic disease such as atherosclerosis, the contribution of each of the UPR arm has not been defined well. It has been shown that the endoribonuclease activity of IRE1 promotes atherosclerosis in hyperlipidemia induced Apoe$^{-/-}$ mice, but its kinase activity has not been investigated in this disease (154,266). Inhibiting the UPR pathway kinases such as IRE1 and PERK with small molecule inhibitors has not been investigated in the context of atherosclerosis. This strategy could also have off-target effects and this may be circumvented with tissue specific UPR modulation in the future (230) .Hopefully, ongoing studies in many labs will enlighten us about the role of UPR arms to metabolic diseases and lay out the foundation of specific and effective therapeutic targeting of these UPR arms in future.

1.7. Hypothesis and Study Aims

Excess nutrients cause chronic inflammation in metabolically active tissues and known as Metaflammation (273). Metabolism and inflammatory pathways are inter-related and ER is an organelle that is central to both of these processes. As such, ER plays an important role in metaflammation. Both ER and neighboring mitochondria are stressed by metabolic overload. These organelles form an immunometabolic synapse that harbors the inactive form of the inflammasome. Metabolically stressed organelles are in a position to relay this information to the inflammasome and activate downstream inflammatory pathways. Whether the ER stress response that involves UPR signaling plays a role in inflammasome activation by organelle stress is not well understood. Importantly, inflammasome activation is seen in atherosclerosis and plays a causal role in the progression of this inflammatory, vascular disease.

In my thesis work, I sought to understand the contribution of one of the UPR arms that is controlled by PERK to activation of the inflammasome by lipid overload in macrophages. PERK is not only one of the UPR arms but it is also a central arm of the ISR. It has been known that in acute ER stress, PERK promotes anti-oxidants and survival pathways, but prolonged activation of PERK is associated with pro-apoptotic and inflammatory responses. PERK is also known to induce foam cell formation in macrophages. Therefore, I hypothesized that PERK is important for lipid-induced inflammation and that we interfere with its activity will specifically block the

activation of inflammasome by lipids prevent the progression of atherosclerosis. Towards this goal, I first analyzed the impact of PERK on lipid-induced ER stress in macrophages. To achieve this goal, I used small molecule inhibitors and silencing RNA (siRNA)-mediated knock down approaches to modulate the ISR pathway from multiple nodes in both mouse and human macrophages. Keeping in mind the importance of ER and mitochondria cross-talki and importance of both of these organelles forn inflammasome activation, I also analyzed effects of PERK on mitochondrial ROS production and mitophagy processes under lipid-induced ER stress conditions in macrophages.

In addition to small molecules and genetic knock-down approaches, I also took advantage of a relatively new and unique method, the ATP-analog sensitive kinase allele technology (ASKA), to generate a mutant PERK kinase that can be modulated by bulky side-chain ATP analogs. This technology allowed specific inhibition of PERK kinase activity in macrophages and in mice *in vivo*.

In vivo, I investigated the consequences of ISR inhibition on hyperlipidemia-induced atherosclerosis progression in the apolipoprotein e $(Apoe)^{-/-}$ mouse model. First, I administered two small molecule modulators, namely GSK2606414 (an inhibitor for PERK k inase) and TRANS-ISRIB (an activator of eukaryotic initiation factor 2 B (eiF2B), which selectively inhibited PERK kinase activity or ATF4, translation, respectively. I also utilized homozygous PERK_ASKA-$Apoe^{-/-}$ mice, which were treated with 1-NAPP1, an ATP-analog inhibitor to inhibit PERK kinase activity. I then analyzed atherosclerosis by (*i)* determining total plaque area on the en face aorta preparations, (*ii)* determining plaque area and plaque cell content by immunofluorescence or immunohistochemical staining of the aortic sinus sections, (*iii)* by analyzing plasma samples lipoprotein profiles and inflammatory cytokines levels, and (*iv)* analyzed spleens to evaluate T cell response.

Chapter 2.

Materials and Methods

2.1 Materials

2.1.1 Reagents

General laboratory reagents and chemicals are listed in Table 2.1.

Table 2.1. Chemicals and reagents that are used in laboratory generally

Reagent	**Company**	**Catalog No**
Acrylamide %40 solution(acrylamide-bisacrylamide)	Fisher scientific	BP1408-1
Amersham Prime ECL Western Blotting Detection Reagent	GE Healthcare	RPN2236
β-mercaptoethanol	Applichem	A1108,0100
Glycine	Glentham	GM2385
Fluoroshield Mounting Medium	Abcam	Ab104135
Fluoroshield Mounting Medium with DAPI	Abcam	Ab104139
Bovine Serum Albumin	SantaCruz	Sc23234
DC Protein Assay Reagent	Biorad	5000116
Page Ruler Prestained Protein Ladder	Thermo Fisher Scientific	26620
HEPES Buffer, 1M stock in normal saline	Lonza	17-757F
Protease Inhibitor Cocktail EDTA Free	Sigma	P8340-5ML

Phosphatase Inhibitor Cocktail 3	Sigma	P0044
PVDF Transfer Membrane	Pierce-Thermo Scientific	88518
Chloroform	Sigma-Aldrich	24216
Absolute Ethanol	Sigma-Aldrich	32221
Methanol	Sigma-Aldrich	32213
Triton X Molecular Biology Grade	Applichem	A 1388,0500
Trisure	Bioline	Bio 38033
Tris Base	Sigma	T1503
OCT Compıunt-Tissue Tek	Electron Microscopy Sciences	62550
Roche Light Cycler 480 Sybr green Mix	Roche	4887352001
EDTA	Applichem	A3562,1000
Formalin Solution %10	Sigma-Aldrich	HT501128-4L
Sodium orthovanadate	Sigma	S6508
PMSF	Ambresco	M145-5G
Ammonium Persulfate (APS)	Sigma	A3678

2.1.2. Cell Culture Reagents

Table 2.2. Reagents, chemicals and kits used in cell culture

Reagent	**Company**	**Catalog No**
DMEM 4.5g/H Glucose	Lonza	BE12-604F/U1/12
RPMI	Gibco	21875091
BSA-Fatty Acid Free	Sigma	A7030-500G
Dulbecco's Phosphate Buffered Saline (dPBS)	Biowest	L0625
DMSO	Sigma	472301
Penicillin/Streptomycin 10000U/ml	Gibco	15140-122
MEM Non-Essential Amino Acids Solution (100X)	life technologies	11140050
Sodium pyruvate solution	sigma	S8636
Palmitate	Sigma	P0500
1-Naphthyl PP1 HBr salt	Haoyuan Chemexpress Co	HY-13941A
Neon™ Transfection System 100 µL Kit	Thermo Scientific	MPK10096
Mouse IFNγ ELISA	eBioscience	88-7314-88
Mouse IL-1β ELISA	abcam	ab100704
Mouse IL-18 ELISA	MBL	#7625
Mouse MCP1 ELISA	abcam	ab100721

2.1.3. Antibodies

Antibodies used in Immunofluorescence, FACS analysis and Western blot are listed in Table 2.3.

Table 2.3. Antibodies used in all procedures

Western Blot Antibody	**Company**	**Catalog No**	**Working Conditions**
β-actin(C4)	Santa Cruz	sc-47778-HRP	1 hr RT
Total PERK(C33E10)	Cell Signaling	3192S	o/n 4 °C
P-PERK(Thr980)(16F8)	Cell Signaling	3179S	o/n 4 °C
Total eIF2-α	Thermofisher Scientific	AHO0802	o/n 4 °C
P- eIF2-α	Genetex	GTX24832	o/n 4 °C
PINK1 (Oligoclonal 17HCLC) antibody	Thermo Fisher Scientific	710993	o/n 4 °C
LONP1	Atlas Antibodies	HPA002192	o/n 4 °C
Caspase1(EPR19672)	abcam	ab207802	o/n 4 °C
IL-1β	Abcam	ab9722	o/n 4 °C
Parkin	Cell signaling	PRK8/2132S	o/n 4 °C
SQSTM1/p62	Abcam	ab56416	o/n 4 °C
TOM40	Santa Cruz	D-2/sc-365467	o/n 4 °C
Immunohistochemistry antibodies	**Company**	**Catalog No**	**Working Conditions**
Moma-2	Abcam	ab33451	o/n 4 °C
IL-1β	Abcam	ab9722	o/n 4 °C
P- eIF2-α	Genetex	GTX24832	o/n 4 °C
LONP1	Atlas Antibodies	HPA002192	o/n 4 °C
VCAM-1	BD Pharmingen	550547	o/n 4 °C
Immunohistochemistry antibodies	**Company**	**Catalog No**	**Working Conditions**

α-SMA	Abcam	ab5694	o/n 4 °C
anti-CD3-Alexa488	Biolegend	100212	1,5 hr 37 °C
Flow Cytometry antibodies	**Company**	**Catalog No**	**Working Conditions**
Zombie Green	BioLegend	423111	30min 4 °C
PerCP-Cy5.5-conjugated antiCD4	BD Bioscience	550954	30min 4 °C
PE-conjugated IL-4 antibodies	BD Biosciences	554389	30min 4 °C
APC-conjugated IFNγ	BD Biosciences	554413	30min 4 °C
PE-conjugated IL-17A	BD Biosciences	559502	30min 4 °C

2.1.4 Study Specific Reagents and Kits

Study specific chemicals, reagents and kits are listed in table 2.4.

Table 2.4. Study specific Reagents, chemicals and kits

Chemical Compound	**Company**	**Catalog No**
GSK2606414	Calbiochem	516535
Sephin1	Kindly provided by Anne Bertolotti from Cambridge	
Trans-ISRIB	CaymanChem	16258
1-NAPP1	Toronto Research Chemicals	A603004
CDDO	CaymanChem	11883
MitoSOX™ Red Mitochondrial Superoxide Indicator, for live-cell imaging	Invitrogen	M36008
MitoTracker® Green FM - Special Packaging	Invitrogen	M7514
Thioglycollate	BD Pharmingen	743-22299
Cremophor-EL	Sigma-Milipore	238470

2.1.5. Solutions

Solutions used in this study are listed in table 2.5.

Table 2.5. Solutions used in this study

Solution	**Ingredients**
HBS solution (instead of R buffer in Invitrogen Neon Transfection Kit)	21 mM commercial HEPES (pH; 7.05) 137 mM NaCl 5 mM KCl 0,7 mM Na_2HPO_4 6 mM Glucose Filter prior using keep at 4°C.
Phospholysis Buffer	50 mM HEPES (pH: 7.9) 100 mM NaCl 4 mM $Na_4P_2O_7$ 10 mM EDTA 10 mM NaF 1% Triton Just prior using add: 2 mM Sodium orthovanadate (Na_3VO_4) 1 mM phenylmethanesulfonylfluoride (PMSF) 1X Phosphatase Inhibitor Cocktail 3 (100X) 1X Protease Inhibitor Cocktail (100X)
5X SDS Loading Dye	10% SDS 50% glycerol 25% 2-mercaptoethanol 0.02% bromophenol blue 0.3125 M Tris HCl, pH: 6,8
1.5 M Tris-HCl (pH: 6.8)	12 g Tris Base is dissolved in 60 ml ddH2O pH is adjusted to 6.8 with 1 N HCl complete to 100ml with ddH2O.
1.5 M Tris-HCl (pH: 8.8)	54.45 g Tris Base is dissolved in 150 ml ddH2O pH is adjusted to 8.8 with 1 N HCl

Solution	Ingredients
	complete to 300 ml with ddH2O.
10% Resolving Gel	2,5 ml 40% Acrylamide mix 2,5 ml 1.5 M Tris-HCl (pH: 8.8) 100 ul 10% SDS 100 ul 10% Ammonium persulfate ;4 ul 0.08% TEMED complete to 10 ml with ddH2O
5 % Stacking Gel	620 ul 40% Acrylamide mix 630 ul 1.5 mM Tris-HCl (pH: 6.8) 50 ul 10% SDS 50 ul 20% Ammonium persulfate ; 5 ul 0.1% TEMED complete to 5 ml with ddH2O
10X SDS Running Buffer	30,3g Tris-Base 144g Glycine 10gr SDS 1L dH_2O
10X SDS Transfer Buffer	30,3g Tris-Base 144g Glycine
10X TBS	1,5 M NaCl (87,76 g) 100 mM Trizma Base adjust pH 8.0 with 1N HCl complete volume to 1 liter with ddH2O
1X TBS-T	450 ml ddH_2O 50 ml 10x TBS 500 µl Tween
10X PBS	80 g NaCl 2 g KCl 15,2 g $Na_2HPO_4.2H_2O$ adjust to 1L dH_2O, pH to 7,4
HBSS buffer	8 g NaCl 400 mg KCl 140 mg CaCl2

Solution	Ingredients
	100 mg MgSO4-7H2O 100 mg MgCl2-6H2O 60 mg Na2HPO4-2H2O 60 mg KH2PO4 1g Glucose 350 mg NaHCO3

2.1.6. Transgenic Mice Used

- Apoe^{tm1Unc} (Apoe$^{-/-}$) mice were obtained from Charles River Laboratory and used in atherosclerosis studies.

- Park2^{tm1Shn} (Parkin $^{-/-}$ mice) was obtained from Jackson Laboratory and used for isolation of bone marrow derived macrophages (BMDM) and used in inflammasome experiments.

- PERK_ASKA mice; Eif2αk3$^{\mathbf{tm2201(G646N,M886A)Arte}}$ was received from AMGEN (from Dr. J.R. Lipford) and used for BMDM isolation and in atherosclerosis studies.

2.1.7. Diet Used in Mouse Atherosclerosis Studies

Western Type Diet (Catalog: TD.88137 #E15721); high cholesterol/high fat (0.21% cholesterol and 21% butter fat) was purchased from Ssniff Spezialdiaten, Germany.

2.2. Methods

2.2.1. General Study Design

All cell culture experiments were done in triplicates and at least three independent repeats were performed. quantitative real time polymerase chain reaction (qRT-PCR) analysis was performed as quadruplicate repeats and replicated at least in three independent experiments.

All the mice experiments were done in independent cohorts. Mice were switched from chow diet to western diet (WD) at 6-8 weeks of age, and WD diet continued for a total of 16 weeks. The *in vivo* data analysis (such as atherosclerotic lesion analysis, immunofluorescent and immunohistochemical staining quantifications) were performed blinded. The only elimination criteria used for the mice health related (such as more than 20% weight loss, fighting and injury) and determined in accordance with our mouse experiment ethics protocol and a veterinarian's consultation.

2.2.2. Cell Culture and Treatments

Bone Marrow Derived Macrophages isolation

The Femur and tibiae of the mice were used for isolating bone marrows by purging with a 23G needle. Roswell Park Memorial Institute (RPMI)-1640 medium without serum but with %1 Penicilline/ Streptomycine (P/S) was used during purging. Bone marrow was filter with BD-Cell strainer (70μM) filter and cells were centrifuged at 1000rpm for 5 minutes. The cells were then cultured for 7 days until differentiation in a medium that contained: RPMI-1640 growth medium enriched with %20 L929 cells (ATCC) conditioned medium, %10 Fetal bovine serum (FBS), %1 L-Glutamine and %1 P/S. Using flow cytometry, we analyzed the percentage of anti-F4/80 antibody stained macrophages and determined it to be at least %95 of the cells obtained from the bone marrows.

Lipid-induced inflammasome activation

Differentiated WT or Parkin knock-out BMDMs were primed with 100ng ultrapure bacterial lipopolysaccharide (LPS) for 3 hours, followed by stimulation with either 500μM palmitate/ 1% bovine serum albumin (BSA) for additional 20 hours.

Other treatments included inhibitors in the following doses and were added 1 hour prior to LPS priming: 2μM GSK2606414, 25μM SEPHIN1, 6μM Trans-ISRIB or 1μM CDDO.

In experiements that involved silencing RNA (siRNA) transfection, LPS treatment followed 12 hours after transfection.

Peritoneal macrophage isolation

From the ASKA (C57BL/6-Eif2αk3$^{tm2201(G646N, M886A)Arte}$) mice we isolated peritoneal macrophages 5 days after intraperitoneal injection of %4 thioglycollate (BD Biosciences). We collected these macrophages by washing the peritoneal cavity with 10 ml of PBS. They were then centrifuged at 1000rpm for 5 minutes and seeded to cell culture dishes in an RPMI-1640 medium containing %10 FBS, %20 L929 conditioned medium, %1 P/S, %1 sodium pyruvate and %1 minimum essential medium with non-essential amino acids (NMEM) and cultured for six hours. The unattached cells were removed while the attached macrophages were collected.

The attached macrophages were treated with 20μM NAPP1 overnight, where indicated in the results. For inflammasome activation, the peritoneal macrophages were primed with 100 ng LPS for 3 hours, followed by stimulation with 500 μM palmitate/1% BSA for additional 20 hours. 1-(1,1-dimethylethyl)-3-(1-naphthalenyl)-1H-pyrazolo[3,4-d]pyrimidin-4-amine(1-NAPP1) treatment (at the same dose as before) was refreshed during the palmitate-BSA treatment.

Preparation of palmitate-bovine serum albumin complex

Palmitate for the treatments was prepared from the stock solution of 500 mM (in ethanol) in a 1% BSA containing, RPMI 1640 medium containing 25mM HEPES but no serum and heated to 55^{0}C by regular agitation by vortexing. After cooling to 37^{0}C the palmitate was treated on to the cells.

2.2.3. Mitochondria Isolation & Mitophagy Experiments

For mitophagy experiments: RAW264.7 macrophages were treated with 500 μM palmitate for 6 hours along with either DMSO (control), 3 μM GSK2606414 or 2 μM CDDO treatment.

For mitochondrial protein isolation: Cells were scraped and lysed in homogenization buffer containing: 250 mM sucrose, 1 mM EDTA, 10 mM Hepes (at pH 7.4). Then cells were disrupted by passing through a 27G needle (5 times) and the lysate was centrifuged at 600g for 5 minutes at $+4^0$C. The supernatant was transferred to a new tube, from which 200 μl was saved to be evaluated as the whole cell extract. The rest of the supernatant was spun at 7000g for 10 minutes. This supernatant was saved to be evaluated as the cytoplasm. Finally, the pellet was lysed with phospholysis buffer and centrifuge for 14000g for 10 minutes, and this constituted the mitochondrial protein extract.

2.2.4. siRNA Electroporation

BMDMs were electroproated with 60 nM siRNA against PERK (Qiagen; SI00991319), 100 nM siRNA against Prss15 (Qiagen; SI01390298), 100 nM siRNA against ATF4, (Qiagen;SI00905905 & SI00905891; 50 nM each), 60 nM PINK1 siRNA (Qiagen: SI01378986) or scrambled siRNAs (Qiagen; 1027281) using Neon electroporator (Invitrogen).

2.2.5. mtROS Staining and Quantification

Mitochondria were stained with Mitotracker Green^{FM} (Life Technologies) by incubating cells in complete cell medium that contains mitotracker (200 nM) at 37^0C for 45 minutes. Then cells were stain with the MitoSOX™ Red mitochondrial superoxide indicator (Life Technologies) by incubating cells in HBSS buffer that contains MitoSOX (2.5 μM) for 10 minutes in the dark. Then cells were washed with HBSS and PBS, fixed in ice-cold acetone for 5 minutes and then sealed with

Fluoroshield mounting medium (with 4',6-Diamidine-2'-phenylindole dihydrochloride (DAPI)). The images were analyzed with ImageJ: mtROS (red)-positive cells percentage / DAPI-stained nuclei number. The representative images were taken with

a Leica DMI 4000B equipped with Andor DSD2 spinning disk confocal microscope (Cagdas Son Lab, Middle East Technical University (METU).

2.2.6. Western Blot Analysis

Cell lysates were prepared in the phospholysis buffer after centrifuging at 14000g for 10 minutes. Lysates were loaded to sodium dodecyl sulfate – polyacrylamide gel electrophoresis (SDS-PAGE) gel and transferred to polyviniylidene difluoride (PVDF) membranes. The membranes were blocked with 5% (w/v) milk or BSA in Tris buffered saline with tween(TBS-T) (0.1% Tween-20 (v/v)). The cell culture supernatant was collected after centrifuging with 500g for 5 minutes to remove dead cells and mixed with %5 SDS loading dye prior to loading to protein gels. Before loading samples were boiled at 95°C for 5 minutes. After western blotting with primary antibodies, a secondary, HRP-conjugated antibody incubation followed. All blots were developed using ECL prime reagent (GE Healthcare) and visualized by BioRAD MP imager.

2.2.7. RNA Isolation and Quantitative Real Time -Polymerase Chain Reaction (qRT-PCR)

Total RNA was extracted with Trisure (Bioline) according to company instructions. We synthesize first strand complementary Deoxyribonucleic acid (cDNA) using the Revert-aid first strand cDNA Synthesis Kit (Thermo Scientific) according to company instructions. qRT-PCR reaction used gene specific primers and Syber Green (Roche) and the analysis was carried out in the Rotor Gene (Qiagen) or Thermal Cycler LC480 PCR (Roche). We analyzed the data using relative quantification ΔΔCt method, and we normalized the data according to GAPDH transcript levels using the formula: ΔΔCt =(primer efficiency)^(−ΔΔCt), where ΔΔCt means ΔCt (target gene) – ΔCt (reference gene). Results were obtained from 3 or more biological replicants and analyzed with a students t-test.

The primers used for mRNA analysis in q-RT PCR experiments are listed in Table 2.6.

Table 2.6. q-RT PCR Primers used in the study

Gene	Forward	Reverse
Mouse		
LONP1	CTCATGGTGGAGGTTGAGAATG	CAGAGGGTTCAAGGCGATGATA
NLRP3	ATTACCCGCCCGAGAAAGG	TCGCAGCAAAGATCCACACAG
Caspase1	AGGCATGCCGTGGAGAGAAACAA	AGCCCCTGACAGGATGTCTCCA
PYCARD	CTTGTCAGGGGATGAACTCAAAA	GCCATACGACTCCAGATAGTAGC
IL-1β	CAACCAACAAGTGATATTCTCCATG	GATCCACACTCTCCAGCTGCA
TNFα	CATCTTCTCAAAATTCGAGTGACAA	TGGGAGTAGACAAGGTACAACCC
CCL2	CTTCTGGGCCTGCTGTTCA	CCAGCCTACTCATTGGGATCA
ATF4	TCGATGCTCTGTTTCGAATG	AGAATGTAAAGGGGGCAACC
ATF3	GAGGATTTTGCTAACCTGACACC	TTGACGGTAACTGACTCCAGC
CHOP	CCTAGCTTGGCTGACAGAGG-	CTGCTCCTTCTCCTTCATGC
PINK1	CCTTCCTATCAGCACCCAAAC	TCCGCTAGTTGAACATACAGGAT
GAPDH	GTGAAGGTCGGTGTGAACG	GGTCGTTGATGGCAACAATCTC
Human		
GAPDH	GACCACAGTCCATGCCATCACT	TCCACCACCCTGTTGCTGTAG
CHOP	AGGCGACCAAACTAAAGAAGG	TGCTGAGTTGAGCGTTATACTG
LONP1	GACGATCCCCGATGTGTTTCC	GGGCGAGACGAACTTTCCTT
ATF4	CTCCGGGACAGATTGGATGTT	GGCTGCTTATTAGTCTCCTGGAC

2.2.8. Mouse Cytokine Measurements with Enzyme Linked Immunosorbent Assay (ELISA)

Mouse IL-1β ELISA kit (Abcam), mouse IL-18 ELISA kit (MBL International), mouse MCP1 ELISA kit (abcam) and mouse IFNγ ELISA kit (e-Bioscience) were used to quantify the respective cytokine's levels in conditioned medium according to the manufacturer instructions.

2.2.9. Mice Studies and Treatments

Apoe$^{-/-}$ mice (Charles River) were used. Male mice were fed with Western Diet from the age of week 8 for 10 weeks. Then mice were injected daily by intraperitoneal method with 30mg/kg of GSK2606414 (Atomole) or DMSO with vehicle (%12.5 vol/vol cremophor EL (Sigma-Aldrich)-saline) for 6 weeks. In a separate group, mice were treated with either 5 mg/kg SEPHIN1 or DMSO with vehicle (%16 vol/vol cremophor EL (Sigma-Aldrich)-saline) for 5 weeks. Furthermore, in another independent experiment mice were treated with 1 mg/kg or 2 mg/kg of Trans-ISRIB (Cayman CHEM) or DMSO with vehicle (%16 vol/vol cremophor EL (Sigma-Aldrich)-saline) for 6 weeks. The Apoe$^{-/-}$ or the PERK-ASKA mice (Eif2αk3$^{tm2201(G646N,M886A)Arte}$ mice) were treated with 60 mg/kg 1-NAPP1 or DMSO in

vehicle (%20 vol/vol cremophor EL- saline) for four weeks. Mice weight was measured weekly and blood glucose measurements were done at the beginning and at the end of injections before sacrifice. In addition, BMDMs or peritoneal macrophages were isolated form Parkin$^{-/-}$ mice (from R.A. Gottlieb's labaroty in Cedars Sinai Medical Center) and PERK_ASKA mice or C57BL/6-Eif2αk3$^{tm2201(G646N,M886A)Arte}$ mice (from J.R. Lipford in Amgen, California). All animal experiments were performed according to protocols approved by the Experimental Animal Care Committee at Bilkent University and Cedars Sinai Medical Center.

2.2.10. Plasma Lipids and Lipoprotein Analysis

Mouse plasma isolation was carried out from whole blood obtained via heart puncture; after centrifugation of the whole blood the plasma was stored at -80^{0}C. We sent the samples for fast protein liquid chromatography (FPLC) analysis at the Mouse Metabolic Phenotyping Center at the University of Cincinnati. For the resolution of major lipoprotein classes from plasma; the columns were equilibrated in 50 mM PBS. Using a microtiter plate enzyme-based assay, the major lipoprotein classes were measured in cholesterol or triglyceride assays from collected fractions.

2.2.11. Flow Cytometry

Spleens were collected at the sacrifice day and splenocytes were isolated. First, erythrocytes were from the splenocytes by the red blood cell lysis buffer and cells were stimulated for 4 hours with phorbol-myristate-acetate (PMA; 50 ng/mL; Abcam) and ionomycin (1 μg/mL; Abcam) in the presence of Golgi stop (BD Biosciences). We differentiated the living cells with Zombie Green (Bio Legend). Surface markers were stained with PerCP-Cy5.5–conjugated anti-CD4 antibody (BD Biosciences) followed by incubation in Cytofix/Cytoperm Solution (BD Biosciences) at room temperature for 15 min. Then, the intracellular cytokines were stained with phycoerythrin (PE)-conjugated IL-4 antibodies, allophycocyanin (APC)-conjugated IFN-γ, phycoerythrin (PE)-conjugated IL-17A, and (all from BD Biosciences). Analysis was carried out using the BD Accuri C6 device and software.

2.2.12. Immunohistochemistry

7-μm thick aortic root cryosections (from OCT embedded heart tissue) were stained with antibodies for: anti-α-smooth muscle actin (abcam-ab5694), MOMA-2 (abcam/ab33451), CD3-Alexa488 (Biolegend/100-210), α-SMA (abcam/ab5694), P-eIF2α (Invitrogen/144-28G), eIF2α (Invitrogen/AH00802), IL-1β (abcam/ab9722), LONP1 (Atlas/HPA002192), VCAM-1(BD-Pharmingen/ 550547) and DAPI (abcam/ab104140) and images were captured with Zeiss fluorescent microscope. Cryosections were stained with Masson's Trichrome (Bio-Optica), OilRedO (Sigma), FAM/FLICA caspase1 detection kit (Immunochemistry Tech FAM-YVAD-FMK (655) # 97), TUNEL (In situ Cell Death detection Kit, Fluorescenin; Roche 11684795910) and hematoxylin and eosin (H&E).

Cryosections were stained with H&E stain for morphometric lesion analysis. The total lesion area and necrotic area were quantified as previously described from 4 sequential sections (60μM apart, beginning at the base of the aortic root (246,274,275). Foam cell area was calculated from OilRedO stained 4 sequential sections and collagen content from Masson's Trichrome stained sections using ImageJ as previously described (246).

The fluorescent immunostainings were carried out on cryosections that were fixed in cold acetone for 10 minutes, blocked in %4-6 BSA/PBS with %10-20 species specific serum (compatible with the primary antibody) as previously described (276). All stained sections were mounted with Fluorosave mounting reagent with DAPI. Florescent signal calculations: (a) P-eIF2α, LONP1, FAM/FLICA and IL-1β staining: the sections were double stained with MOMA-2 to mark the macrophage-enriched area. The Mean Fluorescent Intensity (MFI) corresponding to primary antibody signal was calculated from this MOMA-2 positive area. The background fluorescence of the non-stained area inside the lesion was subtracted from the total MFI corresponding to each signal. Data were quantified as total MFI signal compared with baseline (277-279) (b) CD3 and Tunel stainings: The total T cell number (cells/mm^2) to the lesion area was quantified from CD3 or Tunel stained sections as previously described. (154,280,281). (c) other fluorescent stainings was calculated as percentage of MOMA-2, α-SMA or VCAM-1 positive stained area over total lesion area.(154,246)

2.2.13. *En face* Aorta Lesion Analysis

The aortas obtained from mice were cleaned from fat and surrounding tissue and then, cut opened longitudinally. The aortas were pinned on a black wax surface and lesions were analyzed after Sudan IV staining. Data was quantified as the percentage of Sudan IV stained plaque area in the aortas, as described earlier (246,278,282).

2.2.14. Statistical Analysis

All results are reported as mean ± standart error measurement (SEM). I used Student's t-test with Welch's Correction for determining the statistical significance of the results from the *in vitro* cell culture experiments. I used *Mann Whitney_U* test in analyzing the results from the *in vivo* studies. I used non- parametric Mann *Whitney U* test in these animal experiments to account for the variation in sample size in the various groups and the results displaying great variation among subjects does not fit to the normal distribution rules. I concluded a P value less than 0.05 is statistically significant. All of the statistical tests to determine significance were conducted with the Graphpad *Prism 6* software.

Chapter 3.

In Vitro Results

3.1 Regulation of Inflammasome Activation

ER stress plays significant role in metabolic diseases such as obesity, diabetes and atherosclerosis. (273). ER stress is also known to alter inflammatory responses by UPR pathways through engaging the ER membrane-resident proteins, IRE, PERK and ATF6. In particular, chemical toxins (such as thapsigargin and tunicamycin) that lead to ER stress induction and PERK kinase activation were previously shown to induce NFκB pathway and initiate and inflammatory responses. It is known that lipids can also induce inflammation, specifically inflammasome activation, simultaneous to PERK kinase activation (283). However, it is not known whether PERK plays a role in mediating these lipid-induced inflammatory responses. I hypotesized PERK plays a role in lipid-induced inflammasome activation and inflammatory cytokine secretion, which is an important process that drives atherogenesis.

3.1.1 The Impact of Silencing PERK During Lipid-Induced ER Stress in Bone Marrow-Derived Mouse Macrophages

I first investigated PERK's contribution to lipid-induced inflammasome activation by suppressing PERK expression using a specific silencer Ribonucleic Acid (siRNA) targeting PERK. Successful silencing of PERK kinase in bone marrow-derived mouse macrophages (BMDMs) is shown in Figure 3.1 A. Jenny P. Ting's group showed LPS-primed and palmitate-stimulated BMDMs induce NLRP3 inflammasome activation (148). Upon activation of the NLRP3 inflammasome, the zymogen form of caspase-1 is cleaved by the inflammasome into the mature and active caspase-1 form (10 kDa) that is secreted. The activated caspase-1 then cleaves pro-IL-1β into its mature form (284,285). I observed lipid-induced ER stress is associated with

subsequent inflammasome activation and cleaved caspase1 production, however, this was profoundly suppressed in the PERK siRNA-transfected BMDMs (Figure 3.1 A). This result suggests that PERK might be regulating inflammasome activation. For certainty, I analyzed the cell culture supernatants with ELISA to detect the mature IL-1β levels. Consistent with the caspase-1 levels, I observed IL-1β secretion is significantly suppressed in the PERK siRNA-transfected BMDMs when compared control siRNA transfected BMDMs (Figure 3.1 B). These results show inhibition of PERK can significantly suppress lipid-induced inflammasome activation.

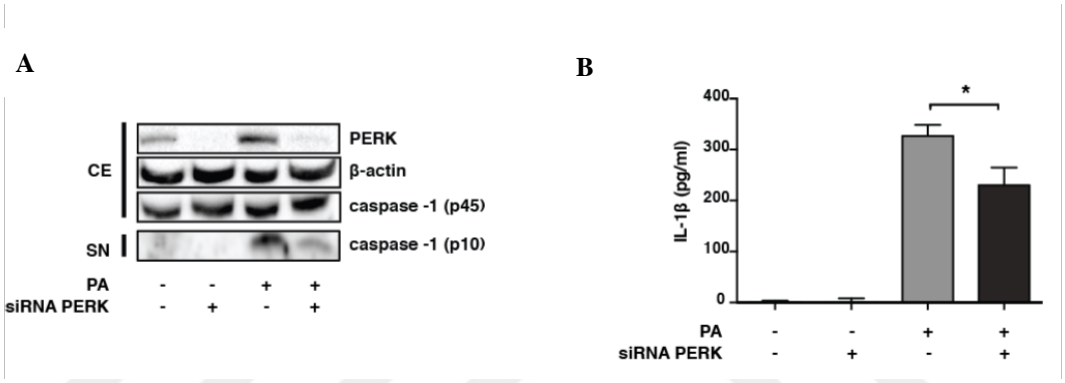

Figure 3.1. PERK expression silencing with siRNA can suppress lipid-induced NLRP3 inflammasome activation in BMDM cells. Inflammasome is activated by 500μM palmitate treatment in 100 ng LPS-primed BMDMs, which were transfected with PERK-specific or scrambled siRNA: (A) PERK, caspase-1 (p45) and actin expression is detected from cell lysates and caspase 1 (p10) from the cell supernatant by Western blotting using specific antibodies against these proteins. (B) Supernatants were analyzed for IL-1β B protein by ELISA. Data: mean value ± SEM; (n=3). Student's t-test. *P≤ 0.05, **P≤ 0.01, ***P≤ 0.001, ns = non-significant.

3.1.2 Effect of Silencing PERK Kinase Activity Under Lipid-induced ER Stress Conditions in Bone-marrow Derived Macrophages

I next examined whether PERK is required for inflammasome activation or just its kinase activity is sufficient. To address this issue, I used '7-Methyl-5-(1-{[3-(trifluoromethyl)phenyl]acetyl}-2,3-dihydro-1*H*-indol-5-yl)-7*H*-pyrrolo[2,3-*d*] pyrimidin-4-amine (GSK2606414)', a selective PERK kinase inhibitor. In BMDMs, using this inhibitor, PERK kinase activity was inhibited (as assessed by autophosphorylation of PERK) (Figure 3.2 A). The analysis of cleaved caspase-1 (p10

fragment) from the cell culture supernatants ,showed a significant reduction upon inhibitor treatment (Figure 3.2 A) Also, the analysis of the supernatants with ELISA for secreted mature IL-1β levels demonstrated a significant reduction upon inhibitor treatment (Figure 3.2 B). These results therefore demonstrate ablation of kinase activity significantly inhibits lipid-induced inflammasome activation and that kinase activity of PERK mediates an important signal necessary for robust activation of the NLRP3 inflammasome.

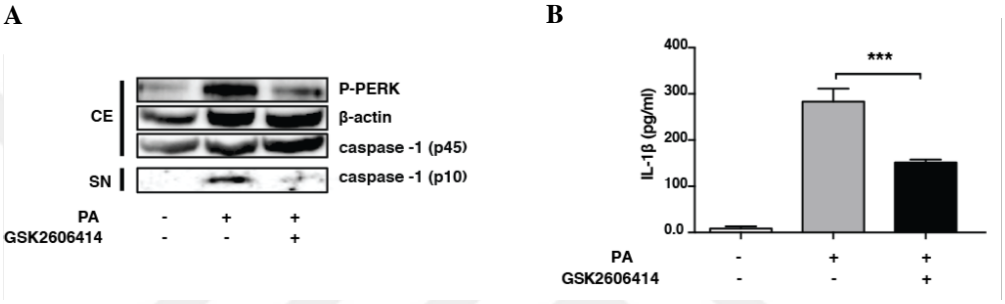

Figure 3.2. Inhibition of PERK kinase activity leads to suppression of lipid-induced NLRP3 inflammasome activation in BMDMs. Inflammasome activation is induced by 500μM palmitate treatment in (100ng) LPS-primed BMDMs, treated with 2μM GSK2606414 or control: (A) P-PERK, actin and caspase-1 (p45) were analzyed from cell lysates and caspase-1 (p10) from the supernatant by Western blotting with specific antibodies against these proteins. (B) The supernatnat was analzyed by ELISA for IL-1β B protein levels. Data: mean value ± SEM; (n=3). Student's t-test. *P≤ 0.05, **P≤ 0.01, ***P≤ 0.001, ns = non-significant.

3.1.3 Alternative Approach Confirms PERK Kinase Activity is Necessary for Lipid-Induced Inflammasome Activation in Macrophages *In Vivo*

The application of chemical genetics as a tool to study kinase activity and substrates was previously described by Kevan Shokat (286). This approach, which requires a point mutation in the kinase of interest allows the manipulation of kinase activity with bulky ATP analogs: A point mutation in a 'gate-keeper' amino acid in the ATP-binding cavity to convert a bulky side chain amino acid to a smaller one result in enlargement of the ATP binding cavity and entry of bulky side-chain ATP analogs. This allows selective modulation of the mutant kinase activity with bulky ATP analogs (287). The ASKA (ATP-analog sensitive kinase allele) mutant of PERK kinase was

previously reported (288). PERK_ASKA mutant bears a single mutation on the gatekeeper residue of PERK; methionine in 886th position was mutated to alanine (M886A). However, some kinases were shown to be destabilized by this kind of mutation (286). By generating another stabilizing mutation at the position G646N, our collaborators at AMGEN aimed to prevent kinase instability. This mutated allele of PERK kinase was then inserted to C57/BL6 mice by our collaborators. The point mutations were generated in exon 12 (G646N) and in exon 13 (M886A), which is depicted in figure 3.3 A. After receiving heterozygous mice bearing the PERK_ASKA allele, I inter-bred them with a mouse model of atherosclerosis, the apolipoprotein-E-deficient (Apoe$^{-/-}$) mice (Figure 3.3 B).

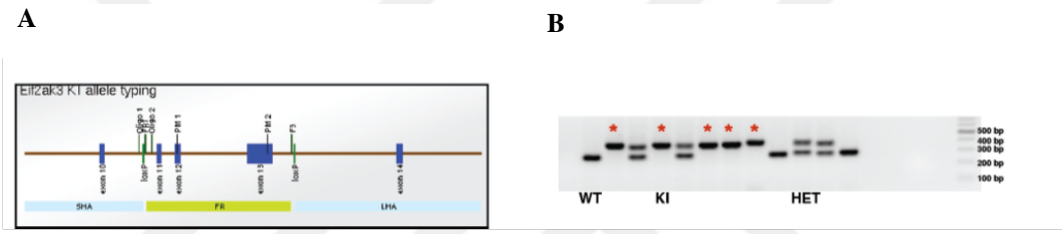

Figure 3.3. Design of PERK_ASKA mice and successful breeding of homozygous mice. (A) Two point mutations G646N and M886A were introduced in the eIF2αk3 gene's exons 12 and 13 . (B) These mice were bred to homozygosity and genotyped to determine incorporation of the mutations (KI (mutant) depicted by higher molecular weight, and wild-type (WT) depicted by lower molecular weight product of PCR reaction using mutation specific primers.

To confirm the regulatory role of PERK kinase in inflammasome activation, thioglycollate- elicited primary peritoneal macrophages were isolated from the PERK_ASKA or WT mice and NLRP3 inflammasome was induced as before and treated them with the bulky ATP analog/inhibitor known as 4-Amino-1-tert-butyl-3-(1′-naphthyl)pyrazolo[3,4-d]pyrimidine (1-NAPP1). 1-NAPP1 inhibited PERK kinase activity in PERK_ASKA macrophages but not in WT macrophages (Figure 3.4). Also, 1-NAPP1 significantly suppressed cleaved caspase-1 and mature IL-1β levels in the supernatants of of PERK_ASKA macrophages but not WT macrophages. In summary, by using this additinonal method (in addition to a specific PERK kinae inhibitor and siRNA-mediated PERK silencing), I demonstrated PERK activity is critical for robust activation of the inflammasome by lipids.

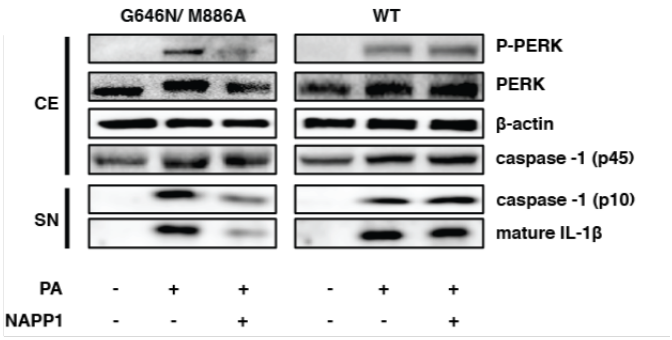

Figure 3.4. PERK kinase activity is critical for robust activation of the NLRP3 inflammasome by lipids was confirmed in peritoneal macrophages by an alternative approach involving chemical genetics. Inflammasome activation was induced in the peritoneal macrophages obtained from PERK_ASKA and WT mice, which were treated with or without 20μM 1-NAPP1 or DMSO as well as inflammasome was induced by 500μM palmitate after LPS (100ng) priming. P-PERK, PERK, actin, caspase-1 (p45) was analyzed from cell lysate and caspase-1 (p10) from supernatatns by Western blotting. (n=3, a representative blot is shown).

3.2 The Impact of eIF2α Phosphorylation on Inflammasome Activation

In previous section of my thesis, I showed that PERK is required for inflammasome activation. We next sought to determine which protein or pathway is responsible for the inflammasome regulatory role of PERK. We searched for whether this effect of PERK is through its target substrate eIF2α and its PERK dependent phosphorylation, whether it is through CHOP, ATF4 or through other independent mechanism.

3.2.1 Effect of eIF2α Phosphorylation in Inflammasome Activation

To study the role of eIF2α phosphorylation in inflammasome activation, I took advantage of a published inhibitor of the protein phosphatase-1 regulatory subunit-15A (PPP1R15A) known as Sephin1 (270,289). Sephin1 has been shown to work by sustaining eif2α phosphorylation only in the ER stress conditions (270). PPP1R15A recruits the phosphatase that dephosphorylates eIF2α. The treatment with Sephin1, however, inhibits PPP1R15A and prolongs the stress response by sustaining the eIF2α phosphorylation. This makes Sephin1 a good tool for study the consequences of prolonged eIF2α phosphorylation on inflammasome activation (270,289).

First, I confirmed that sephin1 can also sustain eif2α phosphorylation induced by a lipid stress. Indeed, sephin1 treatment of lipid-stressed BMDMs led to enhanced and prolonged of CHOP, downstream target of ATF4 in the eif2α signaling pathway, mRNA induction (figure 3.5.A). Persistent eIF2α phosphorylation (caused by Sephin1) lead to induction of CHOP mRNA levels. GSK2606414 inhibited lipid-induced cleaved caspase-1 and secreted mature IL-1β, but not in cells that has persistent eIF2α phosphorylation (sephin1 treated) (Fig.3.5A-C). These findings reveal eIF2α phosphorylation is a key contributor to lipid-induced inflammasome activation.

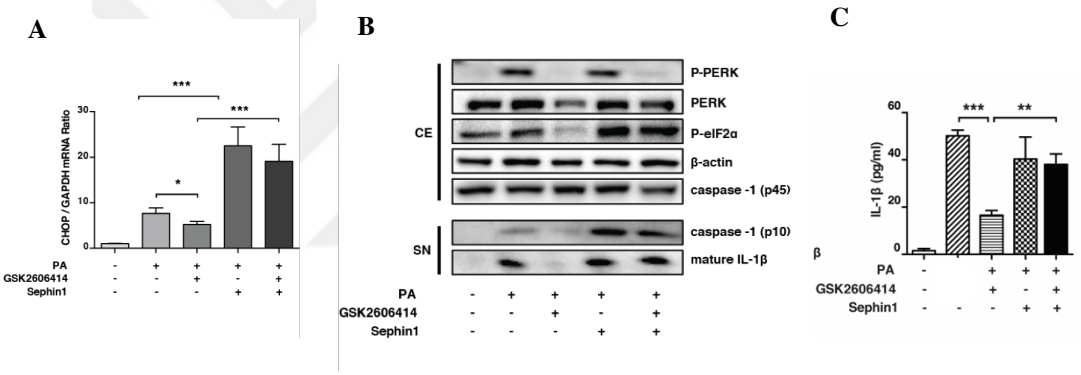

Figure 3.5. Sephin1 prolongs eIF2α phosphorylation and bypassess PERK inhibitor's suppression of NLRP3 inflammasome. BMDMs were trated with 500μM PA and 100ng LPS to induce the inflammasome and treated with GSK260514 (2μM) and sephin1(25μM): (A) CHOP mRNA levels are determined by qRT-PCR. (B) P-PERK, PERK, P-eIF2α, actin and caspase-1 (p45) levels were determined by Westerned blotting from the cell lysate while caspase-1 (p10) and mature IL-1β was determined from cell supernatants using antibodies against these proteins. (C) IL-1β was also measured from the cell supernatant with ELISA. Data: mean value ± SEM; (n=3). Student's t-test. *P≤ 0.05, **P≤ 0.01, ***P≤ 0.001, ns = non-significant. For western blots, a representative blot of three repeat experiments was shown.

3.2.2 Delinating eIF2α to Inflammasome Signaling

After discovereing the critical role of eIF2α phosphorylation for lipid-induced inflammasome activation, I next assessed the contribution of the signaling downstream of eIF2α on inflammasome activation by lipids. For this purpose, I took advantage of a specific activator of eIF2B, a guanine exchange factor (GEF) for eif2α. The ISRIB small molecule can thus repress the translation, but does not interfere with PERK kinase activity or eIF2α phosphorylation. As a consequence of eIF2B activation, ISRIB but inhibit CHOP mRNA levels (289-291). In my experiments, I first confirmed that ISRIB inhibits CHOP mRNA levels that were induced by lipid stress in BMDM (Figure 3.6 A). Also, I confirmed that ISRIB does nto have an impact on PERK autophosphorylation or eIF2α phosphorylation. However, ISRIB inhibited the cleavage of caspase-1 and secretion of IL-1β in same conditions, (Figure 3.6 B-C), suggesting a role for ATF4 and/or CHOP in inflammasome activation by lipids.

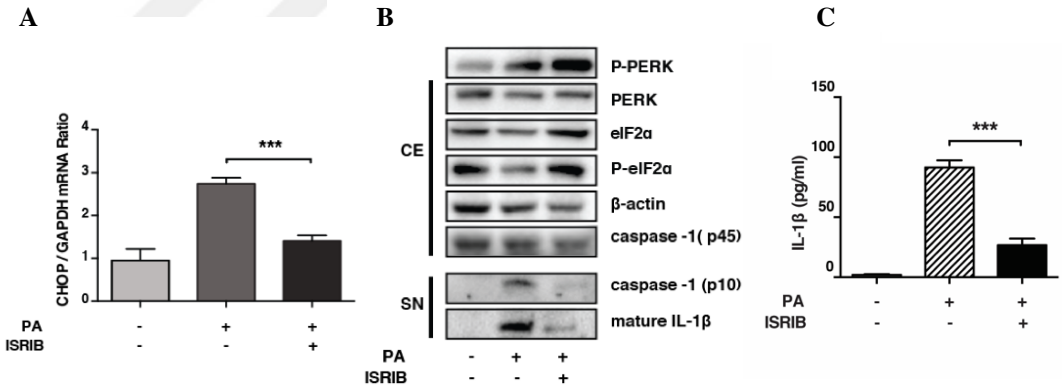

Figure 3.6. ISRIB inhibits NLRP3 inflammasome activation in lipid stressed BMDMs. Inflammasome was induced by 500μM palmitate in the LPS-primed (100ng) BMDMs, which were treated with or without ISRIB(6μM): (A) CHOP mRNA was determined by qRT-PCR analysis. (B) P-PERK, PERK, P- eIF2α, actin and caspase1 (p45) were assessed by Western blotting from the cell lysate while caspase1 (p10) and IL-1β protein were assessed from the cell culture supernatants using antibodies specific for these proteins. (C) Also, cell superantants were analyzed for mature IL-1β with ELISA. Data: mean value ± SEM; (n=3). Student's t-test. *P≤ 0.05, **P≤ 0.01, ***P≤ 0.001, ns = non-significant. A representative blot is shown from three replicates.

Because ISRIB prevented inflammasome activation, I next examined the impact of ATF4, on inflammasome activation. To study ATF4 loss of function, I used a specific siRNA for it. Successful knockdown of ATF4 led to significant inhibition of inflammasome activation by lipids as shown by suppression of caspase1 cleavage and secretion of IL1β (figure 3.7 A-B).

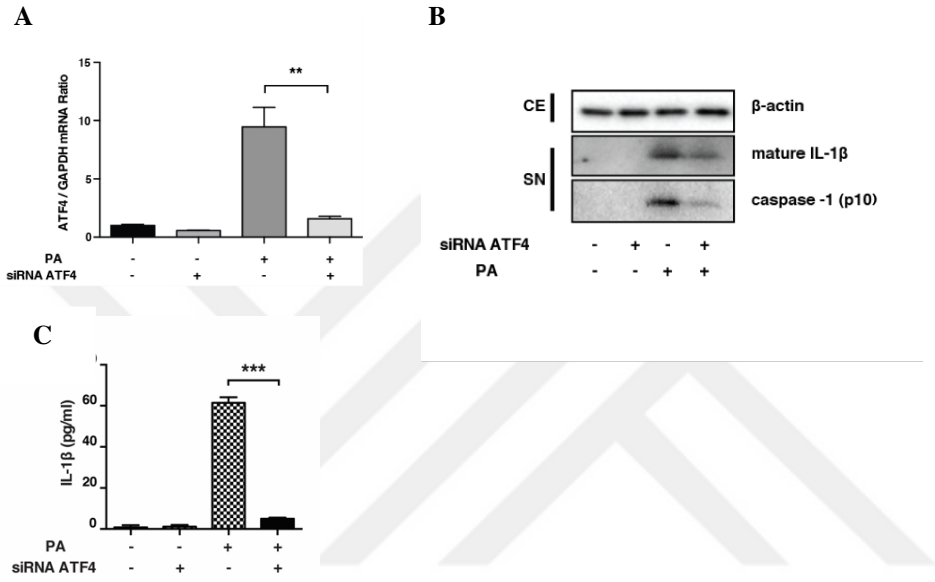

Figure 3.7. ATF4 mediates lipid-induced NLRP3 inflammasome activation in BMDMs. Inflammasome was induced by 500μM palmitate in LPS(100ng) primed BMDMs that were transfected with siRNA against ATF4 or scrambled siRNA: (A) ATF4 mRNA levels was determined by qRT-PCR. (B) Cleaved caspase-1 (p10) and IL-1β protein levels were analyzed by Western blot from cell culture supernatants and actin from cell lysates using specific antibodies against these proteins. (C) Cell culture supernatants was analyzed for mature IL-1β with ELISA. Data: mean value ± SEM; (n=3). Student's t-test. *P≤ 0.05, **P≤ 0.01, ***P≤ 0.001, ns = non-significant. A representative blot is shown from three replicates.

In conclusion, the data generated by using Sephin1, ISRIB and ATF4 siRNA confirms that the ISR signaling has a regulatory effect on lipid induced inflammasome activation.

3.3. The Impact of Silencing ISR on Lipid - Induced Activation in Human Macrophages

Next, I sought to determine the impact of silencing ISR pathway on lipid-induced inflammasome condition in human macrophages. For this, I examined this pathway in human THP-1 monocyte-derived macrophages and human peripheral blood mononuclear (PBMC) cells. In THP-1 macrophages, the inhibitin of PERK kinase activity (with GSK2606414) or activation of eIF2B (with ISRIB) resulted in a significant decrease in mature IL-1β and cleaved caspase-1 levels that are induced by lipid stress (Figure 3.8 A-B). Also in PBMC cells, interfering with PERK kinase activity (with GSK2606414), led to a significant reduction in in mature IL-1β and cleaved caspase-1 levels (Figure 3.8 C).

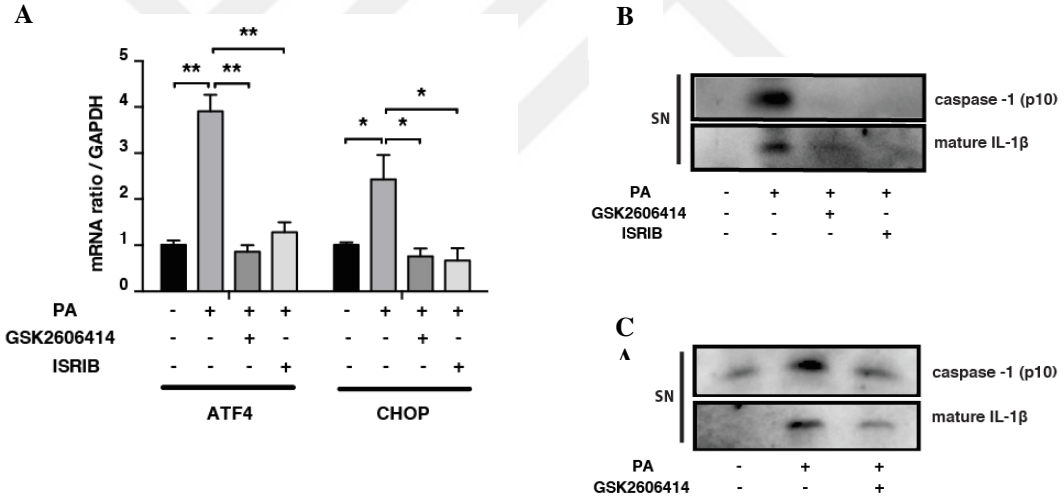

Figure 3.8. ISR signaling plays a critical role in lipid-induced inflammasome activation in human macrophages. Inflammasome activation is induced with 500μM palmitate treatment in LPS (100ng)- primed (A-B) THP-1 macrophages or (C) PBMCs that were treated with GSK2606414 (3μM) or ISRIB (6μM). (A) ATF4 and CHOP mRNA levels were analyzed by qRT-PCR. (B-C) Cell culture supernatants were analyzed for mature IL-1β and cleaved caspase-1. Data: mean value ± SEM; (n=3). Student's t-test. *P≤ 0.05, **P≤ 0.01, ***P≤ 0.001, ns = non-significant.

3.4 Regulation of Mitochondrial Oxidative Stress by the Integrated Stress Response

3.4.1 Regulation of Mitochondrial Reactive Oxygen Species (mtROS) Production by PERK

My findings demonstrates ISR regulates lipid-induced inflammasome activation (292). The lipid we used, palmitate, is a saturated fatty acid (SFA), which has already been shown to induce inflammasome activatity by increasing the generation of mitochondrial reactive oxygen species (mtROS) (292). Therefore, next, I sought to undersand ISR's impact on lipid-induced mtROS production.

LPS-primed and palmitate-stimulated BMDMs were treated with GSK2606414, Sephin1 or ISRIB to study the impact of ISR inhibition on mtROS production. As shown in Figure 3.9, the lipid challenge increased mtROS production, whereas GSK2606414 (left) and ISRIB (right) treatments resulted in a profound reduction in mtROS. Consistent with previous results, Sephin1 treatment, which leads to prolonged eIF2α phosphorylation, did not reduce mtROS production. These results therefore demonstrate that PERK-eIF2α signaling is required for mtROS production in response to lipid-stress and this is consistent with the role of ISR in mediating lipid stress to inflammasome activation.

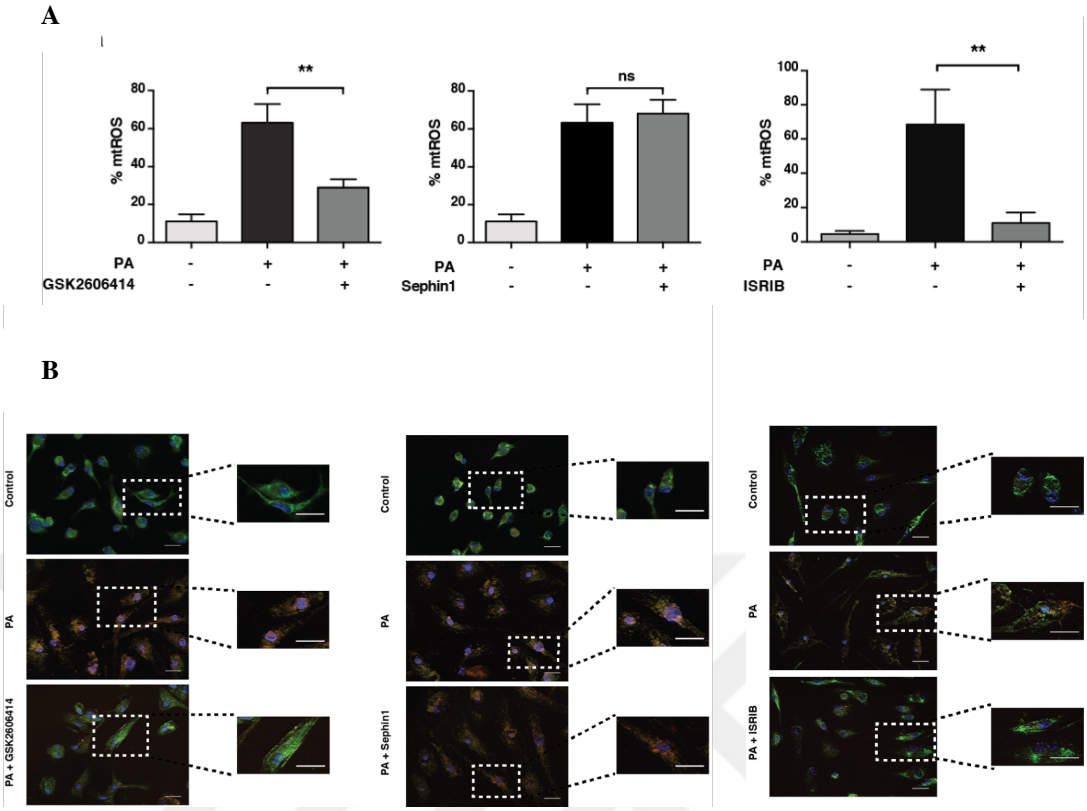

Figure 3.9. Regulation of lipid-induced mtROS production by ISR (A) LPS (100ng) primed and palmitate (500μM) stimulated BMDM cells were subjected to GSK2606414 (2μM), Sephin1 (25 μM) or ISRIB (6μM) treatments and mitochondrial ROS production was measured with Mitosox Red Mitochondrial Superoxide Indicator. (B) Representative confocal images of mtROS production colocalized with mitochondria. Red: Mitosox Red, Green Mitotracker Green Data: mean value ± SEM; (n=3). Student's t-test. *P≤ 0.05, **P≤ 0.01, ***P≤ 0.001,ns = non-significant.

3.4.2 Regulation of Mitochondrial LON Protease by ISR Signaling

3.4.2.1 Regulation of Mitochondrial LON Protease by ISR in Mouse BMDMs

The link between PERK- eIF2α signaling and mitochondria were established in the earlier sections of my thesis. I next sought to understand the detailed molecular mechanisms that connect ISR to mtROS production and inflammasome induction in lipid-stressed macrophages.

A previous study showed a mitochondrial protease, LON protease-1, is induced by ER stress and in a PERK-dependent manner (293). Another study reported that ATF4 and CHOP can transcriptionally activate LONP1 mRNA production (294). Moreover, LONP1 has been suggested to have a role in altering electron transport in mitochondria (295), which might may also be releveant to how PERK effects mtROS production. To test this idea, I first analyzed if LONP1 is induced in lipid stressed BMDMs. LPS-primed, palmitate-treated BMDMs indeed displayed a significant increase in LONP1 mRNA levels, which was blocked by GSK2606414 and ISRIB treatment but not Sephin1. In fact, Sephin1 caused further induction of LONP1 in the GSK2606414-treated cells (Figure 3.10 A-B). I also analzyed LONP1 induction in BMDMs transfected with specific siRNA against PERK or ATF4. The findings in this experimental set up was similar to inhibitor-treated cells. LONP1 induction by lipids was significantly suppressed upon PERK or ATF4 knock down in macrophages (Figure 3.10 C). These findigs demonstrate the induction of LONP1 with SFA is dependent on PERK-eIF2α-ATF4 signaling.

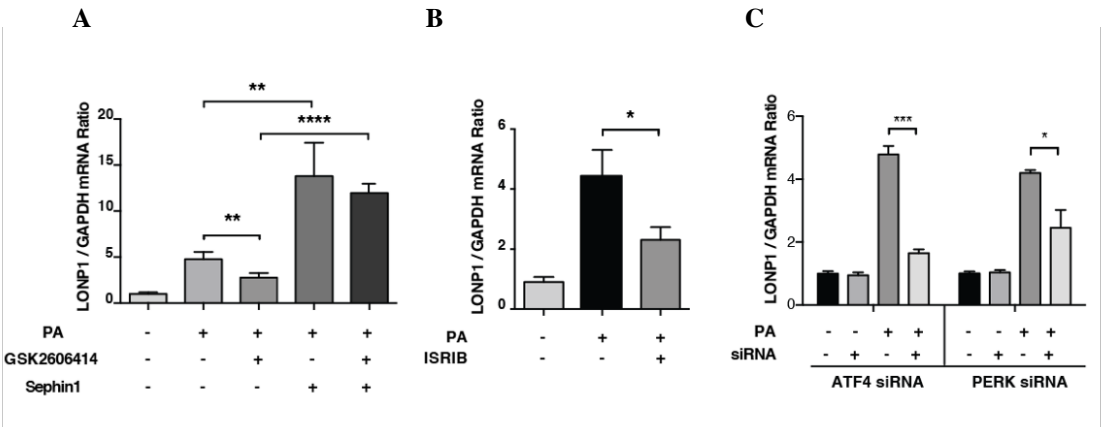

Figure 3.10. Mitochondrial LONP1 is regulated by ISR in lipid-stressed macrophages. LPS (100ng) primed-BMDMs were treated with 500μM palmitate and (A) treated wtih GSK2606414 (2μM), Sephin1 (25μM), or (B) ISRIB (6μM), or (C) transfected with siRNA against ATF4 or PERK or scrambled siRNA. In (A-C) LON protease levels was analyzed by qRT-PCR. Data are mean value ± SEM; (n=3). Student's t-test. *P≤ 0.05, **P≤ 0.01, ***P≤ 0.001, ns = non-significant.

3.4.2.2 Regulation of Mitochondrial LONP1 by ISR in Human Macrophages

After observing the regulation of LONP1 by the ISR pathway in mouse macrophages, next I sought to confirm this is also applicapble to human macrophages. For this, I analyzed LONP1 protein levels in human THP-1 macrophages (Figure 3.11 A-B) and in human PBMC cells (3.11 C) that were stressed with lipids. Interfering with PERK kinase activity (with GSK2606414) or interfere with PERK downstream signaling (with ISRIB), led to a significant reduction in LONP1 mRNA and protein levels. (Figure 3.11 A-C).

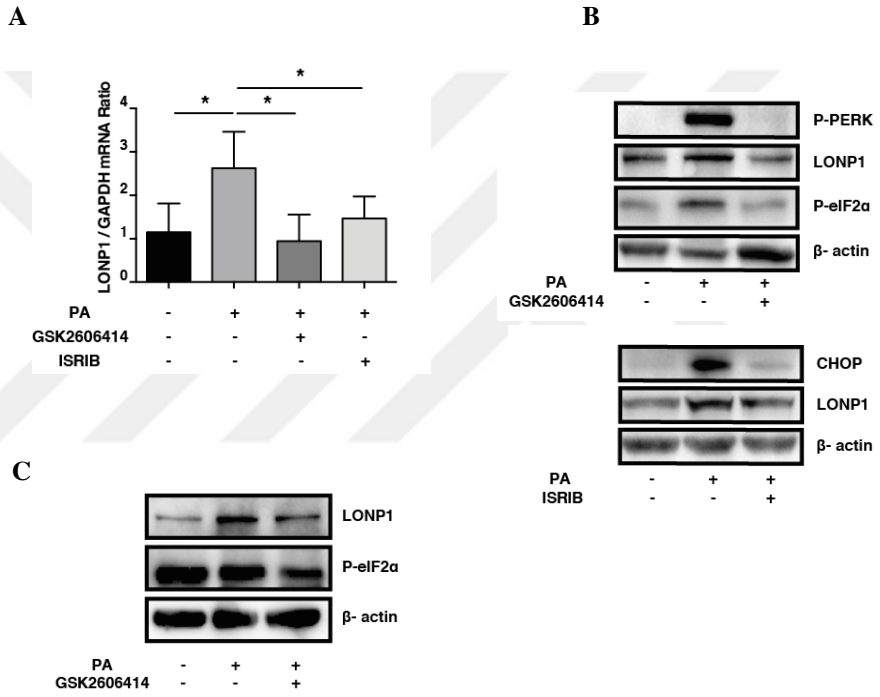

Figure 3.11. Lipid-induced mitochondrial LONP1 is dependent on ISR signaling in human macrophages. LPS-primed (100ng), and palmitate-stimulated (500μM) human macrophages were treated with either GSK2606414 (3μM) or ISRIB (6μM): (A) RNA lysates from THP-1 macrophages were analyzed for LONP1 mRNA by qRT-PCR. (B) Protein lysates of THP1 macrophages were analyzed with Western blotting for P-PERK, LONP1, P-eIF2α ,CHOP and β-actin using specific antibodies for these proteins. (C) PBMC protein lysates were analyzed with Western blotting for LONP1, P-eIF2α and β-actin using specific antibodies for these proteins. Data: mean value ± SEM; (n=3). Student's t-test. *P≤ 0.05, **P≤ 0.01, ***P≤ 0.001, ns = non-significant. A representative blot is shown out of three replicates.

3.4.3 Regulation of Mitochondrial Reactive Oxygen Species (ROS) Production by LONP1

My findings demonstrate the mitochondrial LONP1 is induced in ISR-dependent manner by lipids. Due to its previously reported role in regulating electron transport in the mitochondria, I hypothesized that ISR-induced LONP1 may mediate mtROS production in response to lipid stress in macrophages. Using specific siRNA for LONP1 to knock down this protein's expression in LPS-primed and palmitate-stimulated BMDM cells, I evaluated LONP1's role in mediating lipid stress to the mitochondria. Successful silencing of LONP1 and transcriptional induction of LONP1 was achieved, which resulted in significant block in mtROS production upon lipid challenge (Figure 3.12 A-C). This result confirmed my previous findings and revealed that PERK-eIF2α-LONP1 signaling regulates SFA-induced mtROS production.

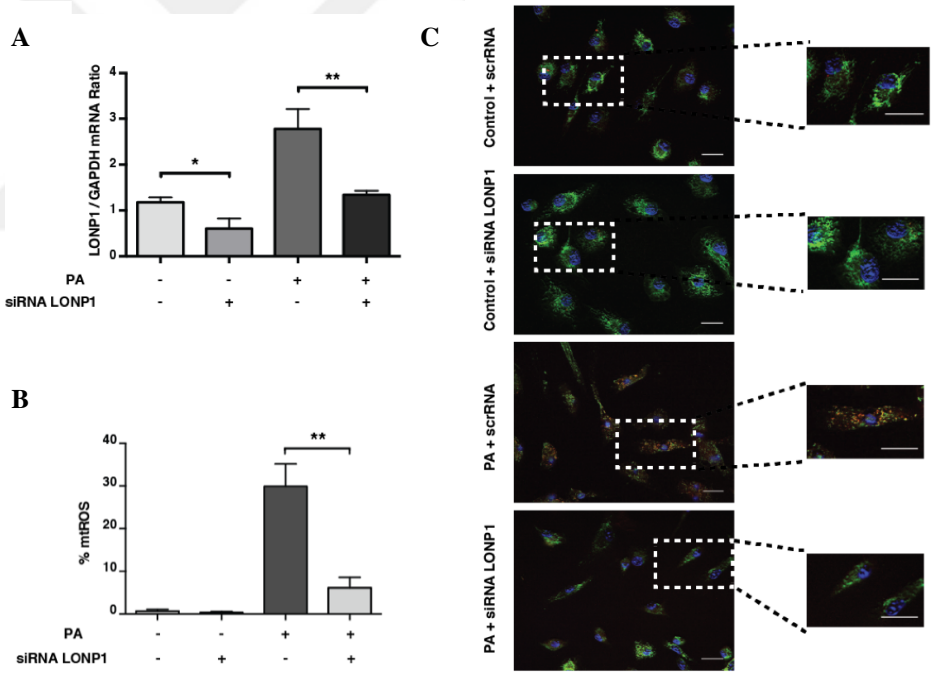

Figure 3.12. Regulation of mtROS production by LONP1. Palmitate (500 μM) treated, LPS-primed (100ng) BMDMs were transfected with siRNA agasint LONP1 or scrambled siRNA: (A) Total RNA was analyzed for LONP1 by qRT-PCR(B) mtROS levels analyzed after silencing of LONP1 (B) levels analyzed with mitosox kit after LON siRNA transfection (C) representative images showing reduced mtROS levels analyzed by Mitosox Red Mitochondrial Superoxide Indicator (red), Mitotracker Green for mitochondrial colocalization(Green), after LON siRNA transfection. Data: mean value ± SEM; (n=3). Student's t-test. *P≤ 0.05, **P≤ 0.01, ***P≤ 0.001, ns = non-significant.

3.4.4 Regulation of Inflammasome Activation by LONP1

In previous section, my findings demonstrated PERK-eIF2α-LONP1 signaling plays a critical role in mediating lipid stress to mtROS generation. This data suggests that lipid-induced transcriptional upregulation of LONP1 can mediate mtROS production that is upstream of inflammasome activation. In order to modulate LONP1 levels or activity and address its role in lipid-induced inflammasome activation, I utilized LONP1 specific siRNA as well as a specific inhibitor of LONP1, 2-cyano-3,12-dioxo-oleana-1,9(11)-dien-28-oic acid (CDDO-ME). Either silencing LONP1 with siRNA or inhibiting its protease activity with CDDO, led to significant inhibition of inflammasome activation by lipid stress as shown by decreased caspase1 cleavage and IL-1β secretion (Figure 3.13). These findings thus cofirm that PERK-eIF2α-LONP1 signaling is responsible for the SFA induced mtROS production and NLRP3 inflammasome activation

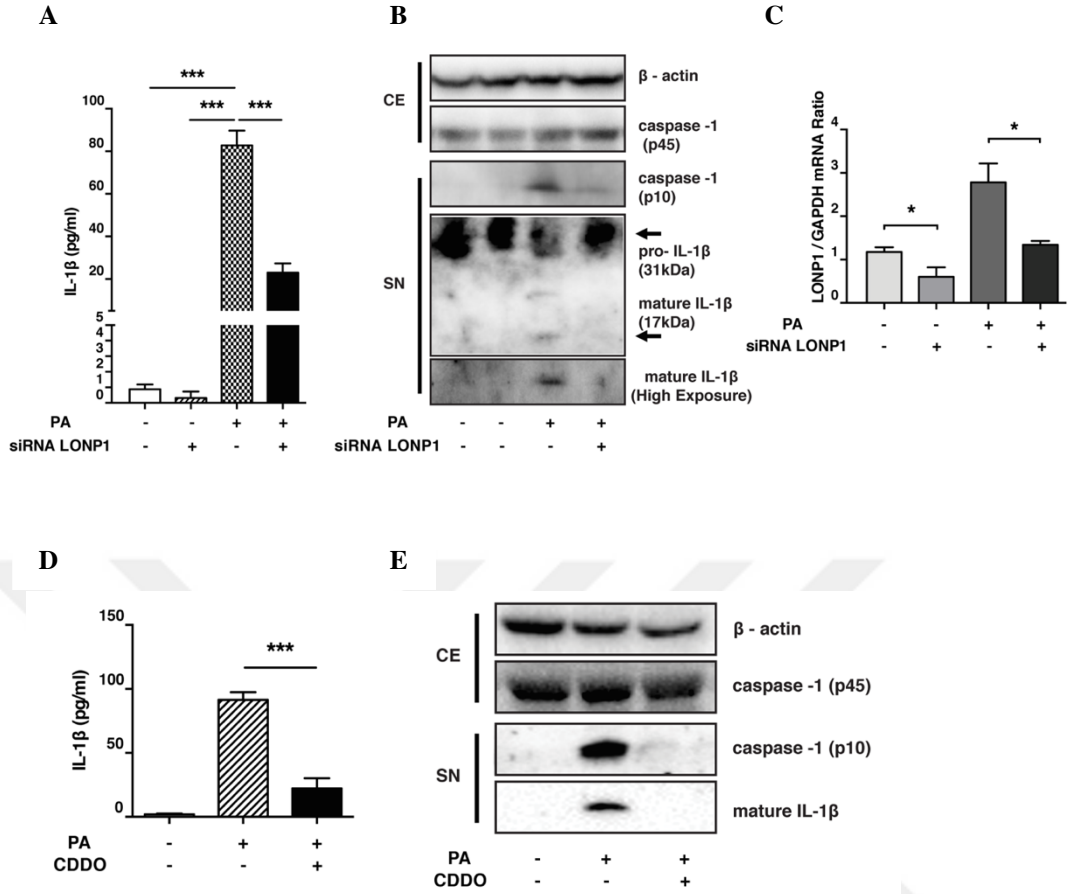

Figure 3.13. LONP1 regulates lipid-induced inflammasome activation. Palmitate (500μM) was used to stimulate the inflammsome in LPS-primed (100ng) BMDM that were (A-C) transfected with LONP1 siRNA or (D-E) treated with CDDO(1μM). In (A), cell culture supernatants were analyzed for mature IL-1β with ELISA and in (B) cell culture supernatants (SN) and total cell extract protein lysates (CE) were analyzed by Western blotting for caspase1, IL1β and β-actin using specific antibodies against these proteins. (C) RNA lysates were analyzed for LONP1 by qRT-PCR. (D) Cell culture supernatants were analyzed for mature IL-1β with ELISA. (E) Cell culture supernatants (SN) and total cell extract protein lysates (CE) were analyzed by Western blotting for caspase1, IL1β and β-actin, using specific antibodies against these proteins. Data are mean value ± SEM; (n=3). Student's t-test. *P≤ 0.05, **P≤ 0.01, ***P≤ 0.001, ns = non-significant. A representative blot is shown for n=3 experiments.

3.4.5 Regulation of PINK1 by PERK-eIF2α-LONP1 Signaling Axis

One of the substrates for LONP1 protease is PTEN-induced kinase-1 (PINK1). While it has been suggested that LONP1 may play a role in PINK1-Parkin-dependent mitophagy, this has not been shown directly (296). I first sought to establish LONP1 dependent regulation of PINK1 in lipid-stressed macrophages. Using specific siRNA against LONP1 resulted in increased, PINK1 protein levels (Figure 3.14 A). Then we checked whether there are any changes with the inhibition of PERK from upstream (GSK2606414), or from downstream (ISRIB) will affect PINK1 levels. Furthermore, inhibitors of the ISR pathway (GSK2606414 and ISRIB) resulted in the suppression of LONP1 expression that is is induced by SFA while enhancing PINK1 expression in the same cells (Figure 3.14 B). These results therefore show that PERK-P-eIF2α-LONP1 axis regulates PINK1 protein levels, as would be expected considering PINK1 is a LONP1 substrate.

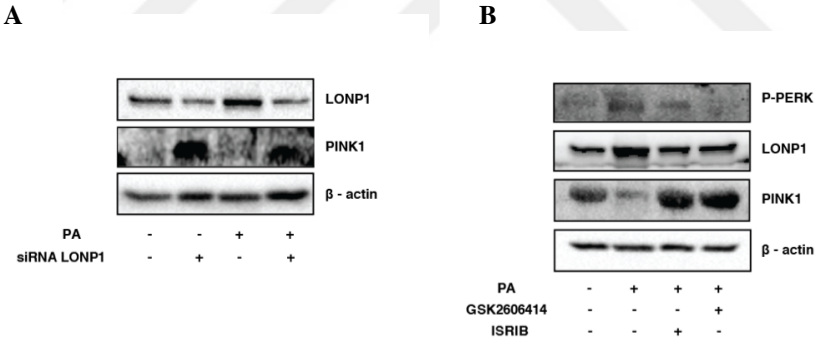

Figure 3.14. PERK regulates inflammasome activation through mitochondrial LONP1 and PINK1. LPS –primed (100ng), palmitate-stimulated (500μM) BMDMs were (A) transfected with siRNA against LONP1 or scrambled siRNA, or (B) treated with GSK2606414(2μM) or ISRIB (6μM). In (A) mitochondrial protein lysates were analyzed for LONP1 and PINK1 by Western blotting using specific antibodies against these proteins were used to show effected PINK1 levels by LON protease directly. (B) successful silencing of PERK kinase activity by GSK2606414 is shown by P-PERK and LONP1 and PINK1 levels are analyzed by Western Blot under the indicated conditions.

3.5 Regulation of Mitophagy by ISR

Mitophagy is the process to remove damaged mitochondria from cells, in turn, relieving mitochondrial oxidative stress and subsequent inflammasome activation (148). Since ISR regulates PINK1, a central player in mitophagy, I next saught to understand ISR's impact on mitophagy in lipid-stressed macrophages.

3.5.1 PINK1-Parkin Dependent Mitophagy Response

To address the role of PERK-eif2α-LONP1 axis in PINK1-Parkin-dependent mitophagy, I isolated mitochondria from lipid-stressed macrophages and checked for the mitophagy markers such as Sequestosome 1(SQSTM1/P62) and Parkin in lipid-stressed RAW264.7 macrophages. According to the results, GSK2606414 (to inhibit PERK kinase) or CDDO (to inhibit LONP1) treatments both increased these mitophagy markers (Figure 3.15). Also, the decrease in mitochondrial outer membrane protein translocase of outer mitochondrial membrane 40 (TOM40) in the whole cell extracts is consistent with decreased number of mitochondria due to increased mitophagy in cells.

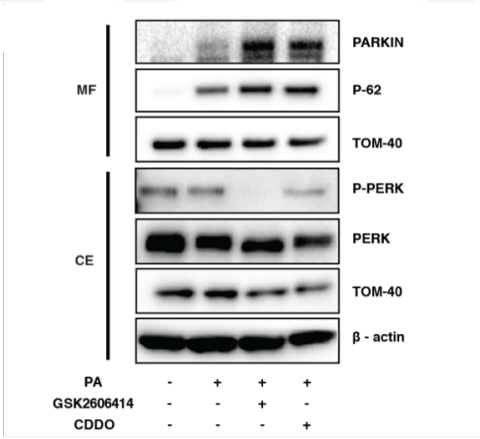

Figure 3.15. PERK-eif2α-LONP1 signaling axis regulates mitophagy. Palmitate-stimulated (500μM), GSK2606414 (2μM), CDDO (1μM) or control treated RAW264.7 cells were analyzed for mitohagy markers: (A) Parkin, p-62, TOM-40 were analyzed from the mitochondrial fraction (MF) protein lysates whereas P-PERK, PERK and actin were analyzed from total cell extract protein lysates (CE) by Western blot using antibodies against these proteins. A representative blot is shown for n=3 experiments.

3.5.2 Confirming the Role of Mitophagy in Inflammasome Regulation by ISR

My findings thus far indicate a role for PERK in PINK1-Parkin-dependent mitohpahagy regulation. To connect PERK's role in mitophagy regulation to lipid-induced inflammasome activation, I used specific siRNA against PINK1 to silence this pathway in lipid-stressed BMDMs and analyzed the impact of PINK1 suppression on caspase-1 cleavage and IL-1β secretion. Successful reduction in PINK1 mRNA levels in BMDMs prevented GSK2606414's ability to block SFA-induced IL-1β secretion or caspase-1 cleavage (Fig.3.16A-B). As a secondary confirmation, I used Parkin-deficient primary mouse BMDMs and treated them with GSK2606414, CDDO-Me or ISRIB. The results of this experiment showed that the ability of all three drugs to block SFA-induced IL-1β secretion or caspase-1 cleavage was disrupted in Parkin-deficient cells (Figure 3.16 D&E). Collectively, my findings show PERK controls PINK1-Parkin dependent mitophagy pathway to control mtROS release and inflammasome activation.

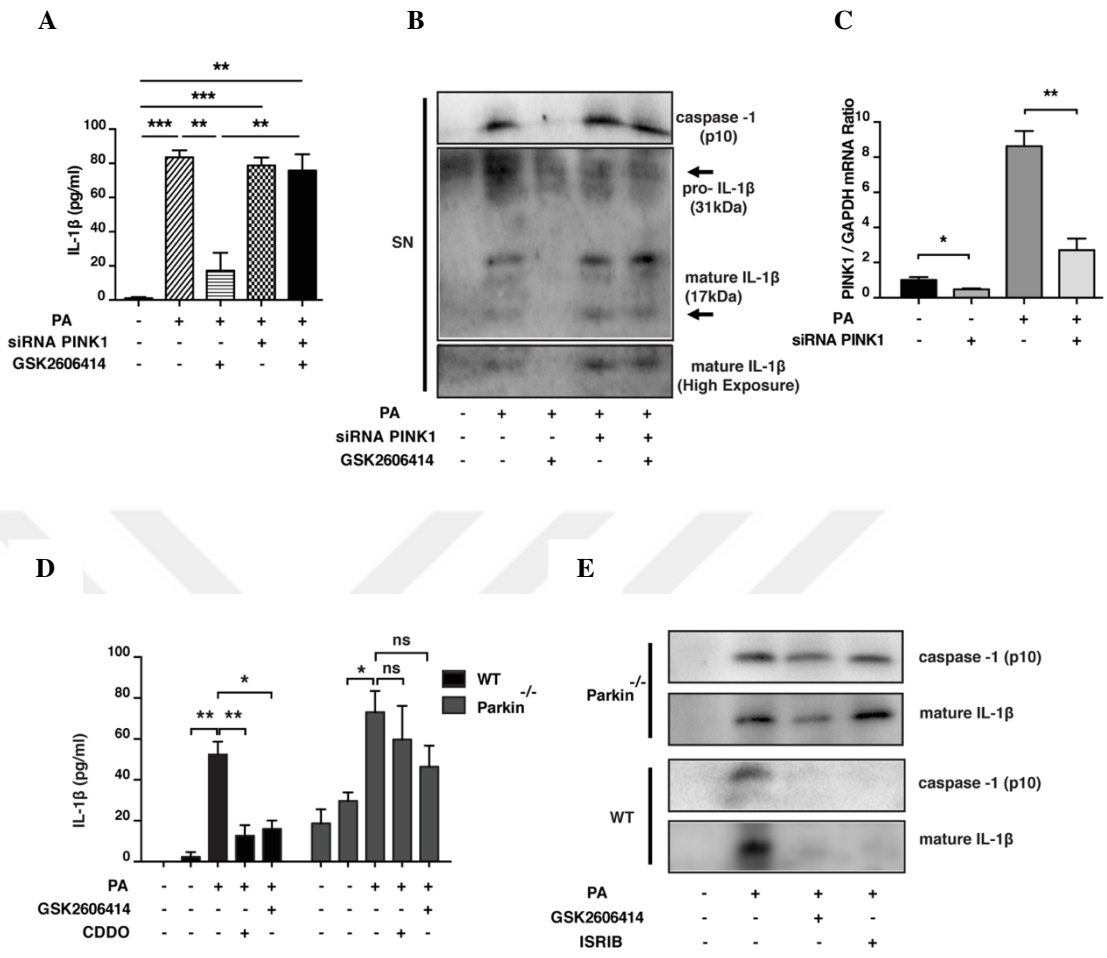

Figure 3.16. Inflammasome regulation via PERK–LONP1 axis is dependent on PINK1- PARKIN-mediated mitophagy. (A-C) LPS-primed (100ng), palmitate-stimulated (500μM) BMDMs were transfected with siRNA against PINK1. (A) Protein lysates from cell culture supernatants were analyzed via western blot for mature caspase1 (p10) and mature IL-1β or (B) mature IL-1β with ELISA. (C) RNA lysates were analyzed for PINK1 levels with qRT-PCR. (D-E) LPS-primed (100ng), palmitate-stimulated (500μM) WT and Parkin$^{-/-}$ BMDMs were treated with GSK2606414, ISRIB or CDDO and analyzed for inflammasome activation: (D) cell culture supernatant was analzyed for IL-1β using ELISA and (E) mature caspase-1 (p10) and mature IL-1β by western blotting using specific antibodies against these preoteins. Data: mean value ± SEM; (n=3). Student's t-test. *P≤ 0.05, **P≤ 0.01, ***P≤ 0.001, ns = non-significant. (a representative blot is shown from three replicate experiments.

Chapter 4.

PERK's Role in High Fat-Induced Inflammation and Atherogenesis *In Vivo*

Based on the findings in previous chapter, PERK pathway plays an important role in inflammatory pathways, particularly inflammasome activation, by lipids. These findings suggest that PERK-eIF2α pathway could have a role in atherosclerotic plaque development *in vivo*. Furthermore, PERK has been shown to promote foam cell formation in earlier studies, further implicating this pathway in atherogenesis (297,298).

4.1 *In Vivo* Administration of GSK2606414 to Inhibit PERK Kinase Activity in a Mouse Model of Atherosclerosis

4.1.1 General Study Design and Correlation of The Efficacy of GSK2606414 *In Vivo*

The apolipoportein E-deificient ($Apoe^{-/-}$) mice were subjected to 16 weeks of hypercholesterolemic Western diet (WD). During the last 6 weeks of WD, mice were administered GSK2606414 (30 mg/kg/day in 12.5 % Cremophor-EL-Saline solution) via intraperitoneal injection (Figure 4.1 A). The delivery method of this specific drug as well as the effective dose was determined according to the previous studies that used GSK2606414 *in vivo* (299,300).

To test the efficiency of the *in vivo* administration of GSK3606414, I extracted protein from pancreatic tissue, where PERK kinase is highly expressed, and analyzed WD-

induced PERK activation (by detecting PERK auto-phosphorylation in Western blots). As expected, GSK2606414 significantly inhibited PERK phosphorylation without affecting its total protein levels (Figure 4.1 B). Also in the RNA lysates obtained from the spleens of these mice, I analyzed CHOP, ATF4, ATF3 and LONP1 mRNA expression by qRT-PCR. All of these PERK downstream mediators were suppressed in the inhibitor-administrated mice (Figure 4.1 C). These findings also validate the PERK-eif2α-LONP1 pathway I discovered in lipid-induced macrophages.

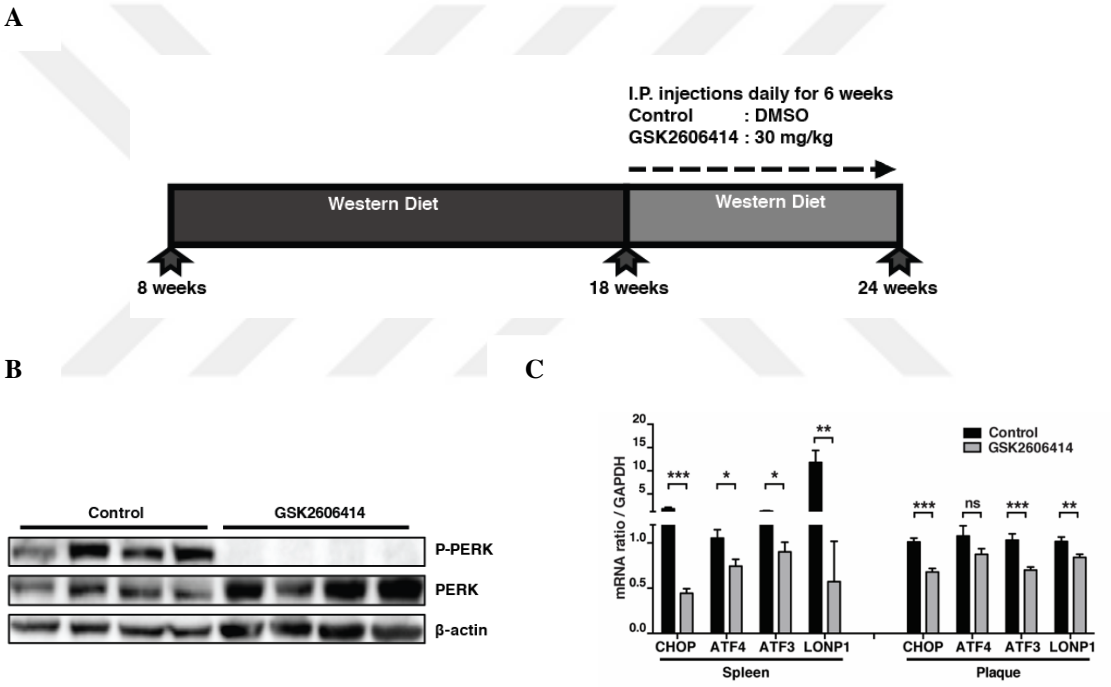

Figure 4.1. Inhibition of PERK kinase Activity *In Vivo* During Athersclerosis Progression. (A) Experimental design and the time course for 30mg/kg/day GSK2606414 administration to Apoe$^{-/-}$ mice *in vivo*. (B) Pancreatic protein extracts were analzyed for P-PERK, total PERK levels and actin levels by western blotting using specific antibodies against these proteins. (C) RNA lysates extracted from spleens or aortic plaques of same animals were analyzed by qPCR for CHOP, ATF4, ATF3 and LONP1. Data: mean value ± SEM; (n=15-15). Mann-Whithney Test. *P≤ 0.05, **P≤ 0.01, ***P≤ 0.001, ns = non-significant. (A representative blot is shown from three replicate experiments).

4.1.2 Analysis of Bodyweight, Blood Glucose and Plasma Insulin Levels in Animals

To assess, whether GSK2606414 altered the metabolism of the mice, I weighed them every 3 days and also measured blood glucose levels before beginning inhibitor injection and at the day of sacrifice. Treated and control mice did not show any differences in blood glucose levels, however, there was some bodyweight loss (up to 10%) that is associated with inhibitor treatment, which was expected based on earlier reports using this inhibitor in mice (Figure 4.2 A). Because, I used 1/3rd of the drug does in those studies, the bodyweight effect was less severe than reported and did not impact the experimental design. Because chronic inhibiton of PERK can lead to pancreatotoxicity, I also analyzed plasma insulin levels by ELISA. There were no significant changes in plasma insulin levels of the inhibitor-treated animal groups (Figure 4.2 B).

A

Variables	Treatment	Control	GSK2606414
n		15	15
Bodyweight(g)	Before	30,27 ± 1,350	28,87 ± 0,7096
	After	31,87 ± 0,9850	25,43 ± 0,4651
Glucose(mg/dl)	Before	111,7 ± 6,455	111,2 ± 5,372
	After	116,5 ± 6,862	120,8 ± 5,477

B

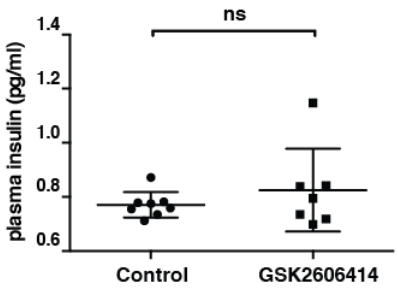

Figure 4.2. Metabolic characterization of 30mg/kg/day GSK2606414-treated mice. GSK2606414 or vehicle-treated Apoe$^{-/-}$ mice were fed WD: (A) Blood blucose and bodyweight measurements (n=15-15) (B) Plasma insulin measurement by ELISA (n=8-7). Data: mean value ± SEM; (n=15-15). *Mann-Whitney U*Test. *P≤ 0.05, **P≤ 0.01, ***P≤ 0.001, ns = non-significant.

4.1.3 Analysis of Atherosclerotic Lesion Formation in PERK Kinase Inhibited Apoe $^{-/-}$ Mice

To evaluate the effect of GSK2606414 plaque development, I analyzed en face aorta preparations as well as aortic root cryosections from GSK2606414- or DMSO-(control) treated Apoe$^{-/-}$ mice on WD. En face aorta were analyzed after staining lipids with SUDAN IV. As expected from previous studies, lipid plaques were mainly located to artery branching areas on the aorta and near the aortic root connecting to the heart (282). GSK2606414 administration effectively reduced SUDAN IV-stained plaque area (44%) when compared to the control mice (Figure 4.3 A).

Aortic sinus is located at the artic root area. According to the literature, most of the atherosclerotic lesions present in mice are located at the aortic sinus and extend throughout the ascending aorta The aortic sinus can be analyzed from multiple, serial sections after immunofluorescent or immunohistochemical staining for lipids (301,302).

Using four serial sections that are 7 μM thick and 60μM apart from each other, I analyzed the aortic sinuses of GSK2606414-treated and control mice by first staining with Oil RedO stain for visualizing the lipid accumulation in foamy macrophages. After staining, I calculated the total Oil RedO-stained area from these two groups. There was a significant reduction in foam cell area of atherosclerotic Apoe$^{-/-}$ mice in the GSK2606414-administered group when compared to the control group (Figure 4.3 C). I also analyzed the total lesion area and the necrotic core areas from the aortic sinuses of same mice after hematoxylin and eosin (H&E) staining of the aortic root cryosections. I observed a reduction in both total lesion area and the necrotic core area in GSK2606414-administered mice when compared to the control mice (Figure 4.3 B&D).

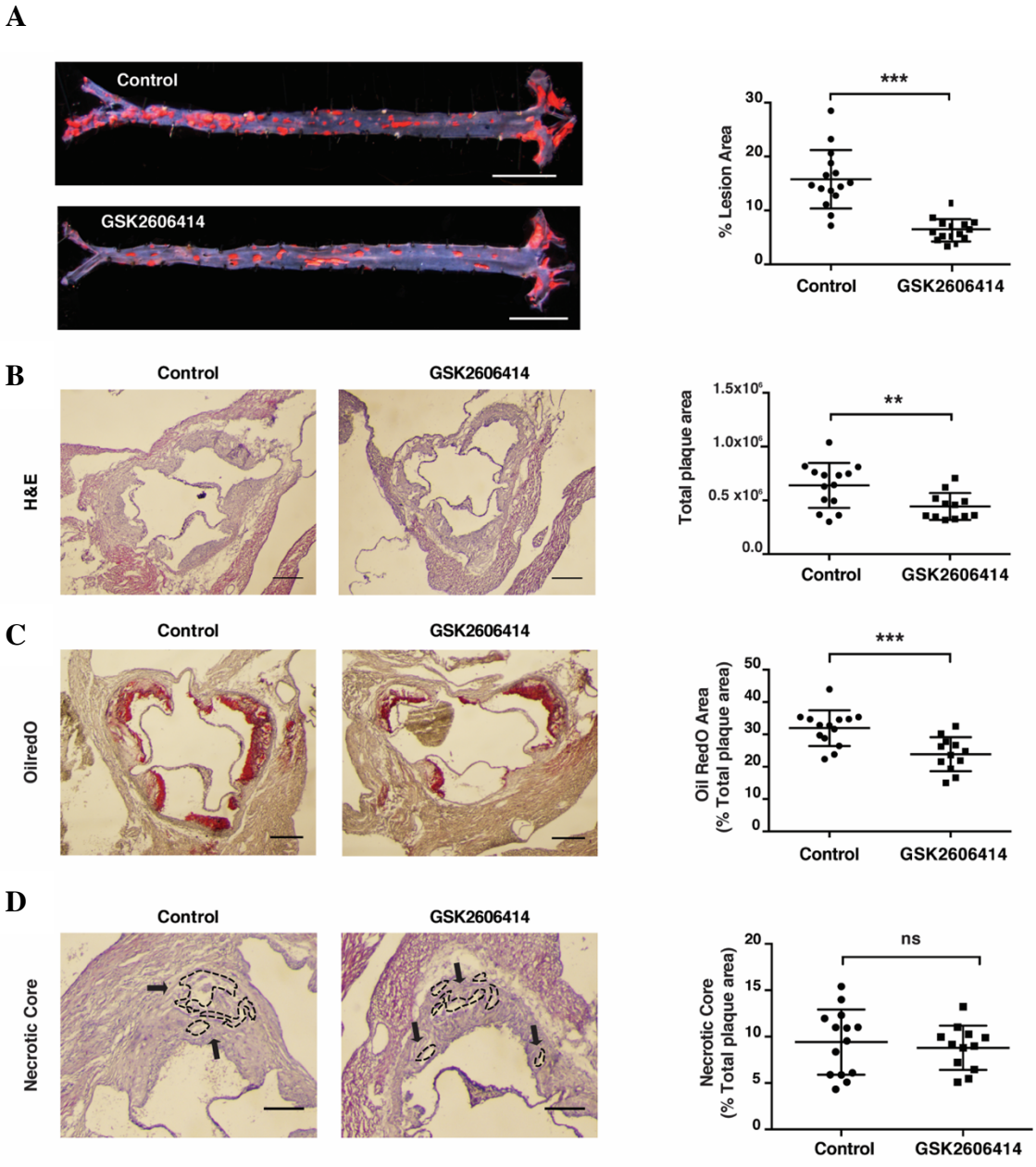

Figure 4.3. PERK inhibition leads to reduction in atherosclerotic plaque formation *in vivo*. 30 mg/kg/day GSK2606414-administered Apoe$^{-/-}$ mice were fed with WD: (A) Lesion area was calculated from en face aorta preparations that were stained with Sudan IV (n=15-15; scale bar: 5 mm). (B) Total plaque area was calculated from H&E-stained aortic root lesions. (C) Foam cell area was calculated from Oil RedO stained aortic root sections. (D) Necrotic area was calculated from H&E-stained aortic root sections (n=14-12, scale bar: 300 μm). Data: Data are means ± SEM. *Mann-Whitney U* Test *P≤ 0.05, **P≤ 0.01, ***P≤ 0.001, ns = non-significant.

4.1.4 The Impact of PERK Inhibition on Atherosclerotic Plaque Cellular Composition

Atheroslerotic lesions contain a variet of cell types that play important roles in plaque development, progression and rupture. These include endothelial cells, vascular smooth muscle cells (VSMC), and immune cells such as macrophages, dentritic cells and T and B lymphocytes. These cells secrete a variety of immune-modulatory proteins including cytokines, which can be detected in lesion area (303). In the previous sections, I showed that GSK2606414 has a s significant impact on macrophage inflammatory responses as wells as atherosclerotic lesion area and foam cell accumulation *in vivo*. Therefore, I next analyze the plaques to determine PERK's impact on cellular composition during atherosclerosis development.

4.1.4.1 Analysis of Aortic Sinuses for P-eIF2α and LONP1 Axis

As previously described, GSK2606414 is kinase inhibitor of PERK and as a consequence of this inhibition, eIF2α phosphorylation is blocked. I first confirmed the impact of PERK kinase inhibitor on the plaque cells by analyzing eIF2α phosphorylation. I analyzed aortic root cryosections that were obtained from GSK2606414- or DMSO-treated $Apoe^{-/-}$ mice (fed with WD) after immunohistochemical staining with a specific antibody for phosphorylated-e)F2α (P-eIF2α) and macrophages (MOMA2). The analysis of P-eIF2α (green) signal in macrophage-enriched areas (MOMA-2 stained; red) showed that GSK2606414 significantly reduced P-eIF2α levels when compared to control animals (Figure 4.4.A). This finding thus confirmed the effective silencing of PERK kinase activity in plaque cells.

Next, I decided to analyze LONP1 expression in the aortic sinus macrophages as I previously showed in the earlier sections to be suppressed by GSK2606414 treatment in lipid-stressed macrophages. Aortic root cryosections were stained with a specific antibody against LONP1 (green) in the macrophage positive area (stained with MOMA-2; red). The analysis revealed GSK2606414 significantly reduced LONP1 expression in macrophages and in correlation with my previous *in vitro* findings.

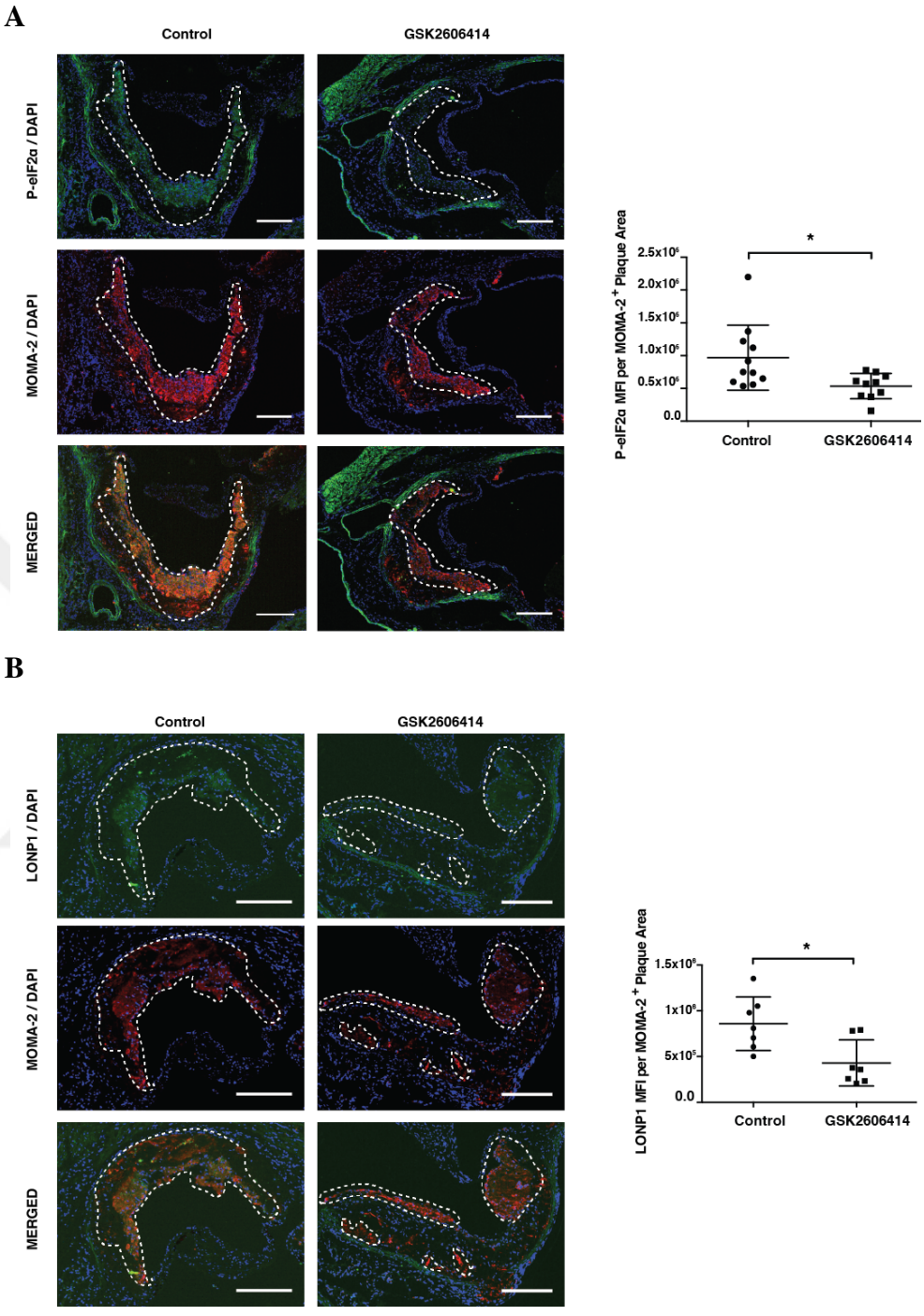

Figure 4.4. Loss of PERK kinase activity reduces of p-eIF2α and LONP1 levels in Apoe$^{-/-}$ mice *in vivo*. Immunohistochemical analysis of aortic root cryosections from 30mg/kg/day GSK2606414 injected *Apoe*$^{-/-}$ vs DMSO injected control mice. For each figure, quantifications are at the right of the representative figures. (A) P-eIF2α staining (green) quantified in Macrophage positive area (red)(n=7-7) (B) LONP1 staining (green) quantified in Macrophage positive area (red). Data: mean value ± SEM; (n=3). Mann-Whitney U Test *P≤ 0.05, **P≤ 0.01, ***P≤ 0.001. ns means not significant; a.u. means arbitrary units. (Scale bar: 200 μm).

4.1.4.2 Analysis of PERK Kinase Inhibitor's Impact on Macrophage and T Cell Content in the Aortic Sinus Atherosclerotic Plaque Areas

As GSK2606414 treatment reduced atherosclerotic lesion size in Apoe$^{-/-}$ mice that were fed with WD, I next investigated the impact of PERK kinase inhibitor on the immune cell composition in the plaques. Macrophages are the major immune cell type found in plaques. The infiltration of monocytes to the plaque area is the main source of inflammation (201).

To determine whether GSK2606414 effects plaque immune cell composition, I began my analsys by assessint the macrophage-enriched plaque areas in the aortic root cryosections that were stained with a specifica antibody for MOMA-2 (red). I observed GSK2606414 treatment led to a significant reduction in macrophage population in aortic sinus plaque area (Figure 4.5 A). This result is consistent with the reduction in foam cell area that was observed in the previous section (in Figure 4.3 C). Next I sought to determine GSK2606414's impact on plaque T cell composition. By staining the aortic root cryosections with a specific antibody against cluster of differentiation 3 (CD3, green) on T cells, I quantified the CD3 positive cell numbers in plaques. I observed a significant reduction in T cell counts in GSK2606414- vs vehicle-treated Apoe$^{-/-}$ mice on WD (Figure 4.5 B).

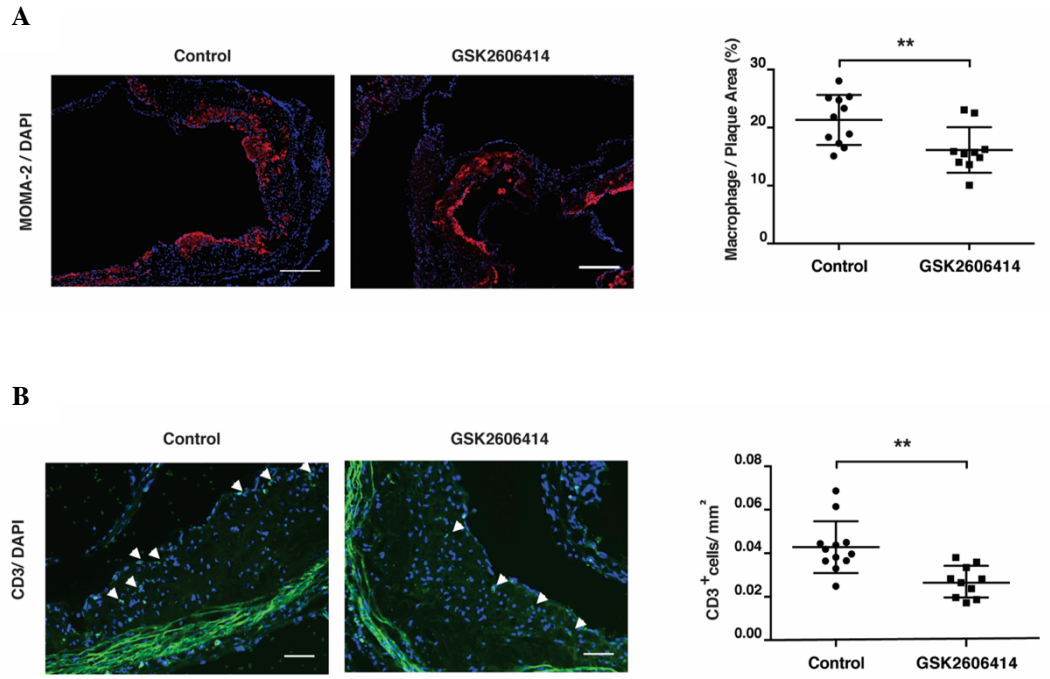

Figure 4.5. Loss of PERK kinase activity mitigates hyperlipidemia induced Immune cell accumulation in Apoe$^{-/-}$ mice. In-vivo Immunohistochemical analysis of aortic root cryosections from 30mg/kg/day GSK2606414 injected *Apoe*$^{-/-}$ vs DMSO injected control mice. For each figure, quantifications are at the right of the representative figures. (A) MOMA-2 staining (red) (n=12-12) (B) CD3 staining (green). Data: mean value ± SEM;. Mann-Whitney U Test *P≤ 0.05, **P≤ 0.01, ***P≤ 0.001. ns means not significant. (Scale bar: 200 μm for A, 50 μmfor B).

4.1.4.3 Analysis of Inflammatory Cytokine levels

After I noted the convincing changes in macrophage and T-cell content in aortic plaque area, I sought to determine PERK kinase inhibitor's impact on inflammatory cytokine secretion in the plaques. Mature IL-1β, an indicator of inflammasome activation, is secreted from the macrophages and is causally associated with plaque progression (201). According to the literature, IL-1β inhibition results in the reduction of atherosclerotic plaques (304). To evaluate if GSK2606414 inhibits IL-1β maturation or caspase-1 cleavage in the plaques, I stained the aortic root sections for mature IL-1β and caspase-1 together with MOMA-2 (for macrophage-enriched area determination). I saw a significant reduction in these inflammasome markers in MOMA2- positive areas of the aortic roots obtained from GSK2606414-treated mice when compared to control mice (Figure 4.6 - 4.7). This reduction of IL-1β and

caspase-1 by GSK2606414 treatment is consistent with this inhibitor's effect in macrophages *in vitro*, as shown in the previous sections (Figure 3.2)

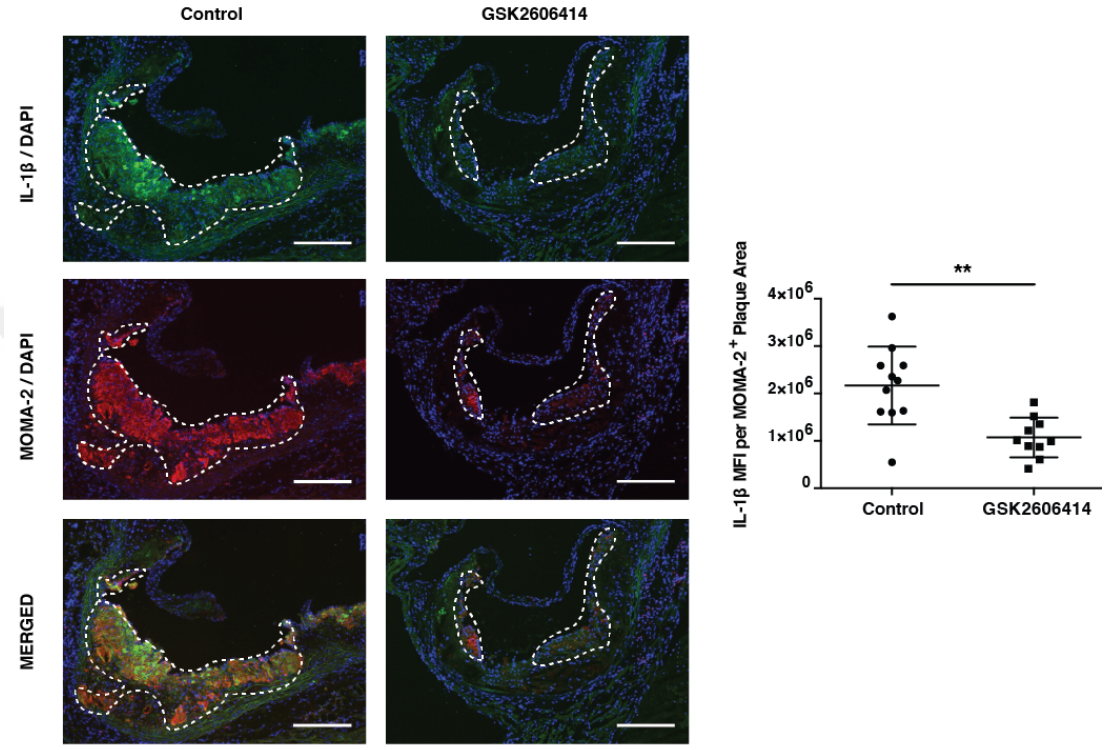

Figure 4.6 Inhibition of PERK kinase activity reduces hyperlipidemia-induced IL-1β production in aortic plaque macrophages. Immunohistochemical analysis of aortic root cryosections from 30mg/kg/day GSK2606414-treated or control mice. Quantification is shown at the right of the representative figure. IL-1β staining (green) quantified from macrophage positive (MOMA2- stained; red) area. (n=11-10) Data: mean value ± SEM;. Mann-Whitney U Test *P≤ 0.05, **P≤ 0.01, ***P≤ 0.001. ns means not significant. (Scale bar: 200 μm).

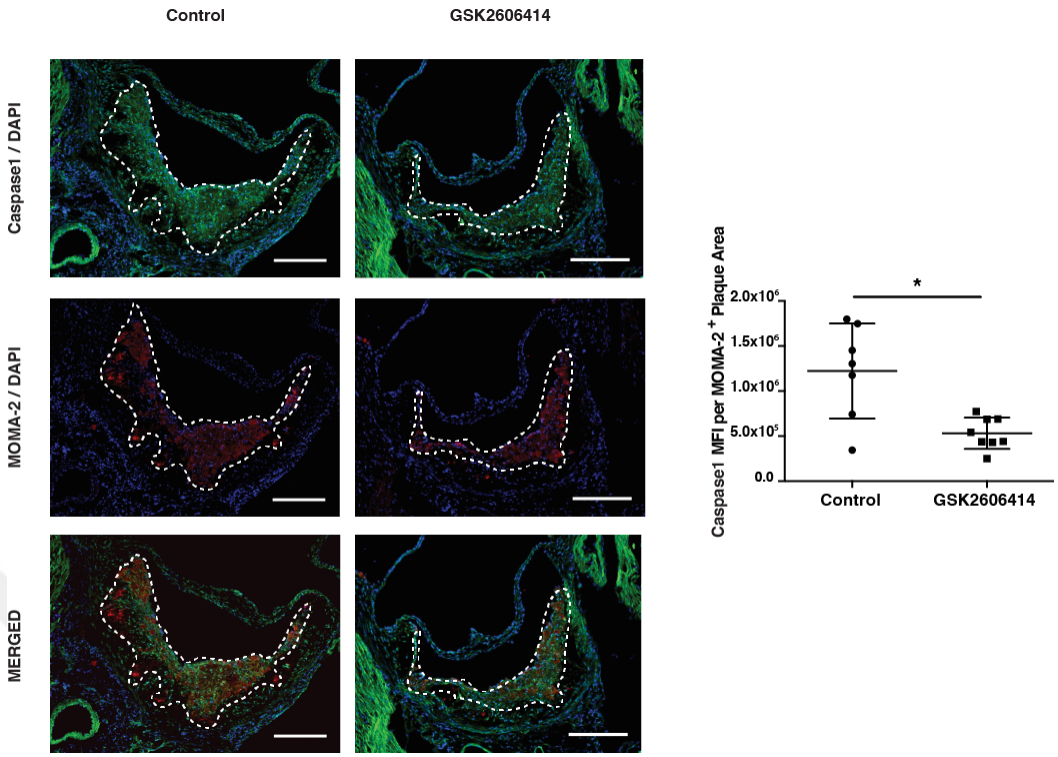

Figure 4.7. Inhibition of PERK kinase activity reduces hyperlipidemia-induced cleaved caspase1 levels in aortic plaque macrophages. Immunohistochemical analysis of the aortic root cryosections from 30mg/kg/day GSK2606414-treated and control mice. Quantification is shown at the right of the representative figure. Caspase-1 (FAM/FLICA) staining (green) quantified from macrophage positive (red) area. (n=7-8) Data: mean value ± SEM;. Mann-Whitney U Test *P≤ 0.05, **P≤ 0.01, ***P≤ 0.001. ns means not significant. (Scale bar: 200 μm).

Because I saw these significant reductions in plaque inflammatory cells, IL-1β and cleaved caspase1, next, I analyzed systemic inflammatory cytokine levels. GSK2606414-treated mice displayed significantly lower IL-18, monocyte chemoattractant protein 1(MCP1) and interferon gamma (IFNγ) concentrations in the plasma (Figure 4.8 A-C). Furthermore, assessment of the plaque mRNA demonstrated reduced TNFα and MCP1 mRNA but not IL-1β mRNA in inhibitor-treated mice when compared to control Apoe$^{-/-}$ mice on western diet (Figure 4.8 D-F). Taken together, these results show that GSK2606414 not only reduces lipid-induced inflammatory cell content and cytokine levels in the plaque area, but also systemically. These findings also demonstrate that the suppression of IL-1β is at the transcript level.

Next, I analyzed aortic plaque area stained with vascular cell adhesion protein 1 (VCAM-1), which show a significant reduction in GSK2606414-treated lesions when compared to lesiosn from the control mice (Figure 4.9 A). Finally, I assessed macrophage apoptosis in the cryosections by staining with the TUNEL assay kit. Importantly, there were no significant changes in the apoptotic cell numbers in the aortic root cryosections from the inhibitor-treated mice (Figure 4.9.B). This finding suggests the reduced macrophage counts by inhibitor treatment is not a result of macrophage death and is consistent with no changes detected regarding the necrotic core area in the same mice (Figure 4.3. D).

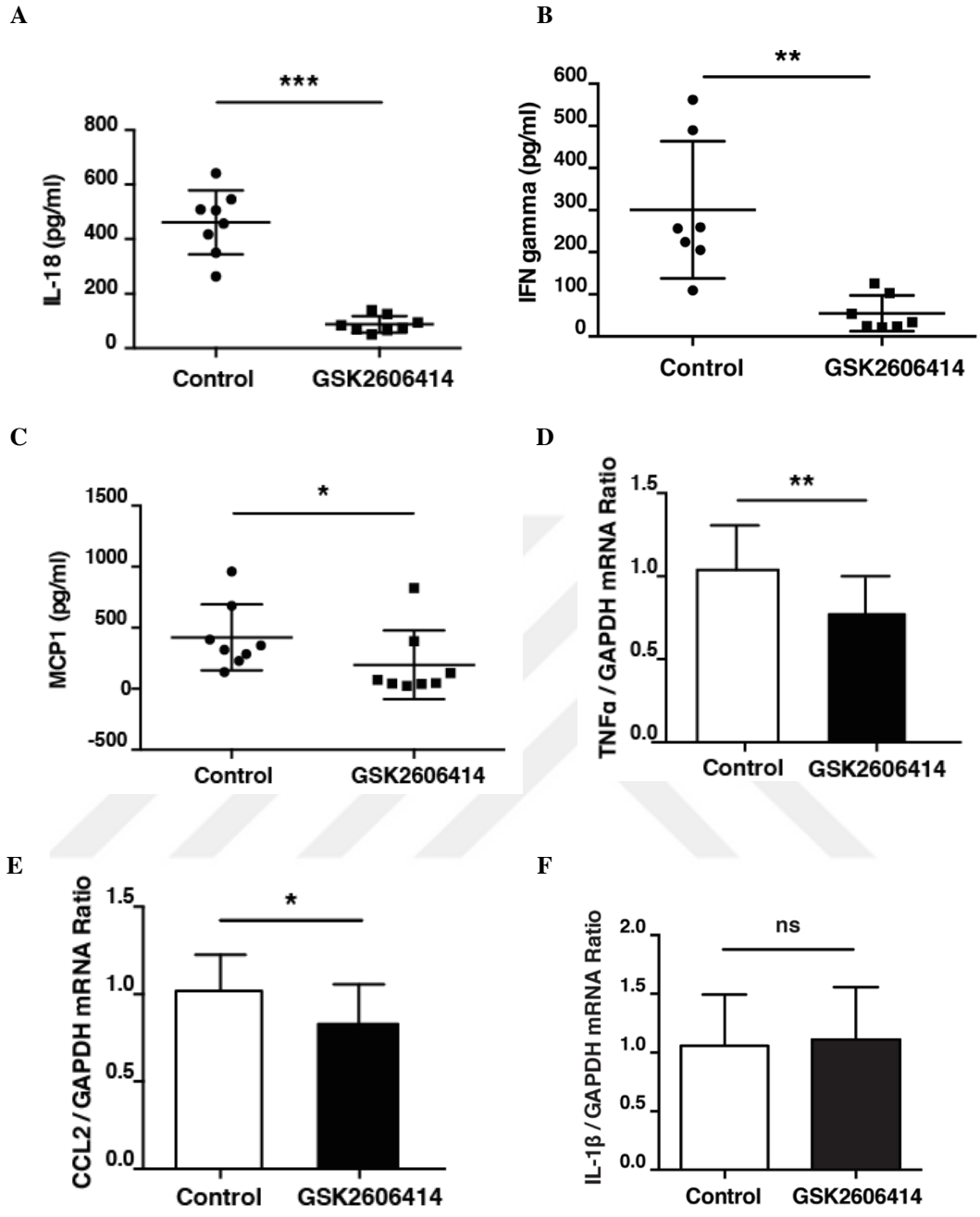

Figure 4.8. Inhibition of PERK kinase activity suppresses hyperlipidemia-indued cytokine levels in the Apoe$^{-/-}$ mice on WD. (A-C) Serum cytokine levels was measured with ELISA: (A) IL-18 (n=8-8), (B) IFNγ (n=7-7), (C) MCP1(n=8-8). (D-F) RNA lysates from aortic root plaques were analyzed with qRT-PCR for (D) TNFα (n=14-12), (E) CCL2 (n=14-12), (F) IL-1β (n=14-12). Data: mean value ± SEM;. Mann-Whitney U Test *P≤ 0.05, **P≤ 0.01, ***P≤ 0.001. ns means not significant.

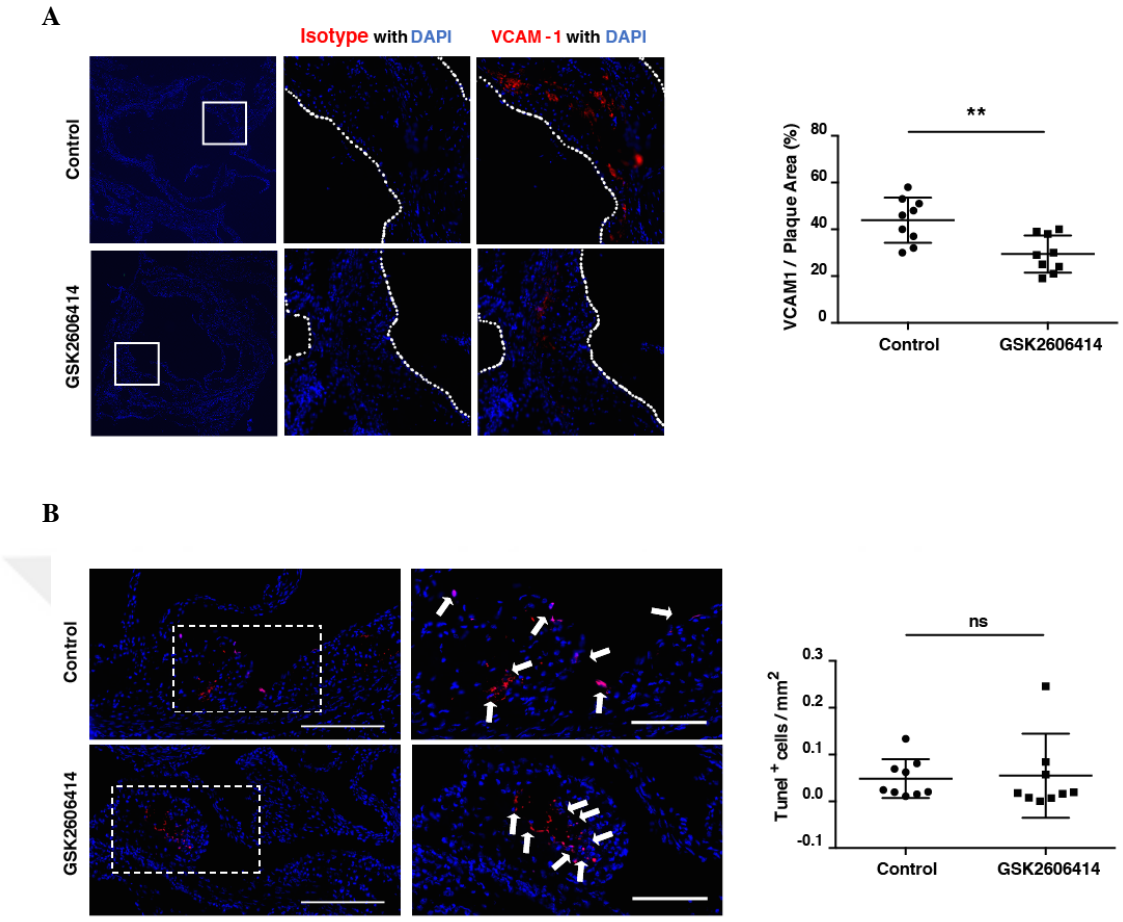

Figure 4.9. Analysis of VCAM-1 and Cell Death in Plaques from PERK Kinase-inhibited Apoe$^{-/-}$ Mice. Aortic root plaque cryosections were stained with: (A) VCAM-1 antibody (red; n=9-9). (B) Tunel assay (red; n=9-8) Data: mean value ± SEM;. Mann-Whitney U Test *P≤ 0.05, **P≤ 0.01, ***P≤ 0.001, ns means not significant. (scale bar: A,100μM; B, 50μM)

4.1.4.4 PERK Kinase Inhibitor's Impact on Aortic Plaque Collagen Content

Vascular smooth muscle cells (VSCMc),migrate towards the lesion area and secrete collagen to seal up the plaque with a 'fibrous cap' that makes the plaque less vulnerable to shear stress caused by blood flow (213). The plaque vulnerability is impacted directly by the amount and function of the infiltrated VSMCs . That is why I sought to assess if GSK2606414 has a significant effect on VSMC infilatration or collagen secretion into the plaques.

First, the aortic root sections were stained for vascular smooth muscle actin (α-sma) to assess the changes in vascular smooth muscle cell. This analysis showed no significant changes by the GSK2606414 treatment (Figure 4.10.A). Then, the aortic root sections were stained with Masson's Trichrome, which stains for collagen. Once again, I observed no significant changes in plaque collagen amount after GSK2606414 treatement (Figure 4.10.B). These results show that neither the amount of smooth muscle cells nor collagen content of the plauques is altered by GSK2606414 treatment and that plaque inflammation is the main target for GSK2606414.

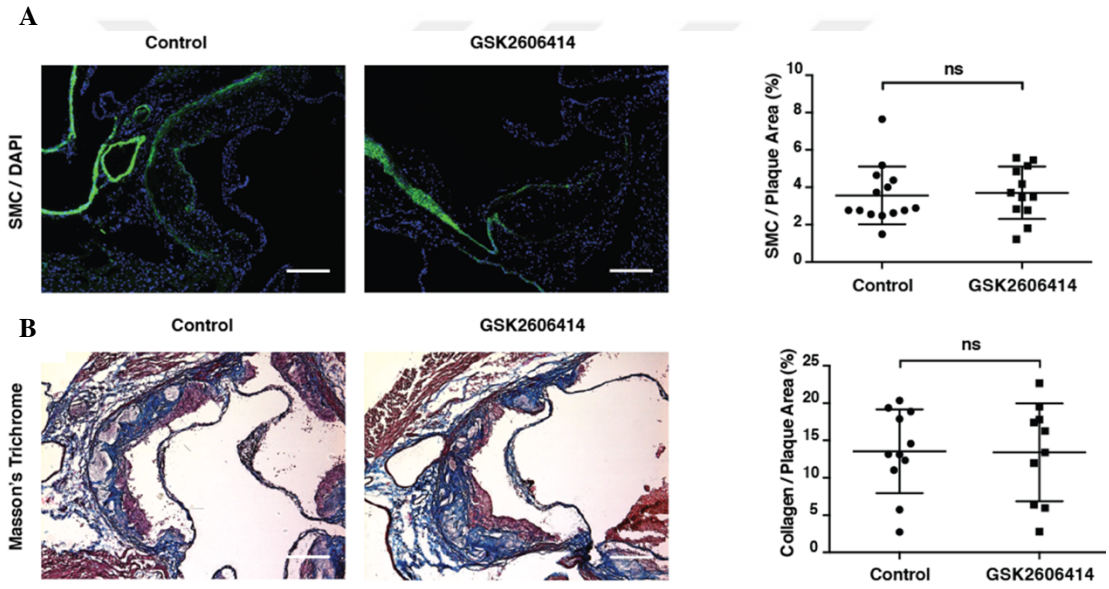

Figure 4.10. Loss of Perk kinase activity does not affect smooth muscle cell migration or collagen secretion. Immunohistochemical analysis of aortic root cryosections from 30mg/kg/day GSK2606414 injected *Apoe*$^{-/-}$ vs DMSO injected control mice. For each figure, quantifications are at the right of the representative figures. (A) α-sma staining (green) (n=12-12) (B) Masson's Trichrome staining (n=12-12). Data: mean value ± SEM; Mann-Whitney U Test *P≤ 0.05, **P≤ 0.01, ***P≤ 0.001. ns means not significant. (Scale bar: 200 μm).

4.1.5 PERK Kinase Inhibitor's Impact on Inflammatory Cell Numbers in the Circulation

Findings in the preivous sections showed that GSK2606414 treatment leads to significant reductions in inflammatory cells in plaques and inflammatory cytokines in both plaques and the circulation (Figure 4.9 B). These findings demonstrate a key target of the PERK kinase inhibitor is hyperlipidemia-induced inflammation. Next, I examined whether this marked effect is related to potential changes in immune cell numbers. According to the results shown in Figure 4.11, there were no changes in the major inflammatory cell types between inhibitor- and vehicle-treated mice. Therefore, the changes in serum and plaque cytokine levels are independent of systemic effects of the PERK kinase inhibitor on inflammatory cell counts in these mice.

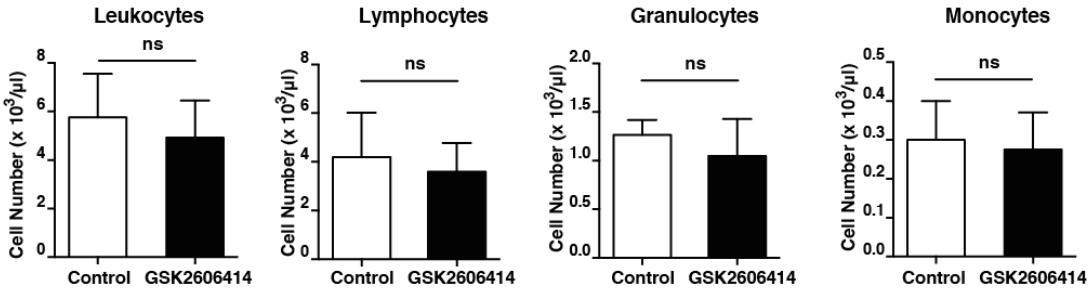

Figure 4.11. Loss of Perk kinase activity does not affect numbers of immune cells in bloodstream. Blood immune cells were counted in 30mg/kg/day GSK2606414 or vehicle treated Apoe$^{-/-}$ mice in Western Diet. Data: mean value ± SEM; Mann-Whitney U Test *P≤ 0.05, **P≤ 0.01, ***P≤ 0.001. ns means not significant.

4.1.6 The Impact of PERK Kinase Inhibitor on T Lymphocytes in the $^{Apoe-/-}$ Mice Fed with Western Diet

T helper cell response is important for atherosclerosis progression. Th1 and Th17 cells are reported to be pro-atherogenic whereas Th2 response is considered anti-atherogenic (305). These cells infiltrate to atherosclerotic lesion area to modulate plaque inflammatory responses. The majority of T helper cells in atherosclerotic lesions are Th1 type cells, known to produce interferon gamma (IFNγ). IFNγ cytokine

production is important for activation of monocytes and macrophages that infiltrate the lesion area. Also, IFNγ reduces the fibrous cap thickness and consequently, reduce plaque stability (222,306). Inflammatory cytokines such as IL-18 and IL-1β can impact T helper cell polarization (307). As GSK2606414 alters these cytokines levels, I sought to analyze the Th cell response more closely. For this, I collected mouse spleens to generate fresh splenocytes and compare the Th cell subpopulation counts (via flow cytometry) in GSK2606414-treated and control Apoe-/- mice that were fed with WD. Consistent with anti-inflammatory effects of GSK2606414 in the previous sections of this thesis, I saw a significant reduction in Th1 and Th17 subpopulation and the secreted cytokines IFNγ and IL-17A, respectively. On the other hand, increase the Th2-secreted IL-4 cytokine was detected in GSK2606414-treated mice when compared to control mice. Collectively, these results demonstrate that PERK kinase activity regulates hyperlipidemia-induced Th cell differentiation (Figure 4.12).

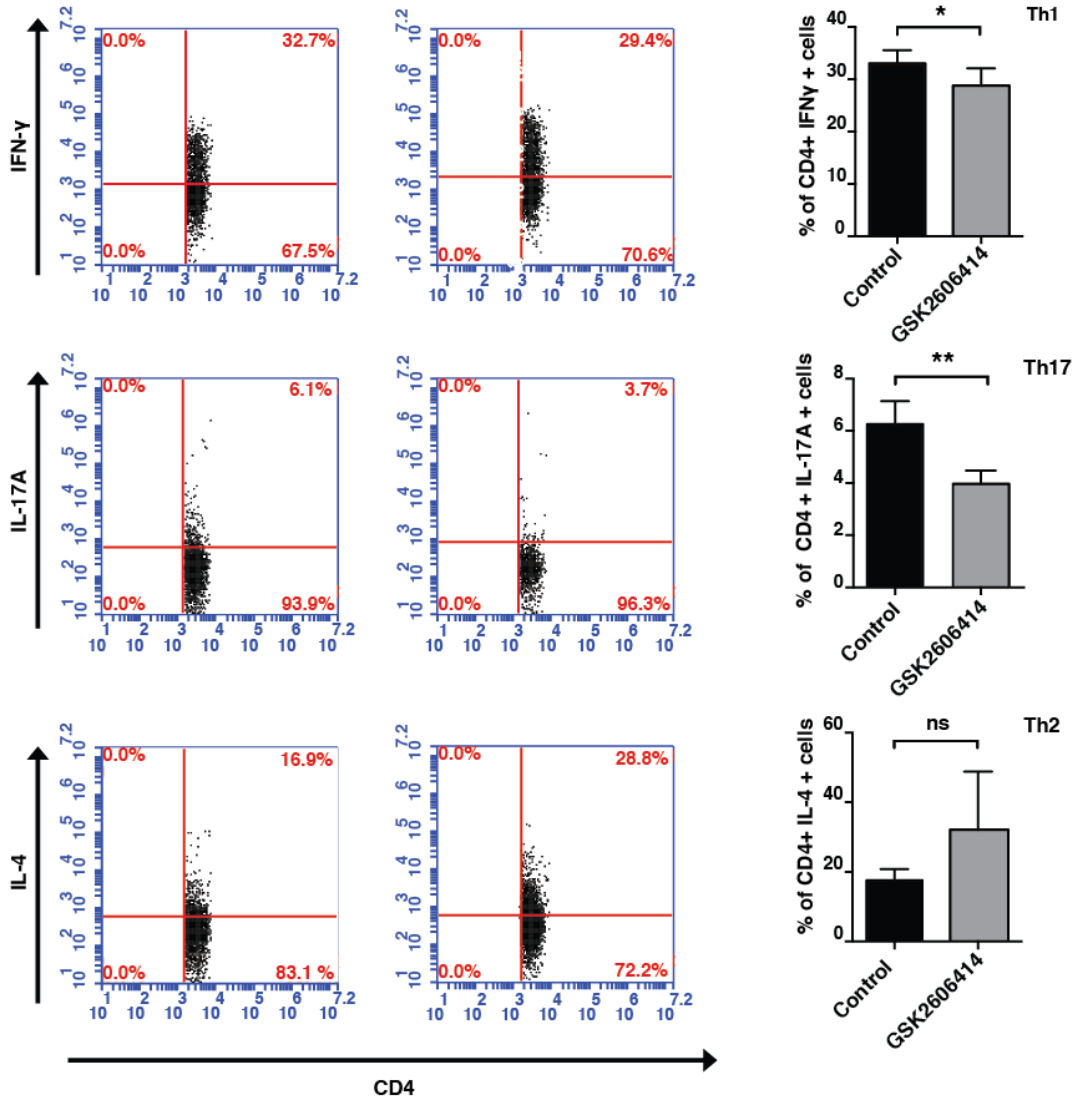

Figure 4.12. Inhibition of PERK kinase activity impacts Th lymphocyte differentiation induced by hyperlipidemia in Apoe$^{-/-}$. Flow cytometry analysis of IFNγ (Th1), IL-17 (Th17), IL-4 (Th2) levels in splenocytes stimulated with parathoxyamphetamine/ionomycin (n=5, 5). Data are mean ± SEM; unpaired two-tailed Student's t test. *P≤ 0.05, **P≤ 0.01, ***P≤ 0.001. ns means not significant

4.1.7 The Impact of PERK Kinase Inhibitor on Lipoprotein Profiles of Apoe$^{-/-}$ Mice Fed with Western Diet

Increased lipid levels in bloodstream especially lipid-loaded Low Density Lipoprotein (LDL), is associated with the progression of atherosclerotic lesions (308). Here, I determined the lipid and lipoprotein profiles of the plasma obtained from the GSK2606414-treated and control Apoe$^{-/-}$ mice fed with WD. The lipid and lipoprotein

profiles, analyzed by fast protein liquid chromatography (FPLC), did not show any significant changes in total cholesterol (Figure 4.13 A), total triglyceride (Figure 4.13 B), lipoprotein class distribution or lipoprotein cholesterol and triglyceride content (Figure 4.13 C&D). These results show the impact of GSK2606414 on atherosclerosis is not a result of improved lipoprotein profiles. Collectively, my findings strongly suggest that inhibition of PERK kinase activity with GSK2606414 reduces atherosclerosis by suppressing hyperlipidemia-induced inflammation.

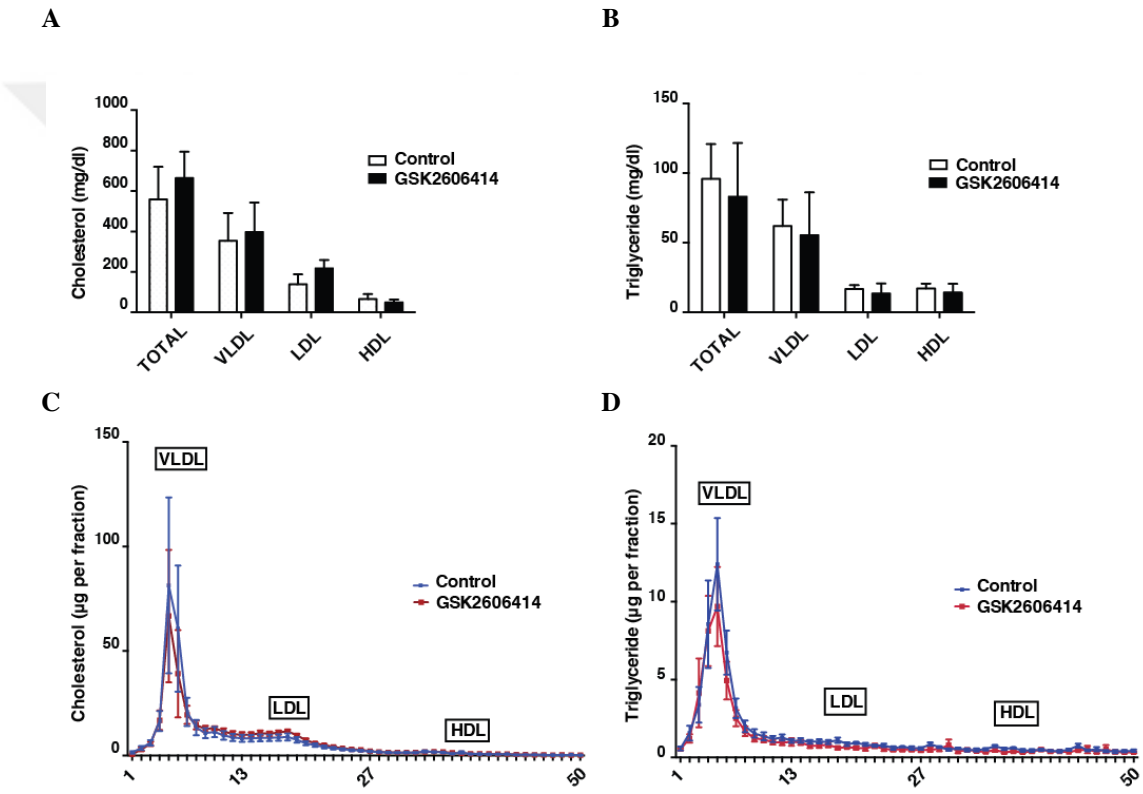

Figure 4.13. Plasma Lipid and Lipoprotein Profiles from 30mg/kg/day GSK2606414-treated and control Apoe$^{-/-}$ mice. (A) Total plasma cholesterol and lipoprotein (VLDL, LDL, HDL) cholesterol levels, (B) Total plasma trigyceride and lipoprotein (VLDL, LDL, HDL) triglyceride levels. (C-D) Lipoprotein profiles for in vehicle (blue) and GSK2606414 (red) treated mice: (C) cholesterol and (D) trigyceride content. Data are represented as means ± SEM; (n=5) by two-tailed student's *t* test. *P≤ 0.05, **P≤ 0.01, ***P≤ 0.001. ns means not significant.

4.1.8 Analysis of Aortic Lesion Progression in PERK Kinase Inhibitor-Treated Mice

The results of my experiments have shown a marked impact of PERK kinase inhibition on atherosclerotic plaque formation. Furthermore, the reduction in atherosclerotic plaques is related to reduced inflammation in these mice. To understand whether treatment with GSK2606414 inhibits progression, a group of mice were sacrificed at 12 weeks of WD, while two other groups were kept on WD for 4 more weeks (total WD duration of 16 weeks). The latter group of mice were either injected with GSK2606414 or vehicle. In comparision to the 12 weeks diet group, further WD led to increase in lesion size whereas GSK2606414 administration blocked the further progression of atherosclerotic lesion formation but did not reduce lesion size compared to the 12 weeks WD group (4.14 A&B). These findings suggest PERK kinase inhibition prevents atherosclerosis progression but does not cause its regression.

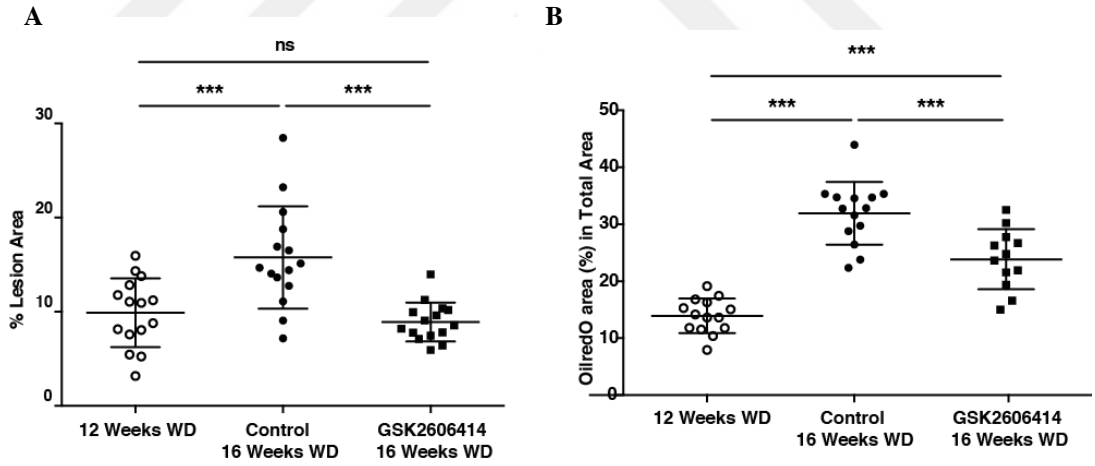

Figure 4.14. The impact of PERK kinase inhibitior on atherosclerosis progression. (A) % Lesion area is compared in the Sudan IV- stained aortas of Apoe-/- mice fed with WD for 12 or 16 weeks and treated with 30mg/kg/day GSK2606414 or vehicle (n=15-15-15) (B) From the same mice in A, % foam cell area is determined by staining the aortic root sections with Oil redO (n=14-14-12). Data are represented as means ± SEM; by *Mann-Whitney U* test. *P≤ 0.05, **P≤ 0.01, ***P≤ 0.001. ns means not significant.

4.2 Modulating ATP Analog-Sensitive Kinase Allele of PERK *In Vivo*

Findings in the previous section demonstrate inhibition of PERK kinase activity by a small molecule inhibitor, GSK260641, can reduce the atherosclerosis development. However, nonspecific effects have been attribute to GSK2606414 (309), Therefore, I sough to use a complementary approach to show PERK kinase activity plays a critical role in atherogenesis. For this, I used PERKASKA mice that were bred to homozygosity wit the Apoe$^{-/-}$ (Apoe$^{-/-}$ - Eif2αk3$^{tm2201(G646N,M886A)Arte}$). Treatment of these mice with a bulky ATP analog inhibitor such as 4-Amino-1- tert-butyl-3-(1′-naphthyl)pyrazolo[3,4-d]pyrimidine(1-NAPP1) is expected to bind an inhibit only the mutant allele of PERK. In other words, 1-NAPP1 is expected to bind to the slightly enlarged ATP binding cavity of PERK kinase kinase as explained before in this thesis. This in turn provides an alternative and specific way to modulate PERK kinase activity *in vivo* (310).

4.2.1 General Study design and Correlation of The Efficacy of 1-NAPP1 *In Vivo*

Because the excess usage of 1-NAPP1 can inhibit normal kinase, I sought to determine the effective and selective dose of 1-NAPP1 that inhibits mutant PERK allele. For this purpose, I utilized both Apoe$^{-/-}$ and Apoe$^{-/-}$ - Eif2αk3$^{tm2201(G646N,M886A)Arte}$ mice (ASKA, Apoe$^{-/-}$)_ side by side in my experiments. These mice were subjected to 14 weeks of WD and in the last 4 weeks of diet, the mice were treated with 60 mg/kg/day 1-NAPP1 (in 20 % Cremophor-EL-Saline solution) by intraperitoneal injection, The delivery method of the drug as well as the dosage was determined according to the previous studies that used 1-NAPP1 *in vivo*.

The general study design is provided in Figure 4.15 A and B. In figure 4.15 C, I assessed the phosphorylation status of eIF2α in conjunction with total eIF2α levels and actin levels. Inhibitiono of eIF2α phosphorylation was onbserved in the ASKA, Apoe$^{-/-}$ mice by 1-NAPP1, confirming efficient silencing of PERK pathway. Importantly, 60 mg/kg/day 1-NAPP1, did not reduce P-eIF2α levels in Apoe$^{-/-}$ mice, bearing a wild type copy of PERK.

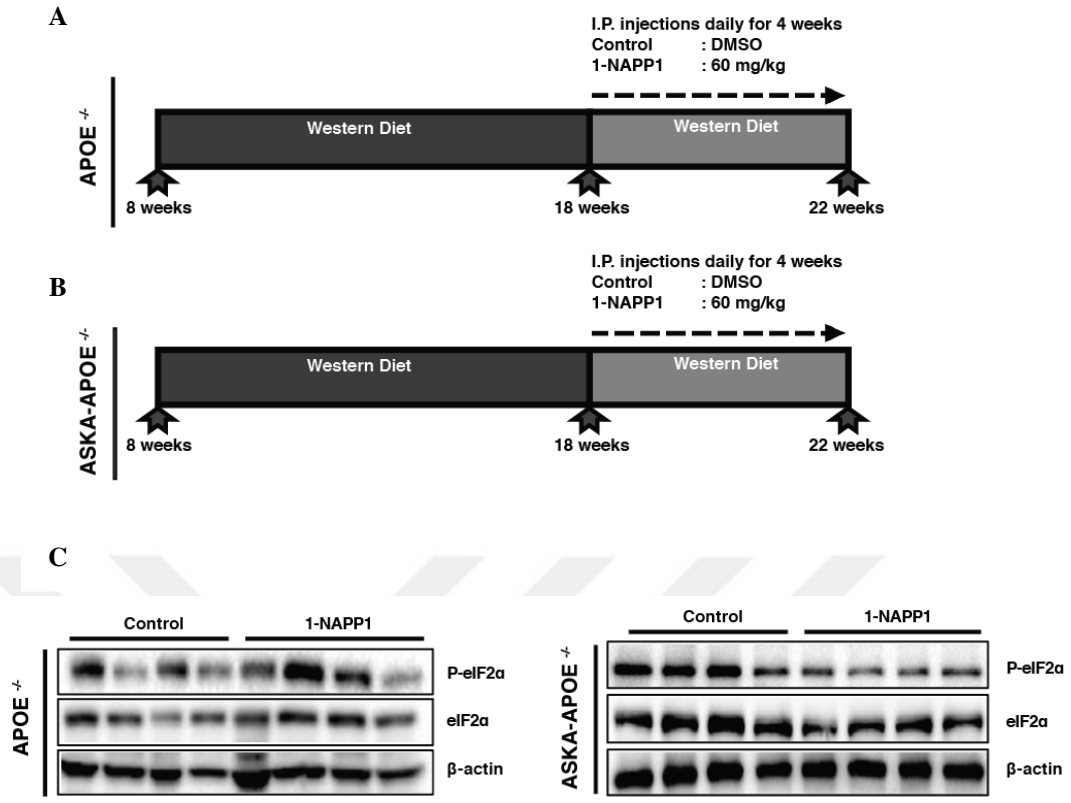

Figure 4.15. Experimental Design for Monospecific Inhibition of ASKA mutant *in vivo* during atherosclerosis development. (A) Experimental design and the time course for 60mg/kg/day 1-NAPP1 administration *in vivo* to Apoe$^{-/-}$ and ASKA- Apoe$^{-/-}$mice. (B) Pancreatic protein extracts were analyzed P-PERK, total PERK and actin levels bu Western blotting using specific antibodies for these proteins. (n=8-9 for Apoe$^{-/-}$ and 12-12 for ASKA-Apoe$^{-/-}$ mice)

4.2.2 Analysis of bodyweight, blood glucose

Despite reported unwanted side effects of GSK2606414 on bodyweight (Figure 4.2 A), there was no significant changes in terms of blood glucose or bodyweight by 1-NAPP1 treatement in either ASKA, Apoe$^{-/-}$ or Apoe$^{-/-}$ mice fed with WD. These results suggest that 1-NAPP1 administration at the dosage used in this thesis inhibits PERK kinase activity without systemic metabolic side effects. (Figure 4.2 vs Figure 4.15)

A

	Variables	Treatment	Control	1-NAPP1
APOE $^{-/-}$	n		8	9
	Bodyweight(g)	Before	35,13 ± 1,172	33,44 ± 1,425
		After	36,50 ± 1,000	34,11 ± 1,419
	Glucose(mg/dl)	Before	70,00 ± 5,007	74,22 ± 4,425
		After	75,50 ± 6,044	82,44 ± 6,803

B

	Variables	Treatment	Control	1-NAPP1
ASKA-Apoe $^{-/-}$	n		12	12
	Bodyweight(g)	Before	35,08 ± 1,294	33,58 ± 2,207
		After	34,50 ± 1,384	32,92 ± 2,155
	Glucose(mg/dl)	Before	68,00 ± 2,290	65,00 ± 2,964
		After	74,92 ± 4,490	72,00 ± 2,839

Figure 4.16. Bodyweight and glucose levels in 60mg/kg/day 1-NAPP1 injected Apoe$^{-/-}$ (control) vs ASKA-Apoe$^{-/-}$ mice *in vivo*. (A) Bodyweight and glucose changes of 1-NAPP1 injected Apoe$^{-/-}$ (control) (B) Bodyweight and glucose changes of 1-NAPP1 injected ASKA, Apoe$^{-/-}$ - mice. Data: mean value ± SEM; (n=3). Student's t-test. *P≤ 0.05, ** P≤ 0.01,***P≤ 0.001, ns = non-significant.

4.2.3 The Impact of PERK ASKA Kinase Inhibition by 1-NAPP1 on Atherosclerotic Plaque Development

The analysis of en face aorta preparations from Apoe$^{-/-}$ mice fed with WD and treated with 1-NAPP1 or DMSO administration demonstrated 1- NAPP1 administration did not cause any changes in plaque area in en face aorta preparations (Figure 4.17 A) or foamy macrophage accumulation (Figure 4.17 B) and the total plaque area (Figure 4.17 B) in the aortic root cryosections.

Next, I analyzed en face aorta preparations from 1-NAPP1- or DMSO-treated (control) ASKA-Apoe$^{-/-}$ mice fed with WD. Plaque area in en face aorta preparations were reduced significantly in 1-NAPP1-treated group when compared to DMSO-treated mice (Figure 4.18 A). Analysis of the aortic root cryosections further showed the lipid rich, foam cell area was reduced in the NAPP1-treated mice when compared to control mice (Figure 4.18 B), However, there was no change in the total plaque area of the 1-NAPP1-treated ASKA, Apoe$^{-/-}$ mice (Figure 4.18 C). These results confirm that inactivation of PERK kinase activity reduces atherosclerotic plaque formation.

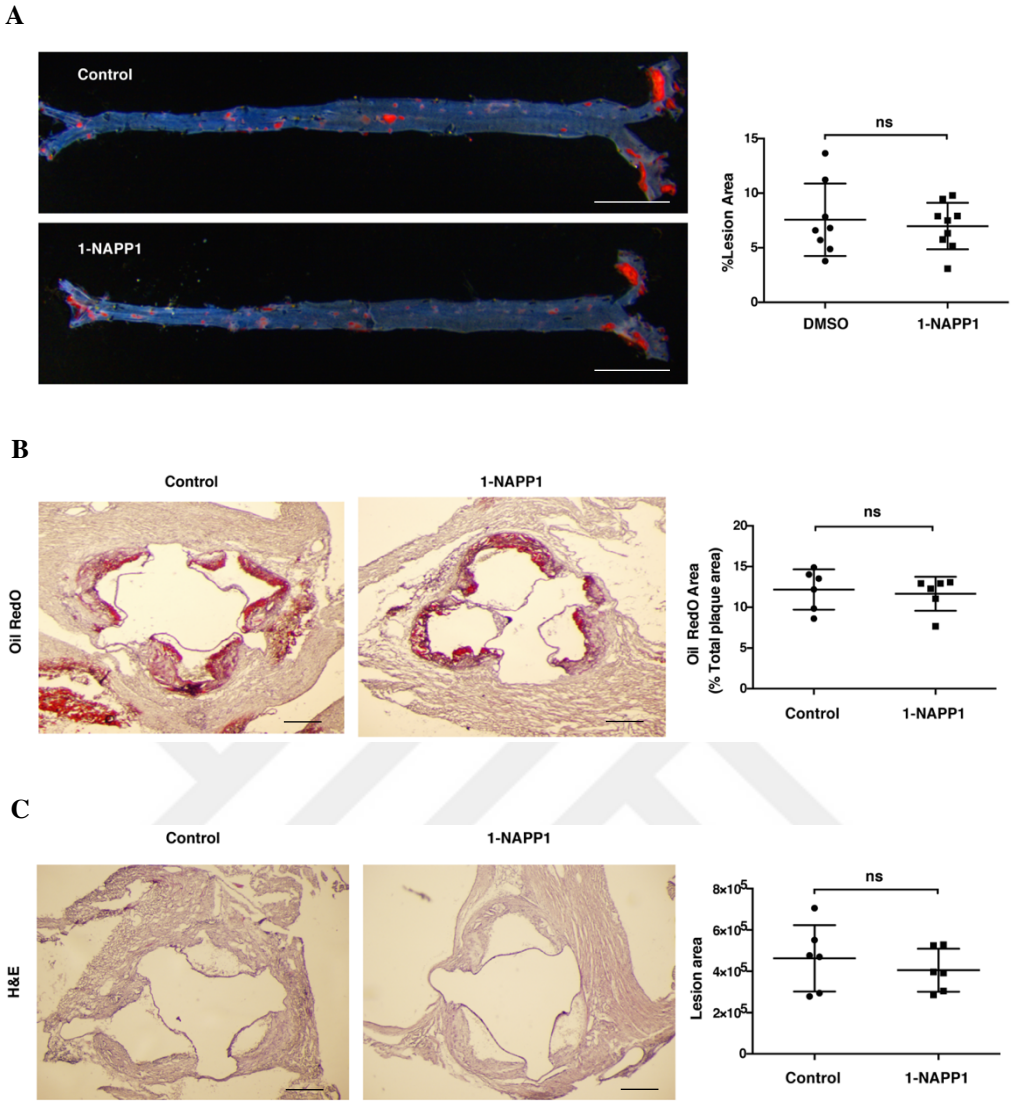

Figure 4.17. 1-NAPP1 Does Not Effect Atherosclerorsis in Control Apoe$^{-/-}$ mice. 1-NAPP1 (60 mg/kg/day) was administered to Apoe$^{-/-}$ while on WD: (A) Lesion area was calculated from en face aorta preparations stained with Sudan IV (n=9-8; scale bar: 5 mm). (B) Foam cell area was calculated from Oil RedO stained aortic root sections. (C) Total plaque area was calculated from H&E stained aortic root lesions. (n=9-8, scale bar: 300 μm). Data: Data are means ± SEM. Mann-Whithney U Test *P≤ 0.05, **P≤ 0.01, ***P≤ 0.001,ns = non-significant.

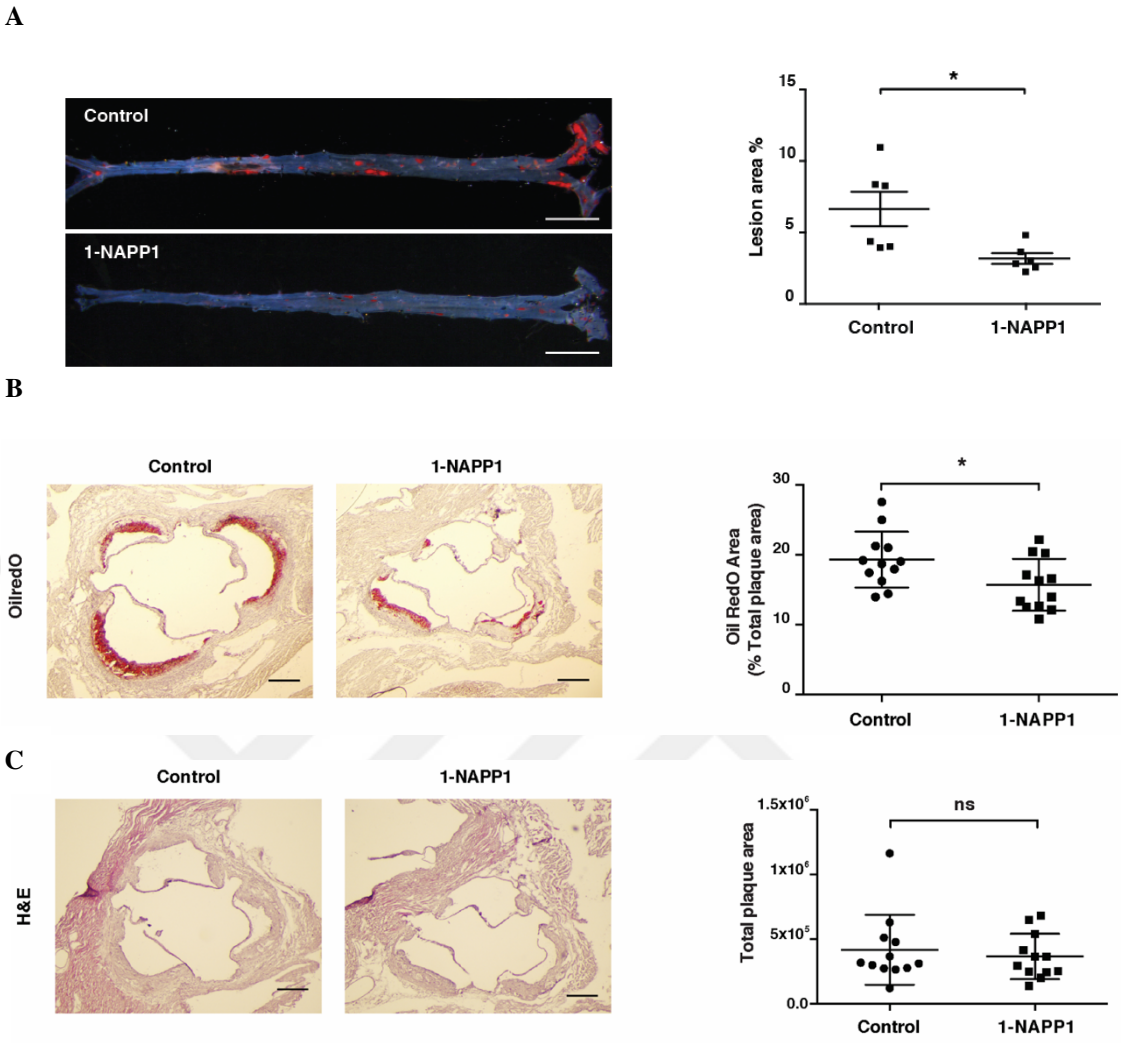

Figure 4.18. 1-NAPP1 administration to ASKA-Apoe$^{-/-}$ mice reduced atherosclerosis development. 1-NAPP1 (60 mg/kg/day) was administered to ASKA-Apoe$^{-/-}$ mice fed WD: (A) Lesion area was calculated from en face aorta preparations stained with Sudan IV (n=6-6; scale bar: 5 mm). (B) Total plaque area was calculated from H&E stained aortic root lesions. (C) Foam cell area was calculated from Oil RedO stained aortic root sections. (n=12-12, scale bar: 300 μm). Data: Data are means ± SEM. Mann-Whithney U Test *P≤ 0.05, **P≤ 0.01, ***P≤ 0.001, ns = non-significant.

4.2.4 1-NAPP1 Treatment Reduces Stress, Inflammation and Atherosclerosis Progression in the Aortic Roots of ASKA-Apoe$^{-/-}$ mice

As 1-NAPP1 administration impacted PERK kinase activity and atherosclerosis in only the ASKA-Apoe$^{-/-}$ mice but not in the Apoe$^{-/-}$ mice, the analysis of stress and inflammatory signaling and plaque progression was performed only in the ASKA-Apoe$^{-/-}$ mice's aortic root cryosections.

4.2.4.1 Analysis of aortic sinuses for P-eIF2α and LONP1

To analyze eIF2α phosphorylation status, the aortic sinus cryosections from the ASKA-Apoe$^{-/-}$ mice (fed with WD) that were treated with 1-NAPP1 vs DMSO (control) were stained with a specific antibody for P-eIF2α (green). Consistent with the *in vitro* data in macrophages, inhibition of PERK kinase activity with 1-NAPP1 led to a significant reduction in P-eIF2α levels, for which the fluoresenct signal was quantified from within the macrophage-enriched (MOMA-2 stained; red) plaque area (Figure 4.19 A). I also analyzed LONP1, CHOP, ATF3 and ATF4 mRNA expression in the aortic root plaques, in which 1-NAPP1 administration led to significant reductions in all of the genes analyzed and similar to what I had observed with GSK2606414 administration in mice (Figure 4.19 B). Together, these findins confirm PERK-eIF2α signaling regulates lipid-induced LONP1 production in macrophages *in vitro* and atherosclerotic plaque macrophages *in vivo*.

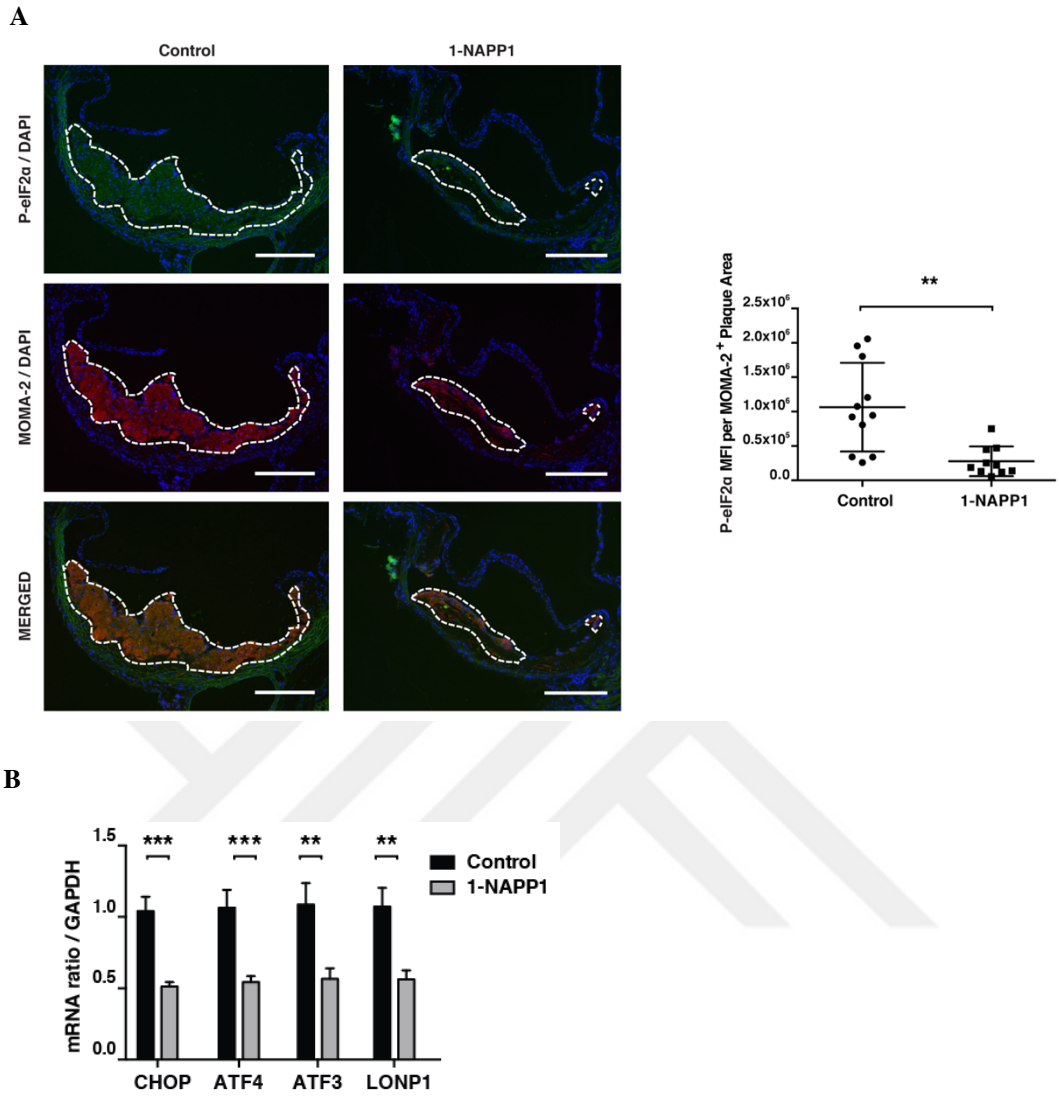

Figure 4.19. PERK kinase activity is critical for hyperlipidemia-induced eIF2α-LONP1 signaling *in vivo*. Analysis of aortic root cryosections from 60mg/kg/day 1-NAPP1- or DMSO-treated (control) ASKA-Apoe$^{-/-}$mice; (A) P-eIF2α staining (green) was quantified from macrophage-enriched (MOMA-2 stained) positive area (red) (n=11-11). quantification is at the right of the representative figüre: (A(B) Aortic root RNA lysates were analyzed for CHOP, ATF4, ATF3 and LONP1 by qRT-PCR (n=12-12). Data: mean value ± SEM; (n=3). Mann-Whitney U Test *P≤ 0.05, **P≤ 0.01, ***P≤ 0.001. ns means not significant; a.u. means arbitrary units. (Scale bar: 200 μm).

4.2.4.2 The Impact of PERK Inhibition on Plaque Immune Cell Content

Next, I sought to examine whether 1-NAPP1 treatment in the ASKA, Apoe$^{-/-}$ mice has an impact on plaque macrophage or T cell population as did GSK2606414. Staining cryosections from the 1-NAPP1- or DMSO (control)-treated ASKA, Apoe$^{-/-}$ mice with a specific antibody for MOMA-2 (red), revealed that 1- significantly reduced lesion macrophage counts (Figure 4.20). This reduction in macrophage content with PERK inhibition is consistent with previous results I obtained from plaques of GSK2606414-treated mice.

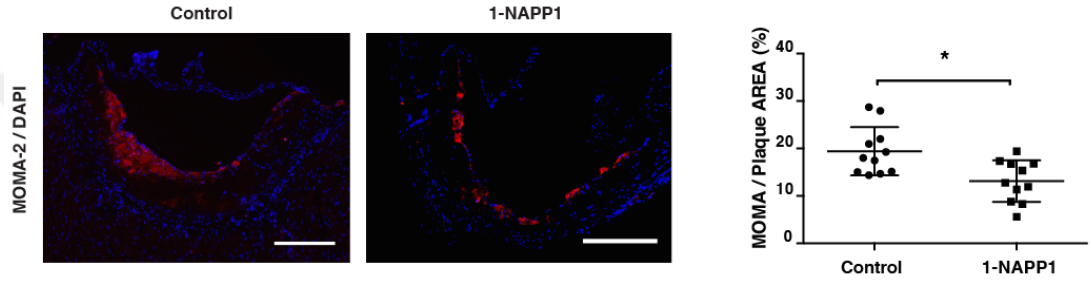

Figure 4.20. Inhibition of PERK kinase activity reduces hyperlipidemia-induced macrophage infiltration in plaques. Immunohistochemical staining with MOMA-2 antibody and analysis of aortic root cryosections from 60mg/kg/day 1-NAPP1- and DMSO-treated (control) ASKA- Apoe$^{-/-}$ mice. Quantification is at the right of the representative figure. MOMA-2 staining (red) (n=11-11). Data: mean value ± SEM;. Mann-Whitney U Test *P≤ 0.05, **P≤ 0.01, ***P≤ 0.001. ns means not significant. (Scale bar: 200 μm)

4.2.4.3 PERK Kinase Inhbition Suppressed Hyperlipidemia-Induced Inflammatory Cytokine Levels

After confirming, plaque macrophage counts are reduced with PERK inhibition, I sought to analyze inflammatory cytokines levels. Previous findings with GSK2606414 in this thesis, showed that secreted, mature IL-1β and cleaved caspase-1, two indicators of inflammasome activation in immune cells, are significantly suppressed by PERK inhibition.

Here, aortic root cryosections from 1-NAPP1 or DMSO-treated ASKA-Apoe $^{-/-}$ mice (fed with WD) were stained for IL-1β (green) using a specific antibody (Figure 4.21 A) or FAM/FLICA for caspase-1 (green) as shown in Figure 4.21 B.

The analysis of the signal intensities from the macrophage positive areas (stained with MOMA2; red) revealed that 1-NAPP1 treatment in ASKA-Apoe$^{-/-}$ mice led to a significant reduction in these cytokines' levels, confirming the previous results related to PERK inhibition *in vitro* and *in vivo*.

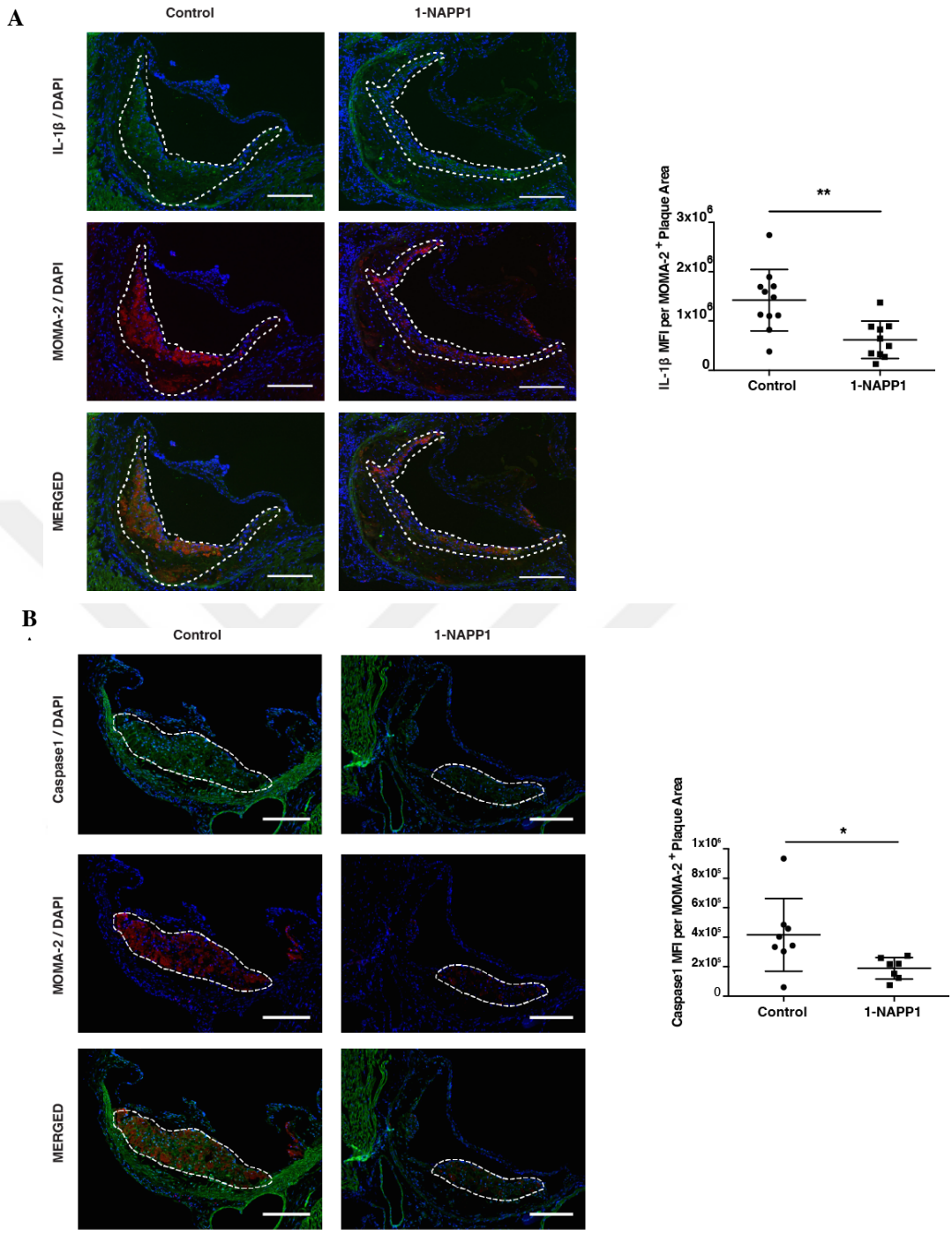

Figure 4.21. Inhibition of PERK kinase activity reduces hyperlipidemia-induced inflammasome activation in mice. Immunohistochemical analysis of aortic root cryosections from 60mg/kg/day 1-NAPP1- and DMSO (control)-treated ASKA-*Apoe*$^{-/-}$ mice fed with WD. Quantifications are shown at the right of the representative figures: (A) IL-1β (n=11-10) and (B) FAM/FLICA staining (green) (n=8-7) intensities were quantified from macrophage-enriched (MOMA2-positive; red) area. Data: mean value ± SEM;. Mann-Whitney U Test *P≤ 0.05, **P≤ 0.01, ***P≤ 0.001. ns means not significant. (Scale bar: 200 μm).

I next examined the aortic root plaques for RNA levels of inflammatory cytokines. According to the results in Figure 4.22, 1-NAPP1-treated mice aortic roots displayed significant reduction in TNFα and CCL2 mRNA levels, but not in IL-1β mRNA levels. These findings also confirm the previous results I obtained from mice treated with GSK2606414. Here also, IL-1β levels are not altered at the transcript level.

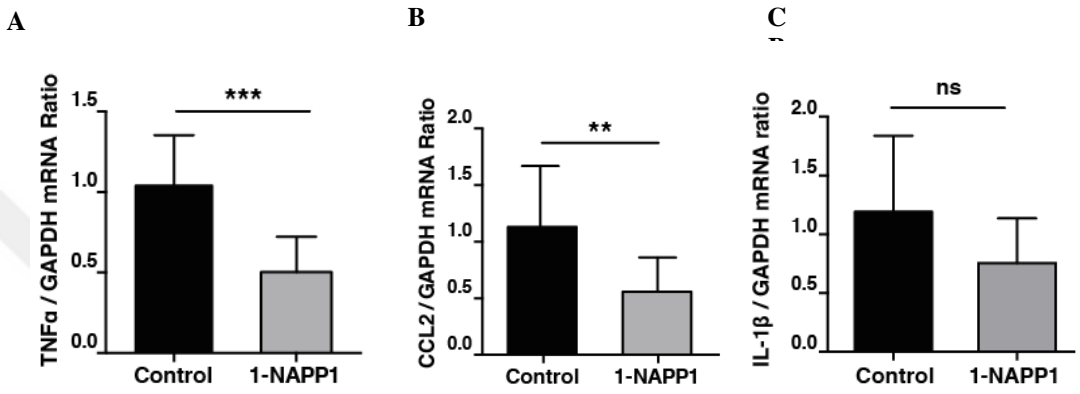

Figure 4.22. Inhibition of PERK kinase activity reduces hyperlipidemia-induced serum and plaque cytokine levels in mice. ASKA_Apoe-/- mice (fed with WD) were treated with 1-NAPP1 or DMSO (control): (A-C) RNA lysates from aortic root plaques were analyzed with qRT-PCR for (A) TNFα (n=14-12), (B) CCL2 (n=14-12), (C) IL-1β(n=14-12). Data: mean value ± SEM;. Mann-Whitney U Test *P≤ 0.05, **P≤ 0.01, ***P≤ 0.001. ns means not significant.

4.2.5 The Impact of PERK Kinase Inhibition on Lipid Profiles of Mice

I analyzed cholesterol and triglyceride levels in the plasma of 1-NAPP1 or DMSO (control)-treated ASKA, Apoe$^{-/-}$ mice that were fed with WD. Neither total cholesterol and triglyceride levels nor lipoprotein coetent were different between the groups (Figure 4.23)

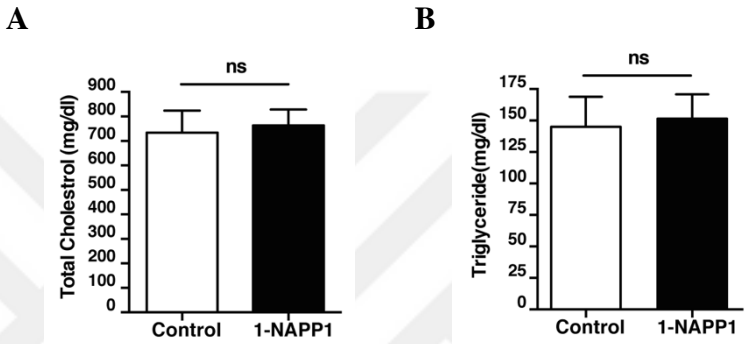

Figure 4.23. Selective inhibition of PERK kinase activity with 60 mg/kg/day 1-NAPP1 does not affect blood lipid measurements in ASKA-Apoe$^{-/-}$ mice on western diet (A) Total Cholesterol (B) Total Triglyceride levels was measured by ELISA from blood plasma of 1-NAPP1 or vehicle treated ASKA-Apoe$^{-/-}$ mice on Western Diet. Data: mean value ± SEM; *Mann-Whitney U* Test *P≤ 0.05, **P≤ 0.01, ***P≤ 0.001. ns means not significant.

Chapter 5.

Effect of Integrated Stress Response in atherosclerosis

The findings presented in the previous section shows that eIF2B activator, ISRIB, inhibits downstream of eIF2α and has a suppressive effect on lipid-induced inflammasome activation. Here, I sought to determine whether ISRIB has a suppressive effect on atherosclerosis progression *in vivo*. In this study, the dose and the route of administration for ISRIB were selected based on earlier studies using this inhibitor *in vivo* in mice (291,311,312), either 1mg/kg/day or 2mg/kg/day ISRIB was injected intra-peritoneally.

Alternatively, Sephin1, a PPPR15A inhibitor that de-phosphorylates and inactivates phosphorylation of eIF2α. This, in turn, causes prolonged phosphorylation and activation of eIF2α. The earlier vitro studies in this thesis showed that prolonged activation of PERK signaling prevents the anti-inflammatory effects of GSK2606414 (such as inflammasome activation and inflammatory cytokine production). For example, when Sephin1 is applied to cells undergoing lipid-induced stress, Sephin1 further induced inflammasome activation and proinflammatory cytokine production in macrophages. Due to these reults, I next sought to determine the consequences of Sephin1 usage on inflammaion *in vivo* on the dose selected based on earlier studies (270).

5.1 The Impact of ISRIB on Hyperlipidemia-Induced Inflammation and Atherosclerosis *In Vivo*

5.1.1 General Study design and Correlation of The Efficacy of Trans-ISRIB 1mg/kg/day

The doses and administration route used for *in vivo* ISRIB treatment in mice was based on previously published studies (291,311,312). In my experiments, I used two different doses of ISRIB (1-2 mg/kg/day). After 10 weeks of WD, the $Apoe^{-/-}$ mice were daily injected (intraperitoneal) ISRIB for additional 6 weeks. This general study design is shown in figure 5.1 A. After sacrifice, I analyzed eIf2α phosphorylation. As expected from an eIF2B activator, ISRIB did not effect eif2α phosphorylation in these mice (Fig.5.1 B). I also analyzed the mRNA levels of downstream effectors such as CHOP, ATF3 as well as LONP1 (that I demonstrated to be regulated by ISR). ISRIB treatment reduced the expression of all three mRNA that are normally induced by WD (Figure 5.1 B&C). This is also consistent with the data obtained from ISR inhibition with GSK2606414 (Figure 5.1 C).

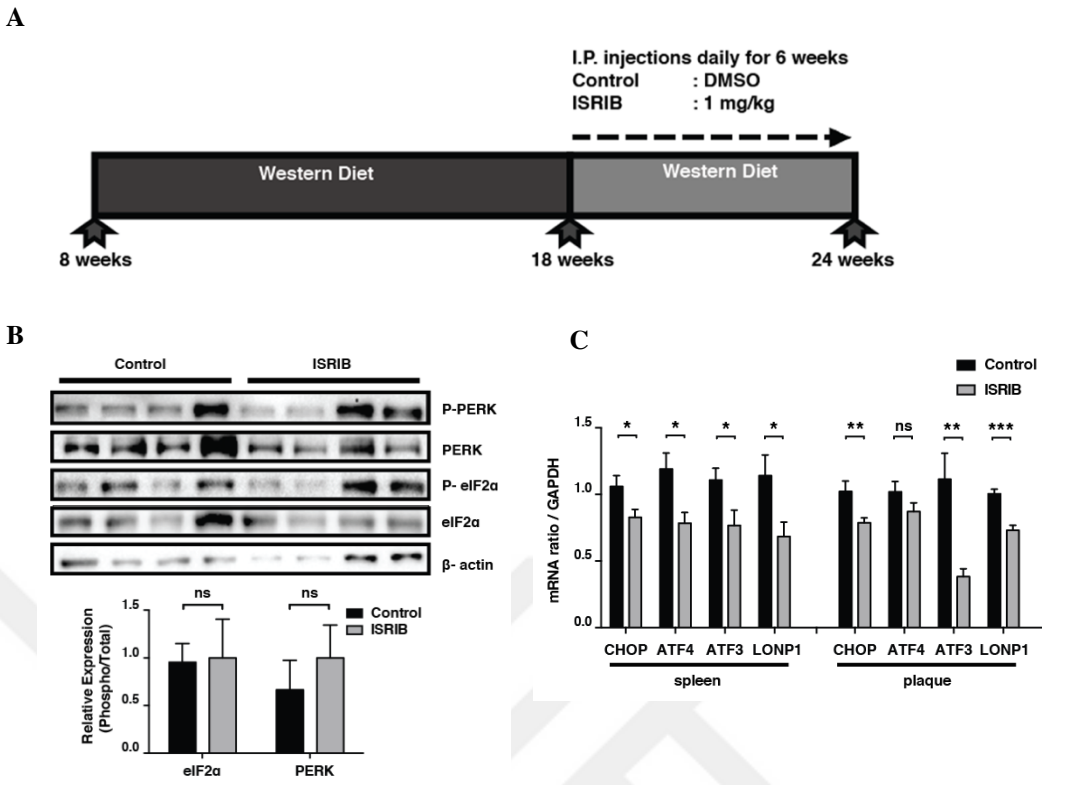

Figure 5.1. Experimental design and the efficacy of ISRIB administration *in vivo*. (A) Experimental design: Apoe$^{-/-}$ mice fed with WD were treated with ISRIB (1 mg/kg/day) or vehicle (control) (B) Protein lysates from the pancreas were analyzed by Western blotting with specific antibodies against P-PERK, PERK, P-eIF2α, eIF2α, β-actin, quantification is below the figure, and (C) RNA lysates from Spleen(left) or Plaque (right were analyzed by q-RT PCR for CHOP, ATF4, ATF3 and LONP1 mRNA levels (n=7, 7). Data: mean value ± SEM; *Mann-Whitney U* Test. *P≤ 0.05, **P≤ 0.01, ***P≤ 0.001, ns = non-significant.

5.1.2 The Impact of ISRIB on Metabolic Parameters

Previous reports on ISRIB demonstrated it is non-toxic inhibitor for ISR, however, I reasssed the ISRIB treatment on metabolic parameters that could be relevant to the atherosclerosis experiments in my thesis. Fort this purpose, I analyzed bodyweight and blood glucose levels before ISRIB treatment and at the end of the experiment, during sacrifice. Also, blood insulin levels were analyzed at the end of the experiment. According to the results presented in Figure 5.2, neither bodyweight nor blood glucose and insulin levels changed due to ISRIB.

A

1 mg/kg

Variables	Treatment	Control	ISRIB
n		7	7
Bodyweight(g)	Before	31,13 ± 1,407	32,25 ± 0,8183
	After	32,00 ± 1,512	33,00 ± 0,8660
Glucose(mg/dl)	Before	85,00 ± 0,8315	110,9 ± 10,54
	After	109,9 ± 7,354	113,0 ± 10,71

B

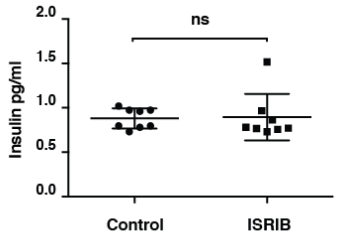

Figure 5.2. Analysis of Metabolic Parameters in ISRIB- Treated Apoe$^{-/-}$ Mice. Apoe$^{-/-}$ mice were treated with ISRIB (1mg/kg/day) or vehicle (control). (A) Glucose and bodweight measurements of Control vs ISRIB administered mice. (B) Insulin ELISA measured from serum(n=7-7). *Mann-Whitney U* Test. *P≤ 0.05, **P≤ 0.01, ***P≤ 0.001, ns = non-significant.

5.1.3 The Impact of ISRIB in Atherosclerotic Plaque Development

Next, I sought to determine the impact ISRIB administration on plaque development. En face aorta total plaque area (Sudan IV-stained) analysis showed, ISRIB significantly reduced plaque area (Figure 5.3 A). Furthermore, the analysis of aortic root cryosections (stained with Oil RedO) showed reduced foam cell area (Figure 5.3 C). However, there were no significant changes in total plaue (H&E-stained) area in aortic sinuses (Figure 5.3 B). Finally, the necrotic core analysis from the H&E stained sections showed that there were not changes in necrotic area after ISRIB treatment (Figure 5.3 D). These findings also are consistent with the findings from mice where ISR was inhibited by PERK kinase inhibitors.

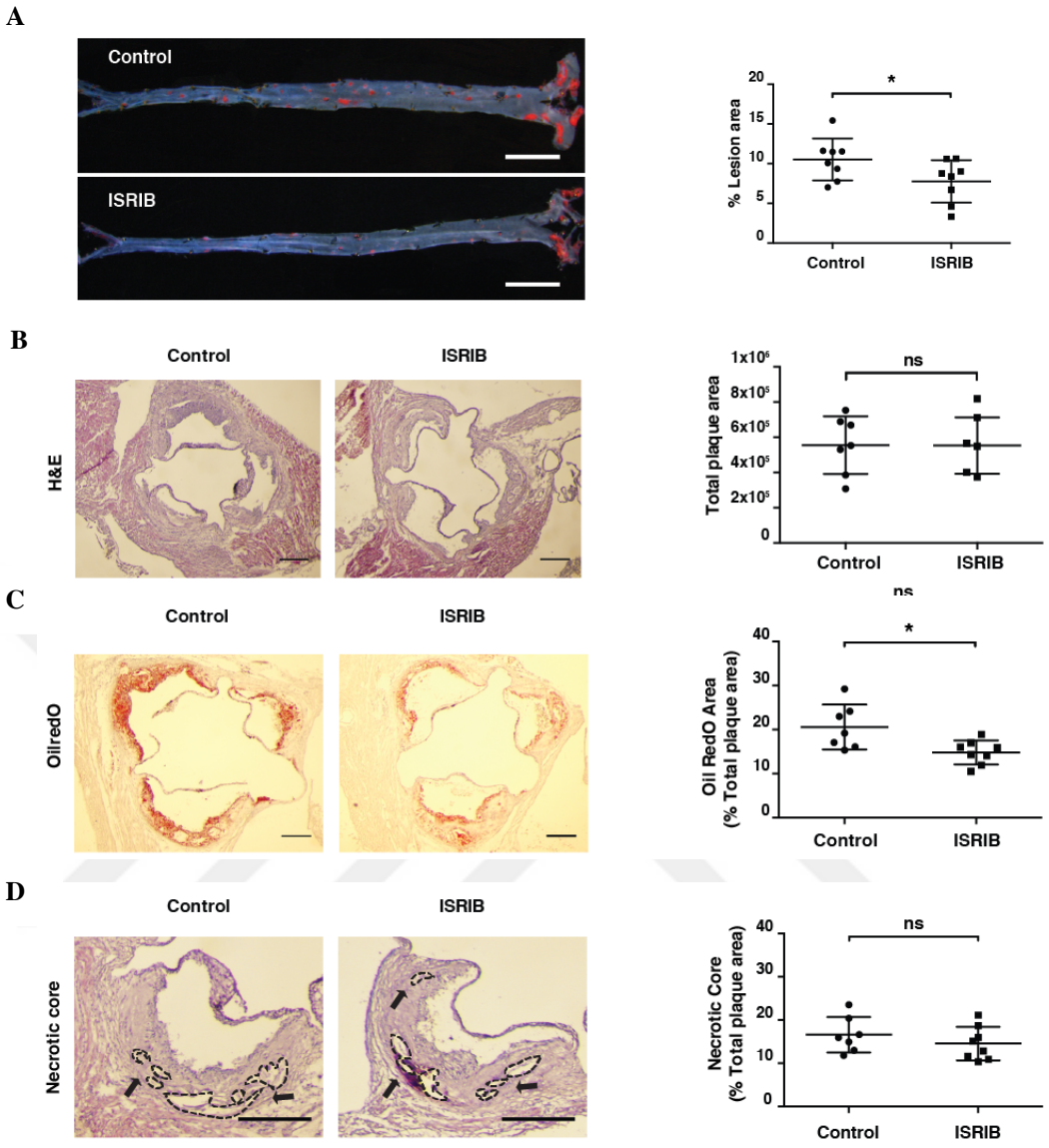

Figure 5.3. Blocking ISR by ISRIB alleviates atherosclerosis in Apoe$^{-/-}$mice. Apoe$^{-/-}$ mice fed with WD were treated with ISRIB (1 mg/kg/day) or vehicle (control): (A) Lesion area was calculated from en face aorta preparations stained with Sudan IV (n=8, 8), (B) the foam cell area was calculated from Oil RedO-stained aortic root lesions (n=7, 8), (C) total plaque area was calculated from H&E-stained aortic root lesions (n=7, 8), and (D) the mecrotic Core analysis from H&E stained aortic root sections. (n=7, 8). Data: mean value ± SEM; . *Mann-Whitney U* Test. *P≤ 0.05, **P≤ 0.01, ***P≤ 0.001,ns = non-significant.

5.1.4 The Impact of ISRIB on Plaque Immune Cell Composition

Because significant changes in atherosclerotic plaque size were observed after administration of ISRIB *in vivo*, I next sought to determine whether ISRIB alters the cellular contents of plaques in the Apoe$^{-/-}$ mice fed with WD.

5.1.4.1 The Impact of ISRIB on Hyperlipidemia-induced LONP1 Expression in Plaques

I fist analyzed the heart aortic root tissue sections for LONP1 expression, which is induced by lipid stress and suppressed by ISR inhibition via various approaches, including PERK kinase inhibition. For this, aortic root cryosections were stained with a specific antiobody for LONP1 and macrophages (MOMA-2), and the mean fluorescent intensity (MFI) for LONP1 (green) was analyzed from macrophage-enriched or MOMA-2 positive (red) area. LONP1 expression (green) was significantly reduced by ISRIB treatment in these mice (Figure 5.4).

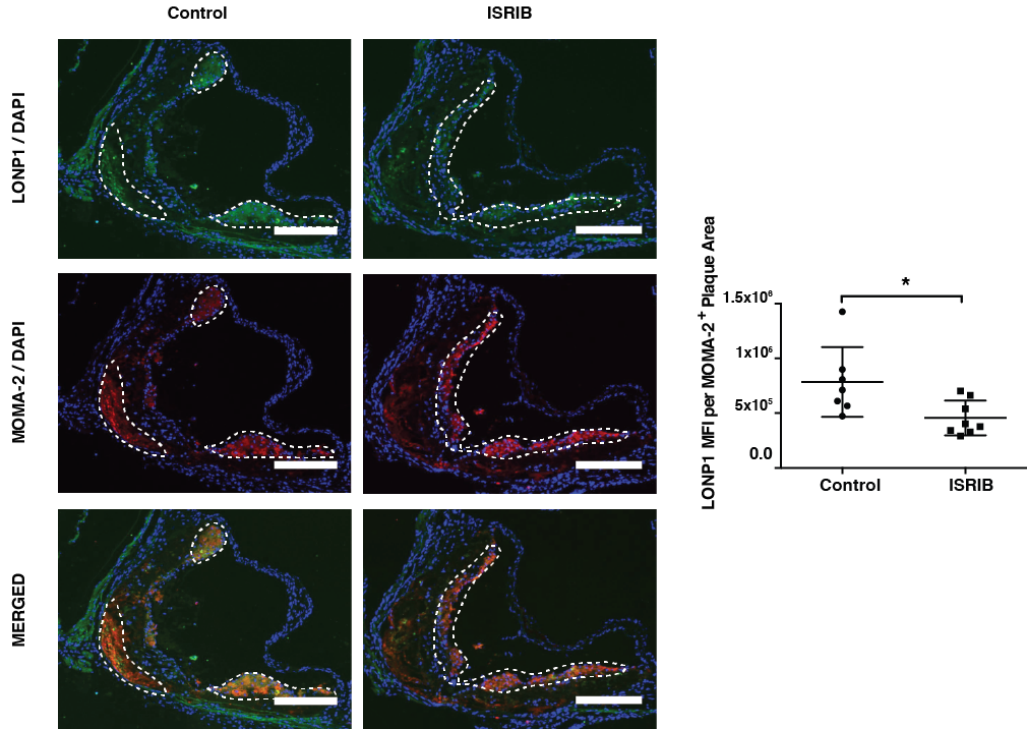

Figure 5.4. ISRIB supresses LONP1 expression in *Apoe*$^{-/-}$ aortic root sections. Aortic root cryosections from ISRIB and vehicle-treated (control) mice were stained with specific antibodies against LONP1 and MOMA2. MFI for LONP1 (green) was calculated from MOMA2-positive (red) area. Data are means ± SEM; *Mann-Whitney U* test *P≤ 0.05, **P≤ 0.01, ***P≤ 0.001. ns means not significant. (Scale bar: 200 μm).

5.1.4.2 The Impact of ISRIB on Plaque Immune Cell Content

In section 4.1.3, ISRIB's impact on reducing foam cell area was shown. As I explained in previous chapter, aortic root plaques are composed of inflammatory cells, mainly macrophages and T cells. To analyze the impact of ISRIB on plaque immune cell conent, I first stained the aortic root cryosections with an antibody against macrophages (MOMA-2; red) and analyzed the size of macrophage-enriched plaque areas in aortic sinus. ISRIB administration resulted in a significant reduction in the macrophage area (Figure 5.5 A). Next, I stained the T cell population with a T cell marker (CD3; green) and analyzed the number of T cells in each mm^2 of plaque area. My analysis showed that ISRIB led to a significant reduction in CD3 positive T cell counts (Figure 5.5 B).

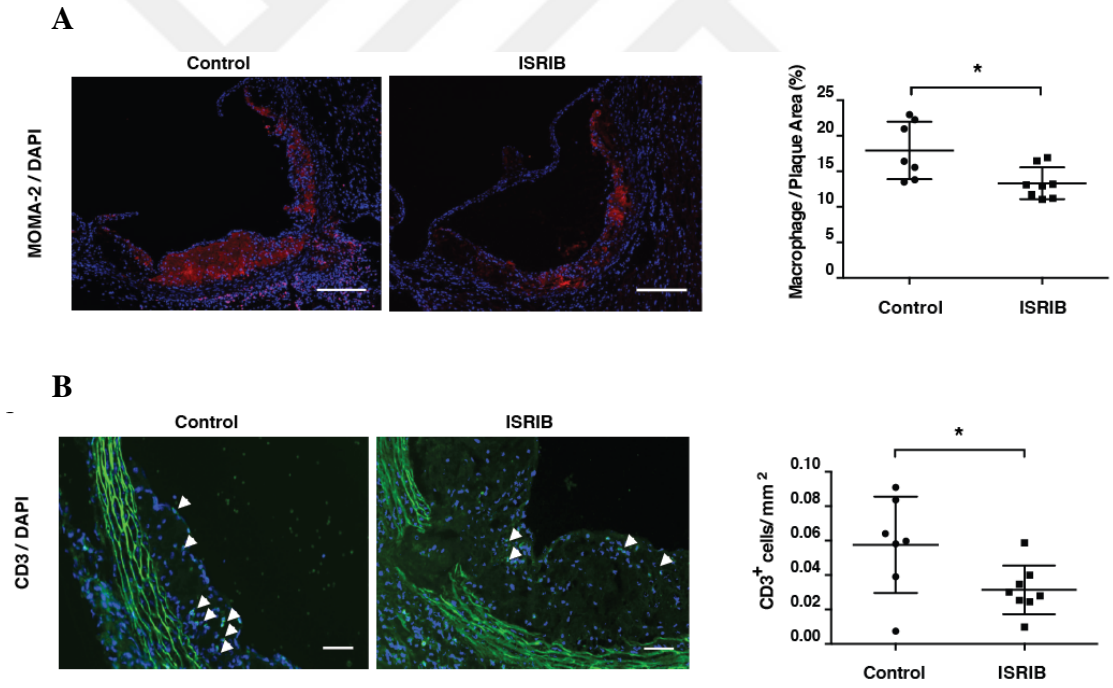

Figure 5.5. ISRIB supresses hyperlipidemia-induced inflammation in *Apoe*$^{-/-}$ mice Immunohistochemical analysis of aortic root cryosections from ISRIB-treated (1mg/kg/day) or vehicle-treated (control) mice was performed. For all stainings, a representative image is shown to the left of the quantification:(A) MOMA-2 (red), (B) CD3 (green) (n=7-8). Data are means ± SEM; *Mann-Whitney U* test *P≤ 0.05, **P≤ 0.01, ***P≤ 0.001. ns means not significant. (Scale bar: 200 μm)

5.1.4.3 The Impact of ISRIB on Inflammatory Cytokine Levels Induced by Hyperlipidemia

The reduction of macrophage and T cell counts in the aortic root plaque area with ISRIB prompted my analysis of inflammatory cytokines' levels in the aortic root plaque area. First, I analyzed the aortic roots for mature IL-1β and cleaved caspase-1 protein levels, which are two indicators of inflammasome activation. The aortic root cryosections were stained with specific antibodies for these proteins along with MOMA-2 macrophage marker. The analysis of both of these protein levels (mean fluorescence intensity (MFI)) were done from macrophage-positive areas in the lesions Confirming the results in the previous chapters of my thesis, I observed a significant reduction in mature IL-1β (Figure 5.6 A) and cleaved caspase-1 (Figure 5.6 B) levels in the macrophage-enriched areas of the plaques from ISRIB-treated Apoe $^{-/-}$ mice fed with WD. This finding with ISRIB confirming that ISR inhibition, whether upstream at PERK level or downstream ISR signaling, blocks lipid-induced inflammasome activation.

After confirming effects of ISRIB on caspase-1 and IL-1β in the atherosclerotic plaques, I analyzed the systemic consequence of ISRIB on inflammation. I measured IL-18 from the serums of ISRIB-treated and control Apoe$^{-/-}$ mice fed with WD. Consistent with the findings the previous chapters, ISR pathway inhibition via ISRIB administration significantly lowered plasma IL-18 levels in the cirucation (Figure 5.7 A) as well as plasma MCP1 levels (Figure 5.7 B), which is also consistent with the decrease observed in lesion macrophage and T cell counts and lesion IL-1β levels.

After confirming systemic effects of ISRIB on inflammation, I next analyzed RNA levels of the inflammatory cytokines in aortic root sections. Confirming the results with GSK2606414 administration in the previous sections of this thesis and consistent with the reduced inflammatory cell counts in ISRIB-treated mice, I observed significantly reduced mRNA levels of TNFα (Figure 5.7 C) and CCL2 (Figure 5.7 D) but not IL-1β mRNA (Figure 5.7 E) in the ISRIB-treated mice.

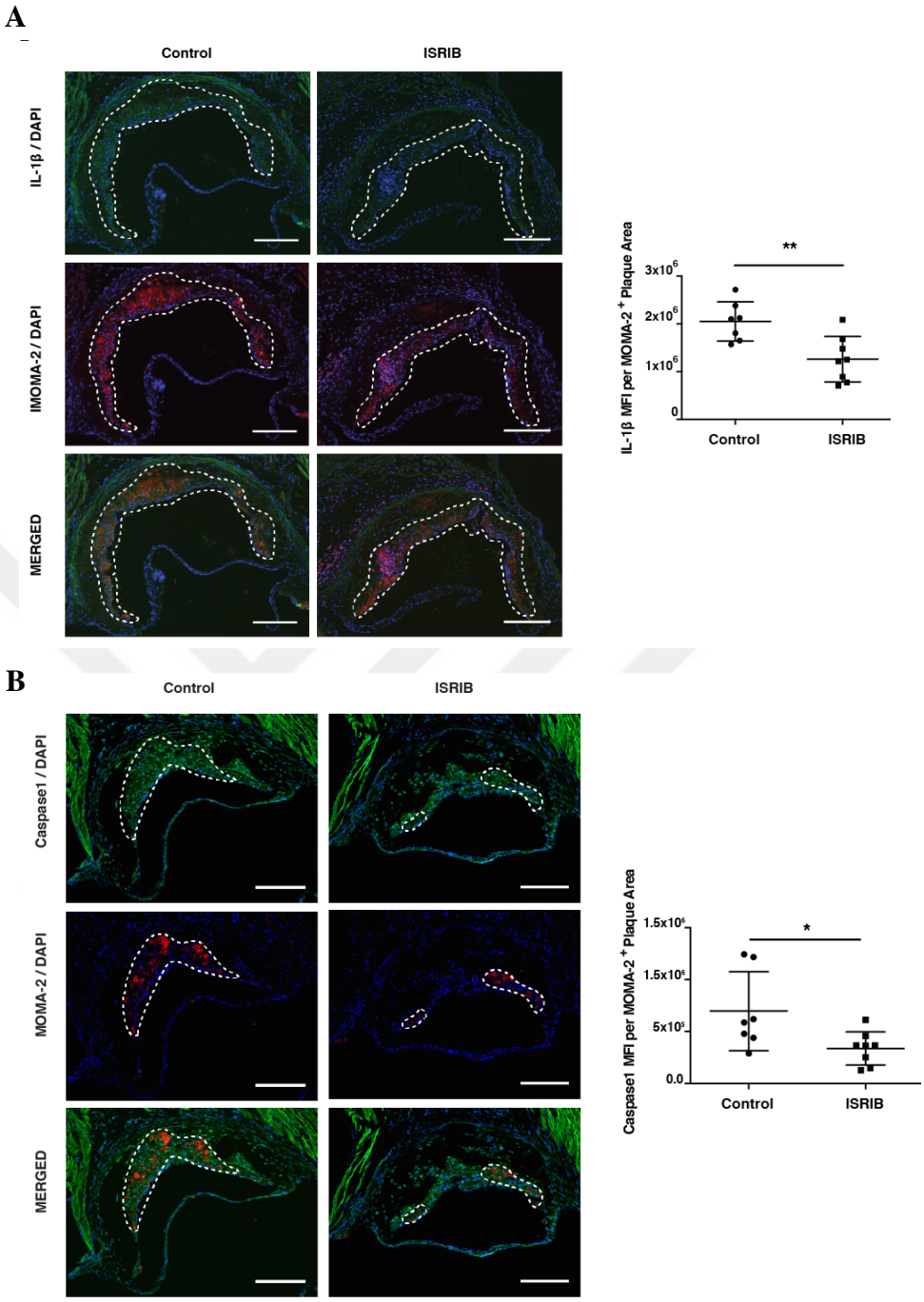

Figure 5.6. ISRIB supresses hyperlipidemia-induced IL-1β and cleaved caspase-1 levels *in vivo*. Immunohistochemical analysis of aortic root cryosections from ISRIB-treated (1 mg/kg/day) or vehicle-treated (control) *Apoe*$^{-/-}$ mice. Quantifications (MFI: quantificaiton of green signal from the red-stained area) are shown at the right of the each representative figure: (A) IL-1β (green), MOMA2 (red), DAPI/nuclear stain (blue), and (B) Caspase-1 (FAM/FLICA) staining (green), MOMA2 (red), DAPI/nuclear stain (blue). (n=7-8) Data: mean value ± SEM;. *Mann-Whitney U* Test *P≤ 0.05, **P≤ 0.01, ***P≤ 0.001. ns means not significant. (Scale bar: 200 μm).

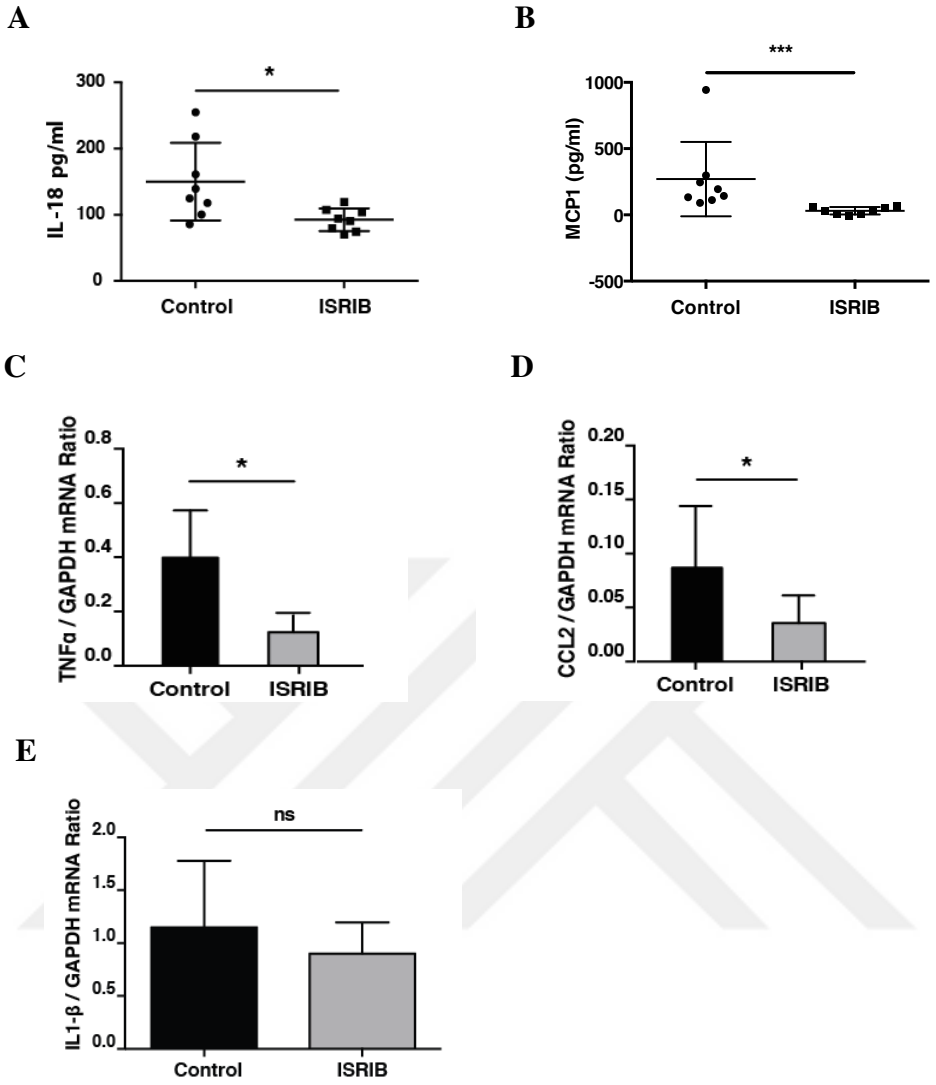

Figure 5.7. ISRIB administration reduces serum and plaque cytokine levels in Apoe$^{-/-}$ mice. Apoe-/- mice were fed with WD and treated with ISRIB (1 mg/kg/day) or vehicle (control): (A-B) Serum cytokine levels were measured with ELISA for (A) IL-18 (n=8-8) and (B) MCP1 (n=8-8). (C-E) RNA lysates from aortic root plaques were analyzed with qRT-PCR for (C) TNFα (n=7-8), (D) CCL2 (n=7-8), and (E) IL-1β mRNAs(n=7-8). Data: mean value ± SEM;. *Mann-Whitney U* Test *P≤ 0.05, **P≤ 0.01, ***P≤ 0.001. ns means not significant.

5.1.5 The Impact of ISRIB on Circulating Immune Cell Counts

Next, I analyzed the impact of ISRIB on circulating blood immune cell counts. Based on the cell count results in Figure 5.8, ISRIB did not alter immune cell counts in the circulation. This finding limits ISRIB's action to mainly preventing hyperlipidemia-induced inflammatory response in the atherosclerotic lesion area.

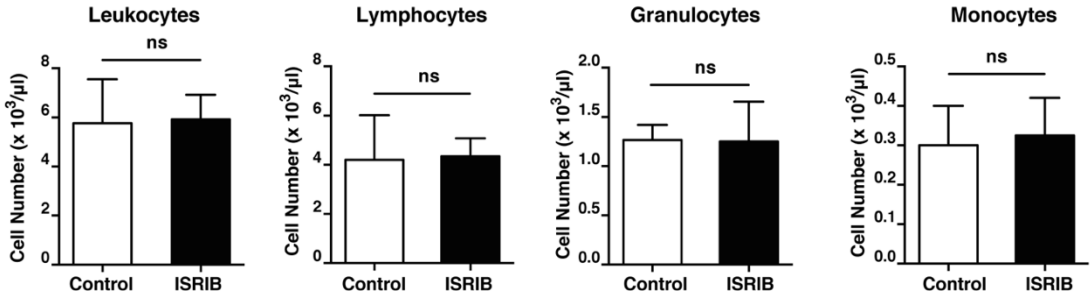

Figure 5.8. Blockade of ISR with ISRIB does not alter circulating immune cells counts. Blood immune cells were counted from ISRIB- or vehicle-treated (control) Apoe$^{-/-}$ mice on Western Diet. Data: mean value ± SEM; *Mann-Whitney U* Test *P≤ 0.05, **P≤ 0.01, ***P≤ 0.001. ns means not significant.

5.1.6 The Impact of ISRIB on Sytemic Lipoprotein and Lipid Profiles in Apoe$^{-/-}$ Mice Fed with Western Diet

To determine if ISRIB has an effect on systemic lipid metabolism in addition to its anti-inflammatory actions, I next analyzed lipid profiles of the Apoe$^{-/-}$ mice treated with ISRIB (1 mg/kg/day) or vehicle (control) ApoE$^{-/-}$ mice fed with WD. I did observe any changes in total cholesterol (Figure 5.9 A) or total triglyceride (Figure 5.9 B) levels. These results suggest that the effect of ISRIB on atherosclerosis is not based on the changes in systemic lipid metabolism.

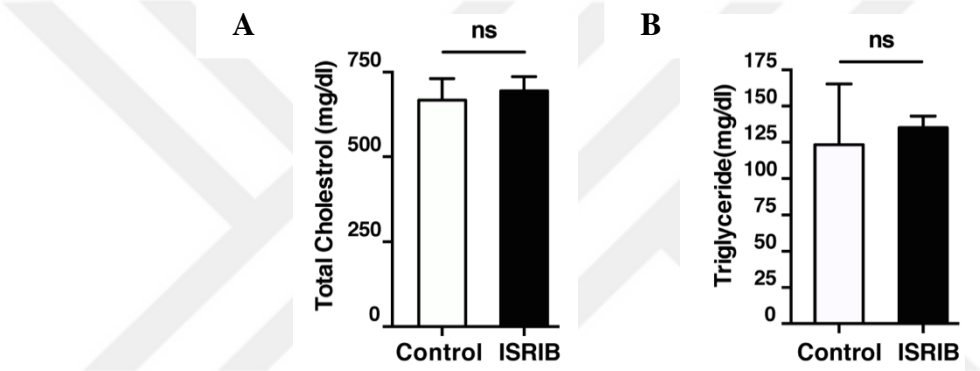

Figure 5.9. ISRIB administration does not affect systemic lipid measurements (A) Total Cholesterol (B) Total Triglyceride levels was measured by ELISA from plasma of ISRIB- or vehicle-treated Apoe$^{-/-}$ mice on WD. Data: mean value ± SEM; *Mann-Whitney U* Test *P≤ 0.05, **P≤ 0.01, ***P≤ 0.001. ns means not significant.

5.1.7 The Impact of ISRIB on Atherosclerosis Progression

As in previous chapter with PERK kinase inhibitor treatment, I sought to determine that whether ISRIB administration impacts atherosclerosis progression. For this, Apoe$^{-/-}$ mice were fed with WD for 12 weeks. And, a second group was fed with WD for 16 weeks. This group was divided in itself as those that received 1mg/kg ISRIB and those that received vehicle treatment. According to the results in Figure 5.10, ISRIB treatment prevented only the progression of the total plaque area in the en face aortas and foamy macrophage and plaque size in the aortic roots (Figure 5.10 A&B). It did not however, regress lesion size in these parts of the aorta and aortic root below the 12 week WD group's plaque size, suggesting ISRIB only interferes with atherosclerosis progression and not remission.

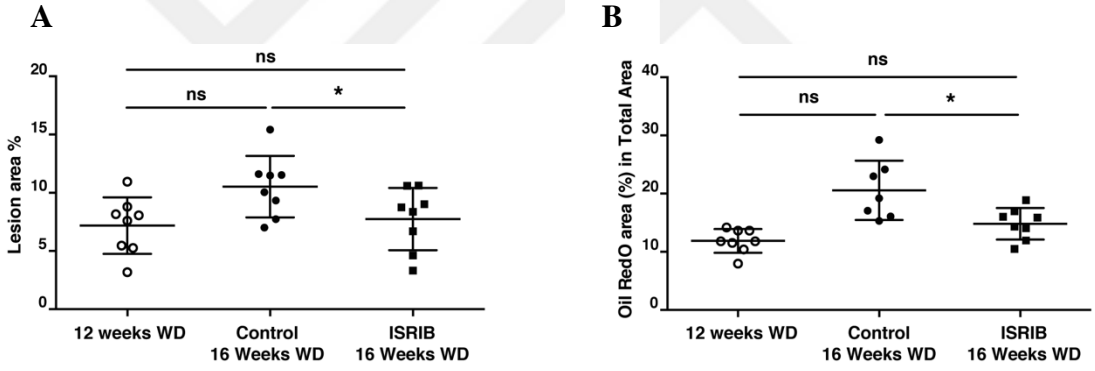

Figure 5.10. ISRIB Prevents Atherosclerosis Progression. Apoe$^{-/-}$ mice were fed with Western Diet for 12 to 16 weeks and treated with 1mg/kg ISRIB or vehicle (control) as indicated. (A) % lesion area was determined from en face aorta stained with SUDAN IV (n=15-15-15) (B) % foam cell area was calculated from teh aortic root sections stained with Oil RedO (n=14-14-12). Data are represented as means ± SEM; by *Mann-Whitney U* test. *P≤ 0.05, **P≤ 0.01, ***P≤ 0.001. ns means not significant.

In conclusion, the findings from my study with 1 mg/kg/day ISRIB administration in Apoe-/- mouse model of atherosclerosis confirms the findings related to ISR inhibition by PERK kinase inhibitor; The inhibition of ISR pathway from either upstream (by PERK kinase inhibitors) or downstream (by ISRIB), both significantly lowers the inflammatory response to hyperlipidemia and inhibits the progression of atherosclerotic plaque formation.

5.2. The Impact of Higher Dose of ISRIB Administration on Atherosclerosis

In order to evaluate if higher dose of ISRIB will be more effective in preventing atherosclerosis, I set up another atherosclerosis study with ISRIB, using 2 mg/kg/day dose in Apoe$^{-/-}$ mice that were fed with WD (291,311,312).

5.2.1 The Impact of Higher Dose of ISRIB administration on Metabolic Parameters

The experimental design of this experiment was: after 12 weeks of WD, Apoe$^{-/-}$ mice were treated with 2 mg/kg/day ISRIB for 5 weeks, while animals continued to be fed with WD (Figure 5.11 A). Body weight and blood glucose levels were measured before drug treatment and at the time of sacrifice. The higher dose of ISRIB did not alter bodyweight or blood glucose levels as shown in Figure 5.11 B.

A

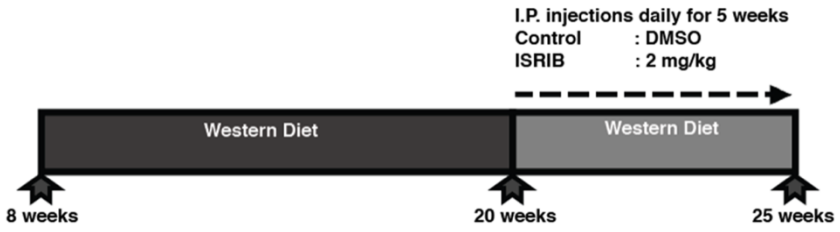

B

	Variables	Treatment	Control	ISRIB
2 mg/kg	n		5	5
	Bodyweight(g)	Before	29,31 ± 1,857	32,46 ± 2,947
		After	29,59 ± 1,607	31,44 ± 2,660
	Glucose(mg/dl)	Before	89,60 ± 3,501	97,80 ± 1,020
		After	89,20 ± 6,785	110,6 ± 6,728

Figure 5.11. Experimental design and metabolic characteristics of ISRIB administration *in vivo*. (A) Experimental design in Apoe$^{-/-}$ mice treated with ISRIB (2 mg/kg/day) or vehicle (DMSO) in the control mice. (B) Glucose and bodweight measurements of control vs ISRIB administered mice. Data: mean value ± SEM; (n=5-5). Two-tailed student's T-test *P≤ 0.05, ** P≤ 0.01,***P≤ 0.001, ns = non-significant.

5.2.2 The Impact of Higher Dose of ISRIB Administration on Atherosclerosis

Here, I assessed the impact of higher dose ISRIB (2 mg/kg/day) on the progression of atherosclerosis. Consistent with the previous results, administration of 2 mg/kg/day ISRIB significantly reduced aortic plaque area (in en-face aorta preparations) and more than 1mg/kg administration (compare to Figure 5.12 A). Also, Oil RedO stained foamy macrophage area was significantly reduced by higher dose ISRIB (Figure 5.12 B). Consistent with the previous results using lower dose of ISRIB, total plaque area was not altered in the H&E- stained of aortic root tissue sections higher dose ISRIB 2mg/kg administered mice (Figure 5.12 C). Taken together, both doses of ISRIB can effectively reduce atherosclerotic plaque formation.

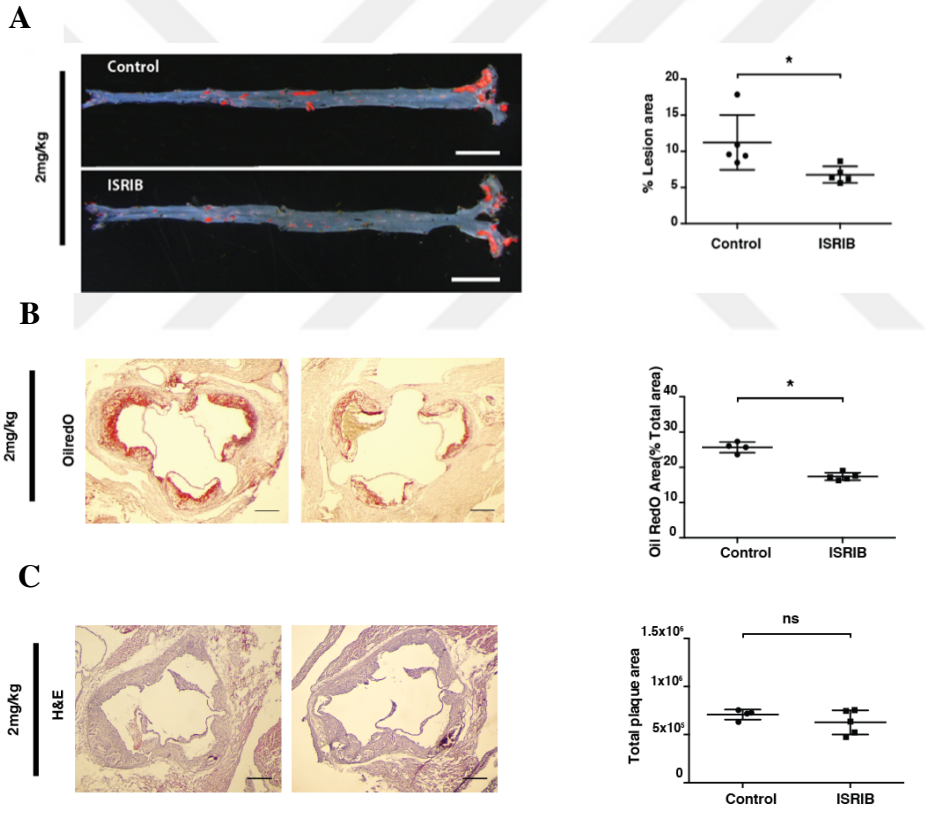

Figure 5.12. Blocking ISR by higher dose of ISRIB alleviates atherosclerosis. Apoe$^{-/-}$ mice were injected with 2 mg/kg/day of ISRIB or vehicle (control): (A) the lesion area was calculated from en face aorta preparations stained with Sudan IV (n= 5, 5), (B) the foam cell area was calculated from Oil RedO stained aortic root lesions (n= 5, 5), and (C) total plaque area was calculated from H&E-stained aortic root lesions (n=4, 5). Data: mean value ± SEM; (n=4-5). *Mann-Whithney U* Test. *P≤ 0.05, **P≤ 0.01, ***P≤ 0.001, ns = non-significant.

Chapter 6.

Discussion

In the last century, obesity and obesity-related cardiometabolic health problems have dramatically risen across the world in the last century. Intense research into the mechanisms of obesity-induced pathologies has revealed chronic inflammation and organelle stress can as common mechanisms. Upon metabolic stress, organelles like the ER and mitochondria are stressed and signal this stress to inflammatory pathways through mechanisms not well understood. One of these stress signaling pathways that is associated with ER stress is the ISR. Oner of the ways ISR can be induced is through the activation of the ER stress sensor PERK. In chronic ER stress conditions, this pathway is continuously activated. Persistent phosphorylation of eIF2α by PERK by chronic hyperlipidemia is evident in atherosclerotic lesions in mice and humans. These observations suggest that ISR may play a causal role in atherogenesis and that ISR pathway could potentially be targeted for the prevention of this complex disease (230,278,313).

In literature, targeting of ISR in neurodegenerative diseases has been achieved by inhibiting PERK (such as GSK2606414) or inhibiting downstream ISR by activating eIF2B (with ISRIB). Both approaches attempt to reduce ISR activation and inhibit the downstream detrimental effects in the target cells that lead to neurodegeneation. These studies are not addressing mechanisms related to atherosclerosis development or assessing ISR's role in systemic inflammation, however, they provide proof of concept that ISR inhibition is possible in a chronic disease settting (270,289-291,312,314-319) . Furthermore, these studies provide important guidance in dosage and administration route of the ISR drugs. In this study, we took advantage of the previously published

ISR inhibitors to investigate mechanisms related to lipid-induced ER stress and to assess the druggability of ISR in atherosclerosis.

Because of concerns related to serious side effects of the PERK kinase inhibitors, I conducted my macrophage studies with three different drugs that exert their effects at multiple levels of ISR. These were GSK2606414 (the PERK kinase inhibitor), Sephin1, (the PPPR15A inhibitor), and ISRIB (the eIF2B activator that inhibits the ISR response downstream of eIF2□ phosphorylation) (309,318-320). From these inhibitors, I further analyzed the impact of GSK2606414 and ISRIB *in vivo* using an atherosclerosis mouse model. Furthermore, I used a chemical-genetics as a complementary approach to modulate PERK kinase activity in macrophages. My study showed that 1-NAPP1 blocks the activation of ASKA_PERK mutant efficiently and specifically without off target effects both in macrohpages and *in vivo*. Importantly, results obtained using ASKA_PERK mutant confirmed the findings using the PERK kinase inhibitor in macrophages and *in vivo*. Additionally, I used specific siRNA to knockdown ISR at multiple levels (such as PERK and ATF4 siRNA), which also generated results similar to those obtained by applying small molecule inhibitors for ISR in macrophages.

In the *in vivo* studies in this thesis, I only used male mice due to male mice developing lesion sizes that are less variable than in females. One possible reason why female mice develop highly variable sizes of atherosclerosis may be related to the hormonal variations due to the female menstrual cycle (154,246,321). Also in literature, female mice have been shown to produce more aortic lesions compared to male mice fed with same diet in the same timeline (322). However, female mice can develop resistance to high-fat diet induced metabolic changes and atherosclerosis by simply increasing the regulatory T cell population (323). As it was conducted, my study does not address if there are differences in ISR activation or ISR inhibitor efficacy in the two sexes. This should be further assessed in future studies. In these *in vivo* studies, the mice were switched to start western diet at 8 weeks of age and the diet study continued for maximum 16 weeks. Due to limitations of resoruces, I have not assessed longer time course for atherosclerosis and longer treatment regimens with the inhibitors. There are studies in literature that conduct the atherosclerosis diet experiments for up to 54 weeks of age. Certainly, it will be important to determine how ISR contributes to

vascular aging. One plausible reason to use younger mice and shorter diet regimens is that younger mice generate mild atherosclerotic lesions and therefore it is easir to observe atherosclerosis in progress. Older mice have elevated levels of plasma cholesterol and triglycerides and increased systemic inflammation compared to the young, which correlates with advanced atherosclerosis (324). Older mice and longer duration of WD would be useful to study aging, cholesterol, inflammation link with ISR in the future.

While the *in vitro* usage of the various ISR inhibitors yield similar outcomes (inhibition of inflammation) in macrophages *in vitro*, their application in vivo requires careful consideration of toxicity and off target effects. For example, the PERK kinase inhibitor GSK2606414 was reported to cause serious pancreatic toxicity, weight loss and death in chronic administration, albeit at higher doses than used in my study (309). As opposed to GKS2606414, ISRIB does not lead to pancreatoxicity and has not reported toxicity or systemic side effects in earlier studies (291). ISRIB is also a unique drug with memory enhancing effects (319). These important properties of the two drugs suggest that targeting eIF2B by ISRIB may be more advantegous by preventing both atherosclerosis and age related memory decline and circumvent the toxicity associated with inhibitin ISR more upstream. In summary, the toxicity associated with GSK2606414 prevents its further utility in humans while the non-toxic nature of ISRIB makes it as a valuable drug to develop for using in many diseases that share a common pathology based on ISR activation (289,309,318-320). However, testing ISRIB in human vascular disease will be the only way to provide conclusive data regarding its utility in atherosclerosis.

Findings in my thesis studies demonstrated ISR plays a regulatory role on lipid-induced inflammasome activation. Using GSK2606414 effectively reduced inflammatory cytokines such as IL-1β as well as the inflammasome activation (as assessed by cleaved caspase-1). Both ISRIB and Sephin1 generated further data in lipid-stressed macrophages supporting the causality of eIF2α phosphorylation in inflammasome activation. This conclusion was further strengthened with the results obtained in macrophages using complementary approaches such as PERK or ATF4 siRNA to knock down these critical players in ISR signaling. Furthermore, inhibition

of PERK_ASKA by 1-NAPP1 in macrophages further strengthened the data regarding PERK's contributin to lipid-induced inflammasome activation, which was obtained by using GSK2606414 to inhibit PERK. Also, in vivo, both GSK2606414 and ISRIB administration to Apoe$^{-/-}$ mice resulted in significantly reduced inflammation and atherosclerotic plaque formation. Moreover, in these plaques, the most prominent change ws related to reduced macrophage and T cell counts, suggesting anti-inflamamatory action of ISR inhibitors plays a prominent role in preventing atherosclerosis. As would expected based on my *in vitro* findings, the ISR inhibitors also blocked hyperlipidemia-induced IL-1β in plaques and in the circulation and reduced hyperlipidemia-induced systemic IL-18 levels. Importantly, I obtained same results in the ASKA-APOE$^{-/-}$ mice after 1-NAPP1 administration, further strenghthening PERK kinase's role in hyperlipidemia-induced inflammation. These results collectively show that PERK to eIF2α signaling palys a critical role in promoting inflammation in the face of chronic lipid stress and as such, contribute to the atherogenic process.

In both the *in vitro* and in vivo studies, using multiple approaches to block ISR generated consistent results that confirm a central PERK-eIF2α-LONP1 pathway is activated by lipid stress and is causally associated with chronic inflammation that drives atherogenesis. This pathway also establishes an ER to mitochondria signaling that is important for inflammasome activation. My findings *in vitro* show that PERK kinase is required for lipids to induce LONP1, a mitochondrial protease. Aslo, silencing of ISR signaling either with GSK2606414 or ISRIB, significantly reduces LONP1 levels *in vitro* as well as *in vivo*. This was also confirmed by analyzing LONP1 levels in plaques obtained from ASKA-mice.

How does LONP1 mediate lipid stress to inflammsome activation? A previous study has shown LONP1 can degrade PINK1, implicating LONP1 in PINK1-PARKIN dependent mitophagy regulation (325,326). According to literature, mitochondrial ROS production is important for NLRP3 inflammasome activation. In my own experiments, ISR inhibition (at all levels) and inhibiting LONP1 can all prevent lipid-induced mtROS production. This observation formed my hypothesis that ISR regulates mitochondrial oxidative stress through regulating mitochondrial clearance by LONP1

induction and thereby, ISR plays an important role in lipid-induced, robust inflammasome activation. The results I obtained from the in vitor macrophage experiments clearly showed that inhibition of ISR at multiple levels causes both the activation of mitophagy (by preventing the degradation of PINK1 through inhibing LONP1 transcripition) and inhibits inflammasome activation. Key data supporting this notion was obtained by using PINK1 siRNA to silence PINK1-Parkin-dependen mitophagy in macrophages as well as by using PARKIN$^{-/-}$ BMDMs. In these, I observed neither GSK2606414 nor ISRIB treatment could prevent lipid-induced inflammasome activation. These findings depict significant information transmission regarding cellular stess between ER and mitochondria is coordinate by PERK-eIF2α-LONP1 signaling, leading to mitophagy and inflammsome regulation.

Previous studies have demonstrated NLRP3 inflammasome activation is associated with increased atherosclerosis in mice. NLRP3 acivation in plaques can occur by the accumulation of elevated cholesterol crystals or saturated fatty acids. In these studies, NLRP3$^{-/-}$ mice have reduced levels of IL-1β and IL-18 and are protected against atherosclerosis (220,327,328). In these mice, there was no improvement in lipid metabolism. In our study as we showed that both Attempts to translate these findings in mice to humans culminated in the CANTOS trial. In the CANTOS trial, IL-1β neutralizing antibody 'canakinumab' was used in patients that had endured a preivous cardiovascular event. The treated patients had significantly lower recurrent rate of cardiovascular events but with a possibility of enhanced infection rates (265,329). Circumventing organelle stress upstream of inflammasome activation may be an alternative approach to preventing inflammation and atherosclerosis but without the unwanted side effect of inflammation.

In summary, the main focus of my study was on ISR's role in inflammation as a cenral mechanism that drives atherogenesis. My findings show that ISR signaling through PERK-eiF2□-ATF4 induces LONP1 mitochondrial protease expression. LONP1, by cleaving its substrate PINK1, is an important regulator in PINK1/PARKIN dependent mitophagy. My findings further show that the disruption in mitophagical clearance by chronic ISR can cause the accumulation mtROS, which in turn, induces NLRP3 inflammasome activation. The activation of inflammasome and subsequent

inflammation can advance and destabilize the atherosclerotic plaque. In this study, I demonstrated the consequences of blocking lipid- induced ISR to inflammasome activation and atherosclerosis. The summary of pathways studied and the inhibitors that were used is depicted in figure 6.1.

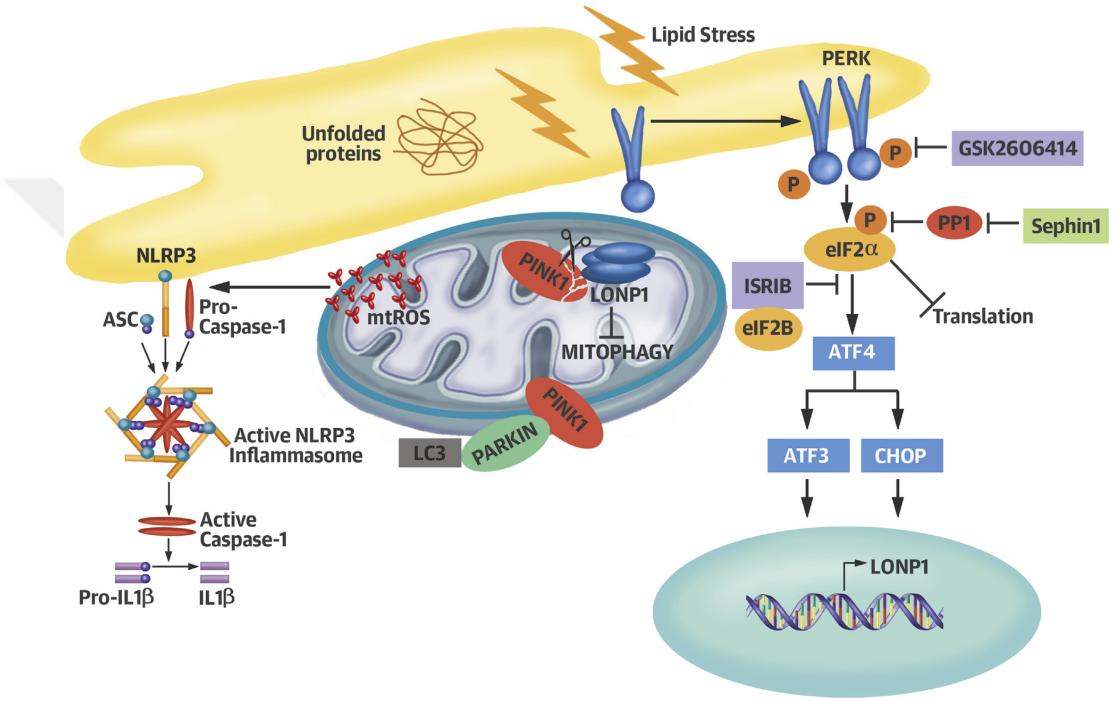

Figure 6.1. Lipid-induced ISR Regulates Mitochondrial Cleareance, Mitochondrial Oxidative Stress and Subsequent Inflammasome Activation

Chapter 7.

Future Perspectives

ER stress is causally associated with the progression of atherosclerosis and previous studies have shown interrupting ER stress signaling can alleviate atherosclerosis (268,269). ER stress sensor proteins function in UPR activation and their downstream effectors are also upregulated or activated in the atherosclerotic lesion area (118,230). As stated before, according to the cell type and duration of the stress UPR can have different outcomes, good and badd, in target cells/tissues (117,271,330). Thererfore, the applicaiton of ER stress reduction strategies for the treatment of metabolic disorders will be more specific if they ban be targeted to key cell/tissue types. Drugs that are systemically administred require higer dosage and their half-life is reduced. On the other hand, coupling agents such as cremophor-EL can increase the drug half-life, however, in most cases the drug's administration through intraperitoneal injection needs to ocur on a daily basis. As opposed to systemic delivery, targeted delivery can increase the half-life and on-target effect of the administered drug. This is because the drug would be internalized directly by the target cell/tissue and won't be subjected to degradation during transportation (such as from intraperitoneal cavity and through the circulation). In targeted delivery, the dosage of drugs can be lower, which would also decrease any undesired off-target effects. In my thesis, I studied two different small molecule inhibitors that can interfere with ISR pathway at different molecular nodes. I used an inhibitor for PERK kinase, however, its systemic administration has a low probability to be successful due to this drug's known toxic effects on pacnreas. The best way to circumevent this is to deliver PERK kinase inhbitors directly to macrohages such as in drug-encapsulated nanoparticles that are decorated with target proteins for specific receptors for macrophages (331).

In my thesis, based on the generated data, I proposed LONP1 connects ER – mitochondria stress responses to inflammatory pathways. I have not tested the conseqeunces of inhibiting LONP1 on atherosclerosis. However, in theory, inhibiton of LONP1 can potentially be atheroprotective. But this needs to be tested. Finally, I have not addressed the possibility to target ATF4 directly for atherosclerosis. Future studies should be considered to define ATF4's role in athesclerosis progression and regression.

Finally, future studies should be designed ot addressed the connection of ISR to sex-based differences in vascular disease and vascular aging. One possible way to do is to include female mice and male mice in ISR-atherosclerosis studies and compare the results obtained from both sexes to determine the gender effect on the atherosclerotic readouts. If we face high variability due to hormonal cycle in females, atherosclerosis can be studied in female mice after over ablation (chemical or surgical) (332). ISR's role can be tested in older age group mice to determine the connection of ISR with vascular aging. While these can increase the timeline and the cost of the experiment significantly, the results will illuminate unknown aspects of ISR signaling *in vivo* as well as the role of gender and age in complex diseases pathogenesis.

Bibliography

1. Westrate LM, Lee JE, Prinz WA, Voeltz GK. Form follows function: the importance of endoplasmic reticulum shape. Annu Rev Biochem 2015;84:791-811.
2. Schwarz DS, Blower MD. The endoplasmic reticulum: structure, function and response to cellular signaling. Cell Mol Life Sci 2016;73:79-94.
3. Fagone P, Jackowski S. Membrane phospholipid synthesis and endoplasmic reticulum function. J Lipid Res 2009;50 Suppl:S311-6.
4. Braakman I, Hebert DN. Protein Folding in the Endoplasmic Reticulum. Cold Spring Harb Perspect Biol 2013;5.
5. Araki K, Nagata K. Protein Folding and Quality Control in the ER. Cold Spring Harb Perspect Biol 2011;3.
6. Jaffe LF. Sources of calcium in egg activation: a review and hypothesis. Dev Biol 1983;99:265-76.
7. Clapham DE. Calcium Signaling. Cell;131:1047-1058.
8. Gilkey JC, Jaffe LF, Ridgway EB, Reynolds GT. A free calcium wave traverses the activating egg of the medaka, Oryzias latipes. J Cell Biol 1978;76:448-66.
9. Krols M, Bultynck G, Janssens S. ER–Mitochondria contact sites: A new regulator of cellular calcium flux comes into play. The Journal of Cell Biology 2016;214:367-370.
10. Cardenas C, Miller RA, Smith I et al. Essential regulation of cell bioenergetics by constitutive InsP3 receptor Ca2+ transfer to mitochondria. Cell 2010;142:270-83.
11. Booth David M, Enyedi B, Geiszt M, Várnai P, Hajnóczky G. Redox Nanodomains Are Induced by and Control Calcium Signaling at the ER-Mitochondrial Interface. Molecular Cell 2016;63:240-248.
12. Rizzuto R, Marchi S, Bonora M et al. Ca(2+) transfer from the ER to mitochondria: when, how and why. Biochimica et biophysica acta 2009;1787:1342-1351.
13. Vance JE. Phospholipid synthesis in a membrane fraction associated with mitochondria. Journal of Biological Chemistry 1990;265:7248-7256.
14. Rowland AA, Voeltz GK. Endoplasmic reticulum-mitochondria contacts: function of the junction. Nat Rev Mol Cell Biol;13:607-25.
15. Basseri S, Austin RC. ER stress and lipogenesis: a slippery slope toward hepatic steatosis. Dev Cell 2008;15:795-6.
16. Basseri S, Austin RC. Endoplasmic Reticulum Stress and Lipid Metabolism: Mechanisms and Therapeutic Potential. Biochemistry Research International 2012;2012:13.

17. Vallim T, Salter A. Regulation of hepatic gene expression by saturated fatty acids. Prostaglandins Leukot Essent Fatty Acids 2010;82:211-8.

18. Vembar SS, Brodsky JL. One step at a time: endoplasmic reticulum-associated degradation. Nat Rev Mol Cell Biol 2008;9:944-57.

19. McGuckin MA, Eri RD, Das I, Lourie R, Florin TH. ER stress and the unfolded protein response in intestinal inflammation. American Journal of Physiology - Gastrointestinal and Liver Physiology 2010;298:G820-G832.

20. Taouji S, Wolf S, Chevet E. Chapter Seventeen - Oligomerization in Endoplasmic Reticulum Stress Signaling. In: Jesús G, Francisco C, editors. Progress in Molecular Biology and Translational Science: Academic Press, 2013:465-484.

21. Hetz C. The unfolded protein response: controlling cell fate decisions under ER stress and beyond. Nat Rev Mol Cell Biol 2012;13:89-102.

22. Hetz C, Martinon F, Rodriguez D, Glimcher LH. The unfolded protein response: integrating stress signals through the stress sensor IRE1alpha. Physiol Rev 2011;91.

23. Ron D, Walter P. Signal integration in the endoplasmic reticulum unfolded protein response. Nat Rev Mol Cell Biol 2007;8:519-29.

24. Tabas I, Ron D. Integrating the mechanisms of apoptosis induced by endoplasmic reticulum stress. Nat Cell Biol 2011;13.

25. Chen Y, Brandizzi F. IRE1: ER stress sensor and cell fate executor. Trends in cell biology 2013;23:547-555.

26. Lee AH, Iwakoshi NN, Glimcher LH. XBP-1 regulates a subset of endoplasmic reticulum resident chaperone genes in the unfolded protein response. Mol Cell Biol 2003;23:7448-59.

27. Acosta-Alvear D, Zhou Y, Blais A et al. XBP1 controls diverse cell type- and condition-specific transcriptional regulatory networks. Mol Cell 2007;27:53-66.

28. Harding HP, Zhang Y, Bertolotti A, Zeng H, Ron D. Perk is essential for translational regulation and cell survival during the unfolded protein response. Mol Cell 2000;5:897-904.

29. Harding HP, Zhang Y, Ron D. Protein translation and folding are coupled by an endoplasmic-reticulum-resident kinase. Nature 1999;397.

30. Liu Z, Lv Y, Zhao N, Guan G, Wang J. Protein kinase R-like ER kinase and its role in endoplasmic reticulum stress-decided cell fate. Cell Death Dis 2015;6:e1822.

31. Cullinan SB, Zhang D, Hannink M, Arvisais E, Kaufman RJ, Diehl JA. Nrf2 Is a Direct PERK Substrate and Effector of PERK-Dependent Cell Survival. Mol Cell Biol 2003;23:7198-209.

32. Akai R, Hosoda A, Yoshino M, Iwawaki T. Constitutive role of GADD34 and CReP in cancellation of phospho-eIF2alpha-dependent translational

attenuation and insulin biosynthesis in pancreatic beta cells. Genes Cells 2015;20:871-86.

33. Tam AB, Mercado EL, Hoffmann A, Niwa M. ER stress activates NF-kappaB by integrating functions of basal IKK activity, IRE1 and PERK. PLoS One 2012;7:e45078.

34. Haze K, Yoshida H, Yanagi H, Yura T, Mori K. Mammalian transcription factor ATF6 is synthesized as a transmembrane protein and activated by proteolysis in response to endplasmic reticulum stress. Mol Biol Cell 1999;10.

35. Shen J, Chen X, Hendershot L, Prywes R. ER stress regulation of ATF6 localization by dissociation of BiP/GRP78 binding and unmasking of Golgi localization signals. Dev Cell 2002;3:99-111.

36. Yoshida H, Matsui T, Yamamoto A, Okada T, Mori K. XBP1 mRNA is induced by ATF6 and spliced by IRE1 in response to ER stress to produce a highly active transcription factor. Cell 2001;107.

37. Chen X, Shen J, Prywes R. The luminal domain of ATF6 senses endoplasmic reticulum (ER) stress and causes translocation of ATF6 from the ER to the Golgi. J Biol Chem 2002;277:13045-52.

38. Ye J, Rawson RB, Komuro R et al. ER stress induces cleavage of membrane-bound ATF6 by the same proteases that process SREBPs. Mol Cell 2000;6:1355-64.

39. Yamamoto K, Sato T, Matsui T et al. Transcriptional induction of mammalian ER quality control proteins is mediated by single or combined action of ATF6alpha and XBP1. Dev Cell 2007;13:365-76.

40. Adachi Y, Yamamoto K, Okada T, Yoshida H, Harada A, Mori K. ATF6 is a transcription factor specializing in the regulation of quality control proteins in the endoplasmic reticulum. Cell Struct Funct 2008;33:75-89.

41. Bommiasamy H, Back SH, Fagone P et al. ATF6alpha induces XBP1-independent expansion of the endoplasmic reticulum. J Cell Sci 2009;122:1626-36.

42. Belmont PJ, Chen WJ, San Pedro MN et al. Roles for endoplasmic reticulum-associated degradation and the novel endoplasmic reticulum stress response gene Derlin-3 in the ischemic heart. Circ Res 2010;106:307-16.

43. Ron D. Translational control in the endoplasmic reticulum stress response. The Journal of clinical investigation 2002;110:1383-1388.

44. Harding H. An Integrated Stress Response Regulates Amino Acid Metabolism and Resistance to Oxidative Stress. Molecular Cell 2003;11:619-633.

45. Brostrom CO, Prostko CR, Kaufman RJ, Brostrom MA. Inhibition of Translational Initiation by Activators of the Glucose-regulated Stress Protein and Heat Shock Protein Stress Response Systems: ROLE OF THE INTERFERON-INDUCIBLE DOUBLE-STRANDED RNA-ACTIVATED

EUKARYOTIC INITIATION FACTOR 2α KINASE. Journal of Biological Chemistry 1996;271:24995-25002.

46. Dever TE, Feng L, Wek RC, Cigan AM, Donahue TF, Hinnebusch AG. Phosphorylation of initiation factor 2α by protein kinase GCN2 mediates gene-specific translational control of GCN4 in yeast. Cell 1992;68:585-596.

47. Wek RC, Jiang H-Y, Anthony TG. Coping with stress: eIF2 kinases and translational control. Biochemical Society Transactions 2006;34:7-11.

48. Rzymski T, Milani M, Pike L et al. Regulation of autophagy by ATF4 in response to severe hypoxia. Oncogene 2010;29:4424.

49. Ye J, Kumanova M, Hart LS et al. The GCN2-ATF4 pathway is critical for tumour cell survival and proliferation in response to nutrient deprivation. The EMBO journal 2010;29:2082-2096.

50. García MA, Meurs EF, Esteban M. The dsRNA protein kinase PKR: Virus and cell control. Biochimie 2007;89:799-811.

51. Donnelly N, Gorman AM, Gupta S, Samali A. The eIF2α kinases: their structures and functions. Cellular and Molecular Life Sciences 2013;70:3493-3511.

52. Pakos-Zebrucka K, Koryga I, Mnich K, Ljujic M, Samali A, Gorman AM. The integrated stress response. EMBO Reports 2016:1374-1395.

53. Lu PD, Harding HP, Ron D. Translation reinitiation at alternative open reading frames regulates gene expression in an integrated stress response. The Journal of cell biology 2004;167:27-33.

54. Novoa I, Zhang Y, Zeng H, Jungreis R, Harding HP, Ron D. Stress-induced gene expression requires programmed recovery from translational repression. The EMBO Journal 2003;22:1180-1187.

55. Dey S, Baird TD, Zhou D, Palam LR, Spandau DF, Wek RC. Both transcriptional regulation and translational control of ATF4 are central to the integrated stress response. The Journal of biological chemistry 2010;285:33165-33174.

56. Scheuner D, Patel R, Wang F et al. Double-stranded RNA-dependent Protein Kinase Phosphorylation of the α-Subunit of Eukaryotic Translation Initiation Factor 2 Mediates Apoptosis. Journal of Biological Chemistry 2006;281:21458-21468.

57. Castilho BA, Shanmugam R, Silva RC, Ramesh R, Himme BM, Sattlegger E. Keeping the eIF2 alpha kinase Gcn2 in check. Biochimica et Biophysica Acta (BBA) - Molecular Cell Research 2014;1843:1948-1968.

58. Vazquez de Aldana CR, Wek RC, Segundo PS, Truesdell AG, Hinnebusch AG. Multicopy tRNA genes functionally suppress mutations in yeast eIF-2 alpha kinase GCN2: evidence for separate pathways coupling GCN4 expression to unchanged tRNA. Molecular and cellular biology 1994;14:7920-7932.

59. Clemens MJ, Elia A. The Double-Stranded RNA-Dependent Protein Kinase PKR: Structure and Function. Journal of Interferon & Cytokine Research 1997;17:503-524.

60. Lemaire PA, Anderson E, Lary J, Cole JL. Mechanism of PKR Activation by dsRNA. Journal of molecular biology 2008;381:351-360.

61. Dey M, Cao C, Dar AC et al. Mechanistic Link between PKR Dimerization, Autophosphorylation, and eIF2α Substrate Recognition. Cell 2005;122:901-913.

62. Zhang F, Romano PR, Nagamura-Inoue T et al. Binding of Double-stranded RNA to Protein Kinase PKR Is Required for Dimerization and Promotes Critical Autophosphorylation Events in the Activation Loop. Journal of Biological Chemistry 2001;276:24946-24958.

63. Vattem KM, Staschke KA, Wek RC. Mechanism of activation of the double-stranded-RNA-dependent protein kinase, PKR. European Journal of Biochemistry 2001;268:3674-3684.

64. Balachandran S, Roberts PC, Brown LE et al. Essential Role for the dsRNA-Dependent Protein Kinase PKR in Innate Immunity to Viral Infection. Immunity 2000;13:129-141.

65. Lee SB, Esteban M. The Interferon-Induced Double-Stranded RNA-Activated Human p68 Protein Kinase Inhibits the Replication of Vaccinia Virus. Virology 1993;193:1037-1041.

66. Shimazawa M, Hara H. Inhibitor of double stranded RNA-dependent protein kinase protects against cell damage induced by ER stress. Neuroscience Letters 2006;409:192-195.

67. Lee E-S, Yoon C-H, Kim Y-S, Bae Y-S. The double-strand RNA-dependent protein kinase PKR plays a significant role in a sustained ER stress-induced apoptosis. FEBS Letters 2007;581:4325-4332.

68. García MA, Gil J, Ventoso I et al. Impact of protein kinase PKR in cell biology: from antiviral to antiproliferative action. Microbiology and molecular biology reviews : MMBR 2006;70:1032-1060.

69. Williams BR. PKR; a sentinel kinase for cellular stress. Oncogene 1999;18:6112-20.

70. Han AP, Yu C, Lu L et al. Heme-regulated eIF2alpha kinase (HRI) is required for translational regulation and survival of erythroid precursors in iron deficiency. The EMBO journal 2001;20:6909-6918.

71. Rafie-Kolpin M, Chefalo PJ, Hussain Z et al. Two Heme-binding Domains of Heme-regulated Eukaryotic Initiation Factor-2α Kinase: N TERMINUS AND KINASE INSERTION. Journal of Biological Chemistry 2000;275:5171-5178.

72. Rafie-Kolpin M, Han A-P, Chen J-J. Autophosphorylation of Threonine 485 in the Activation Loop Is Essential for Attaining eIF2α Kinase Activity of HRI. Biochemistry 2003;42:6536-6544.

73. Acharya P, Chen J-J, Correia MA. Hepatic heme-regulated inhibitor (HRI) eukaryotic initiation factor 2alpha kinase: a protagonist of heme-mediated translational control of CYP2B enzymes and a modulator of basal endoplasmic reticulum stress tone. Molecular pharmacology 2010;77:575-592.

74. Korennykh A, Walter P. Structural Basis of the Unfolded Protein Response. Annual Review of Cell and Developmental Biology 2012;28:251-277.

75. Gardner BM, Walter P. Unfolded proteins are Ire1-activating ligands that directly induce the unfolded protein response. Science (New York, NY) 2011;333:1891-1894.

76. de la Cadena SG, Hernández-Fonseca K, Camacho-Arroyo I, Massieu L. Glucose deprivation induces reticulum stress by the PERK pathway and caspase-7- and calpain-mediated caspase-12 activation. Apoptosis 2014;19:414-427.

77. Moore CE, Omikorede O, Gomez E, Willars GB, Herbert TP. PERK activation at low glucose concentration is mediated by SERCA pump inhibition and confers preemptive cytoprotection to pancreatic β-cells. Molecular endocrinology (Baltimore, Md) 2011;25:315-326.

78. Jackson RJ, Hellen CUT, Pestova TV. The mechanism of eukaryotic translation initiation and principles of its regulation. Nature reviews Molecular cell biology 2010;11:113-127.

79. Pain VM. Initiation of Protein Synthesis in Eukaryotic Cells. European Journal of Biochemistry 1996;236:747-771.

80. Aitken CE, Lorsch JR. A mechanistic overview of translation initiation in eukaryotes. Nature Structural &Amp; Molecular Biology 2012;19:568.

81. Lomakin IB, Steitz TA. The initiation of mammalian protein synthesis and mRNA scanning mechanism. Nature 2013;500:307.

82. Hinnebusch AG. Molecular mechanism of scanning and start codon selection in eukaryotes. Microbiology and molecular biology reviews : MMBR 2011;75:434-467.

83. Lee Y-Y, Cevallos RC, Jan E. An upstream open reading frame regulates translation of GADD34 during cellular stresses that induce eIF2alpha phosphorylation. The Journal of biological chemistry 2009;284:6661-6673.

84. Palam LR, Baird TD, Wek RC. Phosphorylation of eIF2 Facilitates Ribosomal Bypass of an Inhibitory Upstream ORF to Enhance CHOP Translation. The Journal of Biological Chemistry 2011;286:10939-10949.

85. Novoa I, Zeng H, Harding HP, Ron D. Feedback inhibition of the unfolded protein response by GADD34-mediated dephosphorylation of eIF2alpha. The Journal of cell biology 2001;153:1011-1022.

86. Jousse C, Oyadomari S, Novoa I et al. Inhibition of a constitutive translation initiation factor 2alpha phosphatase, CReP, promotes survival of stressed cells. The Journal of cell biology 2003;163:767-775.

87. Marciniak SJ, Yun CY, Oyadomari S et al. CHOP induces death by promoting protein synthesis and oxidation in the stressed endoplasmic reticulum. Genes & development 2004;18:3066-3077.

88. Ma Y, Hendershot LM. Delineation of a Negative Feedback Regulatory Loop That Controls Protein Translation during Endoplasmic Reticulum Stress. Journal of Biological Chemistry 2003;278:34864-34873.

89. Ameri K, Harris AL. Activating transcription factor 4. The International Journal of Biochemistry & Cell Biology 2008;40:14-21.

90. Karpinski BA, Morle GD, Huggenvik J, Uhler MD, Leiden JM. Molecular cloning of human CREB-2: an ATF/CREB transcription factor that can negatively regulate transcription from the cAMP response element. Proceedings of the National Academy of Sciences of the United States of America 1992;89:4820-4824.

91. Vallejo M, Ron D, Miller CP, Habener JF. C/ATF, a member of the activating transcription factor family of DNA-binding proteins, dimerizes with CAAT/enhancer-binding proteins and directs their binding to cAMP response elements. Proceedings of the National Academy of Sciences of the United States of America 1993;90:4679-4683.

92. B'Chir W, Maurin A-C, Carraro V et al. The eIF2α/ATF4 pathway is essential for stress-induced autophagy gene expression. Nucleic acids research 2013;41:7683-7699.

93. Siu F, Bain PJ, LeBlanc-Chaffin R, Chen H, Kilberg MS. ATF4 Is a Mediator of the Nutrient-sensing Response Pathway That Activates the Human Asparagine Synthetase Gene. Journal of Biological Chemistry 2002;277:24120-24127.

94. Han J, Back SH, Hur J et al. ER-stress-induced transcriptional regulation increases protein synthesis leading to cell death. Nat Cell Biol 2013;15:481-490.

95. Harding HP, Novoa I, Zhang Y et al. Regulated Translation Initiation Controls Stress-Induced Gene Expression in Mammalian Cells. Molecular Cell 2000;6:1099-1108.

96. Huret J-L, Ahmad M, Arsaban M et al. Atlas of genetics and cytogenetics in oncology and haematology in 2013. Nucleic acids research 2013;41:D920-D924.

97. Afonyushkin T, Oskolkova Olga V, Philippova M et al. Oxidized Phospholipids Regulate Expression of ATF4 and VEGF in Endothelial Cells via NRF2-Dependent Mechanism: Novel Point of Convergence Between Electrophilic and Unfolded Protein Stress Pathways. Arteriosclerosis, Thrombosis, and Vascular Biology 2010;30:1007-1013.

98. Lassot I, Ségéral E, Berlioz-Torrent C et al. ATF4 degradation relies on a phosphorylation-dependent interaction with the SCF(betaTrCP) ubiquitin ligase. Molecular and cellular biology 2001;21:2192-2202.

99. Rutkowski DT, Arnold SM, Miller CN et al. Adaptation to ER stress is mediated by differential stabilities of pro-survival and pro-apoptotic mRNAs and proteins. PLoS biology 2006;4:e374-e374.

100. Yang X, Matsuda K, Bialek P et al. ATF4 Is a Substrate of RSK2 and an Essential Regulator of Osteoblast Biology: Implication for Coffin-Lowry Syndrome. Cell 2004;117:387-398.

101. Elefteriou F, Ahn JD, Takeda S et al. Leptin regulation of bone resorption by the sympathetic nervous system and CART. Nature 2005;434:514-520.

102. Hollien J. Evolution of the unfolded protein response. Biochimica et Biophysica Acta (BBA) - Molecular Cell Research 2013;1833:2458-2463.

103. Kimmig P, Diaz M, Zheng J et al. The unfolded protein response in fission yeast modulates stability of select mRNAs to maintain protein homeostasis. eLife 2012;1.

104. Moreno AA, Mukhtar MS, Blanco F et al. IRE1/bZIP60-mediated unfolded protein response plays distinct roles in plant immunity and abiotic stress responses. PLoS One 2012;7:e31944.

105. Jelitto-Van Dooren EP, Vidal S, Denecke J. Anticipating endoplasmic reticulum stress. A novel early response before pathogenesis-related gene induction. Plant Cell 1999;11:1935-44.

106. Shen X, Ellis RE, Lee K et al. Complementary signaling pathways regulate the unfolded protein response and are required for C. elegans development. Cell 2001;107:893-903.

107. Richardson CE, Kooistra T, Kim DH. An essential role for XBP-1 in host protection against immune activation in C. elegans. Nature 2010;463:1092-5.

108. Feng B, Yao PM, Li Y et al. The endoplasmic reticulum is the site of cholesterol-induced cytotoxicity in macrophages. Nat Cell Biol 2003;5:781-92.

109. Kharroubi I, Ladriere L, Cardozo AK, Dogusan Z, Cnop M, Eizirik DL. Free fatty acids and cytokines induce pancreatic beta-cell apoptosis by different mechanisms: role of nuclear factor-kappaB and endoplasmic reticulum stress. Endocrinology 2004;145:5087-96.

110. Hotamisligil GS. Inflammation and metabolic disorders. Nature 2006;444:860-7.

111. Cao SS, Kaufman RJ. Endoplasmic Reticulum Stress and Oxidative Stress in Cell Fate Decision and Human Disease. Antioxid Redox Signal 2014;21:396-413.

112. Chaudhari N, Talwar P, Parimisetty A, Lefebvre d'Hellencourt C, Ravanan P. A Molecular Web: Endoplasmic Reticulum Stress, Inflammation, and Oxidative Stress. Front Cell Neurosci 2014;8.

113. Raturi A, Simmen T. Where the endoplasmic reticulum and the mitochondrion tie the knot: the mitochondria-associated membrane (MAM). Biochim Biophys Acta 2013;1833:213-24.

114. Flis VV, Daum G. Lipid Transport between the Endoplasmic Reticulum and Mitochondria. Cold Spring Harb Perspect Biol 2013;5.

115. Kaufman RJ. Orchestrating the unfolded protein response in health and disease. J Clin Invest 2002;110:1389-98.

116. Hotamisligil GS. Inflammation and endoplasmic reticulum stress in obesity and diabetes. Int J Obes (Lond) 2008;32 Suppl 7:S52-4.

117. Hotamisligil GS. Endoplasmic reticulum stress and the inflammatory basis of metabolic disease. Cell 2010;140:900-17.

118. Hotamisligil GS. Endoplasmic reticulum stress and atherosclerosis. Nat Med 2010;16:396-9.

119. Navid F, Colbert RA. Causes and consequences of endoplasmic reticulum stress in rheumatic disease. Nat Rev Rheumatol 2017;13:25-40.

120. Kaneko M, Niinuma Y, Nomura Y. Activation signal of nuclear factor-kappa B in response to endoplasmic reticulum stress is transduced via IRE1 and tumor necrosis factor receptor-associated factor 2. Biol Pharm Bull 2003;26:931-5.

121. Raha S, Robinson BH. Mitochondria, oxygen free radicals, disease and ageing. Trends Biochem Sci 2000;25:502-8.

122. Rius J, Guma M, Schachtrup C et al. NF-kappaB links innate immunity to the hypoxic response through transcriptional regulation of HIF-1alpha. Nature 2008;453:807-11.

123. Pahl HL, Baeuerle PA. Activation of NF-kappa B by ER stress requires both Ca2+ and reactive oxygen intermediates as messengers. FEBS Lett 1996;392:129-36.

124. Lawrence T. The Nuclear Factor NF-ϰB Pathway in Inflammation. Cold Spring Harb Perspect Biol 2009;1.

125. Keestra-Gounder AM, Byndloss MX, Seyffert N et al. NOD1 and NOD2 signalling links ER stress with inflammation. Nature 2016;532:394-397.

126. Jiang HY, Wek SA, McGrath BC et al. Phosphorylation of the alpha subunit of eukaryotic initiation factor 2 is required for activation of NF-kappaB in response to diverse cellular stresses. Mol Cell Biol 2003;23:5651-63.

127. Bai D, Ueno L, Vogt PK. Akt-mediated regulation of NFϰB and the essentialness of NFϰB for the oncogenicity of PI3K and Akt. International Journal of Cancer 2009;125:2863-2870.

128. Yamazaki H, Hiramatsu N, Hayakawa K et al. Activation of the Akt-NF-kappaB pathway by subtilase cytotoxin through the ATF6 branch of the unfolded protein response. J Immunol 2009;183:1480-7.

129. Allen D, Seo J. ER Stress Activates the TOR Pathway through Atf6. Journal of molecular signaling 2018;13:1-1.

130. Smith JA. Regulation of Cytokine Production by the Unfolded Protein Response; Implications for Infection and Autoimmunity. Frontiers in immunology 2018;9:422-422.

131. Oslowski Christine M, Hara T, O'Sullivan-Murphy B et al. Thioredoxin-Interacting Protein Mediates ER Stress-Induced β Cell Death through Initiation of the Inflammasome. Cell Metabolism 2012;16:265-273.

132. Lerner AG, Upton JP, Praveen PV et al. IRE1alpha induces thioredoxin-interacting protein to activate the NLRP3 inflammasome and promote programmed cell death under irremediable ER stress. Cell Metab 2012;16:250-64.

133. Ozcan U, Cao Q, Yilmaz E et al. Endoplasmic reticulum stress links obesity, insulin action, and type 2 diabetes. Science 2004;306:457-61.

134. Urano F, Wang X, Bertolotti A et al. Coupling of stress in the ER to activation of JNK protein kinases by transmembrane protein kinase IRE1. Science 2000;287:664-6.

135. Smith JA, Turner MJ, DeLay ML, Klenk EI, Sowders DP, Colbert RA. Endoplasmic reticulum stress and the unfolded protein response are linked to synergistic IFN-beta induction via X-box binding protein 1. Eur J Immunol 2008;38:1194-203.

136. Martinon F, Chen X, Lee AH, Glimcher LH. TLR activation of the transcription factor XBP1 regulates innate immune responses in macrophages. Nat Immunol 2010;11:411-8.

137. Goodall JC, Wu C, Zhang Y et al. Endoplasmic reticulum stress-induced transcription factor, CHOP, is crucial for dendritic cell IL-23 expression. Proc Natl Acad Sci U S A 2010;107:17698-703.

138. Iwasaki Y, Suganami T, Hachiya R et al. Activating Transcription Factor 4 Links Metabolic Stress to Interleukin-6 Expression in Macrophages. Diabetes 2014;63:152.

139. Cheng Y-L, Lin Y-S, Chen C-L et al. Activation of Nrf2 by the dengue virus causes an increase in CLEC5A, which enhances TNF-α production by mononuclear phagocytes. Scientific Reports 2016;6:32000.

140. Ting JP, Lovering RC, Alnemri ES et al. The NLR gene family: a standard nomenclature. Immunity 2008;28:285-7.

141. Sharma D, Kanneganti T-D. The cell biology of inflammasomes: Mechanisms of inflammasome activation and regulation. The Journal of Cell Biology 2016;213:617-629.

142. Thornberry NA, Bull HG, Calaycay JR et al. A novel heterodimeric cysteine protease is required for interleukin-1 beta processing in monocytes. Nature 1992;356:768-74.

143. Dinarello CA. IL-18: A TH1 -inducing, proinflammatory cytokine and new member of the IL-1 family. Journal of Allergy and Clinical Immunology 1999;103:11-24.

144. Faustin B, Lartigue L, Bruey JM et al. Reconstituted NALP1 Inflammasome Reveals Two-Step Mechanism of Caspase-1 Activation. Molecular Cell 2007;25:713-724.

145. Vance RE. The NAIP/NLRC4 inflammasomes. Curr Opin Immunol 2015;32:84-9.

146. Tenthorey JL, Kofoed EM, Daugherty MD, Malik HS, Vance RE. Molecular basis for specific recognition of bacterial ligands by NAIP/NLRC4 inflammasomes. Mol Cell 2014;54:17-29.

147. Man SM, Kanneganti TD. Regulation of inflammasome activation. Immunol Rev 2015;265:6-21.

148. Wen H, Gris D, Lei Y et al. Fatty acid-induced NLRP3-PYCARD inflammasome activation interferes with insulin signaling. Nature immunology 2011;12:408-415.

149. Hornung V, Ablasser A, Charrel-Dennis M et al. AIM2 recognizes cytosolic dsDNA and forms a caspase-1-activating inflammasome with ASC. Nature 2009;458:514-518.

150. Bauernfeind FG, Horvath G, Stutz A et al. Cutting edge: NF-kappaB activating pattern recognition and cytokine receptors license NLRP3 inflammasome activation by regulating NLRP3 expression. J Immunol 2009;183:787-91.

151. Zhou R, Yazdi AS, Menu P, Tschopp J. A role for mitochondria in NLRP3 inflammasome activation. Nature 2011;469:221-225.

152. Cruz CM, Rinna A, Forman HJ, Ventura AL, Persechini PM, Ojcius DM. ATP activates a reactive oxygen species-dependent oxidative stress response and secretion of proinflammatory cytokines in macrophages. J Biol Chem 2007;282:2871-9.

153. Shalev A. Minireview: Thioredoxin-Interacting Protein: Regulation and Function in the Pancreatic β-Cell. Molecular Endocrinology 2014;28:1211-1220.

154. Tufanli O, Telkoparan Akillilar P, Acosta-Alvear D et al. Targeting IRE1 with small molecules counteracts progression of atherosclerosis. Proceedings of the National Academy of Sciences 2017;114:E1395-E1404.

155. D'Osualdo A, Anania VG, Yu K et al. Transcription Factor ATF4 Induces NLRP1 Inflammasome Expression during Endoplasmic Reticulum Stress. PLoS One 2015;10:e0130635.

156. Menu P, Mayor A, Zhou R et al. ER stress activates the NLRP3 inflammasome via an UPR-independent pathway. Cell Death &Amp; Disease 2012;3:e261.

157. Bronner DN, Abuaita BH, Chen X et al. Endoplasmic Reticulum Stress Activates the Inflammasome via NLRP3- and Caspase-2-Driven Mitochondrial Damage. Immunity 2015;43:451-62.

158. Lazarou M. Keeping the immune system in check: a role for mitophagy. Immunology & Cell Biology 2015;93:3-10.

159. Halestrap Andrew P. A pore way to die: the role of mitochondria in reperfusion injury and cardioprotection. Biochemical Society Transactions 2010;38:841.

160. Rich PR, Maréchal A. The mitochondrial respiratory chain. Essays In Biochemistry 2010;47:1.

161. Ichimura H, Parthasarathi K, Quadri S, Issekutz AC, Bhattacharya J. Mechano-oxidative coupling by mitochondria induces proinflammatory responses in lung venular capillaries. The Journal of Clinical Investigation 2003;111:691-699.

162. Maass DL, White J, Sanders B, Horton JW. Role of cytosolic vs. mitochondrial Ca2+ accumulation in burn injury-related myocardial inflammation and function. American Journal of Physiology-Heart and Circulatory Physiology 2005;288:H744-H751.

163. Escames G, López LC, García JA, García-Corzo L, Ortiz F, Acuña-Castroviejo D. Mitochondrial DNA and inflammatory diseases. Human Genetics 2012;131:161-173.

164. Kornmann B, Currie E, Collins SR et al. An ER-mitochondria tethering complex revealed by a synthetic biology screen. Science 2009;325:477-81.

165. Chen H, Detmer SA, Ewald AJ, Griffin EE, Fraser SE, Chan DC. Mitofusins Mfn1 and Mfn2 coordinately regulate mitochondrial fusion and are essential for embryonic development. The Journal of Cell Biology 2003;160:189.

166. Verfaillie T, Rubio N, Garg AD et al. PERK is required at the ER-mitochondrial contact sites to convey apoptosis after ROS-based ER stress. Cell Death and Differentiation 2012;19:1880-1891.

167. Mori T, Hayashi T, Hayashi E, Su T-P. Sigma-1 Receptor Chaperone at the ER-Mitochondrion Interface Mediates the Mitochondrion-ER-Nucleus Signaling for Cellular Survival. PLOS ONE 2013;8:e76941.

168. Duchen MR. Roles of Mitochondria in Health and Disease. Diabetes 2004;53:S96.

169. Szabadkai G, Simoni AM, Bianchi K et al. Mitochondrial dynamics and Ca2+ signaling. Biochimica et Biophysica Acta (BBA) - Molecular Cell Research 2006;1763:442-449.

170. Hayashi T, Su T-P. Sigma-1 Receptor Chaperones at the ER- Mitochondrion Interface Regulate Ca2+ Signaling and Cell Survival. Cell 2007;131:596-610.

171. Szabadkai G, Simoni AM, Chami M, Wieckowski MR, Youle RJ, Rizzuto R. Drp-1-Dependent Division of the Mitochondrial Network Blocks Intraorganellar Ca2+ Waves and Protects against Ca2+-Mediated Apoptosis. Molecular Cell 2004;16:59-68.

172. Camacho P, Lechleiter JD. Calreticulin inhibits repetitive intracellular Ca2+ waves. Cell 1995;82:765-771.

173. Roderick HL, Lechleiter JD, Camacho P. Cytosolic phosphorylation of calnexin controls intracellular Ca(2+) oscillations via an interaction with SERCA2b. The Journal of cell biology 2000;149:1235-1248.

174. Nutt LK, Pataer A, Pahler J et al. Bax and Bak Promote Apoptosis by Modulating Endoplasmic Reticular and Mitochondrial Ca2+ Stores. Journal of Biological Chemistry 2002;277:9219-9225.

175. Klionsky DJ, Abdelmohsen K, Abe A et al. Guidelines for the use and interpretation of assays for monitoring autophagy (3rd edition). Autophagy 2016;12:1-222.

176. Georgakopoulos ND, Wells G, Campanella M. The pharmacological regulation of cellular mitophagy. Nature Chemical Biology 2017;13:136.

177. Kondapalli C, Kazlauskaite A, Zhang N et al. PINK1 is activated by mitochondrial membrane potential depolarization and stimulates Parkin E3 ligase activity by phosphorylating Serine 65. Open biology 2012;2:120080-120080.

178. Narendra D, Kane LA, Hauser DN, Fearnley IM, Youle RJ. p62/SQSTM1 is required for Parkin-induced mitochondrial clustering but not mitophagy; VDAC1 is dispensable for both. Autophagy 2010;6:1090-1106.

179. Kazlauskaite A, Kondapalli C, Gourlay R et al. Parkin is activated by PINK1-dependent phosphorylation of ubiquitin at Ser⁶⁵. Biochemical Journal 2014;460:127.

180. Johansen T, Lamark T. Selective autophagy mediated by autophagic adapter proteins. Autophagy 2011;7:279-296.

181. Stolz A, Ernst A, Dikic I. Cargo recognition and trafficking in selective autophagy. Nature Cell Biology 2014;16:495.

182. Wong YC, Holzbaur ELF. Optineurin is an autophagy receptor for damaged mitochondria in parkin-mediated mitophagy that is disrupted by an ALS-linked mutation. Proceedings of the National Academy of Sciences 2014;111:E4439.

183. Nguyen TN, Padman BS, Lazarou M. Deciphering the Molecular Signals of PINK1/Parkin Mitophagy. Trends in Cell Biology 2016;26:733-744.

184. Bouman L, Schlierf A, Lutz AK et al. Parkin is transcriptionally regulated by ATF4: evidence for an interconnection between mitochondrial stress and ER stress. Cell Death Differ 2011;18:769-82.

185. Zhang X, Yuan Y, Jiang L et al. Endoplasmic reticulum stress induced by tunicamycin and thapsigargin protects against transient ischemic brain injury: Involvement of PARK2-dependent mitophagy. Autophagy 2014;10:1801-1813.

186. Hori O, Ichinoda F, Tamatani T et al. Transmission of cell stress from endoplasmic reticulum to mitochondria enhanced expression of Lon protease. J Cell Biol 2002;157:1151-1160.

187. Wu Jea. The Unfolded Protein Response Mediates Adaptation to Exercise in Skeletal Muscle through a PGC-1α/ATF6α Complex. Cell Metabolism 2011;13.

188. Harris J, Deen N, Zamani S, Hasnat MA. Mitophagy and the release of inflammatory cytokines. Mitochondrion 2018;41:2-8.

189. Zhong Z, Umemura A, Sanchez-Lopez E et al. NF-ϰB Restricts Inflammasome Activation via Elimination of Damaged Mitochondria. Cell 2016;164:896-910.

190. Klingenberg R, Hansson GK. Treating inflammation in atherosclerotic cardiovascular disease: emerging therapies. Eur Heart J 2009;30:2838-44.

191. Lopez AD, Mathers CD, Ezzati M, Jamison DT, Murray CJL. Global and regional burden of disease and risk factors, 2001: systematic analysis of population health data. The Lancet;367:1747-1757.

192. von Rokitansky KF. A manual of pathological anatomy: Blanchard & Lea, 1855.

193. Virchow R. Cellular Pathology as Based Upon Physiological and Pathological Histology: JB Lippincott, 1863.

194. Windaus At. Über den Gehalt normaler und atheromatöser Aorten an Cholesterin und Cholesterinestern. Hoppe-Seyler´ s Zeitschrift für physiologische Chemie 1910;67:174-176.

195. Anitschkow N, Chalatow S, Müller C, Duguid J. Ueber experimentelle Cholesterinsteatose und ihre Bedeutehung einiger pathologischer Prozesse. Centrbl Allg Pathol Pathol Anat 1913;24:1-9.

196. Mayerl C, Lukasser M, Sedivy R, Niederegger H, Seiler R, Wick G. Atherosclerosis research from past to present--on the track of two pathologists with opposing views, Carl von Rokitansky and Rudolf Virchow. Virchows Arch 2006;449:96-103.

197. Weber C, Noels H. Atherosclerosis: current pathogenesis and therapeutic options. Nat Med 2011;17:1410-22.

198. Tiwari S, Siddiqi SA. Intracellular Trafficking and Secretion of Very Low Density Lipoproteins. Arterioscler Thromb Vasc Biol 2012;32:1079-86.

199. Libby P. The molecular mechanisms of the thrombotic complications of atherosclerosis. J Intern Med 2008;263:517-27.

200. Williams KJ, Tabas I. The response-to-retention hypothesis of early atherogenesis. Arterioscler Thromb Vasc Biol 1995;15:551-61.

201. Moore KJ, Tabas I. Macrophages in the pathogenesis of atherosclerosis. Cell 2011;145:341-55.

202. Hansson GK, Hermansson A. The immune system in atherosclerosis. Nat Immunol 2011;12:204-12.

203. Virmani R, Burke AP, Kolodgie FD, Farb A. Vulnerable plaque: the pathology of unstable coronary lesions. J Interv Cardiol 2002;15:439-46.

204. Steinl CD, Kaufmann AB. Ultrasound Imaging for Risk Assessment in Atherosclerosis. International Journal of Molecular Sciences 2015;16.

205. Tabas I, García-Cardeña G, Owens GK. Recent insights into the cellular biology of atherosclerosis. J Cell Biol 2015;209:13-22.

206. Gimbrone MA, García-Cardeña G. Vascular endothelium, hemodynamics, and the pathobiology of atherosclerosis. Cardiovasc Pathol 2013;22:9-15.

207. Koo A, Dewey CF, García-Cardeña G. Hemodynamic shear stress characteristic of atherosclerosis-resistant regions promotes glycocalyx

formation in cultured endothelial cells. Am J Physiol Cell Physiol 2013;304:C137-46.

208. Atkins GB, Wang Y, Mahabeleshwar GH et al. Hemizygous Deficiency of Kruppel-like Factor 2 Augments Experimental Atherosclerosis. Circ Res 2008;103:690-3.

209. Zhou G. Endothelial Kruppel-like factor 4 protects against atherothrombosis in mice. 2012;122:4727-31.

210. Dai G, Kaazempur-Mofrad MR, Natarajan S et al. Distinct endothelial phenotypes evoked by arterial waveforms derived from atherosclerosis-susceptible and -resistant regions of human vasculature. Proc Natl Acad Sci U S A 2004;101:14871-6.

211. Hajra L, Evans AI, Chen M, Hyduk SJ, Collins T, Cybulsky MI. The NF-κB signal transduction pathway in aortic endothelial cells is primed for activation in regions predisposed to atherosclerotic lesion formation. Proc Natl Acad Sci U S A 2000;97:9052-7.

212. Alexander MR, Owens GK. Epigenetic control of smooth muscle cell differentiation and phenotypic switching in vascular development and disease. Annu Rev Physiol 2012;74:13-40.

213. Rudijanto A. The role of vascular smooth muscle cells on the pathogenesis of atherosclerosis. Acta Med Indones 2007;39:86-93.

214. Bennett MR, Sinha S, Owens GK. Vascular smooth muscle cells in atherosclerosis. Circ Res 2016;118:692-702.

215. Gu L, Okada Y, Clinton SK et al. Absence of monocyte chemoattractant protein-1 reduces atherosclerosis in low density lipoprotein receptor-deficient mice. Mol Cell 1998;2:275-81.

216. Rajavashisth T, Qiao JH, Tripathi S et al. Heterozygous osteopetrotic (op) mutation reduces atherosclerosis in LDL receptor- deficient mice. J Clin Invest 1998;101:2702-10.

217. Febbraio M, Podrez EA, Smith JD et al. Targeted disruption of the class B scavenger receptor CD36 protects against atherosclerotic lesion development in mice. J Clin Invest 2000;105:1049-56.

218. Moore KJ, Sheedy FJ, Fisher EA. Macrophages in atherosclerosis: a dynamic balance. Nature reviews Immunology 2013;13:709-721.

219. Duewell P, Kono H, Rayner KJ et al. NLRP3 inflammasomes are required for atherogenesis and activated by cholesterol crystals. Nature 2010;464:1357-1361.

220. Duewell P, Kono H, Rayner KJ et al. NLRP3 inflamasomes are required for atherogenesis and activated by cholesterol crystals that form early in disease. Nature 2010;464:1357-61.

221. Bobryshev YV, Lord RS. Ultrastructural recognition of cells with dendritic cell morphology in human aortic intima. Contacting interactions of Vascular Dendritic Cells in athero-resistant and athero-prone areas of the normal aorta. Arch Histol Cytol 1995;58:307-22.

222. Zhou X, Paulsson G, Stemme S, Hansson GK. Hypercholesterolemia is associated with a T helper (Th) 1/Th2 switch of the autoimmune response in atherosclerotic apo E-knockout mice. J Clin Invest 1998;101:1717-25.

223. Huber SA, Sakkinen P, David C, Newell MK, Tracy RP. T helper-cell phenotype regulates atherosclerosis in mice under conditions of mild hypercholesterolemia. Circulation 2001;103:2610-6.

224. King VL, Szilvassy SJ, Daugherty A. Interleukin-4 deficiency decreases atherosclerotic lesion formation in a site-specific manner in female LDL receptor–/– mice. Arteriosclerosis, thrombosis, and vascular biology 2002;22:456-461.

225. Mallat Z, Taleb S, Ait-Oufella H, Tedgui A. The role of adaptive T cell immunity in atherosclerosis. Journal of lipid research 2009;50:S364-S369.

226. Galkina E, Ley K. Immune and Inflammatory Mechanisms of Atherosclerosis. Annu Rev Immunol 2009;27:165-97.

227. Whitman SC, Ramsamy TA. Participatory role of natural killer and natural killer T cells in atherosclerosis: lessons learned from in vivo mouse studies. Can J Physiol Pharmacol 2006;84:67-75.

228. Alcaide P, Jones TG, Lord GM et al. Dendritic cell expression of the transcription factor T-bet regulates mast cell progenitor homing to mucosal tissue. J Exp Med 2007;204:431-9.

229. Maxfield FR, Tabas I. Role of cholesterol and lipid organization in disease. Nature 2005;438:612-21.

230. Zhou AX, Tabas I. The UPR in atherosclerosis. Semin Immunopathol 2013;35:321-32.

231. Gargalovic PS, Gharavi NM, Clark MJ et al. The unfolded protein response is an important regulator of inflammatory genes in endothelial cells. Arterioscler Thromb Vasc Biol 2006;26:2490-6.

232. Zhou J, Lhotak S, Hilditch BA, Austin RC. Activation of the unfolded protein response occurs at all stages of atherosclerotic lesion development in apolipoprotein E-deficient mice. Circulation 2005;111:1814-21.

233. Myoishi M, Hao H, Minamino T et al. Increased endoplasmic reticulum stress in atherosclerotic plaques associated with acute coronary syndrome. Circulation 2007;116:1226-33.

234. Seimon T, Tabas I. Mechanisms and consequences of macrophage apoptosis in atherosclerosis. J Lipid Res 2009;50 Suppl:S382-7.

235. Baigent C, Keech A, Kearney P, Blackwell L. Efficacy and safety of cholesterol-lowering treatment: prospective meta-analysis of data from 90 056 participants in 14 randomised trials of statins. The Lancet 2005;366:1267.

236. Greenland P, Knoll MD, Stamler J et al. Major risk factors as antecedents of fatal and nonfatal coronary heart disease events. Jama 2003;290:891-897.

237. Charo IF, Taub R. Anti-inflammatory therapeutics for the treatment of atherosclerosis. Nat Rev Drug Discov 2011;10:365-76.

238. Moss JWE, Ramji DP. Nutraceutical therapies for atherosclerosis. Nat Rev Cardiol 2016;13:513-32.

239. Minamino T, Komuro I, Kitakaze M. Endoplasmic reticulum stress as a therapeutic target in cardiovascular disease. Circ Res 2010;107:1071-82.

240. Gorinstein S, Leontowicz H, Lojek A et al. Olive oils improve lipid metabolism and increase antioxidant potential in rats fed diets containing cholesterol. J Agric Food Chem 2002;50:6102-8.

241. Dell'Agli M, Fagnani R, Mitro N et al. Minor components of olive oil modulate proatherogenic adhesion molecules involved in endothelial activation. J Agric Food Chem 2006;54:3259-64.

242. Gonzalez-Santiago M, Martin-Bautista E, Carrero JJ et al. One-month administration of hydroxytyrosol, a phenolic antioxidant present in olive oil, to hyperlipemic rabbits improves blood lipid profile, antioxidant status and reduces atherosclerosis development. Atherosclerosis 2006;188:35-42.

243. Osganian SK, Stampfer MJ, Rimm E et al. Vitamin C and risk of coronary heart disease in women. J Am Coll Cardiol 2003;42:246-52.

244. Averill MM, Bennett BJ, Rattazzi M et al. Dietary Antioxidants and Genistein Do Not Inhibit the Progression of Established Atherosclerotic Lesions in Older Apo E Deficient Mice. Atherosclerosis 2009;203:82-8.

245. Slavin JL, Lloyd B. Health benefits of fruits and vegetables. Adv Nutr 2012;3:506-16.

246. Çimen I, Kocatürk B, Koyuncu S et al. Prevention of atherosclerosis by bioactive palmitoleate through suppression of organelle stress and inflammasome activation. Sci Transl Med 2016;8:358ra126.

247. Popa C, Netea MG, Radstake T et al. Influence of anti-tumour necrosis factor therapy on cardiovascular risk factors in patients with active rheumatoid arthritis. Annals of the rheumatic diseases 2005;64:303-305.

248. Zapolska-Downar D, Siennicka A, Kaczmarczyk M, Kołodziej B, Naruszewicz M. Simvastatin modulates TNFα-induced adhesion molecules expression in human endothelial cells. Life sciences 2004;75:1287-1302.

249. Rosenson RS. Future role for selective phospholipase A2 inhibitors in the prevention of atherosclerotic cardiovascular disease. Cardiovascular drugs and therapy 2009;23:93-101.

250. Suckling K. Phospholipase A2s: Developing drug targets for atherosclerosis. Atherosclerosis 2010;212:357-366.

251. Gilbert J, Lekstrom-Himes J, Donaldson D et al. Effect of CC chemokine receptor 2 CCR2 blockade on serum C-reactive protein in individuals at atherosclerotic risk and with a single nucleotide polymorphism of the monocyte chemoattractant protein-1 promoter region. The American journal of cardiology 2011;107:906-911.

252. De Caterina R, Zampolli A. From asthma to atherosclerosis—5-lipoxygenase, leukotrienes, and inflammation. New England Journal of Medicine 2004;350:4-7.

253. Koenen RR, von Hundelshausen P, Nesmelova IV et al. Disrupting functional interactions between platelet chemokines inhibits atherosclerosis in hyperlipidemic mice. Nat Med 2009;15:97-103.

254. Serbina NV, Pamer EG. Monocyte emigration from bone marrow during bacterial infection requires signals mediated by chemokine receptor CCR2. Nature immunology 2006;7:311-317.

255. Tabibiazar R, Wagner RA, Ashley EA et al. Signature patterns of gene expression in mouse atherosclerosis and their correlation to human coronary disease. Physiological genomics 2005;22:213-226.

256. Lötzer K, Funk CD, Habenicht AJ. The 5-lipoxygenase pathway in arterial wall biology and atherosclerosis. Biochimica et Biophysica Acta (BBA)-Molecular and Cell Biology of Lipids 2005;1736:30-37.

257. Hakonarson H, Thorvaldsson S, Helgadottir A et al. Effects of a 5-lipoxygenase–activating protein inhibitor on biomarkers associated with risk of myocardial infarction: a randomized trial. Jama 2005;293:2245-2256.

258. Tardif J-C, L'allier PL, Ibrahim R et al. Treatment with 5-lipoxygenase inhibitor VIA-2291 (Atreleuton) in patients with recent acute coronary syndrome. Circulation: Cardiovascular Imaging 2010:CIRCIMAGING. 110.937169.

259. Aikawa M, Rabkin E, Sugiyama S et al. An HMG-CoA reductase inhibitor, cerivastatin, suppresses growth of macrophages expressing matrix metalloproteinases and tissue factor in vivo and in vitro. Circulation 2001;103:276-283.

260. Steffens S, Mach F. Anti-inflammatory properties of statins. Seminars in vascular medicine: Copyright© 2004 by Thieme Medical Publishers, Inc., 333 Seventh Avenue, New York, NY 10001, USA., 2004:417-422.

261. Dinarello CA, Simon A, van der Meer JWM. Treating inflammation by blocking interleukin-1 in a broad spectrum of diseases. Nature reviews Drug discovery 2012;11:633-652.

262. Nicklin MJ, Hughes DE, Barton JL, Ure JM, Duff GW. Arterial inflammation in mice lacking the interleukin 1 receptor antagonist gene. The Journal of experimental medicine 2000;191:303-312.

263. Isoda K, Kitagaki M, Niida T et al. Deficiency of Interleukin-1 Receptor Antagonist Promotes Spontaneous Femoral Artery Aneurysm Formation in Mice. The American Journal of Pathology 2012;180:1254-1263.

264. Isoda K, Sawada S, Ishigami N et al. Lack of Interleukin-1 Receptor Antagonist Modulates Plaque Composition in Apolipoprotein E–Deficient Mice. Arteriosclerosis, Thrombosis, and Vascular Biology 2004;24:1068-1073.

265. Ridker PM, Everett BM, Thuren T et al. Antiinflammatory Therapy with Canakinumab for Atherosclerotic Disease. New England Journal of Medicine 2017.

266. Ron D, Walter P. Signal integration in the endoplasmic reticulum unfolded protein response. Nat Rev Mol Cell Biol 2007;8:519-529.

267. Todd DJ, Lee AH, Glimcher LH. The endoplasmic reticulum stress response in immunity and autoimmunity. Nat Rev Immunol 2008;8:663-674.

268. Ozcan U, Yilmaz E, Ozcan L et al. Chemical chaperones reduce ER stress and restore glucose homeostasis in a mouse model of type 2 diabetes. Science 2006;313:1137-40.

269. Engin F, Hotamisligil GS. Restoring endoplasmic reticulum function by chemical chaperones: an emerging therapeutic approach for metabolic diseases. Diabetes Obes Metab 2010;12 Suppl 2:108-15.

270. Das I, Krzyzosiak A, Schneider K et al. Preventing proteostasis diseases by selective inhibition of a phosphatase regulatory subunit. Science 2015;348:239-42.

271. Fu HY, Okada K-i, Liao Y et al. Ablation of C/EBP homologous protein attenuates endoplasmic reticulum–mediated apoptosis and cardiac dysfunction induced by pressure overload. Circulation 2010;122:361-369.

272. Chen Y-J, Tan BC-M, Cheng Y-Y, Chen J-S, Lee S-C. Differential regulation of CHOP translation by phosphorylated eIF4E under stress conditions. Nucleic acids research 2009:gkp1034.

273. Hotamisligil GS. Inflammation, metaflammation and immunometabolic disorders. Nature Reviews 2017;542:177-185.

274. Han S, Liang CP, DeVries-Seimon T et al. Macrophage insulin receptor deficiency increases ER stress-induced apoptosis and necrotic core formation in advanced atherosclerotic lesions. Cell Metab 2006;3:257-66.

275. Seimon TA, Wang Y, Han S et al. Macrophage deficiency of p38alpha MAPK promotes apoptosis and plaque necrosis in advanced atherosclerotic lesions in mice. J Clin Invest 2009;119:886-98.

276. Menon P, Fisher EA. Immunostaining of macrophages, endothelial cells and smooth muscle cells in the atherosclerotic mouse aorta. Methods in molecular biology (Clifton, NJ) 2015;1339:131-148.

277. Rinne P, Rami M, Nuutinen S et al. Melanocortin 1 Receptor Signaling Regulates Cholesterol Transport in Macrophages. Circulation 2017;136:83-97.

278. Erbay E, Babaev VR, Mayers JR et al. Reducing endoplasmic reticulum stress through a macrophage lipid chaperone alleviates atherosclerosis. Nat Med 2009;15:1383-91.

279. Doran AC, Ozcan L, Cai B et al. CAMKIIγ suppresses an efferocytosis pathway in macrophages and promotes atherosclerotic plaque necrosis. The Journal of Clinical Investigation 2017;127:4075-4089.

280. Proto JD, Doran AC, Subramanian M et al. Hypercholesterolemia induces T cell expansion in humanized immune mice. The Journal of Clinical Investigation 2018;128:2370-2375.

281. Subramanian M, Thorp E, Hansson GK, Tabas I. Treg-mediated suppression of atherosclerosis requires MYD88 signaling in DCs. The Journal of clinical investigation 2013;123:179-188.

282. Furuhashi M, Tuncman G, Gorgun CZ et al. Treatment of diabetes and atherosclerosis by inhibiting fatty-acid-binding protein aP2. Nature 2007;447:959-65.

283. Lebeaupin C, Proics E, de Bieville CHD et al. ER stress induces NLRP3 inflammasome activation and hepatocyte death. Cell Death Dis 2015;6:e1879-.

284. Lopez-Castejon G, Brough D. Understanding the mechanism of IL-1β secretion. Cytokine & growth factor reviews 2011;22:189-195.

285. Tőzsér J, Benkő S. Natural Compounds as Regulators of NLRP3 Inflammasome-Mediated IL-1β Production. Mediators of Inflammation 2016;2016.

286. Knight ZA, Shokat KM. Chemical genetics: where genetics and pharmacology meet. Cell 2007;128:425-30.

287. Blair JA, Rauh D, Kung C et al. Structure-guided development of affinity probes for tyrosine kinases using chemical genetics. Nature Chemical Biology 2007;3:229-238.

288. Maas NL, Singh N, Diehl JA. Generation and characterization of an analog-sensitive PERK allele. Cancer Biology & Therapy 2014;15:1106-1111.

289. Carrara M, Sigurdardottir A, Bertolotti A. Decoding the selectivity of eIF2[alpha] holophosphatases and PPP1R15A inhibitors. Nat Struct Mol Biol 2017;24,708-716.

290. Sidrauski C, Tsai JC, Kampmann M et al. Pharmacological dimerization and activation of the exchange factor eIF2B antagonizes the integrated stress response. eLife 2015;4:e07314.

291. Halliday M, Radford H, Sekine Y et al. Partial restoration of protein synthesis rates by the small molecule ISRIB prevents neurodegeneration without pancreatic toxicity. Cell Death & Disease 2015;6:e1672.

292. Guo H, Callaway JB, Ting JP. Inflammasomes: mechanism of action, role in disease, and therapeutics. Nat Med 2015;21:677-87.

293. Hori O, Ichinoda F, Tamatani T et al. Transmission of cell stress from endoplasmic reticulum to mitochondria. The Journal of cell biology 2002;157:1151-1160.

294. Han J, Back SH, Hur J et al. ER-stress-induced transcriptional regulation increases protein synthesis leading to cell death. Nat Cell Biol 2013;15:481-90.

295. Gibellini L, Pinti M, Bartolomeo R et al. Inhibition of Lon protease by triterpenoids alters mitochondria and is associated to cell death in human cancer cells. Oncotarget 2015;6:25466-25483.

296. Thomas RE, Andrews LA, Burman JL, Lin W-Y, Pallanck LJ. PINK1-Parkin Pathway Activity Is Regulated by Degradation of PINK1 in the Mitochondrial Matrix. PLOS Genetics 2014;10:e1004279.

297. McAlpine CS, Werstuck GH. Protein kinase R-like endoplasmic reticulum kinase and glycogen synthase kinase-3α/β regulate foam cell formation. Journal of Lipid Research 2014;55:2320-2333.

298. Zhao Y, Guo Z, Lin X et al. Apolipoprotein E-Deficient Lipoproteins Induce Foam Cell Formation by Activation of PERK-EIF-2α Signaling Cascade. Journal of bioanalysis & biomedicine 2010;2:113-120.

299. Moreno JA, Halliday M, Molloy C et al. Oral Treatment Targeting the Unfolded Protein Response Prevents Neurodegeneration and Clinical Disease in Prion-Infected Mice. Science Translational Medicine 2013;5:206ra138-206ra138.

300. Radford H, Moreno JA, Verity N, Halliday M, Mallucci GR. PERK inhibition prevents tau-mediated neurodegeneration in a mouse model of frontotemporal dementia. Acta neuropathologica 2015;130:633-642.

301. Mohanta S, Yin C, Weber C, Hu D, Habenicht AJ. Aorta atherosclerosis lesion analysis in hyperlipidemic mice. Bio-protocol 2016;6.

302. Pedretti M, Rancic Z, Soltermann A et al. Comparative immunohistochemical staining of atherosclerotic plaques using F16, F8 and L19: Three clinical-grade fully human antibodies. Atherosclerosis 2010;208:382-389.

303. Moore KJ, Tabas I. The cellular biology of macrophages in atherosclerosis. Cell 2011;145:341.

304. Bhaskar V, Yin J, Mirza AM et al. Monoclonal antibodies targeting IL-1 beta reduce biomarkers of atherosclerosis in vitro and inhibit atherosclerotic plaque formation in Apolipoprotein E-deficient mice. Atherosclerosis 2011;216:313-320.

305. Elenkov IJ, Chrousos GP. Stress Hormones, Th1/Th2 patterns, Pro/Anti-inflammatory Cytokines and Susceptibility to Disease. Trends in Endocrinology & Metabolism 1999;10:359-368.

306. Ovchinnikova O, Robertson A-KL, Wågsäter D et al. T-cell activation leads to reduced collagen maturation in atherosclerotic plaques of ApoE–/– mice. The American journal of pathology 2009;174:693-700.

307. Ait-Oufella H, Taleb S, Mallat Z, Tedgui A. Recent advances on the role of cytokines in atherosclerosis. Arterioscler Thromb Vasc Biol 2011;31:969-79.

308. Gofman JW, Lindcren F, Elliott H et al. The role of lipids and lipoproteins in atherosclerosis. Science (Washington) 1950;111:166-186.

309. Rojas-Rivera D, Delvaeye T, Roelandt R et al. When PERK inhibitors turn out to be new potent RIPK1 inhibitors: critical issues on the specificity and

use of GSK2606414 and GSK2656157. Cell Death And Differentiation 2017;24:1100.

310. Savitt J, Singh D, Zhang C et al. The in vivo response of stem and other undifferentiated spermatogonia to the reversible inhibition of glial cell line-derived neurotrophic factor signaling in the adult. Stem cells (Dayton, Ohio) 2012;30:732-740.

311. Palam LR, Gore J, Craven KE, Wilson JL, Korc M. Integrated stress response is critical for gemcitabine resistance in pancreatic ductal adenocarcinoma. Cell Death & Disease 2015;6:e1913.

312. Sidrauski C, Acosta-Alvear D, Khoutorsky A et al. Pharmacological brake-release of mRNA translation enhances cognitive memory. Elife 2013;2:e00498.

313. Robblee MM, Kim CC, Porter Abate J et al. Saturated Fatty Acids Engage an IRE1α-Dependent Pathway to Activate the NLRP3 Inflammasome in Myeloid Cells. Cell Rep 2016;14:2611-23.

314. Sidrauski C, McGeachy AM, Ingolia NT, Walter P. The small molecule ISRIB reverses the effects of eIF2α phosphorylation on translation and stress granule assembly. eLife 2015;4:e05033.

315. Tsai JC, Miller-Vedam LE, Anand AA et al. Structure of the nucleotide exchange factor eIF2B reveals mechanism of memory-enhancing molecule. Science 2018;359.

316. Sekine Y, Zyryanova A, Crespillo-Casado A, Fischer PM, Harding HP, Ron D. Mutations in a translation initiation factor identify target of a memory-enhancing compound. Science (New York, NY) 2015;348:1027-1030.

317. Placzek AN, Prisco GVD, Khatiwada S et al. eIF2α-mediated translational control regulates the persistence of cocaine-induced LTP in midbrain dopamine neurons. eLife 2016;5:e17517.

318. Crespillo-Casado A, Chambers JE, Fischer PM, Marciniak SJ, Ron D. PPP1R15A-mediated dephosphorylation of eIF2α is unaffected by Sephin1 or Guanabenz. eLife 2017;6:e26109.

319. Chou A, Krukowski K, Jopson T et al. Inhibition of the integrated stress response reverses cognitive deficits after traumatic brain injury. Proc Natl Acad Sci U S A 2017;114:E6420-E6426.

320. Axten JM, Medina JR, Feng Y et al. Discovery of 7-Methyl-5-(1-{[3-(trifluoromethyl)phenyl]acetyl}-2,3-dihydro-1H-indol-5-yl)-7H-pyrrolo[2,3-d]pyrimidin-4-amine (GSK2606414), a Potent and Selective First-in-Class Inhibitor of Protein Kinase R (PKR)-like Endoplasmic Reticulum Kinase (PERK). Journal of Medicinal Chemistry 2012;55:7193-7207.

321. Cai B, Thorp EB, Doran AC et al. MerTK receptor cleavage promotes plaque necrosis and defective resolution in atherosclerosis. The Journal of Clinical Investigation 2017;127:564-568.

322. Marek I, Canu M, Cordasic N et al. Sex differences in the development of vascular and renal lesions in mice with a simultaneous deficiency of Apoe and the integrin chain Itga8. Biology of Sex Differences 2017;8:19.

323. Pettersson US, Waldén TB, Carlsson P-O, Jansson L, Phillipson M. Female Mice are Protected against High-Fat Diet Induced Metabolic Syndrome and Increase the Regulatory T Cell Population in Adipose Tissue. PLOS ONE 2012;7:e46057.

324. Dinh QN, Chrissobolis S, Diep H et al. Advanced atherosclerosis is associated with inflammation, vascular dysfunction and oxidative stress, but not hypertension. Pharmacological Research 2017;116:70-76.

325. Eiyama A, Okamoto K. PINK1/Parkin-mediated mitophagy in mammalian cells. Current Opinion in Cell Biology 2015;33:95-101.

326. Wu W, Xu H, Wang Z et al. PINK1-Parkin-Mediated Mitophagy Protects Mitochondrial Integrity and Prevents Metabolic Stress-Induced Endothelial Injury. PLOS ONE 2015;10:e0132499.

327. Abderrazak A, Couchie D, Mahmood DF et al. Anti-inflammatory and antiatherogenic effects of the NLRP3 inflammasome inhibitor arglabin in ApoE2.Ki mice fed a high-fat diet. Circulation 2015;131:1061-70.

328. Sheedy FJ, Grebe A, Rayner KJ et al. CD36 coordinates NLRP3 inflammasome activation by facilitating intracellular nucleation of soluble ligands into particulate ligands in sterile inflammation. Nat Immunol 2013;14:812-20.

329. Ridker PM, MacFadyen JG, Everett BM et al. Relationship of C-reactive protein reduction to cardiovascular event reduction following treatment with canakinumab: a secondary analysis from the CANTOS randomised controlled trial. The Lancet 2018;391:319-328.

330. Tabas I. The role of endoplasmic reticulum stress in the progression of atherosclerosis. Circ Res 2010;107:839-50.

331. Kamaly N, Fredman G, Fojas JJR et al. Targeted interleukin-10 nanotherapeutics developed with a microfluidic chip enhance resolution of inflammation in advanced atherosclerosis. ACS nano 2016;10:5280-5292.

332. Mayer Loretta P, Dyer Cheryl A, Eastgard Rebecca L, Hoyer Patricia B, Banka Carole L. Atherosclerotic Lesion Development in a Novel Ovary-Intact Mouse Model of Perimenopause. Arteriosclerosis, Thrombosis, and Vascular Biology 2005;25:1910-1916.

Copyright Permissions

ELSEVIER LICENSE
TERMS AND CONDITIONS

Jun 10, 2019

This Agreement between Bilkent University -- Umut Onat ("You") and Elsevier ("Elsevier") consists of your license details and the terms and conditions provided by Elsevier and Copyright Clearance Center.

License Number	4578761138791
License date	Apr 30, 2019
Licensed Content Publisher	Elsevier
Licensed Content Publication	Biochimica et Biophysica Acta (BBA) - Molecular Basis of Disease
Licensed Content Title	Autophagy: A housekeeper in cardiorenal metabolic health and disease
Licensed Content Author	Guanghong Jia,James R. Sowers
Licensed Content Date	Feb 1, 2015
Licensed Content Volume	1852
Licensed Content Issue	2
Licensed Content Pages	6
Start Page	219
End Page	224
Type of Use	reuse in a thesis/dissertation
Portion	figures/tables/illustrations
Number of figures/tables/illustrations	1
Format	both print and electronic
Are you the author of this Elsevier article?	No
Will you be translating?	No
Original figure numbers	Fig. 1. Proposed dysregulation of autophagy in the development of CRS.
Title of your thesis/dissertation	THE ROLE OF LIPID INDUCED INTEGRATED STRESS RESPONSE IN METAFLAMMATION AND ATHEROSCLEROSIS
Publisher of new work	Bilkent University
Expected completion date	Jul 2019
Estimated size (number of pages)	1
Requestor Location	Bilkent University Ankara Turkey Ankara, Cankaya/Bilkent 06800 Turkey Attn: Bilkent University
Publisher Tax ID	GB 494 6272 12
Total	0.00 USD
Terms and Conditions	

ELSEVIER LICENSE
TERMS AND CONDITIONS

Jun 10, 2019

This Agreement between Bilkent University -- Umut Onat ("You") and Elsevier ("Elsevier") consists of your license details and the terms and conditions provided by Elsevier and Copyright Clearance Center.

License Number	4575930464678
License date	Apr 25, 2019
Licensed Content Publisher	Elsevier
Licensed Content Publication	Mitochondrion
Licensed Content Title	Mitophagy and the release of inflammatory cytokines
Licensed Content Author	James Harris,Nadia Deen,Shahrzad Zamani,Md Abul Hasnat
Licensed Content Date	Jul 1, 2018
Licensed Content Volume	41
Licensed Content Issue	n/a
Licensed Content Pages	7
Start Page	2
End Page	8
Type of Use	reuse in a thesis/dissertation
Intended publisher of new work	other
Portion	figures/tables/illustrations
Number of figures/tables/illustrations	1
Format	both print and electronic
Are you the author of this Elsevier article?	No
Will you be translating?	No
Original figure numbers	Figure 1 Mechanisms of Mitophagy
Title of your thesis/dissertation	THE ROLE OF LIPID INDUCED INTEGRATED STRESS RESPONSE IN METAFLAMMATION AND ATHEROSCLEROSIS
Publisher of new work	Bilkent University
Expected completion date	Jul 2019
Estimated size (number of pages)	1
Requestor Location	Bilkent University Ankara Turkey Ankara, Cankaya/Bilkent 06800 Turkey Attn: Bilkent University
Publisher Tax ID	GB 494 6272 12
Total	0.00 USD
Terms and Conditions	

ELSEVIER LICENSE
TERMS AND CONDITIONS

Jun 10, 2019

This Agreement between Bilkent University -- Umut Onat ("You") and Elsevier ("Elsevier") consists of your license details and the terms and conditions provided by Elsevier and Copyright Clearance Center.

License Number	4575920865502
License date	Apr 25, 2019
Licensed Content Publisher	Elsevier
Licensed Content Publication	Cell
Licensed Content Title	NF-κB Restricts Inflammasome Activation via Elimination of Damaged Mitochondria
Licensed Content Author	Zhenyu Zhong,Atsushi Umemura,Elsa Sanchez-Lopez,Shuang Liang,Shabnam Shalapour,Jerry Wong,Feng He,Daniela Boassa,Guy Perkins,Syed Raza Ali,Matthew D. McGeough,Mark H. Ellisman,Ekihiro Seki,Asa B. Gustafsson,Hal M. Hoffman,Maria T. Diaz-Meco et al.
Licensed Content Date	Feb 25, 2016
Licensed Content Volume	164
Licensed Content Issue	5
Licensed Content Pages	15
Start Page	896
End Page	910
Type of Use	reuse in a thesis/dissertation
Portion	figures/tables/illustrations
Number of figures/tables/illustrations	1
Format	both print and electronic
Are you the author of this Elsevier article?	No
Will you be translating?	No
Original figure numbers	Graphical abstract
Title of your thesis/dissertation	THE ROLE OF LIPID INDUCED INTEGRATED STRESS RESPONSE IN METAFLAMMATION AND ATHEROSCLEROSIS
Publisher of new work	Bilkent University
Expected completion date	Jul 2019
Estimated size (number of pages)	1
Requestor Location	Bilkent University Ankara Turkey Ankara, Cankaya/Bilkent 06800 Turkey Attn: Bilkent University
Publisher Tax ID	GB 494 6272 12
Total	0.00 USD

SPRINGER NATURE LICENSE
TERMS AND CONDITIONS

Jun 10, 2019

This Agreement between Bilkent University -- Umut Onat ("You") and Springer Nature ("Springer Nature") consists of your license details and the terms and conditions provided by Springer Nature and Copyright Clearance Center.

License Number	4575330178680
License date	Apr 24, 2019
Licensed Content Publisher	Springer Nature
Licensed Content Publication	Nature Immunology
Licensed Content Title	Emerging functions of the unfolded protein response in immunity
Licensed Content Author	Sophie Janssens, Bali Pulendran, Bart N Lambrecht
Licensed Content Date	Sep 18, 2014
Licensed Content Volume	15
Licensed Content Issue	10
Type of Use	Thesis/Dissertation
Requestor type	academic/university or research institute
Format	print and electronic
Portion	figures/tables/illustrations
Number of figures/tables/illustrations	2
High-res required	no
Will you be translating?	no
Circulation/distribution	<501
Author of this Springer Nature content	no
Title	THE ROLE OF LIPID INDUCED INTEGRATED STRESS RESPONSE IN METAFLAMMATION AND ATHEROSCLEROSIS
Institution name	Bilkent University
Expected presentation date	Jul 2019
Portions	Figure 3: IRE-1 intersects with inflammatory pathways. and Figure 4: Pathways downstream of PERK are tightly controlled by inflammatory signals.
Requestor Location	Bilkent University Ankara Turkey Ankara, Cankaya/Bilkent 06800 Turkey Attn: Bilkent University
Total	0.00 USD
Terms and Conditions	

ELSEVIER LICENSE
TERMS AND CONDITIONS

Jun 10, 2019

This Agreement between Bilkent University -- Umut Onat ("You") and Elsevier ("Elsevier") consists of your license details and the terms and conditions provided by Elsevier and Copyright Clearance Center.

License Number	4575290276040
License date	Apr 24, 2019
Licensed Content Publisher	Elsevier
Licensed Content Publication	The Lancet Neurology
Licensed Content Title	Harnessing the integrated stress response for the treatment of multiple sclerosis
Licensed Content Author	Sharon W Way,Brian Popko
Licensed Content Date	Apr 1, 2016
Licensed Content Volume	15
Licensed Content Issue	4
Licensed Content Pages	10
Start Page	434
End Page	443
Type of Use	reuse in a thesis/dissertation
Portion	figures/tables/illustrations
Number of figures/tables/illustrations	2
Format	both print and electronic
Are you the author of this Elsevier article?	No
Will you be translating?	No
Original figure numbers	Figure 1. The integrated stress response is sensitive to numerous stress conditions and Figure 2. Translational control and cellular protection in response to stress
Title of your thesis/dissertation	THE ROLE OF LIPID INDUCED INTEGRATED STRESS RESPONSE IN METAFLAMMATION AND ATHEROSCLEROSIS
Publisher of new work	Bilkent University
Expected completion date	Jul 2019
Estimated size (number of pages)	1
Requestor Location	Bilkent University Ankara Turkey Ankara, Cankaya/Bilkent 06800 Turkey Attn: Bilkent University
Publisher Tax ID	GB 494 6272 12
Total	0.00 USD
Terms and Conditions	

SPRINGER NATURE LICENSE
TERMS AND CONDITIONS

Jun 10, 2(

This Agreement between Bilkent University -- Umut Onat ("You") and Springer Nature ("Springer Nature") consists of your license details and the terms and conditions provided Springer Nature and Copyright Clearance Center.

License Number	4575280343334
License date	Apr 24, 2019
Licensed Content Publisher	Springer Nature
Licensed Content Publication	Nature Reviews Cancer
Licensed Content Title	The impact of the endoplasmic reticulum protein-folding environment on cancer development
Licensed Content Author	Miao Wang, Randal J. Kaufman
Licensed Content Date	Aug 22, 2014
Licensed Content Volume	14
Licensed Content Issue	9
Type of Use	Thesis/Dissertation
Requestor type	academic/university or research institute
Format	print and electronic
Portion	figures/tables/illustrations
Number of figures/tables/illustrations	1
High-res required	no
Will you be translating?	no
Circulation/distribution	<501
Author of this Springer Nature content	no
Title	THE ROLE OF LIPID INDUCED INTEGRATED STRESS RESPONSE IN METAFLAMMATION AND ATHEROSCLEROSIS
Institution name	Bilkent University
Expected presentation date	Jul 2019
Portions	Figure 1: The unfolded protein response (UPR) signalling pathways.
Requestor Location	Bilkent University Ankara Turkey Ankara, Cankaya/Bilkent 06800 Turkey Attn: Bilkent University
Total	0.00 USD
Terms and Conditions	

Springer Science and Bus Media B V LICENSE
TERMS AND CONDITIONS

Jul 23, 2019

This is a License Agreement between Bilkent University -- Umut Onat ("You") and Springer Science and Bus Media B V ("Springer Science and Bus Media B V") provided by Copyright Clearance Center ("CCC"). The license consists of your order details, the terms and conditions provided by Springer Science and Bus Media B V, and the payment terms and conditions.

All payments must be made in full to CCC. For payment instructions, please see information listed at the bottom of this form.

License Number	4614950960813
License date	Jun 23, 2019
Licensed content publisher	Springer Science and Bus Media B V
Licensed content title	Seminars in immunopathology
Licensed content date	Jan 1, 2007
Type of Use	Thesis/Dissertation
Requestor type	Academic institution
Format	Print, Electronic
Portion	image/photo
Number of images/photos requested	1
The requesting person/organization is:	Umut İnci Onat, Bilkent University
Title or numeric reference of the portion(s)	Figure 1.Sequential activation of UPR signaling pathways in atherosclerosis
Title of the article or chapter the portion is from	The UPR in atherosclerosis
Editor of portion(s)	N/A
Author of portion(s)	N/A
Volume of serial or monograph.	volume 35
Issue, if republishing an article from a serial	issue 3
Page range of the portion	on page 324
Publication date of portion	2013
Rights for	Main product
Duration of use	Life of current edition
Creation of copies for the disabled	no
With minor editing privileges	no
For distribution to	Worldwide
In the following language(s)	Original language of publication
With incidental promotional use	no
The lifetime unit quantity of new product	Up to 499

Title	THE ROLE OF LIPID INDUCED INTEGRATED STRESS RESPONSE IN METAFLAMMATION AND ATHEROSCLEROSIS
Institution name	Bilkent University
Expected presentation date	Jul 2019
Total (may include CCC user fee)	0.00 USD
Terms and Conditions	

Publications

JOURNAL OF THE AMERICAN COLLEGE OF CARDIOLOGY VOL. 73, NO. 10, 2019
© 2019 THE AUTHORS. PUBLISHED BY ELSEVIER ON BEHALF OF THE AMERICAN COLLEGE OF CARDIOLOGY FOUNDATION. THIS IS AN OPEN ACCESS ARTICLE UNDER THE CC BY-NC-ND LICENSE (http://creativecommons.org/licenses/by-nc-nd/4.0/).

Intercepting the Lipid-Induced Integrated Stress Response Reduces Atherosclerosis

Umut I. Onat, BSc,[a,b] Asli D. Yildirim, MSc,[a,b,c,d] Özlem Tufanli, PhD,[a,b] Ismail Çimen, PhD,[a,b] Begüm Kocatürk, PhD,[a,b,e] Zehra Veli, MSc,[a,b] Syed M. Hamid, PhD,[c,d] Kenichi Shimada, PhD,[c,f,g] Shuang Chen, MD, PhD,[c,g,h] Jon Sin, PhD,[c,d] Prediman K. Shah, MD,[d,f] Roberta A. Gottlieb, MD, PhD,[c,d] Moshe Arditi, MD,[c,d,g,h] Ebru Erbay, MD, PhD[a,b,c,d]

ABSTRACT

BACKGROUND Eukaryotic cells can respond to diverse stimuli by converging at serine-51 phosphorylation on eukaryotic initiation factor 2 alpha (eIF2α) and activate the integrated stress response (ISR). This is a key step in translational control and must be tightly regulated; however, persistent eIF2α phosphorylation is observed in mouse and human atheroma.

OBJECTIVES Potent ISR inhibitors that modulate neurodegenerative disorders have been identified. Here, the authors evaluated the potential benefits of intercepting ISR in a chronic metabolic and inflammatory disease, atherosclerosis.

METHODS The authors investigated ISR's role in lipid-induced inflammasome activation and atherogenesis by taking advantage of 3 different small molecules and the ATP-analog sensitive kinase allele technology to intercept ISR at multiple molecular nodes.

RESULTS The results show lipid-activated eIF2α signaling induces a mitochondrial protease, Lon protease 1 (LONP1), that degrades phosphatase and tensin-induced putative kinase 1 and blocks Parkin-mediated mitophagy, resulting in greater mitochondrial oxidative stress, inflammasome activation, and interleukin-1β secretion in macrophages. Furthermore, ISR inhibitors suppress hyperlipidemia-induced inflammasome activation and inflammation, and reduce atherosclerosis.

CONCLUSIONS These results reveal endoplasmic reticulum controls mitochondrial clearance by activating eIF2α-LONP1 signaling, contributing to an amplified oxidative stress response that triggers robust inflammasome activation and interleukin-1β secretion by dietary fats. These findings underscore the intricate exchange of information and coordination of both organelles' responses to lipids is important for metabolic health. Modulation of ISR to alleviate organelle stress can prevent inflammasome activation by dietary fats and may be a strategy to reduce lipid-induced inflammation and atherosclerosis. (J Am Coll Cardiol 2019;73:1149–69) © 2019 The Authors. Published by Elsevier on behalf of the American College of Cardiology Foundation. This is an open access article under the CC BY-NC-ND license (http://creativecommons.org/licenses/by-nc-nd/4.0/).

Eukaryotic response to diverse stimuli converges at serine-51 phosphorylation on the eukaryotic initiation factor-2α (eIF2α) and activates an adaptive signaling, the integrated stress response (ISR). This leads to global translation attenuation, but a select group of mRNAs (bearing upstream open reading frames), such as activating transcription factor-4 (ATF4) and CCAT/enhancer-binding protein beta homologous protein (CHOP), continues to be translated. Being a key step for

Listen to this manuscript's audio summary by Editor-in-Chief Dr. Valentin Fuster on JACC.org.

From the [a]Department of Molecular Biology and Genetics, Bilkent University, Ankara, Turkey; [b]National Nanotechnology Center, Bilkent University, Ankara, Turkey; [c]Department of Biomedical Sciences, Cedars-Sinai Medical Center, Los Angeles, California; [d]Smidt Heart Institute, Cedars-Sinai Medical Center, Los Angeles, California; [e]Department of Pediatrics, Division of Infectious Diseases and Immunology, Cedars-Sinai Medical Center, Los Angeles, California; [f]Division of Cardiology, Oppenheimer Atherosclerosis Research Center and Atherosclerosis Prevention and Treatment Center, Cedars-Sinai Medical Center, Los Angeles, California; [g]Departments of Medicine and Pediatrics, Division of Pediatric Infectious Diseases, Cedars-Sinai Medical Center, Los Angeles, California; and the [h]David Geffen School of Medicine, University of California, Los Angeles, California. Dr. Tufanli's current address is NYU Langone Medical Center, New York University, New York, New York. Dr. Çimen's current address is the Institute for Cardiovascular Prevention, Ludwig Maximilians University Munich, Munich, Germany. This work was funded by the EMBO installation grant and ERC Starting Grant (336643) (to Dr. Erbay). The authors have reported that they have no relationships relevant to the contents of this paper to disclose.

Manuscript received June 6, 2018; revised manuscript received December 7, 2018, accepted December 10, 2018.

ISSN 0735-1097 https://doi.org/10.1016/j.jacc.2018.12.055

ABBREVIATIONS AND ACRONYMS

ASKA = ATP-analog sensitive kinase allele

ATF4 = activating transcription factor 4

BMDM = bone marrow-derived macrophages

CCL2 = C-D motif ligand-2

CHOP = CCAT/enhancer-binding protein beta homologous protein

CVD = cardiovascular disease(s)

eIF2α = eukaryotic initiation factor 2 alpha

eIF2B = eukaryotic initiation factor 2B

ER = endoplasmic reticulum

GAS = Group A *Streptococcus*

IL = interleukin

IRE1 = inositol-requiring enzyme-1

ISR = integrated stress response

LONP1 = Lon protease 1

mtROS = mitochondrial reactive oxygen species

NLRP3 = Nod-like receptor family, pyrin domain-containing protein-3

PA = palmitate

Parkin = Parkinson juvenile disease protein 2

PERK = protein kinase R-like endoplasmic reticulum kinase/eIF2α kinase

PINK1 = phosphatase and tensin-induced putative kinase1

SFA = saturated fatty acid

siRNA = silencer RNA

TNF = tumor necrosis factor

UPR = unfolded protein response

translational control, eIF2α phosphorylation must be tightly regulated through dephosphorylation by the protein phosphatase-1 (PP1). In prolonged or severe stress, however, ISR can revert to a cell death program (1,2).

SEE PAGE 1170

Endoplasmic reticulum (ER) stress is a trigger for ISR. Unfolded proteins are sensed by the ER-resident eIF2α kinase, protein kinase RNA-activated-like ER kinase (PERK), and trigger eIF2α phosphorylation. This homeostatic pathway is hyperactivated in obesity and dyslipidemia (2–4). Evidently, reducing ER stress in mice reduces insulin resistance, obesity, and atherosclerosis (5–8). ER stress is induced by saturated fatty acids (SFA), which are thought to promote cardiovascular diseases (CVD) (9–11). Replacing 5% of the energy intake from SFA with an equivalent intake of monounsaturated fatty acids or polyunsaturated fatty acids is associated with a reduced risk (15% and 25%, respectively) of CVD (12). A causal relationship between SFA intake and CVD risk was demonstrated in nonhuman primates (11). Other studies have challenged SFA's role in human CVD, and the molecular mechanisms of SFA-induced inflammation in atherosclerosis are not completely understood (10).

Increased cellular lipid influx negatively impacts organelles leading to ER and mitochondrial stress, often intertwined in obesity (13). Organelle stress is causally associated with inflammation and atherosclerosis (14). For example, organelle stress activates the Nod-like receptor family, pyrin domain-containing protein-3 (NLRP3) inflammasome, leading to interleukin (IL)-1β and IL-18 secretion (7,15,16). IL-1β is elevated in plaques and serum during dyslipidemia and drives atherosclerosis (7,17–19).

Persistent ISR activation, as evident by eIF2α and PERK phosphorylation, is observed in atheroma (8). PERK promotes foam cell formation, whereas CHOP deletion in mice reduces atherosclerosis (5,6,8,20). The circumstantial evidence thus suggests that PERK-induced ISR may aggravate atherosclerosis, but can intercepting this homeostatic pathway in a chronic disease provide therapeutic gains? Using small molecules and genetic approaches to modulate multiple ISR nodes, we show lipid-activated PERK induces mitochondrial Lon protease-1 (LONP1). LONP1 degrades phosphatase tensin homolog-induced kinase-1 (PINK1) to suppress mitophagy, thus drives mitochondrial reactive oxygen species (mtROS) production and robust inflammasome activation in lipid-stressed macrophages. Finally, ISR inhibition in vivo can suppress hyperlipidemia-induced inflammation and reduce atherosclerosis progression in mice.

METHODS

GENERAL STUDY DESIGN. Three or more independent replicates were performed for cell-based experiments. Mice were randomly assigned to independent cohorts, and data analysis was performed blind. The only elimination criteria used for mouse studies was based on health. Noted differences in mouse numbers (en face aorta and plaque analysis) is related to technical problems that occurred during sampling before analysis.

MICE STUDIES AND TREATMENTS. C57BL/6.129P2-*Apoe*^{tm1Unc}/J mice (*Apoe*$^{-/-}$ mice; received from Jackson Laboratory, Bar Harbor, Maine, and created by Nabuyo Maeda, University of North Carolina), and C57BL/6.129S4-*Prkn*^{tm1Shn}/J (*parkin*$^{-/-}$ mice; received from Jackson Laboratory and created by Jie Shen, Harvard Medical School) and C57BL/6-eIF2αk3$^{tm2201(G646N,M886A)Arte}$ mice (PERK_ASKA [ATP-analog sensitive kinase allele] mice; received from J.R. Lipford at Amgen, Thousand Oaks, California, and created by Taconic Artemis, Cologne, Germany); G646N/M886A mutations were introduced by Cre-Lox system and bred with *Apoe*$^{-/-}$. *Apoe*$^{-/-}$ mice were injected with GSK2606414 (30 mg/kg/day; Atomole Scientific, Wuhan, China) or trans-ISRIB (1 to 2 mg/kg/day; Cayman Chemical, Ann Arbor, Michigan). PERK_ASKA mice were injected with 4-amino-1-tert-butyl-3-(1-naphthyl)pyrazolo [3,4-d]pyrimidine (1-NAPP1) (60 mg/kg/day; Taconic Artemis). Weight and blood glucose were measured weekly (7,15). The experimental animal ethical care committees at Bilkent University and Cedars Sinai Medical Center approved all animal experiment protocols.

DIETS. Western diet (0.21% cholesterol, 21% fat) was obtained from Ssniff-Spezialdiäten, Soest, Germany (TD.88137/E15721).

RESULTS

ISR REGULATES LIPID-INDUCED INFLAMMASOME ACTIVATION. Lipid stress leads to eIF2α and PERK phosphorylation in macrophages and plaques (5,9,20). Here, we sought to understand the contribution of PERK to SFA-induced inflammasome activation and atherosclerosis. Palmitate (PA)

FIGURE 1 PERK's Role in Lipid-Induced Inflammasome Activation

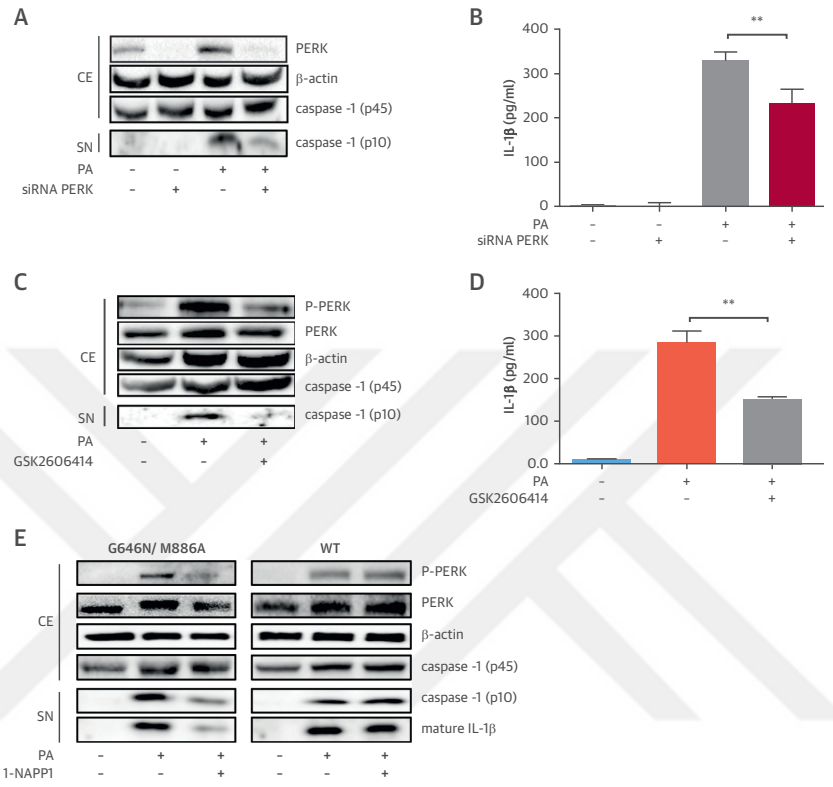

(A and B) LPS-primed, PA-stimulated BMDM were transfected with PERK or control siRNA or **(C and D)** treated with GSK2606414 (2 μmol/l) or vehicle: **(A and C)** protein lysates were analyzed by Western blotting using antibodies against P-PERK, PERK, β-actin, and caspase-1 (p45 and p10), and **(B and D)** conditioned cell medium was analyzed with IL-1β ELISA. **(E)** LPS-primed, PA-stimulated macrophages from PERK_ASKA or WT mice were treated with 1-NAPP1 (20 μmol/l) and protein lysates were analyzed by Western blotting using antibodies against P-PERK, PERK, β-actin, caspase-1 (p45 and p10), and IL-1β. Blots shown are representative of (n = 3) experiments. Data are mean ± SEM; (n = 4) for ELISA. Unpaired *t*-test with Welch's correction. *p ≤ 0.05, **p ≤ 0.01, ***p ≤ 0.001. BMDM = bone marrow–derived macrophages; CE = cell extract; ELISA = enzyme-linked immunosorbent assay; IL = interleukin; LPS = liposaccharide; PA = palmitate; siRNA = silencer RNA; SN = supernatant; WT = wild-type.

treatment of mouse bone marrow–derived macrophages (BMDM) led to profound induction of cleaved caspase-1 (p10 fragment) and IL-1β secretion, but this was significantly reduced by silencer RNA (siRNA)-mediated PERK suppression (**Figures 1A and 1B**, Online Figure 1A). To further assess PERK kinase activity's role in this, lipid-stressed macrophages were treated with a PERK kinase inhibitor (GSK2606414) (21). GSK2606414 suppressed PERK phosphorylation and counteracted lipid-induced caspase-1 cleavage and IL-1β secretion in BMDMs (**Figures 1C and 1D**, Online Figure 1B), human Thp1 macrophages, and human peripheral blood monocytes (PBMC) (Online Figures 1C and 1D). PERK inhibition did not impact the expression of pro-IL-1β, PYD and CARD domain-containing

FIGURE 2 ISR's Critical Role in Lipid-Induced Inflammasome Activation

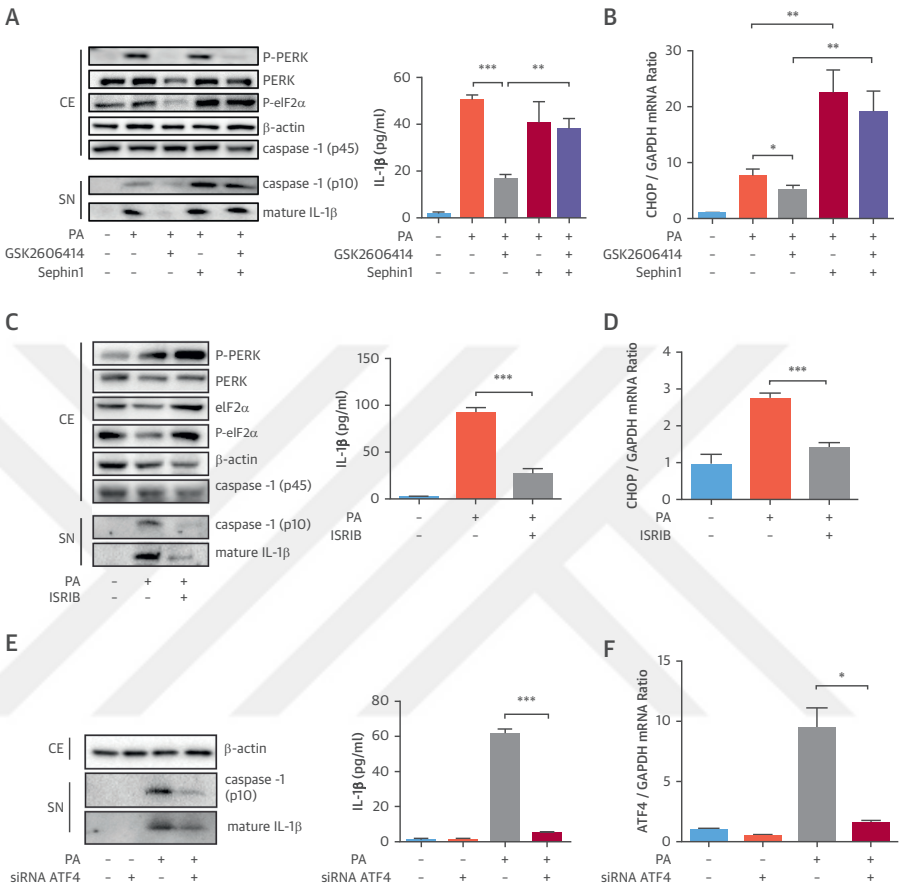

(A and B) LPS-primed, PA-stimulated BMDM were treated with GSK2606414 (2 μmol/l) and/or Sephin1 (25 μmol/l) or **(C and D)** ISRIB (6 μmol/l): **(A and C)** protein lysates were analyzed by Western blotting using antibodies against P-PERK, PERK, P-eIF2α, β-actin, caspase-1 (p45 and p10), and IL-1β, and conditioned cell medium was analyzed with IL-1β ELISA, and **(B and D)** total RNA was analyzed by qRT-PCR for CHOP mRNA. **(E and F)** LPS-primed, PA-stimulated BMDMs were transfected with ATF4 or control siRNAs: **(E)** protein lysates were analyzed by Western blotting using antibodies against: β-actin, caspase-1 (p10), and IL-1β, and conditioned cell medium was analyzed with IL-1β ELISA, and **(F)** total RNA was analyzed by qRT-PCR for ATF4 mRNA. Western blots shown are representative (n = 3) experiments. Data are mean ± SEM; (n = 4) for ELISA and qPCR. Unpaired *t*-test with Welch's correction. *p ≤ 0.05, **p ≤ 0.01, ***p ≤ 0.001. ISR = integrated stress response; qRT-PCR = quantitative reverse transcription polymerase chain reaction; other abbreviations as in Figure 1.

protein, and pro-caspase-1 mRNAs, but a small reduction in NLRP3 mRNA was noted (Online Figures 1E and 1F). PERK inhibition also reduced lipid-induced tumor necrosis factor (TNF)-α and C-C motif chemokine ligand-2 (CCL2) mRNA (Online Figures 1E and 1F).

Additionally, we took advantage of the ATP analog sensitive kinase allele (ASKA) of PERK to specifically

modulate PERK's kinase activity (22). The ASKA approach involves a conserved (gatekeeper) amino acid mutation in the deep, hydrophobic ATP-binding kinase pocket, which unblocks access to bulky ATP analogs (23). The M886A mutation on PERK confers the ability to use ATP analogs with bulky alkyl groups (22). To prevent an unstable kinase (24), the PERK_ASKA mice were designed with a second stabilizing mutation at G646N (Online Figures 1G and 1H). 1-NAPP1 selectively suppressed PERK_ASKA kinase activity (along with lipid-induced caspase-1 cleavage and IL-1β secretion in macrophages) but not wild-type PERK's activity (**Figure 1E**, Online Figure 1I), demonstrating PERK kinase activity's role in lipid-induced inflammasome activation.

We next investigated eIF2α's role in lipid-induced inflammasome activation. Sephin1, a small molecule inhibitor of the stress-induced eIF2α regulatory subunit (25,26), lead to persistent eIF2α phosphorylation and CHOP mRNA induction in PERK inhibitor-treated BMDMs (**Figures 2A and 2B**, Online Figure 2A) GSK2606414 inhibited lipid-induced caspase-1 cleavage and IL-1β secretion, but not in Sephin1-treated BMDMs (**Figure 2A**, Online Figure 2A). This finding confirms PERK acts through eIF2α phosphorylation in controlling inflammasome activation.

We next inhibited PERK signaling downstream of eIF2α with a small molecule activator of eIF2B, ISRIB (27). ISRIB did not inhibit lipid-induced PERK activation or eIF2α phosphorylation but blocked stress-induced CHOP mRNA in BMDM and THP-1 macrophages (**Figures 2C and 2D**, Online Figures 1C and 2B). ISRIB led to a profound suppression of lipid-induced caspase-1 cleavage and IL-1β secretion (**Figure 2C**, Online Figures 1C and 2B). ATF4 knockdown also led to marked suppression of PA-induced caspase-1 cleavage and IL-1β secretion (**Figures 2E and 2F**, Online Figure 2C). ISRIB caused a small reduction in lipid-induced NLRP3 mRNA and unexpectedly in pro-IL-1β (Online Figure 2D), but ATF4 knockdown did not impact pro-Il-1β mRNA (Online Figure 2E). Collectively, these findings demonstrate that interrupting ISR signaling can profoundly block lipid-induced inflammasome activation.

PERK-INDUCED MITOCHONDRIAL LON PROTEASE CONTROLS MITOCHONDRIA CLEARANCE AND INFLAMMASOME ACTIVATION. Inflammasome activation by ER stress requires increased mtROS production (18). SFA leads to dramatic elevation of mtROS levels in BMDMs (16), and we observed this is completely blocked by GSK2606414, but not Sephin1 (**Figure 3A**, Online Figures 3A and 3B). ISRIB also suppressed lipid-induced mtROS (**Figure 3A**, Online Figure 3C), demonstrating ISR's important role in managing mitochondrial oxidative stress.

We next investigated how PERK-eIF2α signaling relays lipid stress to inflammasome activation. ER toxins can up-regulate a mitochondrial matrix, ATP-dependent protease and stress-induced chaperone, LONP1, in a PERK-dependent manner (28,29). PINK1 (a mitochondria localized kinase that phosphorylates Parkinson juvenile disease protein 2 [Parkin] and recruits autophagosomes) is a LONP1 substrate, implicating LONP1 in Parkin-dependent mitophagy (30). Mitophagy counteracts mtROS and inflammasome activation by lipids (16). We asked whether LONP1 plays a role in SFA-induced mtROS production and inflammasome activation. Indeed, PA induced LONP1 expression (**Figure 3B**), which was significantly blocked by GSK2606414 (**Figure 3B**). Sephin1, on the other hand, induced LONP1 and prevented PERK inhibitor's ability to suppress LONP1 (**Figure 3B**). As expected, ISRIB significantly suppressed LONP1 (**Figure 3B**). PERK or ATF4 knockdown also blocked LONP1 induction by lipids (**Figure 3B**). These results demonstrate SFA induces LONP1 through PERK-eIF2α signaling. Furthermore, SFA activates PERK, induces LONP1 (**Figure 3C**, Online Figures 4A to 4D), but reduces PINK1 in macrophages (**Figure 3C**, Online Figure 4A). This inverse regulation is counteracted by GSK2606414 or ISRIB (**Figure 3C**, Online Figures 4A to 4D). To confirm SFA-induced PINK1 reduction was a consequence of LONP1 activation, we silenced LONP1 with siRNA. This led to stabilization of PINK1 levels in lipid-stressed BMDM (**Figure 3D**, Online Figure 4E). These results show SFA leads to PINK1 suppression by activating PERK-eIF2α-LONP1 signaling. Moreover, treatment of lipid-stressed macrophages with GSK2606414 or LONP1 inhibitor (2-cyano-3,12-dioxo-oleana-1,9(11)-dien-28-oic-acid [CDDO]) led to a profound increase in Parkin and autophagy receptor (p62) recruitment to mitochondria (**Figure 3E**, Online Figure 4F). Consistently, expression of a mitochondria import receptor subunit-40 (TOM40) was simultaneously reduced (**Figure 3E**, Online Figure 4F).

We next assessed LONP1's role in mtROS generation. PA induced mtROS in BMDM, but this was significantly blocked by LONP1 knockdown (**Figure 3F**, Online Figure 4G). Suppressing LONP1 also prevented caspase-1 cleavage and IL-1β secretion in lipid-stressed BMDM (**Figures 3G and 3H**, Online Figures 4H and 4I). However, suppressing PINK1 compromised PERK inhibitor's ability to block SFA-induced caspase-1 cleavage and IL-1β secretion (**Figure 3I**, Online Figure 4J). Consistently, GSK2606414, CDDO, or ISRIB could not block SFA-induced IL-1β secretion or caspase-1 cleavage in

FIGURE 3 PERK-Induced Mitochondrial LON Protease Regulates Mitophagy, mtROS, and Inflammasome Activation

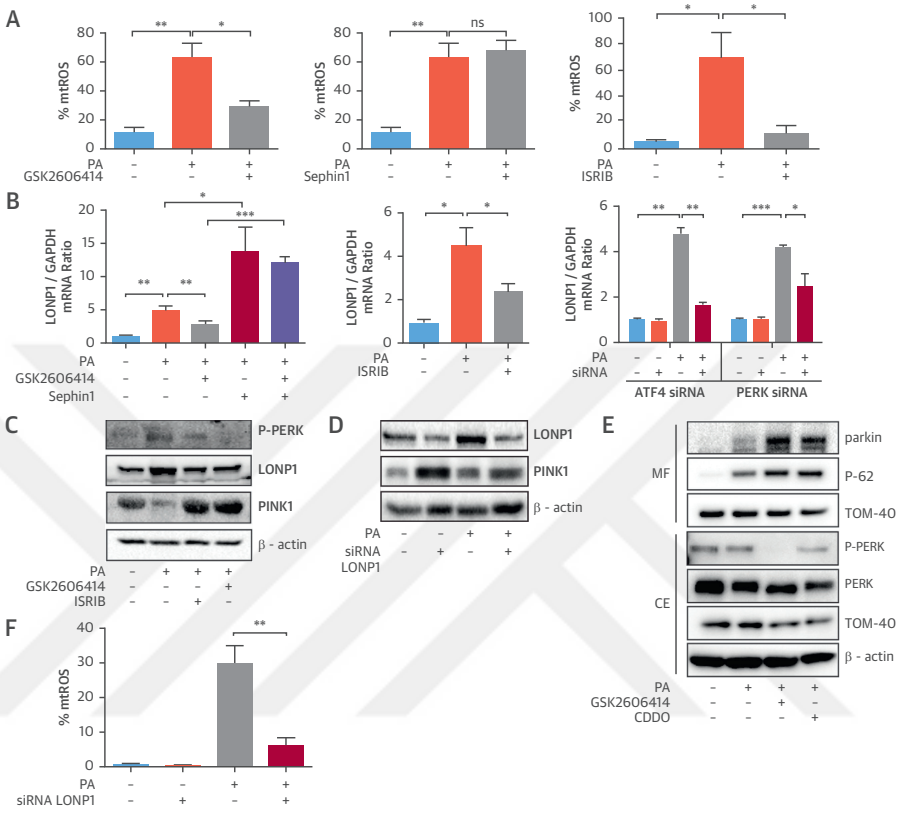

(A to D) LPS-primed, PA-stimulated BMDM were treated with **(A)** GSK2606414 (2 μmol/l), Sephin1 (25 μmol/l) or ISRIB (6 μmol/l) and mtROS was measured with MitoSOX Red mitochondrial superoxide indicator, or **(B)** treated with GSK2606414 (2 μmol/l), Sephin1 (25 μmol/l), or ISRIB (6 μmol/l) or transfected with PERK or ATF4 siRNA and total RNA was analyzed by qRT-PCR for LONP1 and GAPDH mRNA, or **(C)** treated with GSK2606414 (2 μmol/l) or ISRIB (6 μmol/l) and protein lysates were analyzed by Western blotting using antibodies against P-PERK, LONP1, PINK1, and β-actin, or **(D)** transfected with a LONP1 siRNA and protein lysates were analyzed by Western blotting using antibodies against LONP1, PINK1 and β-actin. **(E)** Mitochondrial fraction protein lysates from PA-treated RAW264.7 macrophages were analyzed by Western blotting with antibodies against Parkin, p-62, TOM-40, whereas total cell protein extracts were analyzed using antibodies against P-PERK, PERK, TOM-40, and β-actin. **(F–H)** LPS-primed, PA-stimulated BMDM were **(F)** transfected with LONP1 siRNA, and mtROS was measured with MitoSOX kit, or **(G)** transfected with LONP1 siRNA and supernatants were analyzed with IL-1β ELISA, whereas protein lysates were analyzed by Western blotting using antibodies against caspase-1 (p45 and p10), β-actin, and IL-1β, and total RNA was analyzed by qRT-PCR for LONP1 and GAPDH mRNA, or **(H)** treated with 1 μmol/l CDDO and supernatants were analyzed with IL-1β ELISA, whereas protein lysates were analyzed by Western blotting using antibodies against caspase-1 (p45 and p10), β-actin, and IL-1β, or **(I)** transfected with PINK1 siRNA and/or treated with GSK2606414 (2 μmol/l); the conditioned medium was analyzed by IL-1β ELISA or Western blotting using antibodies against caspase-1 (p10) and IL-1β, whereas total RNA was analyzed by qRT-PCR for PINK1 and GAPDH mRNA. **(J)** LPS-primed *Parkin*$^{-/-}$ or WT BMDM were treated with PA and GSK2606414 (2 μmol/l) or CDDO (1 to 2 μmol/l); conditioned cell medium was analyzed with IL-1β ELISA or by Western blotting using antibodies against caspase-1 (p45 and p10), β-actin, and IL-1β. Western blots shown are representative. Data are mean ± SEM; (n = 3) for Western blots and (n = 4) for ELISA and qPCR. Unpaired *t*-test with Welch's correction. *p ≤ 0.05, **p ≤ 0.01, ***p ≤ 0.001. mtROS = mitochondrial reactive oxygen species; ns = not significant; other abbreviations as in Figures 1 and 2.

Continued on the next page

FIGURE 3 Continued

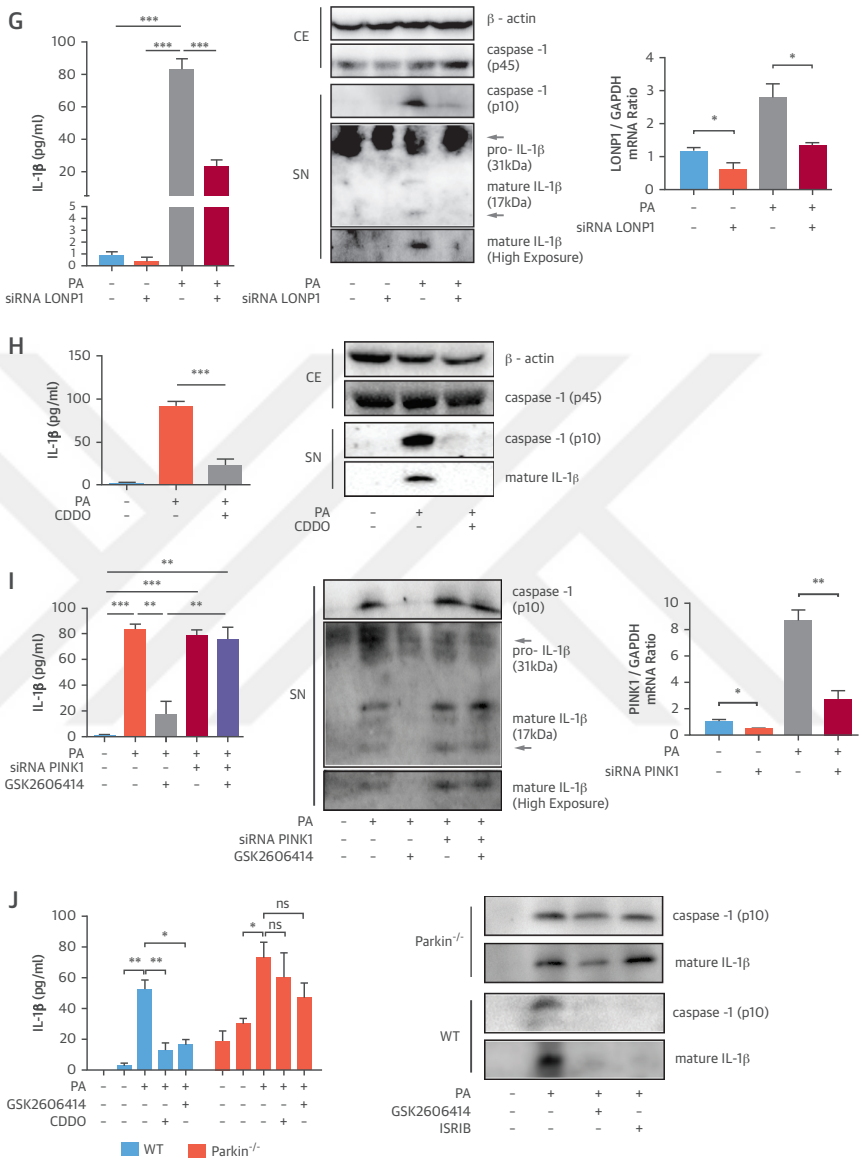

FIGURE 4 PERK Inhibition Leads to Reduction in Plaque Area in *Apoe*$^{-/-}$ Mice

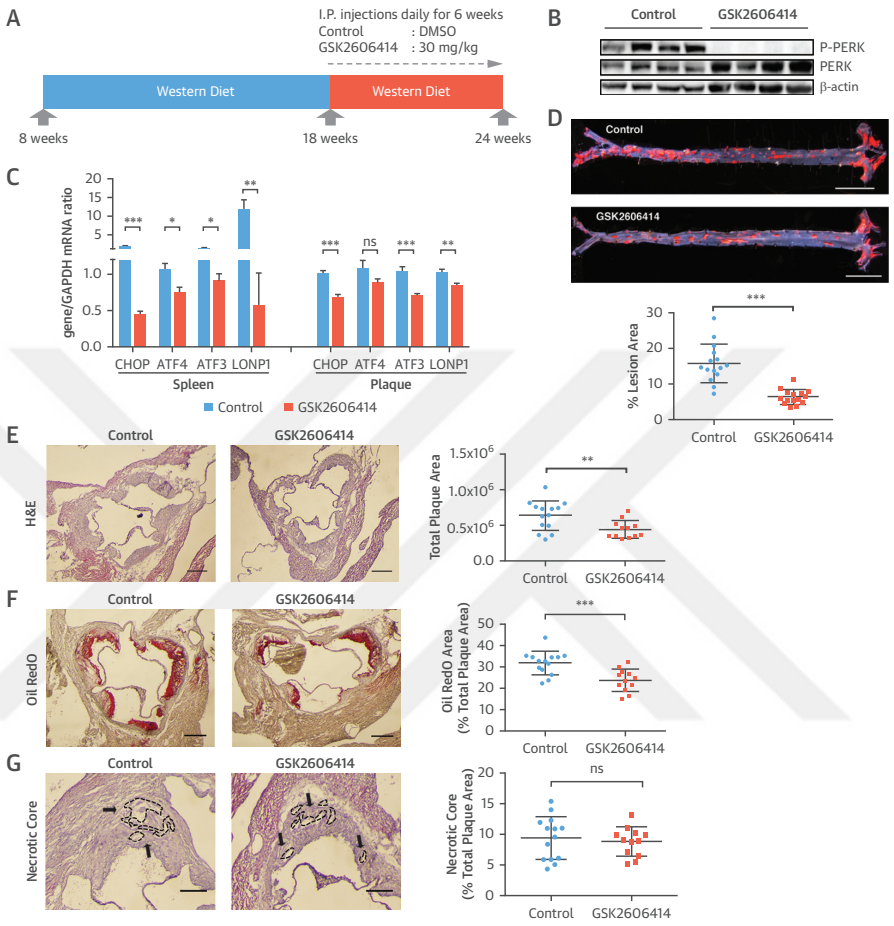

(A to G) Experimental design in *Apoe*$^{-/-}$ mice treated with a PERK inhibitor: **(A)** GSK2606414 (30 mg/kg/day) or vehicle (DMSO). **(B)** Pancreas protein lysates were analyzed by Western blotting using antibodies against P-PERK, PERK, and β-actin (n = 4 control group, 4 treatment group). **(C)** Spleen **(left)** or aortic root plaques **(right)** total RNA were analyzed by qRT-PCR for CHOP, ATF4, ATF3, and LONP1 mRNA (n = 14 control group, 12 treatment group). **(D)** Lesion area was calculated from en face aorta preparations stained with Sudan IV (n = 15 control group, 15 treatment group; scale bar: 5 mm). **(E)** Total plaque area was calculated from H&E-stained (n = 14 control group, 12 treatment group), **(F)** foam cell area was calculated from Oil RedO–stained (n = 14 control group, 12 treatment group), whereas **(G)** necrotic area was calculated from H&E-stained aortic root sections (n = 14 control group, 12 treatment group) (scale bar: 300 μm). **(H)** Experimental design in PERK_ASKA, *Apoe*$^{-/-}$ mice treated with 1-NAPP1 (60 mg/kg/day) or vehicle in the control mice: **(I)** Pancreas protein lysates were analyzed by Western blotting using antibodies against P-eIF2α, eIF2α, and β-actin (bands quantification and displayed next to blot; n = 4 control group, 4 treatment group). **(J)** Aortic root plaque total RNA was analyzed by qRT-PCR for CHOP, ATF4, ATF3, and LONP1 mRNA (n = 10 control group, 10 treatment group). **(K)** Lesion area was calculated from Sudan IV–stained en face aorta preparations (n = 12 control group, 12 treatment group) (scale bar: 5 mm) and **(L)** total plaque area from H&E-stained aortic root sections **(upper panel)**, whereas foam cell area was calculated from Oil RedO-stained sections **(lower panel)** (n = 12 control group, 12 treatment group) (scale bar: 300 μm). Data are mean ± SEM. Mann-Whitney *U* test. *p ≤ 0.05, **p ≤ 0.01, ***p ≤ 0.001. DMSO = dimethyl sulfoxide; H&E = hematoxylin and eosin; other abbreviations as in Figures 1, 2, and 3.

Continued on the next page

FIGURE 4 Continued

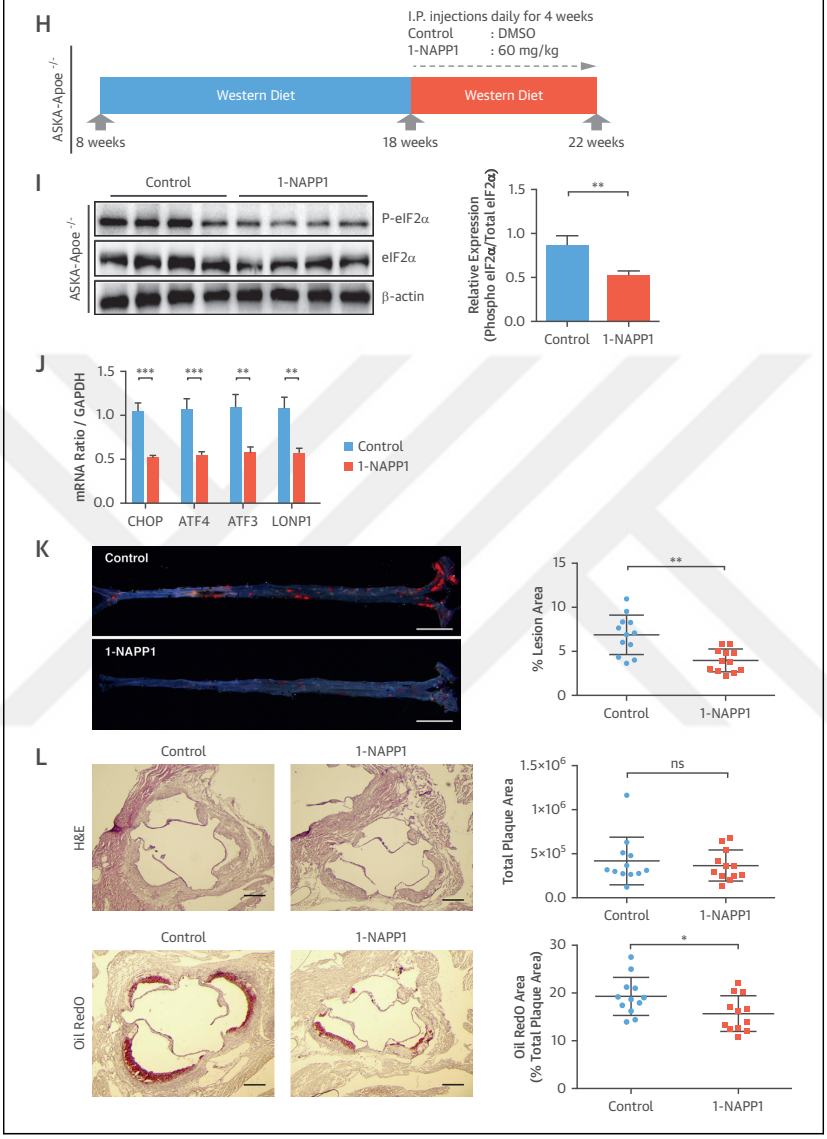

FIGURE 5 PERK Inhibitor Suppresses Hyperlipidemia-Induced Inflammation in *Apoe*$^{-/-}$

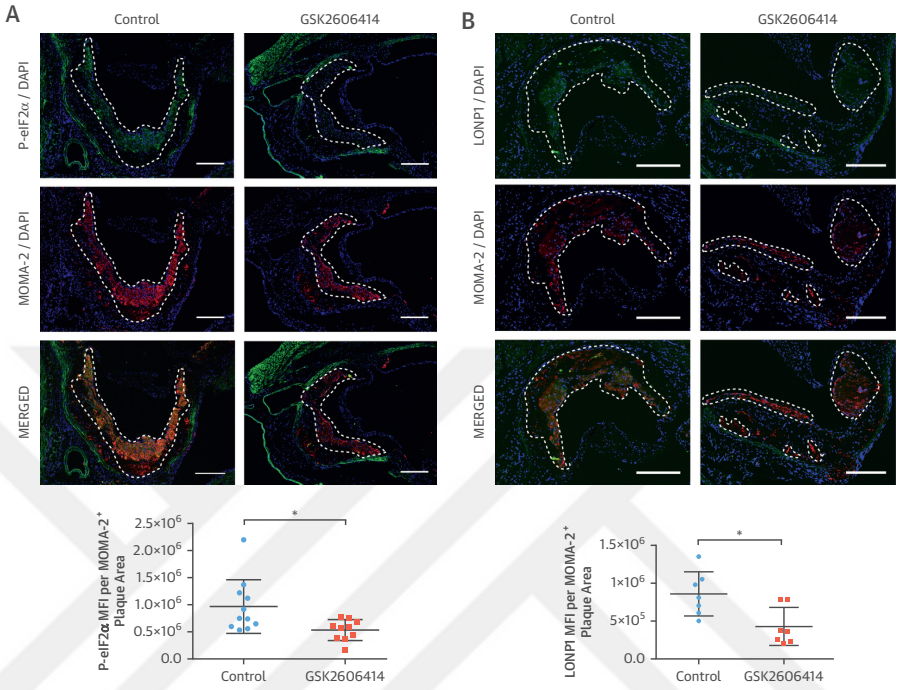

(A–G) Immunohistochemical analysis of aortic root cryosections from GSK2606414- or vehicle (DMSO)-treated *Apoe*$^{-/-}$ (mice as in Figure 4). A representative image is shown for the quantification: **(A and B)** MFI **(green)** quantified from macrophage positive area **(red) (A)** P-eIF2α (n = 11 control group, 10 treatment group), **(B)** LONP1 (n = 7 control group, 7 treatment group), **(C)** MOMA-2 (n = 11 control group, 10 treatment group), **(D)** CD3 (n = 12 control group, 10 treatment group), **(E)** α-SMA (n = 14 control group, 12 treatment group), and **(F)** Masson's Trichrome (n = 11 control group, 10 treatment group), **(G)** IL-1β (MFI) **(green)** quantified from the macrophage area **(red)** (n = 11 control group, 10 treatment group). **(H)** Aortic root plaque RNA was analyzed by qRT-PCR for pro-IL-1β expression (n = 14 control group, 12 treatment group). **(I)** Immunohistochemical analysis of aortic root cryosections for caspase-1 (FAM-FLICA, **green**), from MOMA-2–positive **(red)** area (n = 7 control group, 8 treatment group). **(J)** Plasma IL-18 (**left**; n = 8 control group, 8 treatment group) or IFNγ (**right**; n = 7 control group, 7 treatment group) were measured with ELISA. Data are mean ± SEM; Mann-Whitney *U* test. *p ≤ 0.05, **p ≤ 0.01, ***p ≤ 0.001. (Scale bar: 200 μm except in **D**: 50 μm). MFI = mean fluorescent intensity; other abbreviations as in Figures 1, 2, 3, and 4.

Continued on the next page

Parkin-deficient BMDMs (Figure 3J, Online Figure 4K). These collective results demonstrate ISR inhibits PINK1-Parkin-dependent mitophagy, elevates mtROS, and activates the inflammasome in lipid-stressed macrophages.

INHIBITION OF PERK KINASE MITIGATES ATHEROSCLEROSIS. Organelle stress drives atherosclerosis progression (14,31). We next assessed whether inhibiting PERK could prevent atherosclerosis progression (32). To test this, we challenged *Apoe*$^{-/-}$ mice with the Western diet (16 weeks) and injected GSK2606414 (30 mg/kg/day) (6 weeks) (Figure 4A) (33). No significant differences in plasma glucose and insulin levels or blood cell counts were observed between the groups (Online Figures 5A and 5B). We confirmed the inhibitor engaged its molecular target effectively by assessing PERK autophosphorylation and CHOP and ATF3 mRNA (Figures 4B and 4C, Online Figure 5C). We detected no improvement in plasma lipids or lipoproteins

FIGURE 5 Continued

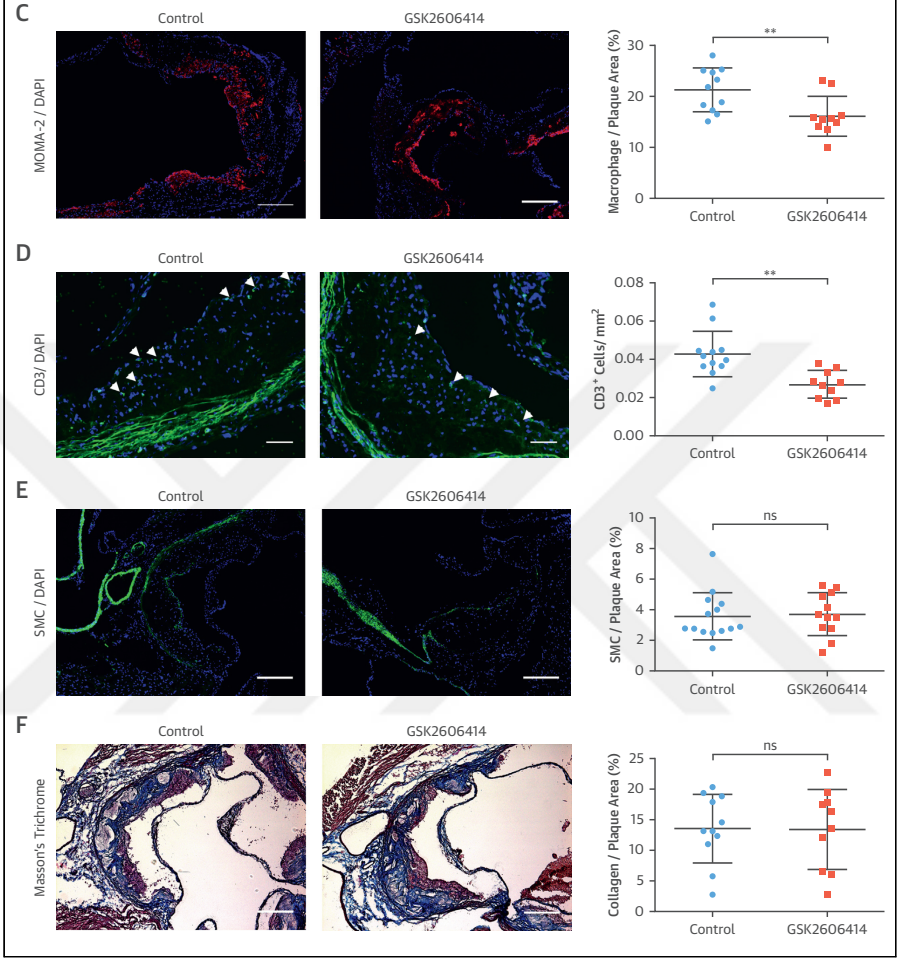

Continued on the next page

(Online Figures 5D-5G); however, GSK2606414 led to a significant decrease in atherosclerotic lesions in en face aorta preparations (44%) (**Figure 4D**, Online Figure 6A). GSK2606414 significantly reduced aortic root plaque (32%) (**Figure 4E**) and foam cell area (25%) (**Figure 4F**, Online Figure 6B). No significant changes in the plaque necrotic area or apoptotic cell numbers were noted between the groups (**Figure 4G**, Online Figure 6C). There was a reduction in plaque VCAM-1 protein (33%) (Online Figure 6D), and CCL2 (20%) (Online Figure 6E), and serum monocyte chemoattractant protein-1 (46%) (Online Figure 6F) after PERK inhibition, suggesting macrophage recruitment is impacted.

We also analyzed atherosclerosis in the PERK_ASKA, *Apoe*$^{-/-}$ transgenic mice. These mice

FIGURE 5 Continued

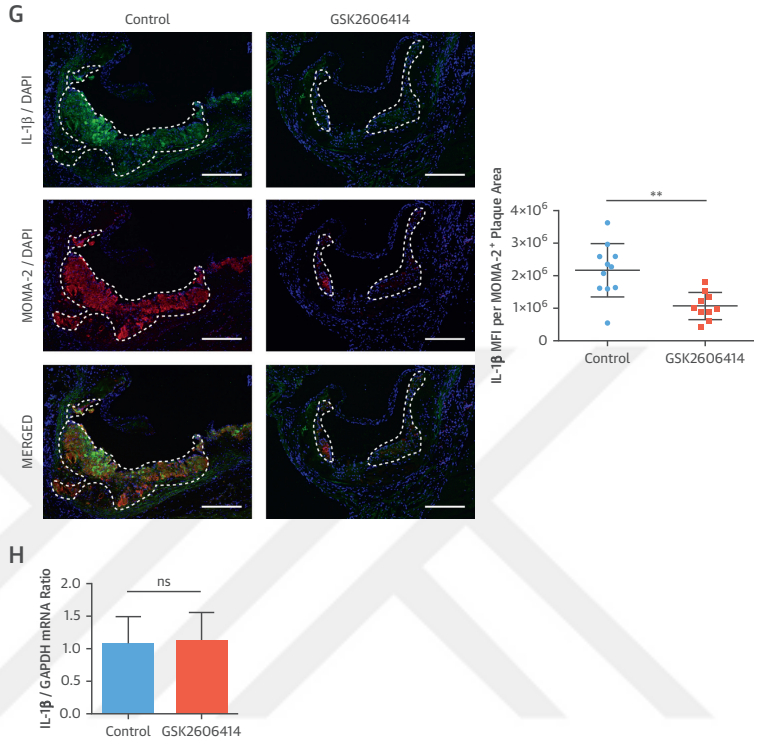

Continued on the next page

were fed the Western diet (14 weeks) and treated with 1-NAPP1 (60 mg/kg/day, 4 weeks) (**Figure 4H**). 1-NAPP1 inhibited eIF2α phosphorylation (**Figure 4I**) and CHOP, ATF4, and ATF3 mRNA (**Figure 4J**). Although there were no significant differences in systemic metabolic parameters between the groups (Online Figures 7A and 7B), 1-NAPP1 significantly reduced atherosclerotic lesions in en face aorta preparations (45%) (**Figure 4K**) and aortic root foam cell area (20%), but not plaque area (**Figure 4L**). These findings in the PERK_ASKA mouse model confirm the atheroprotection we observed in mice treated with the PERK inhibitor.

PERK INHIBITION BLOCKS HYPERLIPIDEMIA-INDUCED INFLAMMATION IN VIVO. Macrophages and other immune cells infiltrate plaques during atherogenesis (34). We next analyzed the impact of PERK inhibition on plaque cellular composition. GSK2606414 and 1-NAPP1 both lead to significant reduction in P-eIF2α in plaque macrophage-rich areas (GSK2606414: 45%) (**Figure 5A**), (1-NAPP1: 50%) (Online Figure 7C), as well as CHOP and ATF3 mRNA (GSK2606414: both 33%) (**Figure 4C**), (1-NAPP1: CHOP 50%; ATF3: 48%) (**Figure 4J**). PERK inhibition reduced LONP1 (GSK2606414: 49%) (**Figure 5B**), (GSK2606414: 20%) (**Figure 4C**), and (1-NAPP1: 48%) (**Figure 4J**). Fewer macrophages (GSK2606414: 25%) (**Figure 5C**) (1-NAPP1: 33%) (Online Figure 7D) and T cells (GSK2606414: 45%) (**Figure 5D**) were observed in plaques, but vascular smooth muscle cells and collagen content were not altered by GSK2606414 (**Figures 5E and 5F**). On the basis of these results, the

FIGURE 5 Continued

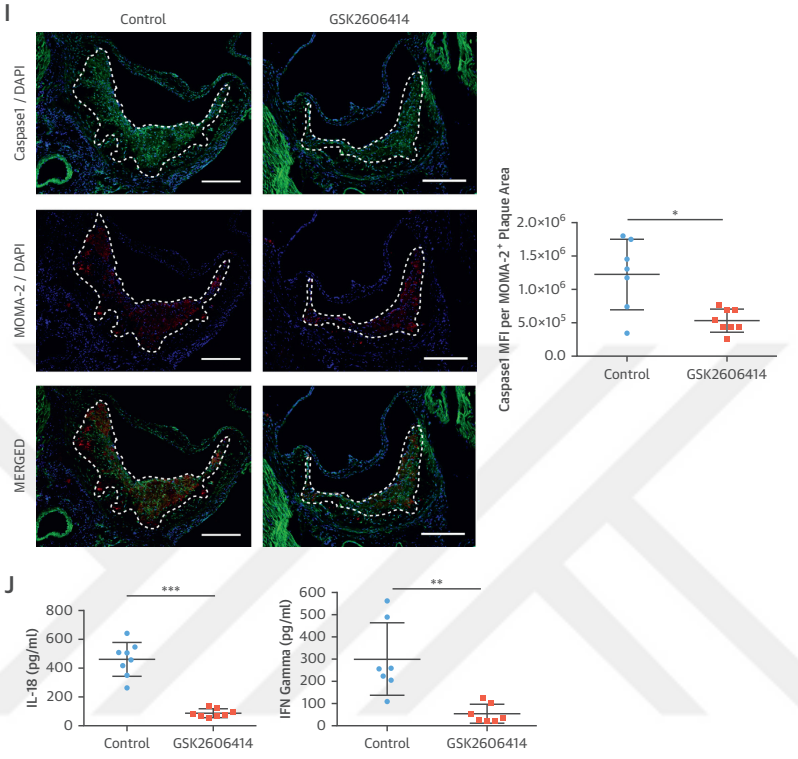

major consequence of PERK inhibition on plaques is reduced immune cells and lipid content.

PERK inhibition led to a significant inhibition of hyperlipidemia-induced expression of plaque IL-1β protein (GSK2606414: 45%) (**Figure 5G**), (1-NAPP1: 47%) (Online Figure 7E), but not IL-1β mRNA (**Figure 5H**, Online Figure 7F). However, PERK inhibition reduced CCL2 and TNFα mRNA levels in plaques (GSK2606414: 20% and 30%, respectively) (Online Figure 6E) (1-NAPP1: 48% and 47%, respectively) (Online Figure 7G). PERK inhibition reduced active caspase-1 (both 50%) (GSK2606414: **Figure 5I**, 1-NAPP1: Online Figure 7H). Consistently, PERK inhibitor reduced IL-18 (80%) (**Figure 5J**) and IFNγ (80%) (**Figure 5J**).

BLOCKING THE ISR WITH ISRIB COUNTERACTS ATHEROSCLEROSIS. We next investigated the consequences of modulating eIF2B for atherosclerosis in vivo. *Apoe*$^{-/-}$ mice on the Western diet (15 to 16 weeks) were injected with ISRIB (1 mg/kg/day; 6 weeks, 2 mg/kg/day; 5 weeks) (**Figure 6A**) (35). ISRIB did not inhibit eIF2α phosphorylation in vivo but reduced CHOP, ATF3, and LONP1 mRNAs (**Figures 6B and 6C**). There were no significant differences in metabolic parameters or blood cell counts between the groups (Online Figures 8A to 8D), but ISRIB caused a significant decrease in lesions in en face aorta preparations (1 mg/kg 26% and 2 mg/kg 39%) (**Figure 6D**, Online Figure 8E). ISRIB did not alter plaque area (**Figure 6E**) but reduced aortic root foam cell area (1 mg/kg 28%, 2 mg/kg 32%) (**Figure 6F**, Online Figure 8F). ISRIB also did not alter plaque necrotic area (**Figure 6G**).

FIGURE 6 Continued

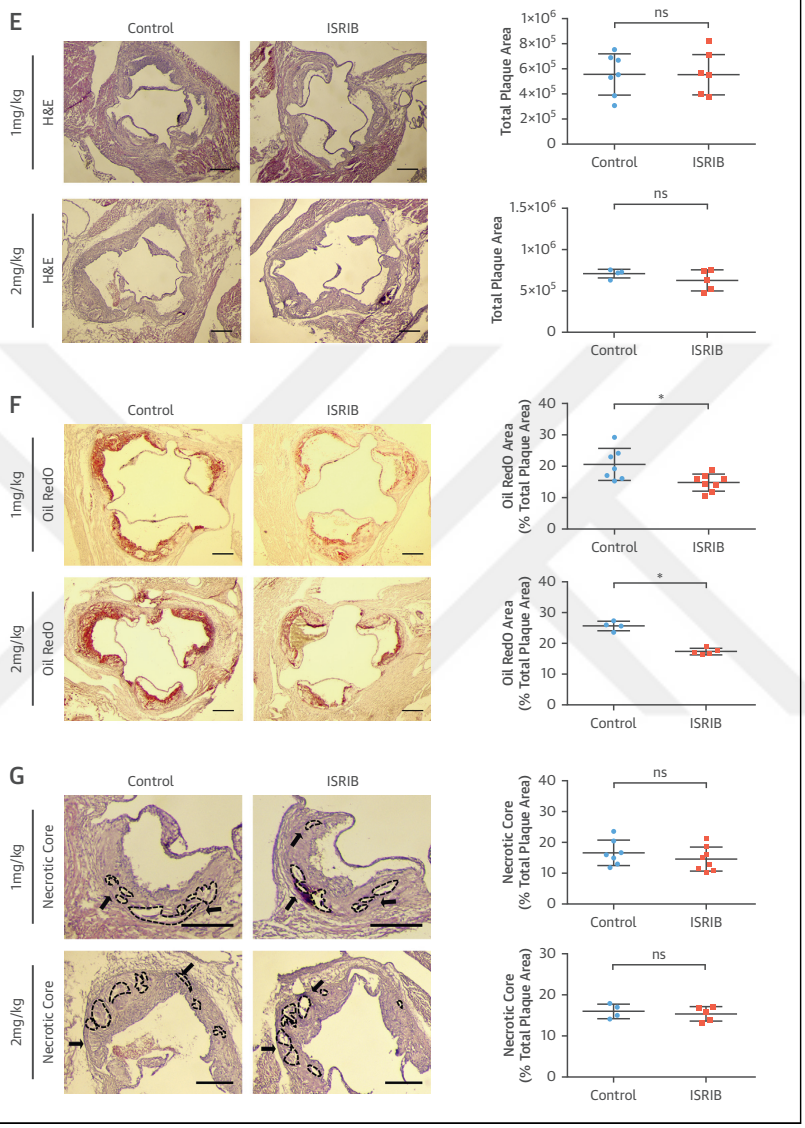

FIGURE 7 ISRIB Suppressed Hyperlipidemia-Induced LONP1 and Inflammation in *Apoe*$^{-/-}$

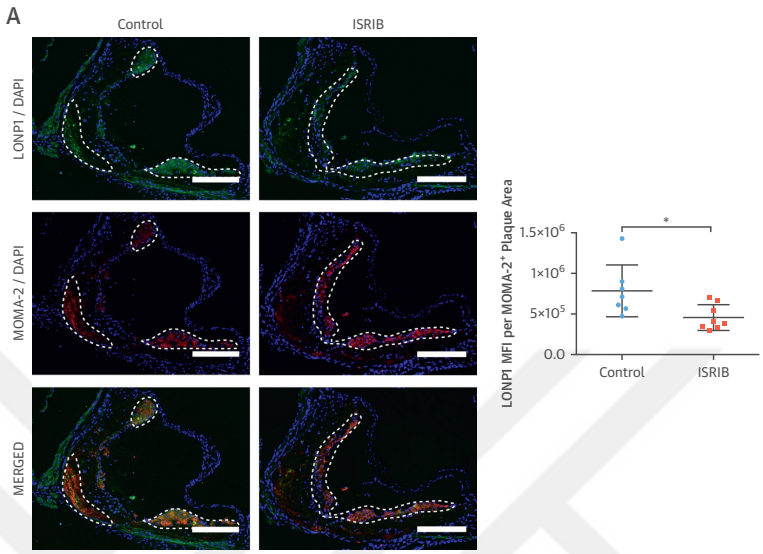

(A–D) Immunohistochemical analysis of aortic root cryosections (1 mg/kg/day ISRIB-injected mice, as in Figure 6); a representative image **(left)** is shown for the quantification: **(A)** LONP1 (MFI) **(green)** quantified from macrophage-positive area **(red), (B)** MOMA-2, **(C)** CD3, and **(D)** IL-1β (MFI) **(green)** quantified from macrophage-positive area **(red)** (n = 7 control group, 8 treatment group). **(E and F)** Total aortic root plaque RNA was analyzed by qRT-PCR for **(E)** IL-1β, and **(F)** CCL2 and TNFα mRNAs (n = 7 control group, 8 treatment group). **(G)** Immunohistochemical analysis of aortic root cryosections for Caspase1 MFI (FAM-FLICA, **green**) quantified from macrophage-positive area **(red)** (n = 7 control group, 8 treatment group). **(H)** Plasma IL-18 levels was measured with ELISA (from mice as shown in Figure 6) (n = 8 control group, 8 treatment group). Data are mean ± SEM; Mann-Whitney *U* Test.*p ≤ 0.05, **p ≤ 0.01, ***p ≤ 0.001. (Scale bar: 200 μm; except **C**: 50 μm). Abbreviation as in Figures 1, 2, 3, and 5.

Continued on the next page

small molecule modulators (25-27,35-39). Using these powerful chemical tools, we investigated ISR's role in lipid-induced inflammation and atherosclerosis. To alleviate concerns with possible off-target effects, we utilized multiple drugs that target 3 different molecular players in ISR (39,40). Complementary approaches such as PERK_ASKA mutant or knockdown of key players in the ISR pathway confirmed our main mechanistic finding that PERK-eIF2α-LONP1 pathway couples the stress responses of ER and mitochondria and potentiates inflammasome activation and inflammation induced by dietary fats, thus promotes atherosclerosis.

ISR's ROLE IN INTERORGANELLE COMMUNICATION AND STERILE INFLAMMATION. LONP1 is an important mitochondrial target that is regulated by lipid-induced PERK-eIF2α signaling in macrophages and in lesions. We discovered that LONP1 plays an unprecedented role during prolonged ER stress by limiting mitochondrial clearance through degrading PINK1. Chronic ER stress caused by dietary fats and activation of PERK-eIF2α-LONP1 signaling can therefore sustain high mtROS levels that flame the inflammasome and drive inflammatory cytokine production during atherogenesis (**Central Illustration**). These findings demonstrate ISR's role in sterile inflammation by modulating organelle stress responses that are important for inflammasome activation by lipids. We observed ISR inhibition suppresses TNFα and CCL2 mRNA induction by lipids, and this may be in part due to the suppression of IL-1β and IL-18 cytokine signaling or ISR's known inhibitory effect on inflammatory transcription factors. Furthermore, yet uncharacterized mitochondria-

FIGURE 7 Continued

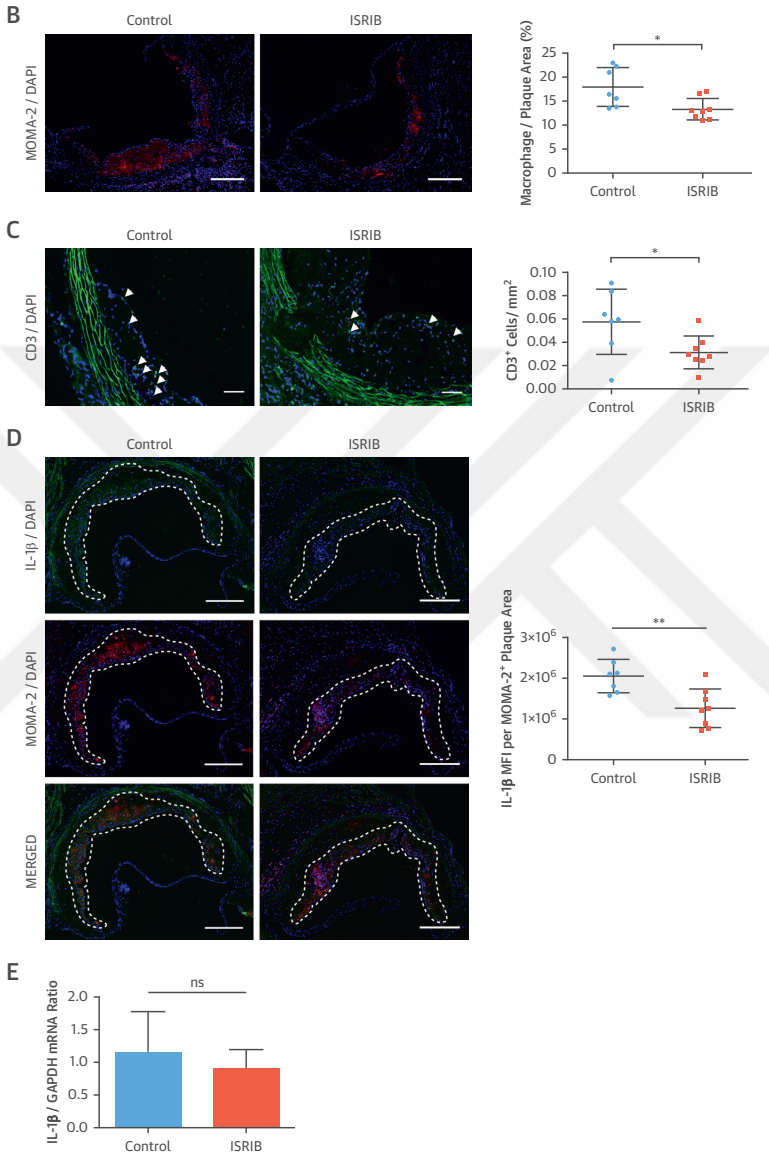

Continued on the next page

FIGURE 7 Continued

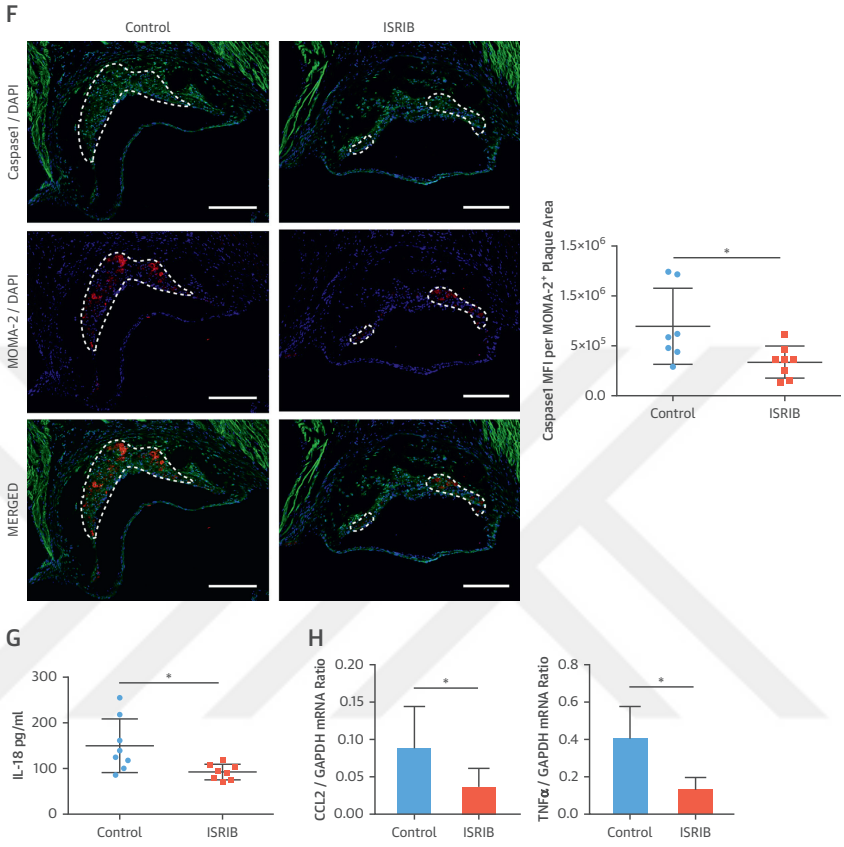

driven metabolic shifts driven by ISR inhibitors could alter the immune epigenome. Our results also suggest LONP1 drives sterile inflammation and atherosclerosis, but this possibility needs to be directly tested. These findings underscore the intricate exchange of information between ER and mitochondria is important for metabolic health and its disruption by dietary fats can promote inflammation and atherosclerosis.

ORGANELLE THERAPEUTICS AS AN UPSTREAM MODULATOR OF IL-1β. Lipid-induced NLRP3 activation in plaque macrophages is an important contributor to atherosclerosis. Previous studies showed inflammasome inhibition or antagonizing IL-1β or IL-18 can reduce atherosclerosis independent of an improvement in dyslipidemia (41–43). Furthermore, the results of the CANTOS (Cardiovascular Risk Reduction Study [Reduction in Recurrent Major CV Disease Events]) (neutralizing IL-1β) showed a modest, but significantly lower, rate of recurrent cardiovascular events in patients with previous myocardial infarction, supporting the inflammatory basis of atherothrombosis in humans (44,45). On the other hand, emerging data suggest that IL-1β inhibition can significantly increase the risk of infections (Group A *Streptococcus* [GAS] [46] and Food and Drug

CENTRAL ILLUSTRATION **Modulation of the Integrated Stress Response in Atherosclerosis**

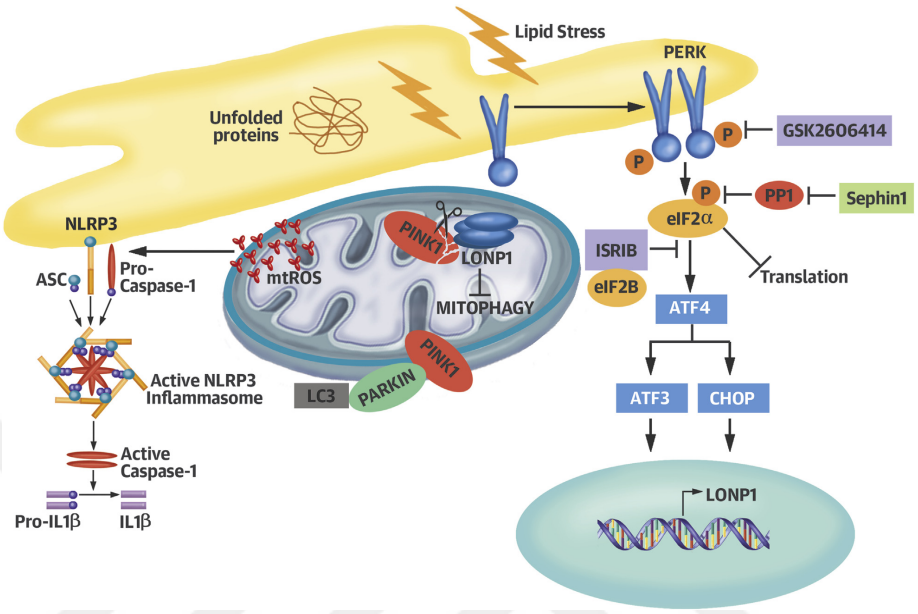

Onat, U.I. et al. J Am Coll Cardiol. 2019;73(10):1149–69.

The integrated stress response (ISR) controls mitochondrial clearance, mtROS production, and NLRP3 inflammasome activation by lipids. Lipid-induced PERK-eIF2α signaling activates a mitochondrial target, LONP1, which degrades its substrate PINK1 and suppresses Parkin-dependent mitophagy. Inhibition of PERK-eIF2α-LONP1 signaling by small molecules promotes mitophagy and counteracts NLRP3 inflammasome by lipids. mtROS = mitochondrial reactive oxygen species.

Administration Adverse Event Reporting System). IL-1 receptor (R)-deficient mice (47) as well as anakinra (IL-1R antagonist)-treated mice display impaired bacterial killing, hypersusceptibility to GAS infection/dissemination (46). However, caspase-1-deficient, NLRP3-deficient mice or NLRP3 inhibitor-treated mice do not display increased GAS susceptibility/dissemination, suggesting that strategies for blocking IL-1β maturation may not carry the same risks for infection as those blocking its receptor (46). These findings illustrate a paradigm in which IL-1β and the inflammasome are not functionally redundant, with implications for atherosclerosis. Therefore, strategies to block the IL-1β pathway in proximal steps such as by relieving organelle stress induced by dietary fats may be beneficial in atherosclerotic patients and bypass the unwanted infection risk associated with ablating IL-1β all together.

STUDY LIMITATIONS. Here, we showed modulation of ISR, especially by targeting eIF2B, is beneficial in atherosclerosis in mice. The feasibility of targeting eIF2B requires further testing in human atherosclerosis in future studies.

CONCLUSIONS

Targeting homeostatic pathways such as unfolded protein response (UPR) and ISR in complex diseases has been challenging, because ablating an essential stress response in a long-term fashion can have unwanted effects (such as pancreas toxicity associated with PERK inhibition) (48). Furthermore, genetic mouse models for important players in these pathways yielded confusing results through unintentional hyperactivation of other pathway components (49). Many groups have tackled this challenge by using

chemical chaperones to relieve general ER stress or small molecules targeting one of the proximal regulators in the tripartite UPR signaling (48). These in vivo studies have taught us lessons about modulating the UPR that were not predictable from cell-based studies. For example, inositol-requiring enzyme-1's (IRE1's) endoribonuclease (RNase) activity has been associated with cell survival as opposed to its kinase activity associated with death (1), but IRE1 RNase inhibitors showed their in vivo anti-inflammatory properties are beneficial by mitigating atherosclerosis (7). Furthermore, in vivo studies with small molecules to modulate key molecular players in the ISR have begun to illuminate how to fine tune this homeostatic response in complex diseases (25,39,48). In this study, using several different approaches to modulate eIF2α phosphorylation, we demonstrated ISR's causal role in lipid-induced inflammasome activation, inflammation, and atherosclerosis progression. Among these strategies, eIF2B activation (by ISRIB) appears to be the most advantageous in atherosclerosis. First, unlike PERK kinase inhibitors ISRIB is not associated with toxicity. Second, detailed mechanism of how ISRIB impacts translation was recently illuminated (36). Third, ISRIB's unique memory enhancing effects combined with its anti-inflammatory and anti-atherosclerotic actions suggest targeting eIF2B locus could combat both memory decline and CVD, especially in an aging population (27,39). Further studies are needed to illuminate ISRIB's impact on aging, but the available information on the specificity, efficacy, and mechanism of action of ISRIB suggest eIF2B could be a desirable, molecular target for the modulation of the ISR in atherosclerosis (26,39,40).

ADDRESS FOR CORRESPONDENCE: Dr. Ebru Erbay, Department of Medicine, Smidt Heart Institute & Department of Biomedical Sciences, Cedars Sinai Medical Center, 127 South San Vincente Boulevard, Advanced Health Sciences Pavilion, A9104, Los Angeles, California 90048. E-mail: ebru.erbay@cshs.org. Twitter: @CedarsSinai.

PERSPECTIVES

COMPETENCY IN MEDICAL KNOWLEDGE: Dietary fats stress anabolic and catabolic organelles and promote inflammation, accelerating atherosclerosis. Inhibition of organelle stress responses in a murine model reduces lipid-induced inflammation and slows the progression of atherosclerosis.

TRANSLATIONAL OUTLOOK: Further research should be directed toward developing methods of modulating organelle stress responses to hyperlipidemia that ameliorate inflammation and prevent atherosclerosis without the risk for infection associated with immunosuppression.

REFERENCES

1. Walter P, Ron D. The unfolded protein response: from stress pathway to homeostatic regulation. Science 2011;334:1081–6.

2. Pakos-Zebrucka K, Koryga I, Mnich K, Ljujic M, Samali A, Gorman AM. The integrated stress response. EMBO Rep 2016:1374–95.

3. Hotamisligil GS. Inflammation, metaflammation and immunometabolic disorders. Nat Rev 2017; 542:177–85.

4. Ozcan U, Cao Q, Yilmaz E, et al. Endoplasmic reticulum stress links obesity, insulin action, and type 2 diabetes. Science 2004;306:457–61.

5. Erbay E, Babaev VR, Mayers JR, et al. Reducing endoplasmic reticulum stress through a macrophage lipid chaperone alleviates atherosclerosis. Nat Med 2009;15:1383–91.

6. Thorp E, Li G, Seimon TA, Kuriakose G, Ron D, Tabas I. Reduced apoptosis and plaque necrosis in advanced atherosclerotic lesions of Apoe-/- and Ldlr-/- mice lacking CHOP. Cell Metab 2009;9:474–81.

7. Tufanli O, Telkoparan Akillilar P, et al. Targeting IRE1 with small molecules counteracts progression of atherosclerosis. Proc Natl Acad Sci U S A 2017; 114:E1395–404.

8. Zhou AX, Tabas I. The UPR in atherosclerosis. Sem immunopathol 2013;35:321–32.

9. Feng B, Yao PM, Li Y, et al. The endoplasmic reticulum is the site of cholesterol-induced cytotoxicity in macrophages. Nat Cell Biol 2003;5: 781–92.

10. Wang DD, Hu FB. Dietary fat and risk of cardiovascular disease: recent controversies and advances. Annu Rev Nutr 2017;37:423–46.

11. Sacks FM, Lichtenstein AH, Wu JHY, et al. Dietary fats and cardiovascular disease: a presidential advisory from the American Heart Association. Circulation 2017;136:e1–23.

12. Li Y, Hruby A, Bernstein AM, et al. Saturated fats compared with unsaturated fats and sources of carbohydrates in relation to risk of coronary heart disease: a prospective cohort study. J Am Coll Cardiol 2015;66:1538–48.

13. Hotamisligil GS, Erbay E. Nutrient sensing and inflammation in metabolic diseases. Nat Rev Immunol 2008;8:923–34.

14. Wang Y, Wang GZ, Rabinovitch PS, Tabas I. Macrophage mitochondrial oxidative stress promotes atherosclerosis and nuclear factor-kappaB-mediated inflammation in macrophages. Circ Res 2014;114: 421–33.

15. Çimen I, Kocatürk B, Koyuncu S, et al. Prevention of atherosclerosis by bioactive palmitoleate through suppression of organelle stress and inflammasome activation. Sci Transl Med 2016;8: 358ra126.

16. Wen H, Gris D, Lei Y, et al. Fatty acid-induced NLRP3-ASC inflammasome activation interferes with insulin signaling. Nat Immunol 2011;12: 408–15.

17. Alexander MR, Moehle CW, Johnson JL, et al. Genetic inactivation of IL-1 signaling enhances atherosclerotic plaque instability and reduces outward vessel remodeling in advanced atherosclerosis in mice. J Clin Invest 2012;122:70–9.

18. Guo H, Callaway JB, Ting JP. Inflammasomes: mechanism of action, role in disease, and therapeutics. Nat Med 2015;21:677–87.

19. Horng T. Calcium signaling and mitochondrial destabilization in the triggering of the NLRP3 inflammasome. Trends Immunol 2014;35:253–61.

20. Myoishi M, Hao H, Minamino T, et al. Increased endoplasmic reticulum stress in atherosclerotic